DEVELOPMENT OF A CELL MOTILITY CHARACTERIZATION SYSTEM FOR INDUSTRIAL BIOTECHNOLOGICAL APPLICATIONS

Valeria Rachela Villella

Dottorato in Scienze Biotecnologiche – XXIII ciclo
Indirizzo Biotecnologie Industriali e Molecolari
Università di Napoli Federico II

Dottorato in Scienze Biotecnologiche – XXIII ciclo
Indirizzo Biotecnologie Industriali e Molecolari
Università di Napoli Federico II

DEVELOPMENT OF A CELL MOTILITY CHARACTERIZATION SYSTEM FOR INDUSTRIAL BIOTECHNOLOGICAL APPLICATIONS

Valeria Rachela Villella

Dottoranda: Valeria Rachela Villella

Relatore: Prof. Stefano Guido

Coordinatore: Prof. Giovanni Sannia

La grandezza di una persona si evince nella perseveranza e nella fermezza che investe nel perseguire e realizzare i suoi grandi sogni.

A chi ha creduto
in me

INDICE

RIASSUNTO

Premesse scientifiche

I fenomeni di interazione e migrazione cellulare sono rilevanti in diversi processi fisiopatologici dallo sviluppo embrionale all'infiammazione. Le tecnologie finora disponibili per lo studio di tali fenomeni in vitro sono in larga parte non adatte per applicazioni biotecnologiche industriali. Infatti, l'analisi delle interazioni cellulari viene spesso effettuata con saggi di biologia cellulare quali osservazioni in immunofluorescenza di campioni fissati, che sono limitate a condizioni statiche e si prestano con difficoltà a fornire misure quantitative di eventi dinamici, come la motilità cellulare, su larga scala. Scopo del progetto di tesi è lo sviluppo di un sistema innovativo per l'analisi della motilità e delle interazioni cellulari in 2D e 3D che, superando i limiti già accennati dei saggi finora disponibili, si presti a utilizzo biotecnologico industriale per future applicazioni in screening di sostanze a potenziale valenza terapeutica. In particolare, è stato sviluppato un sistema che consente l'analisi quantitativa del fenomeno di chemiotassi, in cui un gradiente di chemochine, attraverso recettori di superficie, innesca cascate di segnali intracellulari che culminano nel movimento di cellule infiammatorie in direzione del chemoattrattante (Hynes R.,Cell 2002). Si tratta di un fenomeno in cui una costante e dinamica interazione fra il microambiente e la superficie cellulare induce modificazioni dello stesso fenotipo della cellula che risponde a questi stimoli con movimenti finalistici (Ridley A, et al. Science 2003). Cio' avviene, ad esempio, per il movimento dei neutrofili in risposta all'interlechina 8 (IL-8).
Il lavoro di tesi è stato organizzato nel modo seguente. In un prima fase l'attività di ricerca è stata indirizzata all'individuazione di meccanismi molecolari che regolano la risposta infiammatoria alla base della produzione di fattori chemoattraenti, come IL-8, utilizzando in particolare come modello la fibrosi cistica. Questa prima parte del lavoro di tesi è stata condotta con tecniche classiche di biologia cellulare e molecolare ed è stata finalizzata alla comprensione del meccanismo molecolare alla base della produzione di IL-8. E' stato studiato l'effetto di un ambiente infiammatorio su fattori come la transglutaminasi (TG2) che a sua volta regola la modulazione di IL-8. I risultati ottenuti in questa prima parte del lavoro sono stati utilizzati per la messa a punto di una cella di chemiotassi in cui neutrofili migrano in un gel di collagene tridimensionale sotto l'effetto di un gradiente di IL-8. E' stato inoltre messo a punto un sistema di valenza trasversale per l'analisi quantitativa della migrazione collettiva di una linea cellulare (T84, utilizzata come modello nella patologia celiaca) durante il processo di confluenza in una piastra di coltura 2D. Si tratta di un ulteriore esempio dell'interazione dinamica fra cellule attraverso il quale cellule poste in piastre di coltura in apposito terreno raggiungono la confluenza muovendosi in uno spazio 2D. Questo fenomeno e' particolarmente studiato per le cellule epiteliali ed e' coordinato non solo da non ancora ben definiti stimoli esterni, ma soprattutto da modificazioni dinamiche della cellula, come la proliferazione e il riarrangiamento del citoschelestro che consentono alle cellule di entrare in contatto con le cellule vicine. La complessità di questi eventi e' ulteriormente provata dal fatto che le cellule stesse, interagendo con le cellule vicine vanno incontro a differenziamento come nel caso delle linee cellulari epiteliali intestinali T84 in cui la confluenza induce produzione di enzimi di superficie, quali la lattasi, propri delle cellule mature. Questo processo di migrazione

collettiva viene inoltre influenzato dagli stessi fattori, studiati nella prima parte del lavoro di tesi, che regolano la produzione di IL-8.
Le motivazioni per lo sviluppo del sistema biotecnologico di analisi dei fenomeni di interazione e motilità cellulare oggetto di questa tesi sono da ricercarsi in ambito patologico. Infatti, nel panorama cosi' complesso della motilità e interazione fra cellule in un determinato microambiente la ricerca dei fattori che determinano le modifiche cellulari che conducono all'interazione rappresenta un elemento di grande interesse in patologia umana in quanto il decorso di malattie croniche e' spesso influenzato da alterazioni dei meccanismi di interazione fra cellule. Un esempio e' fornito dal comportamento cellulare in patologie neoplastiche in cui il controllo della invasività delle cellule cancerose rappresenta il goal di terapie anti-tumorali.
Infine lo studio del "movimento" e della sua direzionalità in patologia umana puo' non riguardare cellule in toto o sistemi di cellule in un ambiente specifico. La "motilità" e' infatti anche una caratteristica del compartimento intracellulare in cui organelli, aggregati di proteine e le stesse proteine si muovono all'interno della cellula secondo regole ben definite. Un esempio e' rappresentato dal trafficking di proteine in membrana e dal loro continuo reciclying fra la membrana e gli endosomi nonche' la progressione verso i compartimenti degradativi intracellulari. Meccanismi di "movimenti" intracellulari sono alla base di complessi meccanismi di degradazione quali l'autofagia e compoprtano anche un riarrangiamento del citoscheletro che regola la motilità "esterna" dell'intera cellula.
In un panorama cosi' complesso l'identificazione dei fattori che possono disregolare il complesso sistema della motilità in senso lato e' pertanto di grande interesse e la identificazione di molecole potenzialmente capaci di modulare questi processi puo' avere enormi implicazioni terapeutiche per applicazioni biotecnologiche industriali.
La scelta di modelli di malattia idonei allo studio dei fattori putativamente coinvolti nei meccanismi di motilità/interazione cellulare dovrebbe basarsi essenzialmente sulla evidenza che questi meccanismi costituiscono un elemento patogenetico della malattia e non un semplice evento *bystander*. La comprensione di una pathway specifica puo' aprire la strada alla identificazione di sostanze capaci di modulare questi processi biologici e rappresentare molecole eventualmente implementabili nella terapia di molte patologie umane.
Come già accennato, nel corso del dottorato di ricerca sono stati utilizzati diversi modelli cellulari di due differenti patologie umane, la Fibrosi Cistica e la Celiachia che hanno come fattore comune valori elevati della Transglutaminasi tissutale (TG2), un enzima multifunzionale con un ruolo patogenetico noto in diverse patologie umane, che induce cross-linking di proteine substato o espleta altre funzioni quali una attività isomerasica o di G protein (Malorni, W., et al. 2008, Curr. Pharm. Des).
La Fibrosi Cistica, la piu' comune malattia monogenica ad esito letale nella popolazione caucasica, dovuta a mutazioni del gene CFTR, e' caratterizzata, fra l'altro, da infiammazione polmonare a prevalente componente neutrofilica in risposta ad elevata secrezione di IL8 con ricorrenti infezioni batteriche (Smith, J. J., et al. Cell. 1996; Ratjen, F., and G. Doring. 2003. Lancet). Nella prima parte del lavoro di tesi, sono state utilizzate linee cellulari epiteliali per identificare la pathway mediata da TG2 che porta ad incrementati livelli di IL8 e di infiammazione. Sono stati quindi validati inibitori specifici di questa pathway ed individuato il meccanismo di controllo dell'infiammazione e della secrezione di IL8 in vitro e in vivo in 2 diversi modelli animali di malattia.
La celiachia, una intolleranza permanente a determinate sequenze peptidiche della gliadina del frumento e delle prolamine di orzo e segale, e' una comune intolleranza

alimentare con una prevalenza di 1:100 nella popolazione generale, e caratterizzata da una disregolazione della risposta immune mucosale innata ed adattativa con componente autoimmune (Sollid LM. Nat Rev Immunol 2002). E' ampiamente dimostrato come la gliadina induca aumentata espressione e attivazione della proteina TG2 che esercita un ruolo patogenetico nella malattia. Nella prima parte del lavoro di tesi, sono state utilizzate linee cellulari epiteliali intestinali per studiare i meccanismi di internalizzazione e degradazione di peptidi della gliadina e il loro impatto sulla upregolazione della TG2. Infine sono state utilizzate queste acquisizioni per studiare gli effetti dei peptidi tossici della gliadina sulla motilità delle cellule epiteliali in coltura e sulle loro interazioni e per comprendere se l'inibizione della TG2 possa esercitare un ruolo chiave nel controllare gli effetti dei peptidi della gliadina sulla motilità delle cellule epiteliali in un sistema 2D.

Risultati ottenuti e metodologie

La Fibrosi Cistica (FC) è un nota malattia genetica caratterizzata da uno stato infiammatorio basale, la cui natura è ancora oggetto di controversie.
A) Al fine di comprendere il link tra difetto della Cystic Fibrosis Transmembrane Conductance Regulator (CFTR) e infiammazione con elevati livelli del fattore chemoattrattante IL-8, sono stati condotti esperimenti su linee epiteliali portatrici della piu' comune mutazioni del gene CFTR, la F508del-CFTR, le IB3 e su le corrispondenti linee epiteliali in cui il difetto è stato geneticamente corretto, le linee isogeniche C38 (Smith, J. J., et al. Cell. 1996).
Esperimenti di Western Blot, Immunoprecipitazione, siRNA, Microscopia confocale ed analisi dell'attività enzimatica hanno permesso di evidenziare che nelle cellule epiteliali FC gli elevati livelli di TG2 e la sua conseguente attività enzimatica sono delle funzione della CFTR in quanto sia inibitori della funzione di CFTR, quali il CFTR-inhibitor-172 che il silenziamento del gene CFTR mediante siRNA, aumentano i livelli di TG2 nelle cellule C38. Abbiamo poi dimostrato che l'inibizione della TG2, sia mediante silenziamento genico che con inibitori della sua attività enzimatica (cystamina o R283), riduce drammaticamente alcuni marcatori di attivazione epiteliale, quali la fosforilazione delle MAP-chinasi ERK1/2 (p42/44), e la produzione di citochine infiammatorie, quali TNF-a, sia della chemochina IL-8. Questi dati suggeriscono che il difetto di CFTR induce infiammazione e produzione di IL-8 mediati da TG2.
B) Abbiamo poi voluto comprendere come il difetto di CFTR induca persistenza di elevati livelli di TG2 nelle cellule epiteliali FC. E' noto che la difettiva funzione di CFTR induce un aumento delle Specie Reattive all'Ossigeno (ROS) (Yi, S. J., et al.. 2006. Mol. Cells). Abbiamo dimostrato che molecole scavenger di ROS, quali la N-acetyl-cysteine (NAC) e la catalasi Superossido-Dismutasi(SOD)-mimetica EUK-134 riducono infatti i livelli di TG2 con drammatica riduzione della sua attività enzimatica.
La dipendenza di elevati livelli di TG2 dall' ambiante pro-ossidativo ci ha indotto a pensare che l'incremento di ROS potesse indurre modifiche posttraslazionali della proteina TG2. Fra le piu' comuni modifiche post-traduzionali sono la Sumoylazione (Meulmeester, E., and F. Melchior. 2008. Nature), e l' ubiquitinazione nota per intervenire in processi di degradazione via proteasoma. Entrambe competono per gli stessi residui di Lys e quindi sono mutualmente esclusive e richiedono enzimi E3-ligasi specifici.

I risultati ottenuti in seguito a IP di TG2 in cellule IB3 e C38 hanno evidenziato elevati livelli di Sumo in IB3 rispetto alle C38, e silenziamenti genici di PIASy (specifica E3 ligasi di SUMO) o di SUMO hanno dimostrato uno sbilanciamento a favore della Ubiquitinazione. Tali informazioni hanno suggerito l' idea che la persistenza di TG fosse Sumo-dipendente. L'inibizione della produzione di ROS in cellule IB3 ha evidenziato che i livelli di SUMO e PIASy erano notevolmente abbassati e con essi la SUMOylazione di TG2. I dati sottolineano che l ambiente pro ossidativo della CF giuda la persistenza di TG2 via SUMOylazione PIASy-dipendente.
C) Gli effetti della persistenza di elevati livelli di TG2 mediati da CFTR via ROS hanno dimostrato avere importanti effetti pro-infiammatori che portano ad elevati livelli di IL8. Per individuare le strade più idonee per antagonizzare questa pathway che dal difetto di CFTR conduce all'infiammazione, abbiamo studiato gli effetti della persistenza della TG2 negli epiteli FC.
La TG2 induce modifiche posttraslazionali di proteine substrato ed abbiamo identificato un link diretto tra TG2 e il modulatore anti–infiammatorio PPARγ (Daynes, R. A., and D. C. Jones. 2002. Nat. Rev. Immunol.). Infatti I livelli di PPARγ sono stati ritrovati bassi in IB3 rispetto alle C38. Questa relazione fra TG2 e PPARγ è stata dimostrata dipendere dalla attività cross linkante operata da TG su PPARγ con formazione di legami isopeptidici. Studi con agonisti o inibitori del PPARγ hanno dimostrato che il crosslinking di PPARγ e' uno dei meccanismi attraverso cui TG2 induce infiammazione in epiteli FC.
D) Studi di microscopia confocale hanno poi evidenziato che il PPARγ e' sequestrato in struttre note come aggresomi (Kopito, R. R. 2000. Trends Cell Biol.), che rappresentano stazioni di accumulo di proteine misfolded o modificate post-traslazionalmente e che sono eliminate attravesro un meccanismo alternativo di degradazione, noto come autofagia. Nelle cellule epiteliali FC osserviamo un accumulo di aggresomi, caratterizzati dalla presenza del marcatore HDAC6 (Kawaguchi, Y.,et al. 2003.Cell) e di ubiquitina, con sequestro di PPARg oltre ad aggresomi contenenti la stessa CFTR misfolded. L'accumulo di aggresomi in cellule FC suggerisce una alterazione complessa del degradasoma e suggerisce che le cellule con difettiva CFTR potrebbero presentare un difetto del meccanismo di autofagia.L'autofagia e' un meccanismo che le cellule adottano in condizioni di stress o di carenza nutrizionale come meccanismo di sopravvivenza (Mizushima, N., et al. 2008 Nature; Moreau, K., Luo, S. & Rubinsztein, D. C. 2010 Curr. Opin. Cell Biol.).
Con tecniche di trasfezione, rel time PCR, western blot, immunoprecipitazione, microscopia confocale e microscopia elettronica, Noi abbiamo dimostrato che le cellule epiteliali FC presentano un difetto di autofagia con riduzione di autofagosomi, aumento del pool di proteine ubiquitinate e aumento del marcatore p62 che aumenta in maniera significativa in condizioni di difettiva autofagia.
Abbiamo poi dimostrato che questo difetto di autofagia e' dovuto al crosslinking di beclin 1 da parte di TG2. Beclin 1 e' una proteina cruciale per la formazione di membrane di autofagosomi (Axe, E. L. et al. 2008, J. Cell Biol.) e la sua associazione nel reticolo endoplasmico (ER) con altre proteine del complesso III del phosphatidylinositol-3-kinase complex (PI3K), e' cruciale per iniziare il processo autofagico (Matsunaga, K. et al.2009,Nature Cell Biol.; Zhong, Y. et al. 2009,Nature Cell Biol.). Noi abbiamo dimostrato che le modifiche posttraslazionali (crosslinking) di beclin 1 operato dalla TG2 induce uno spiazzamento del complesso III PI3K dall'ER e suo sequestro in aggresomi con inibizione dell'autofagia. La overespressione di Beclin 1 cosi' come l'inibizione della TG2 ripristina la normale funzionalità del

processo autofagico con eliminazione degli aggresomi e riduzione deli marcatori di infiammazione fra cui IL8.
E) Pertanto il difetto di CFTR induce una attivaione dll'asse ROS-TG2 che attraverso una inibizione dell'autofagia conduce ad infimmazione. Per dimostrare la valenza di questo meccanismo nella patogenesi dell'infiammazione in FC, abbiamo utilizzato altri 2 modelli biologici. Il primo e' rappresentato dalla coltura ex vivo di mucose di polipo nasale di pazienti con FC, e il secondo è il modello murino di malattia. (Mall, M.et al. 2004, Nature Med.).I topi sono stati trattati con cystamine o NAC. Queso trattamento ha indotto riduzione dell'infiammazione polmonare, riduzione di livelli di MIP-2, l'analogo murino della IL8 e riduzione dei neutrofili intratissutali.Nel loro complesso questi dati dimostrano che inibire la TG2 o ridurre i livelli di ROS e' un approccio estremamente utile in vitro e in vivo per controllare l'infiammazione e i livelli di IL-8.
Per ipotizzare un trasferimento dei nostri risultati alla biotecnologia industriale si e' pensato di ipotizzare un device che consentisse lo studio della dinamica del processo di migrazione dei neutrofili in risposta al fattore chemoattrattante IL8 che abbiamo visto giocare un ruolo patogenetico nella infiammazione respiratoria in FC.
E' stata realizzata una matrice tridimensionale di gel di collagene (principale componente delle matrice extracellulare) per mimare le reali condizioni fisiologiche. Sono stati eseguiti esperimenti di motilità su neutrofili in presenza o in assenza di IL8 in una matrice 3D di gel, utilizzando un'appropriata cella di flusso.
La matrice di gel è costituita da una soluzione liquida di collagene al quale è aggiunto e una sospensione cellulare contenente $2 \cdot 10^5$ cell\ml e fatta gelificare per 30minuti in un incubatore per cellule. Per lo studio del fenomeno è stata progettata e realizzata una cella di chemiotassi, costituita da un blocco di alluminio, adeso ad un vetrino portaoggetti, che alloggia un pozzetto al cui centro presenta un blocchetto (inserito tra due guide) sul quale viene fatta aderire una membrana semipermeabile per la realizzazione di un flusso diffusivo.
La cella di chemiotassi contenente le cellule in gel di collagene, in assenza o presenza di chemoattraente, viene alloggiata sul tavolo portaoggetto di un sistema time-lapse, il quale consta di un microscopio rovesciato equipaggiato di motorizzazione per il tavolino portaoggetti e di un micro incubatore per cellule. In maniera completamente automatizzata le immagini vengono acquisite a diverse profondità, effettuando delle scansioni 3D del campione in esame ad intervalli regolari nel tempo.Le immagini sono poi analizzate tramite tecniche di image analysis al fine di: determinare la posizione 3D per ogni istante di tempo, ricostruire la traiettoria seguita, e definire la direzionalità perseguita da ogni singola cellula.
Per validare il sistema è caratterizzare il flusso diffusivo utilizzando destrano fluorescente (FITC-destrano), avente peso molecolare paragonabile a quello del chemoattraente. In seguito, i primi esperimenti di controllo sono stati condotti su neutrofili (da donatori sani) in presenza e assenza di uno stimolo chemiotattico. I risultati ottenuti indicano, come atteso, un movimento cellulare del tutto casuale in assenza di IL8 e fortemente direzionato in condizioni di presenza dello stimolo.
Questo strumento di analisi direzionale e quantitativo potrà consentire innanzitutto di utilizzare questo modello per screening di sostanze con potenziale effetto chemoattrattante per leucociti in diverse patologie umane. La definizione dei meccanismi che regolano la produzione di IL8, come dimostrato nel percorso di dottorato, potrà inoltre aprire la strada ad un nuovo approccio per testare la produzione di chemochine da parte di cellule epiteliali di CF o di altre patologie

infiammatorie croniche poste nel device insieme ai leucociti per screenare "in situ" l'effetto di inibitori di pathways che regolano la produzione di IL8.
I risultati ottenuti nel corso di questo percorso di dottorato di ricerca aprono la strada ad un ulteriore modello di potenziale applicazione alle Biotecnologie Industriali, l'analisi dinamica e direzionale 2D di cellule epiteliali poste in piastre di coltura.
Infatti l'attivazione dell'asse ROS-TG2, oltre ad avere un impatto sui meccanismi patogenetici della FC precedentemente descritti, e' anche in grado di influenzare la fisiologia del citoscheletro cellulare, fattore notoriamente cruciale nel mediare l'interaione fra popolazioni cellulari.
A tale scopo abbiamo utilizzato un modello di un'altra patologia infiammatoria cronica, la celiachia, in cui precedenti evidenze, fra le quali quelle ottenute dal nostro gruppo di ricerca, hanno dimostrato il ruolo determinante della TG2 nella patogenesi della malattia.
La celiachia e' una intolleranza alimentare caratterizzata da una attivazione del sistema immune mucosale a particolari sequenze peptidiche della gliadina, una proteina del frumento. In particolare alcuni peptidi, fra cui quello corrispondente alla sequenza aminoacidica 31-43 della A-gliadina, sono in grado di attivare le cellule epiteliali intestinali predisponendo la mucosa intestinale alla azione di altre frazioni peptidiche, fra cui la 56-68 (a-9) che in un contesto di attivazione della risposta innata sono presentati alle cellule T gliadina-specifiche, evocando in tal modo una attivazione del sistema immune adattativo(Sollid LM.. 2002, Nat Rev Immunol; Sollid LM. 2000 Annu Rev Immunol; Shan L, et al. 2002 Science; Maiuri L, et al. Lancet, 2003).Nel corso del dottorato abbiamo dimostrato come il peptide 31-43 sia internalizzato nelle cellule epiteliali e accumuli nei lisosomi con un ritardo della degradazione che induce un aumento di produzione di ROS e conseguente upregolazione della TG2. Cio' induce un profondo riarrangiamento del citoscheletro con riarrangimento dei filamenti di actina.
Per le ragioni precedentemente dette, abbiamo voluto verificare se la tossicità del peptide 31-43 potesse impattare sul movimento e interazione delle cellule epiteliali intestinali poste in piastra di coltura, in considerazione dei suoi effetti sul citoscheletro.
A tale scopo sono stati condotti esperimenti in 2D in piastre da coltura su linee cellulari epiteliali di T84 in presenza o meno di stimoli infiammatori, quali il p31-43, seguiti da una regolazione della TG2 mediante inibizione con un anticorpo monoclonale (TG 4G3) o mediante inibizione dei ROS utilizzando l' EUK134 (mimetico chimico della catalasi- Superossido Dismutasi).
I movimenti delle cellule sono stati seguiti mediante la tecnologia Time-Lapse; è stato eseguito un esperimento in 2D in cui le immagini dei campi di vista sono acquisite ogni 15 min, per un totale di 48h.
La caratteristica morfologia cellulare delle T84 si esplicita nella formazione di strutture isolari che si accrescono durate le fasi si duplicazione e mostrano movimenti di associazioni di più isole (simile ad un processo di inglobazione).
Le immagini ottenute mostrano una chiara alterazione della motilità delle isole in presenza del solo p31-43 rispetto al controllo non trattato (medium alone). L' aggiunta dei modulatori di TG2 e dei ROS riporta il sistema ad una condizione paragonabile al campione non trattato, mostrando una riduzione di motilità rispetto al p31-43.
Le cellule sono state in seguito fissate e utilizzate per l' osservazione in fluorescenza di un marcatore tipico del citoscheletro, la falloidina; le immagini acquisite tramite microscopia confocale mostrano un chiaro riarrangiamento citoscheletrico nel

campione trattato con p31-43 rispetto al non trattato; analogamente al movimento, in seguito alle inibizioni della TG2, il citoscheletro riprende una struttura paragonabile al non trattato.
I risultati dimostrano quindi che l' alterato profilo infiammatorio impatta sul movimento cellulare e consente di identificare sostanze capaci di modulare le cause che determinano alterazioni della motilità.
Questo modello offre importanti applicazioni potenziali in diverse patologie umane in quanto l'alterazione del citoscheletro e la TG2 sono entrambi coinvolti in processi di migrazione e interazioni cellulari alla base della invasività di cellule neoplastiche.

Conclusioni e prospettive future

I risultati della ricerca svolta nei tre anni di Dottorato offrono innanzitutto un importante contributo alla definizione dei meccanismi patogenetici dell'infiammazione polmonare in FC e identificano nuove opzioni terapeutiche per i pazienti.
In particolare i principali risultati dello studio che hanno riscontro in 4 lavori pubblicati su riviste internazionali definiscono:
a) il ruolo della TG2 come fattore patogenetico nuovo nella FC
b) il ruolo di modifiche posttraslazionali della TG2 come link fra difetto genetico di CFTR ed infiammazione
c) i meccanismi attraverso i quali l'asse ROS-TG2 inibisce l'autofagia nelle cellule epiteliali respiratorie FC. Questo studio definisce per la prima volta la FC come malattia correlata ad autofagia.
Questo percorso di studio fornisce poi il razionale per l'implementazione di modelli di motilità/migrazione cellulare come strumenti idonei per testare l'efficacia di molecole a potenziale impatto farmacologico.
La possibilità di disporre di un modello di analsi quantitativa e qualitativa potrà consentire di saggiare l'efficacia di diversi farmaci che mirano a controllare l'invasività di cellule neoplastiche e per modulare la farmaco-resistenza che costituisce un problema cruciale di terapia. Gli effetti da noi osservati di modulazione di TG2 e di ROS su questi processi dinamici potrà consentire la messa a punto di device idonei sia per finalità di ricerca che per screening dell'efficacia di farmaci.
Infine la difficoltà di utilizzare modelli di malattia e' spesso un limite per effettuare screening di sostanze a potenziale impatto terapeutico. Questo modello dimostra di possedere sia i vantaggi di un "modello in vitro", cioe' la manipolabilità e versatilità, sia le caratteristiche peculiari del modello ex-vivo. E' infatti possibile screenare farmaci sul loro target naturale, cioe' le cellule del paziente poste in coltura con il grande vantaggio di poiter tener conto della variabilità interindividuale di risposta al trattamento che costituisce un problema cruciale nella farmacologia clinica. Queste caratteristiche rendono il sistema per l'analisi quantitativa della motilità e delle interazioni cellulari sviluppato nell'ambito di questo lavoro di tesi adatto per applicazioni biotecnologiche industriali.

Dati ottenuti durante il periodo di PhD sono inseriti nelle seguenti pubblicazioni:

Luciani A, Villella VR, Esposito S, Brunetti-Pierri N, Medina D, Settembre C, Gavina M, Pulze L, Giardino I, Pettoello-Mantovani M, D'Apolito M, Guido S, Masliah E, Spencer B, Quaratino S, Raia V, Ballabio A, Maiuri L. *Defective CFTR induces aggresome formation and lung inflammation in cystic fibrosis through ROS-mediated autophagy inhibition.* Nat Cell Biol. 2010,12(9):863-75.

Luciani A, Villella VR, Vasaturo A, Giardino I, Pettoello-Mantovani M, Guido S, Cexus ON, Peake N, Londei M, Quaratino S, Maiuri L.
stress and tissue transglutaminase-mediated PPARgamma downregulation in intestinal epithelial cells and coeliac mucosa. Gut. 2010; 59(3):311-9.

Luciani A, Villella VR, Vasaturo A, Giardino I, Raia V, Pettoello-Mantovani M, D'Apolito M, Guido S, Leal T, Quaratino S, Maiuri L.
stress and inflammation. J Immunol. 2009; 183(4):2775-84.

Maiuri L, Luciani A, Giardino I, Raia V, Villella VR, D'Apolito M, Pettoello-Mantovani M, Guido S, Ciacci C, Cimmino M, Cexus ON, Londei M, Quaratino S.
modulates inflammation in cystic fibrosis via PPARgamma down-regulation. J Immunol. 2008,180(11):7697-705.

ABSTRACT

Cell migration is a very complex mechanism linked to the inflammatory response as well as to several processes of cell biology and development.
The movement of cells in response to a chemokine gradient is the most popular form of interaction between cell environment and surface and specific surface receptor triggers an intracellular signaling pathway. This phenomenon is known as chemotaxis and is characteristic of neutrophil movements in response to the chemokine Interleuchin-8 (IL8) in a 3D space. Another paradigm of dynamic interaction between cells is the mechanism underlying the confluency of cells cultured in a Petri dish. This process is particularly studied in growing epithelial cell lines, and is influenced by still undefined external stimuli as well as by cell proliferation and cytoskeleton reorganization, that allow the contact and interaction between cells in 2D space. Chronic inflammation is an ideal condition for the study of cell migration and its de-regulation; understanding the mechanisms involved in cell motility and their putative modulation, is the first step in setting new appropriate models of study.
During PhD project, different cellular models have been used: IB3 cell lines belonging to patients with Cystic Fibrosis (caused by mutations of cystic fibrosis transmembrane regulator (CFTR)), and T84 cell lines, a popular model of study of Coeliac Disease, a common intolerance to proteins of wheat. Both disease are characterized by a pro-inflammatory milieu with high level of tissue Transglutaminase (TG2), a multi-functions enzyme with a defined role in several human pathologies.
Cystic Fibrosis is the prototype of diseases in which an uncontrolled production of IL8 leads to a dysregulated neutrophil recruitment. The IB3 cell lines have been used to understand a molecular mechanisms of enhanced IL8 production and their modulation. The results evidence i) the role of TG2 as a new pathogenic factor in Cystic Fibrosis; ii) the role of post-translational modifications of TG2 as a link between genetic defect of CFTR ad inflammation iii) the mechanisms of autophagy inhibition via ROS-TG2 axis, in epithelial airway cell line and mice model of CF. The consequence is a fine modulation of IL8 production. The system allows the design of a 3D model to study cell migration under IL8 diffusive flux in qualitative and quantitative ways.
Another important pathological system with chronic inflammation is celiac disease and the analysis of interactions of alimentary peptides with the frontline gut epithelium is a useful model of study. The epithelial cells are pivot in the innate immune activation in CD and cytoskeleton rearrangement is the earliest event in such a response to gliadin peptides. The data in T84 cell model show a gliadin peptide-driven pro-inflammatory environment as a consequence of its impaired lysosomal degradation. Moreover, alterations of motility and cytoskeletal reorganization emphasize the “toxic” effect of peptide. Therefore, CD offers an ideal opportunity to set up a 2D model of study of cell motility.
Understanding the mechanisms of migration and the identification of appropriate target of modulation of cell recruitment could allow wide industrial applications in biotechnology and will be successful to provide a useful tool to test potential therapeuthic molecules.

INTRODUCTION

Motility and Inflammation

Cellular interaction and migration are common physiological events triggered and finely tuned by different mechanisms either intrinsic to the cell or present in cellular environment. Multiple interactions between environment and cell surface induce dynamic modifications of cellular phenotype (1).

Cell migration, both single and collective, is a highly integrated multistep process that is essential in embryonic morphogenesis, tissue homeostasis and immune surveillance to inflammation. In collective migration a movement of cohesive groups of cells is required (2) and the single migrating cell shows a highly polarization with complex regulatory pathways that are spatiotemporally controlled (1). Migration contributes to several important pathological processes, including cancer progression and metastasis formation. Metastasis, dissemination of malignant tumors to a distant organ, is the major cause of cancer mortality. Tumor cell motility is the hallmark of invasion and is an essential step in metastasis(3).

Cell migration is a very complex phenomenon also linked to the inflammatory response as well as to several processes of cell biology and development.

Cell movements into solid surfaces require a controlled sequence of cell protrusions and retractions that mainly depends on sophisticated regulation of the actin cytoskeleton and the contribution of microtubules (4,5).

The movement of cells in response to a chemokine gradient is the most popular form of interaction between cell environment and surface in which specific surface receptor triggers an intracellular signaling pathway. The final event is the movement of cells in direction of chemoattractant (6). This process is characteristic of neutrophils movements in response to the chemokine Interleuchin-8 (IL8) in a 3D space.

Another paradigm of dynamic interaction between cells is the mechanism underlying the confluency of cells cultured in a Petri dish. This may be considered the prototype of movements in 2D space. This process is particularly studied in growing epithelial cell line, and is influenced by still undefined external stimuli as well as by cell proliferation and cytoskeleton reorganization, that allow the contact and interaction between cells. Cell contact and interaction may in turn impact on cell differentiation, as in confluent intestinal epithelial Caco-2 cell lines, which undergo differentiation with surface expression of brush border enzymes, markers of terminal differentiation.

Both attraction forces that compromise the adhesion of cell to fiber of matrix and cellular adaptative mechanisms are required to respond to matrix resistance. In 3-D ECM, in contrast to 2-D substrate, the cell shape is mostly bipolar and the cytoskeletal organization is less stringent, frequently lacking discrete focal contacts and stress fibers.(7)

Cell migration can be seen as a cyclic process usually driven by several factors, among the others actin polymerisation, stabilized upon adhesion to the extracellular matrix (ECM). Although matrix adhesion dynamic is very important for understanding cell migration behavior, the molecular mechanisms that regulate adhesion dynamics and signalling in disease conditions are still unclear (8,9).

All together these findings indicate that cell motility and migration occur as a consequence of a finely tuned interaction between intracellular and cell surface signaling pathways which can be influenced by a wide range of environmental

factors. Moreover such a signaling cascade may be disrupted in several disease states and migration itself can be considered a key step in disease evolution (10,11).
In the complex overview of motility and interaction between the cells within a specific environment, the research of factors influencing the interaction in human pathology is mandatory. As a matter of fact, the progress of many chronic disease is influenced by alterations of motility or interaction. An important instance is represented by neo-plastic movements of cancer cell and its deregulation during disease progress; understanding the mechanism of modulation of factor involved in this deregulation will be relevant for therapeutic applications.
The study of “moviments” and their directionality in human pathology is not only relevant for cell-to-cell interactions within a specific environment. Such a process is also a feature of intra-cellular processes where cytoplasmatic organelles, proteins aggregates and proteins (nuclear translocation) move within the cell with defined rules. A typical example is the trafficking and reciclying of membrane proteins within endosome-structure or degradation route (proteasome). These movements are the basis of several processes, among the others autophagy and cytoskeleton rearrangement that in turn can influence the “external” motility.
Cell migration may also take place within a proper tissue environment. This is the case of mucosal tissues approaching a luminal cavity, as airways or gut mucosa. In this case the spatial organization of tissues allow a compartmentalization of different cell types whose location reflects a specific function. Epithelial cells are the front line of airways and intestine and represent a set of specialized cells. These cells are also able to orchestrate cell migration within the tissues to maintain a proper tissue homeostasis in response to environmental triggers. In this context they are able to fight "toxic" environmental challenges, either bacterial or alimentary triggers, by secreting specific chemoattractant factors that recruit immunocompetent cells to the "damaged" luminal surface. This process is a well orchestrating event that involves different types of cells moving within the tissue and interacting each other in response to a given triggering factor.
The release of chemoattractants is the results of the activation of complex intracellular signaling cascades also involving a cytoskeleton rearrangement and generating a "stressed" environment (5).
The physiological mechanisms underlying such a complex production of chemoattractant factors is often impaired in disease conditions in which an improper activation of specific pathways or the lack of physiological mechanisms of control, lead to impaired production of chemoattractants with derangement of cell motylity and physiology.
The most popular examples of intra-tissue migration of cells are chronic inflammatory diseases occurring at the mucosal surface. Airway and gut chronic inflammatory diseases are the ideal condition for the study of cell migration and its de-regulation within a controlled environment. In these conditions several cell populations are recruited in response to the enhanced local release of chemo-attractant molecules (chemokines) that favor the infiltration of circulating leukocytes within a disease-target tissue. This phenomena is noted as chemotaxis and the chemical mediators (chemokine, citokine) recall the white cells from blood; the cells must go through different layers(blood vessel, extracellular matrix, epithelia) (12). The formation of chemical gradient (cytokine-chemokine) become an important motor for cell migration.
One of main factors regulating the chemokine-chemical gradient is the presence of an inflammatory status. Inflammation is a physiological process of response to tissue

injury. However, the dysregulation of the proper control of inflammation, induces a massive infiltration of leukocytes (neutrophils, monocytes, lymphocytes) within the target tissue as it occurs in gut, airways, skin, joints leading to chronic inflammatory response and tissue damage. Inflammation is also strictly linked to many events that favor cell motility, such as cytoskeleton rearrangement

In chronic inflammatory diseases at the mucosal sites the rules of cell migration are strictly dependent on disease pathogenesis as well as on the nature of the unwanted triggering event dictating the time-course and the type of the release of chemoattractants by the injured epithelia (13). In arways, bacterial challenge is a common "toxic" event which requires neutrophil recruitment. As a consequence, the release of IL8, a potent neutrophil chemoattractant, is required. The prototype of diseases in which an uncontrolled production of IL8 leads to a dysregulated neutrophil recruitment, is Cystic Fibrosis, a most common lethal genetic disorder in caucasians characterized by chronic inflammation and recurrent pulmonary bacterial infections.

These evidences highlight that the identification of factors that dysregulate the complex mechanism of motility is the key model to develop molecules able to regulate this factor in order to find putative biotechnological applications.

The choice of a suitable disease model for the study of potential factors involved in motility\interaction processes, must take in account that these mechanisms are a pathogenic element of disease and not only a bystander event. Understanding the specific pathways involved may lead to the identification of molecules able to modulate this biological process in human pathology.

During PhD project, different cellular models of these two main diseases have been used as model of study to understand the molecular mechanisms that influence inflammation-triggered cell movements : IB3 and C38 cell lines belonging to patients with Cystic Fibrosis and T84 cell line, a popular model of study of Coeliac Disease, a common intolerance to proteins of wheat. Both disease are characterized by a pro-inflammatory milieu with high level of tissue Transglutaminase (TG2), a multi-functions enzyme with multiple functions, as cross-linking of substrate protein, isomerase or G protein activity, with a defined role in several human pathologies (33).

Cystic fibrosis is caused by mutations of cystic fibrosis transmembrane regulator (CFTR), which functions as a chloride channel in epithelial membranes. More than 1000 mutations in CFTR gene have been identified and they can be grouped into six classes: (1) CFTR is not synthesized; (2) defective processing; (3) regulation; (4) conductance; (5) partial defective production or processing; or (6) defective regulation. The most common CFTR mutation belongs to class 2, and is caused by the deletion of phenylalanine at position 508 (F508del) of CFTR. The impaired chloride transport leads to water/volume depleted periciliary liquid with a increase of mucus viscosity . Bacteria invading the cystic fibrosis lung are trapped within this viscous mucus layer at the surface epithelial layer. As a consequence, recurrent pulmonary infections, principally by Pseudomonas Aeruginosa, colonization together with chronic inflammation are main features of CF lung pathology(14).

CF chronic inflammation is neutrophil-mediated, as circulating neutrophils are recruited within the airways and contribute to the extensive lung damage and to the development of impaired lung function. Accordingly, CF lung pathology is associated with a marked increase of proinflammatory cytokines, such as TNF-α, IL-6, IL-1β, IL-17 (15, 16), and the potent neutrophil chemoattractant and activator IL-8, which recruits large numbers of neutrophils into the airways.

However, conflicting results have been reported on whether CF airways undergo proinflammatory response in the absence of bacterial infections (17-19). Several studies have shown that both cytokine profile secretion and NF-κB activation are similar in CF and normal cells (20, 21). However, mounting evidences suggest that inflammation may occur before infection, and CFTR-defective cells have an intrinsically proinflammatory phenotype (22-24). Recently, it has been shown that CFTR is a negative regulator of NF-κB-mediated innate immune response, and its localization to lipid rafts is involved in control of inflammation (25).

The neutrophil involvement in CF chronic airway inflammation could suggest a development of a 3D motility model to study neutrophils migration under diffusive flux of IL8 and their containment upon identification of the main rules governing IL-8 production.

As chronic inflammation may represent a driving force of cell motility/migration, we could envisage several disease-related models of study, either 3D or 2D models. The study of cell migration in a given disease-related model could help in defining novel devices useful in validating several attracting mechanisms and related molecules with potential implicatrions in human therapy.

Among the others, another important pathological system with chronic inflammation is celiac disease and the analysis of interactions of alimentary peptides with the frontline gut epithelium is a useful model of study (a popular model of study is represented by the T84 cell lines).

Coeliac disease (CD) is a very common pathology that affects 1% of the general population, caused by the ingestion of gluten proteins,in susceptible individuals (26-28). Its strong associations with HLA class II (HLA DQ2 or DQ8) and a well-defined triggering antigen suggest that coeliac disease is a prototype of T-cell-mediated disease.(26). Evidence suggests that CD4(+) T cells are central in controlling the immune response to gluten that causes the immunopathology (29-31). The primary HLA association in the majority of CD patients is with DQ2 and in the minority of patients with DQ8. DQ2 or DQ8 are the predominant restriction elements for gluten-specific T cells. Lesion-derived T cells predominantly recognize deamidated gluten peptides. A number of distinct T cell epitopes within gluten exist. DQ2 and DQ8 bind the epitopes so that the glutamic acid residues created by deamidation are accommodated in pockets that have a preference for negatively charged side chains. Evidence indicates that deamidation in vivo is mediated by the enzyme tissue transglutaminase (TG2). This may result in the formation of complexes of gluten-TG2. These complexes may permit gluten-reactive T cells to provide help to TG2-specific B cells by a mechanism of intramolecular help, thereby explaining the occurrence of gluten-dependent TG2 autoantibodies that is a characteristic feature of active CD(27). Moreover it is well known that a co-operation between the innate and adaptive branches of the immune response are crucial in CD pathogenesis. Some gliadin peptides, which are not recognized by gliadin-specific T cells, are effective in activating the innate response either at epithelial or dendritic cell level. This innate activation is essential in setting the tone of the adaptive response, as the immunodominant peptides turn on toxic only if the gut mucosa has been primed by the so-called "innate" gliadin fractions (77). These peptides are able to induce profound epithelial changes in celiac mucosa as well as in models of CD, as T84 or Caco2 cell lines. Innate epithelial activation include phosphirylation of proteins, cytoskeleton riorganization and even IL-15-mediated apoptosis (77). The peptide p31-43 is the prototype of these peptides and it has been reported as also effective in inducing early TG2 activation.

A link between these two models of human diseases, CF and CD, the first monogenic, the second one multifactorial with a strong involvement of the immune response, is the presence of high tissue levels of the enzyme Tissue Transglutaminase (TG2) a protein with pleiotropic functions, as a consequence of the genetic defect in CF, or triggered by gliadin peptides in CD. In addition, both diseases show a chronic inflammatory phenotype, although neutrophil-mediated in CF and devoid of neutrophil component in CD. Finally in these two pathological conditions surface epithelial cells are key players in disease pathogenesis.
The epithelial cells are pivot in the innate immune activation in CD and cytoskeleton rearrangement is the earliest event in such a response to gliadin peptides; moreover cytoskeletal reorganization is a known factor of cell differentiation (32) . Therefore, CD offers an ideal opportunity to set up a 2D model of study of cell motility. In this study we have also developed a 2D motility model to test i) the effects of gliadin peptides in deranging cell motility and interaction in a 2D monolayer epithelial culture model and ii) to test the role of several modulatory molecules with potential therapeutic application.

AIMS

Cell migration is a very complex phenomenon that regulates the inflammatory response as well as several processes of cell biology and development. The identification of a specific regulatory pathway, offers a potential strategy to modulate many human pathology.

Understanding the mechanisms involved in cell motility and their putative modulation, is the first step in setting the new appropriate model of study.

Therefore, the PhD activity consisted of two main activities:

A) the study of the molecular mechanisms leading i) to release and modulation of major chemoattractant factors' (such as IL8) and their containment; ii) the effects of chronic inflammation in deranging cell-to-cell interaction and the putative mechanisms of control. To this aim two human disease models of chronic inflammation, Cystis Fibrosis with IL8-driven neutrophil-dominated chronic airway inflammation and iii) Celiac disease, the prototype of food induced activation of the mucosal immune response have been used.

B) the development of motility models: i) a 3D model of neutrophil migration in an IL-8-rich environment; ii) a 2D model of interaction of epithelial cells upon challenge with celiac disease-triggering peptide in presence or absence of putative modulator factors.

Both disease models are characterized by increased tissue levels of TG2 and chronic inflammation, as constitutive chronic airway inflammation characterizes Cystic Fibrosis, and gluten-triggered gut inflammation is a feature of Celiac Disease.

The first condition is characterized by a defective CFTR-driven pro-inflammatory environment mediated by increased levels of Reactive Oxygen Species (ROS) and high level of TG2, a pleiotropic enzyme involved in many pro-inflammatory conditions. In such a disease model the modulation of ROS-TG2 axis leads to restoration of cellular homeostasis with inhibition of IL-8 production. To understand the mechanisms of TG2 regulation, we use (i) classical and innovative technique of cellular and molecular biology in CF and control epithelial cell lines; ii) an "*ex vivo"* model of human nasal biopsies; iii) *"in vivo"* mice models of disease. These in vitro and in vivo approaches allow the identification of the link between defective CFTR and inflammation through the disregulation of TG2-ROS axis.

The second condition, Celiac Disease, allow the identification of the rules of TG2 upregulation upon challenge with specific gliadin-derived triggers. In such a condition the study revealed how the modulation of ROS-TG2 controls gliadin-induced mucosal inflammation.

To translate these results into an appropriate study model of motility for putative biotechnological applications, a 3D model for neutrophils migration assay has been set up. The 3D model is an ideal model to study the movements of cells in a 3D matrix of gel, where a diffusive flux of molecule induces migration.

Moreover a 2D model has been used to test whether controlling ROS-TG2 pathway might restore the derangement of cell-to-cell interaction and cytoskeleton reorganization taking place upon challenge of T84 intestinal epithelial cells with gliadin-derived peptides. The results highlight the feasibility of this model as a prototype to screen, in a very fast way, different molecules with potential therapeutic application.

RESULTS

The first part of PhD research program focused on the analysis of the molecular mechanisms responsible for the induction of the pro-inflammatory phenotype that characterizes Cystic Fibrosis airways, and the processes that regulate high TG2 levels.

Transglutaminase 2 (TG2) is an inducible transamidating acyltransferase that catalyzes Ca(2+)-dependent protein modifications. It acts as a G protein in transmembrane signalling and as a cell surface adhesion mediator, this distinguishes it from other members of the transglutaminase family (30). In mammals, nine distinct TGase isoenzymes have been identified at the genomic level; however, only six have so far been isolated and characterized at the protein level. All members of this superfamily possess a catalytic triad of Cys-His-Asp or Cys-His-Asn. Recent structural studies have described the regulatory mechanism of the transamidating activity for the TG2, but can be assumed to act in all the family members. The arrangement of the amino acids of the catalytic centre (Cys277, His 335 and Asp358) in a charge-relay catalytic triad, analogous to that of thiol proteinases such as papain, confers high reactivity on Cys277 to form thioesters with peptidylglutamine moieties in the protein substrate. This high reactivity, in the presence of Ca2þ, of Cys277 has been employed to develop a wide range of active-sitedirected irreversible inhibitors of the enzyme(34)

The sequence motifs and domains revealed in the recent TG2 structure, can each be assigned distinct cellular functions, including the regulation of cytoskeleton, cell adhesion and cell death. Ablation of TG2 in mice results in impaired wound healing, autoimmunity and diabetes, reflecting the number and variety of TG2 functions. An important role for the enzyme in the pathogenesis of coeliac disease, fibrosis and neurodegenerative disorders has also been demonstrated, making TG2 an important therapeutic target.

Understanding the mechanisms of migration and the identification of appropriate target of modulation of cell recruitment could allow wide industrial application in biotechnology.

1.The Inflammatory environment of Cystic Fibrosis

1.1.The up-regulation of TG2 in human CFTR-defective cells

To underpin the molecular link between a defected CFTR and the excessive inflammatory responses typical of CF airways, here we have studied CFTR-defective bronchial epithelial cell lines, IB3-1 human CF bronchial epithelial, (carrying F508del/W1282X CFTR mutation) and isogenic stably rescued C38 .

We demonstrated in CF airway epithelial cell lines and in human CF nasal biopsies increased levels of TG2.

We observed levels of TG2 protein in IB3 and C38 cells, that were analysed by Western Blot. The figure 1A shows high levels of TG2 (72 kDa) in IB3 compared to

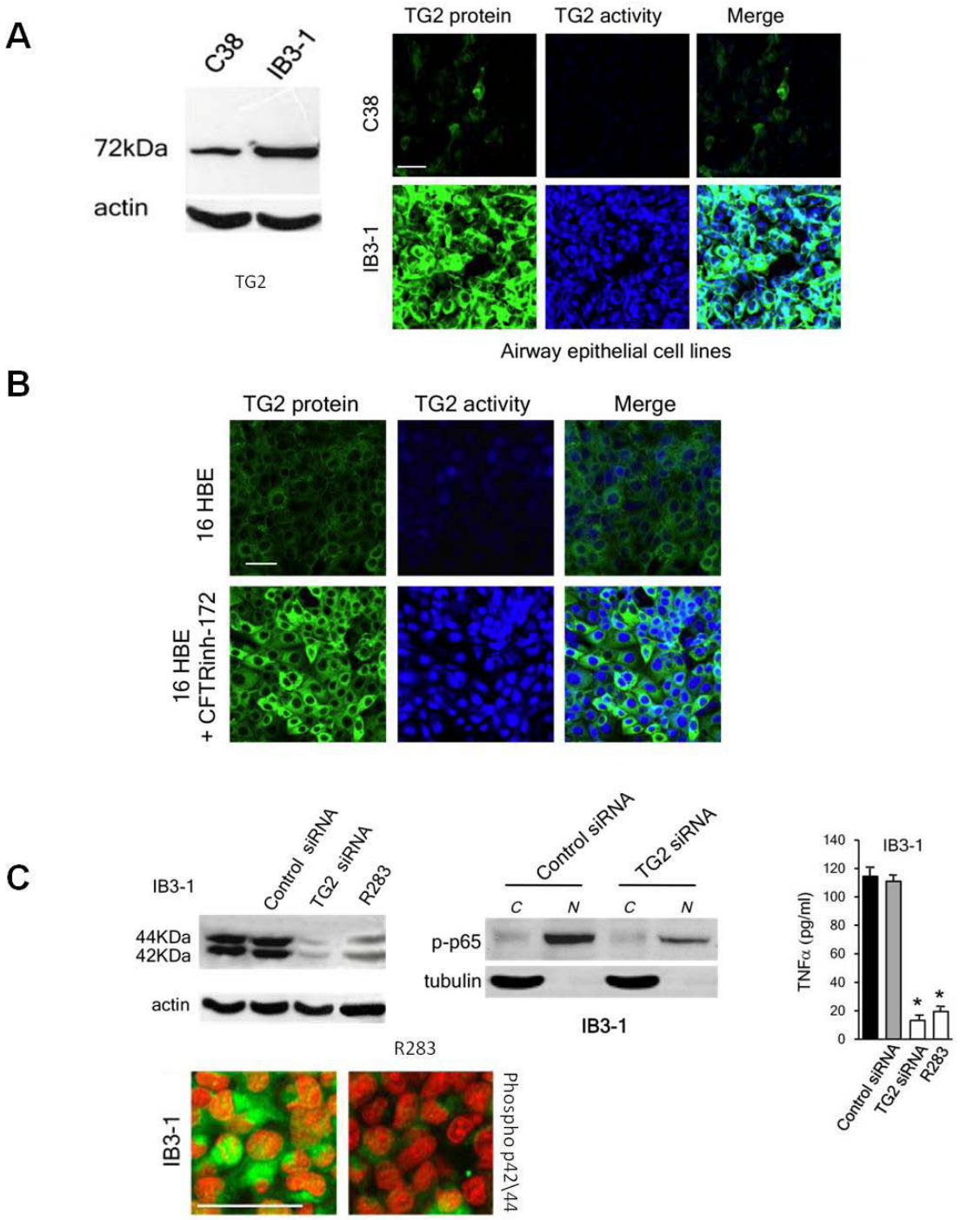

FIGURE 1. TG2 in CF cell line

C38. Therefore, we explored whether ,besides TG2 high levels, also its enzymatic activity were up-regulated in CFTR-defective cell lines. The confocal microscopy images reveled a significant increase of TG2 enzymatic activity in IB3 cell versus C38, upon incubation with biotinylated monodansylcadaverine (bio-MDC; Molecular Probes), a known molecule substrate of TG2 (Fig. 1A).
To assess that the pathway described to date was a direct consequence of CFTR dysfunction, we blocked the functional CFTR in the normal bronchial 16HBE cell line with the selective inhibitor $CFTR_{inh-172}$ (22). The enzymatic activity of TG2 and protein were high increased in presence of $CFTR_{inh-172}$ compared to control without inhibitor, as shown in confocal microscopy images in Fig. 1B.
These results clearly indicate that CFTR-defective epithelial cells are characterized by an intrinsic TG2 functional increase.
Exposure of the IB3-1 cells to the irreversible TG2-specific inhibitor R283 (a gift from M. Griffin, Aston University, Birmingham, U.K.) (35-37) as well as reversible inhibitor cystamine or gene silencing by TG specific siRNA, reveled that TG2 activity also influences other markers of inflammation. Inhibition of TG2 induced a significant reduction of the phosphorylated p42/p44 MAPKs, of the nuclear translocation of NF-κB and TNF-α release in IB3-1 cells(Fig.1C).

TG2 is therefore a master regulator of inflammation in CF airways and mediates the production of inflammatory cytokines and chemokines via targeting key regulatory pathways of inflammation.

1.2. SUMOylation of Tissue Transglutaminase

Because TG2 activity is also regulated by ROS (38) we tested whether ROS influenced the TG2-induced inflammation in CF. In agreement with previous reports, high levels of ROS were only detected in CF tissues and CFTR-defective cells (data not shown) (39). The IB3 cells were treated with ROS scavenger NAC (N-Acetil-Cysteine) or EUK 134 and analysis by confocal microscopy and ELISA assay shown a significantly reduction of TG2 protein and activity, p42/44 phosphorylation (data not shown), and TNF-a release (Fig. 2A) in both CF tissues and IB3-1 cells. The inhibitor $CFTR_{inh-172}$ in 16_HBE normal bronchial cell lines reveled an increase of intracellular ROS (Fig. 2B) and increase of p42/44 phosphorylation.
Altogether, these results clearly demonstrated how pro-oxidative environment influences TG persistence and CFTR disruption directly leads to the development of airway inflammation in CF.
TG2 is regulated by retinoids, steroid hormones, peptide growth factors and cytokines that also lead to a time-dependent decrease in TG2 ubiquitination (40). This indicates that posttranslational control mechanisms may regulate TG2 tissue levels in CF airways. We focused on small ubiquitin like-modifier (SUMO) post-translational modification since this has been defined as a central way of regulating key cellular functions and stability of proteins (41,42). SUMOylation has been defined as a key player of the post-translational network to regulate key cellular functions including transcription, nuclear translocation, stress response and chromatin structure as well as of diversifying localization and even stability of the modified proteins (41,42). Sumoylation is accomplished via an enzymatic cascade involving, among the others, E3 ligases, that catalyze the transfer of SUMO from the

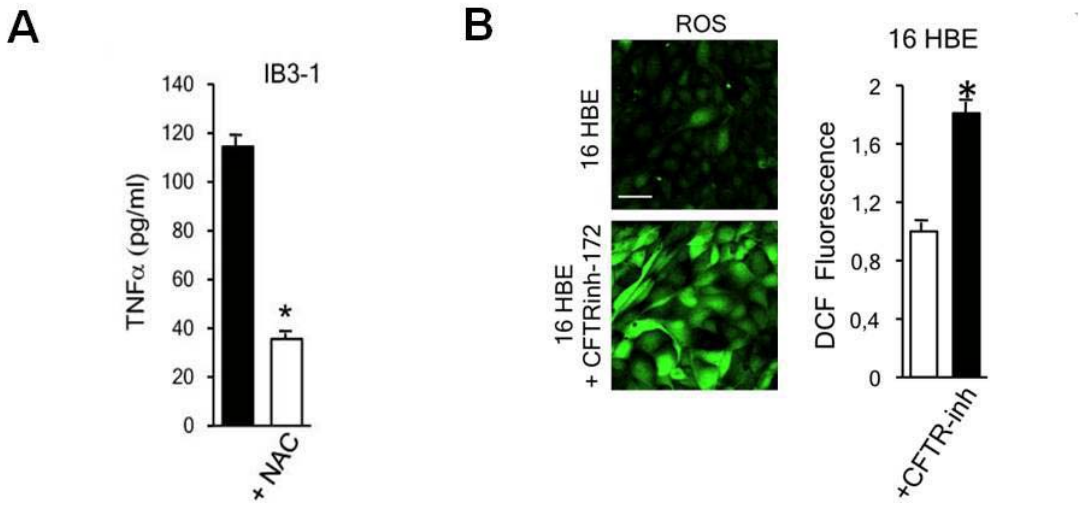

FIGURE 2. CFTR inhibition induces airways inflammation

conjugating enzyme UBC9 to a substrate (41). E3 ligases have gained a central role in the SUMO machinery, since they regulate sumoylation in response to different stresses (41).

To investigate whether posttranslational modifications could result in the persistence of high levels of TG2 protein, the protein extract of IB3-1 and C38 cells were analyzed by Western blots and revealed that SUMO-1 protein level was increased in IB3-1 cells as compared with C38 cell lines (Fig. 3A). Sequence analysis and SUMO motif screening revealed three SUMO acceptor sites (ψ_kxE) (42) in TG2 sequence. The experiments of figure 3A shows, also, that when TG2 immunoprecipitates from IB3-1 cells were probed with the anti-TG2 Antibody, two TG2 bands were detected, with the upper band corresponding to the SUMOylated TG2.

Since Protein Inhibitor of Activated STAT (PIAS)y, a member of the PIAS family (43), has recently been defined as the first SUMO ligase for NF-kB essential modulator (NEMO) (43) and PIASy-NEMO interaction is mediated by Reactive Oxygen Species (ROS) (43), we also investigated whether PIASy-TG2 interaction could mediate ROS-driven post-translational modifications of TG2.

To investigate whether PIASy could mediate TG2 SUMOylation, we performed experiment of Immunoprecipitation of PIASy and TG2 in IB3-1 cells .

IB3 cells were treated or not with virus infection of human manganese superoxide dismutase (MnSOD) to regulate the pro-oxidative environment of cell. The IP analysis underline a direct interaction between PIASy and TG2 shown with band corresponding to reciprocal antibodies of IP, with a strong decrease of interaction in presence of MnSOD; as well as PIASy-TG2 interaction also TG2 Sumoylation is decreased upon MnSOD infection (Fig 3B). The western blot analysis of SUMO, TG2, PIASy evidenced the reduction of level with MnSOD(Fig.3C).

The data of experiments indicate that in CF airway epithelia the pro-oxidative

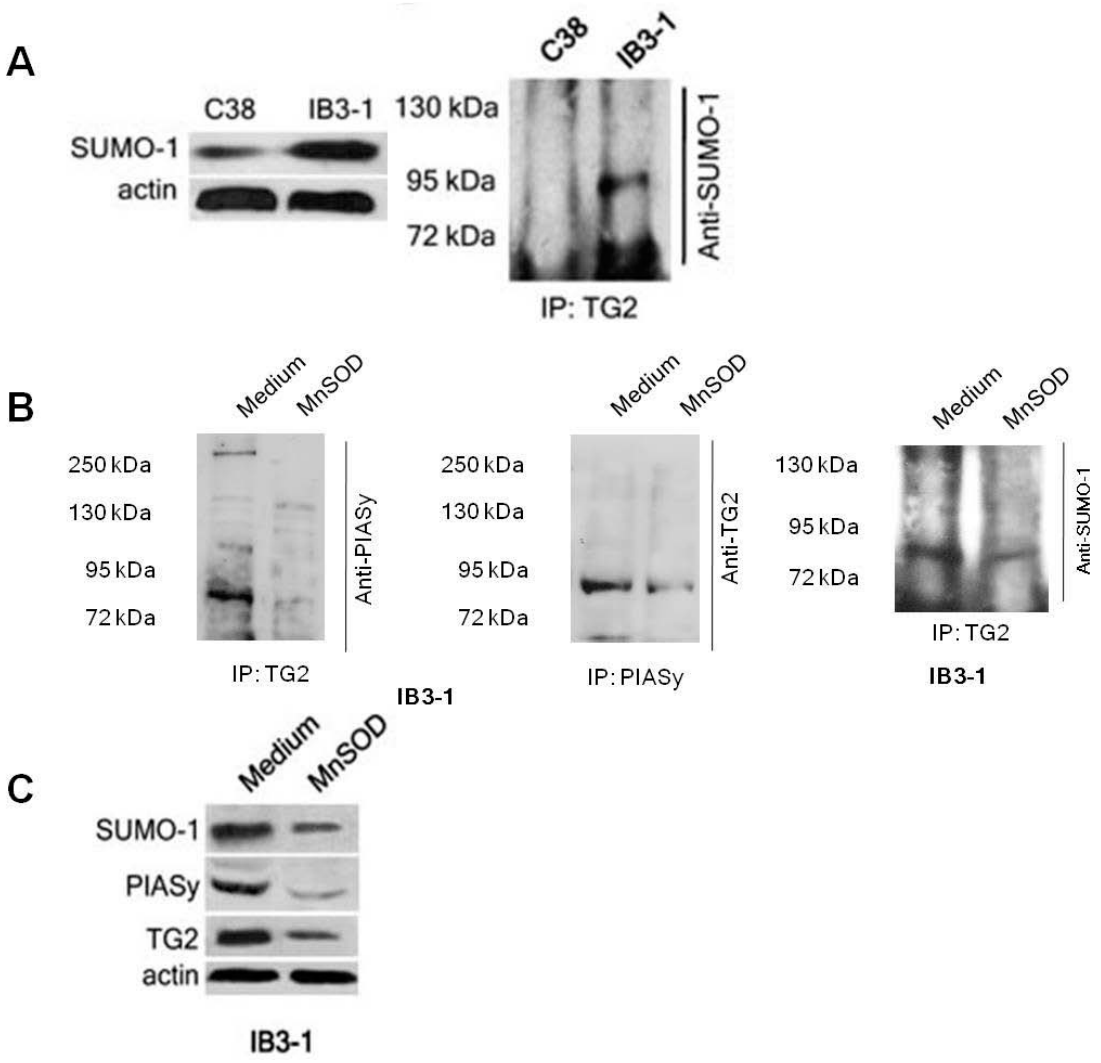

FIGURE 3. PIASy mediates TG2 SUMOylation in CF airway epithelial cells

intracellular milieu leads to PIASy-mediated TG2 sumoylation.
SUMOylation influence ubiquitination since these two main posttranslational changes may compete each other for the same lysine residues on the aminoacid sequence. SUMOylation may induce protein stabilization by blocking ubiquitination of the same lysine residues (44).
We performed experiments of SUMO or PIASy gene silencing. IP studies revealed an increase of TG2 ubiquitination upon proteasome inhibition by MG132 (Fig.4A,B), thus allowing TG2 to be targeted to proteasome for degradation. This induced decreases of TG2 protein (Fig. 4C) and activity.
Therefore, oxidative stress increases PIASy protein levels and favors TG2 SUMOylation that leads to the persistence of high TG2 tissue levels by downregulating TG2 ubiquitination and proteasome degradation.

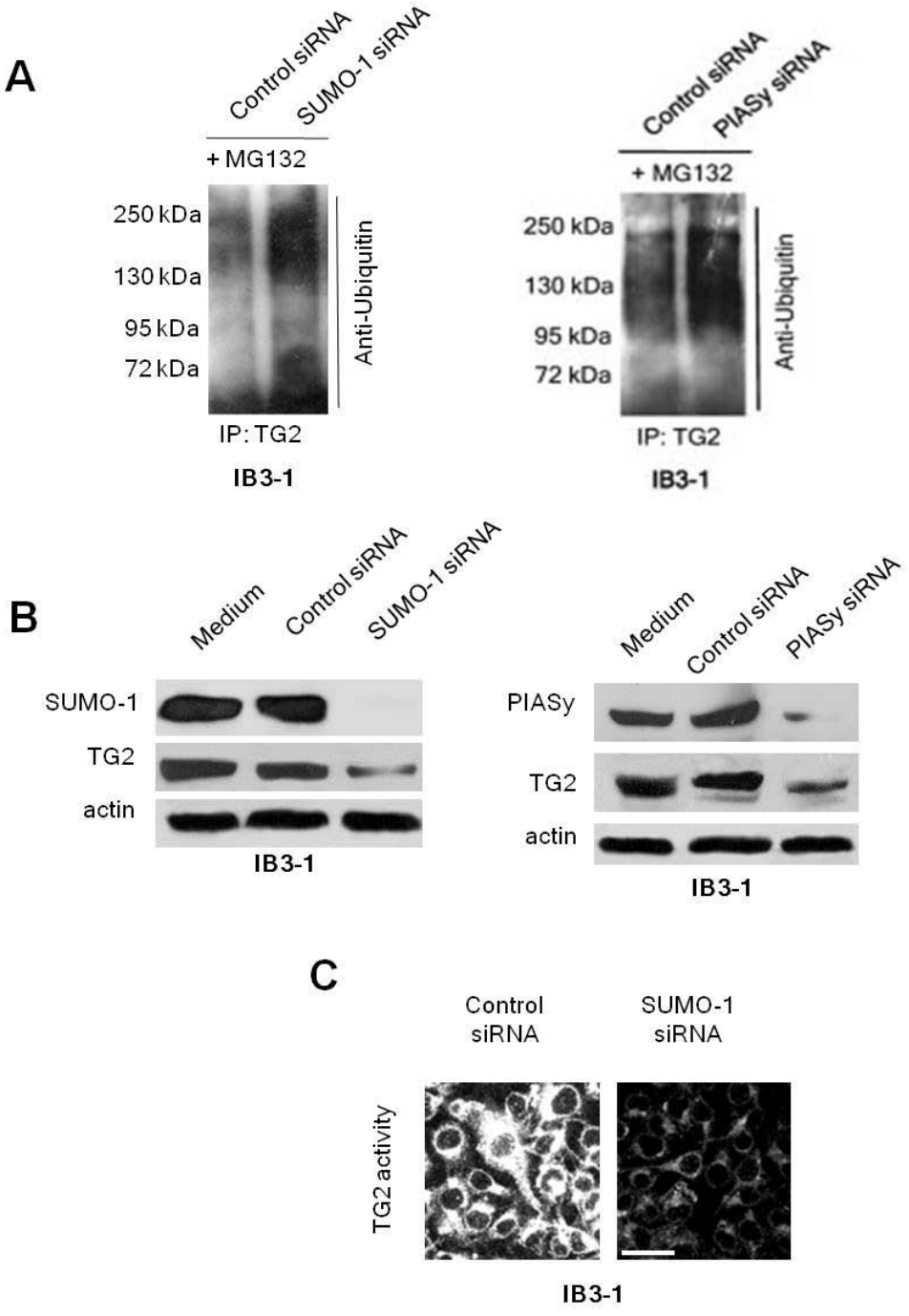

FIGURE 4. Decrease of TG2 protein levels and TG2 activity by either SUMO or PIASy gene silencing

TG2 SUMOylation might provide the missing link between cellular stress and inflammation. We investigated whether the control of TG2 SUMOylation might modulate TG2-driven inflammation (24). The figure 5 demonstrated that gene silencing of either PIASy or SUMO by specific siRNAs induced a significant decrease of p42\44 phosphorylation(Fig.5A) and TNF-α release (Fig. 5*B*) in IB3-1 cells.

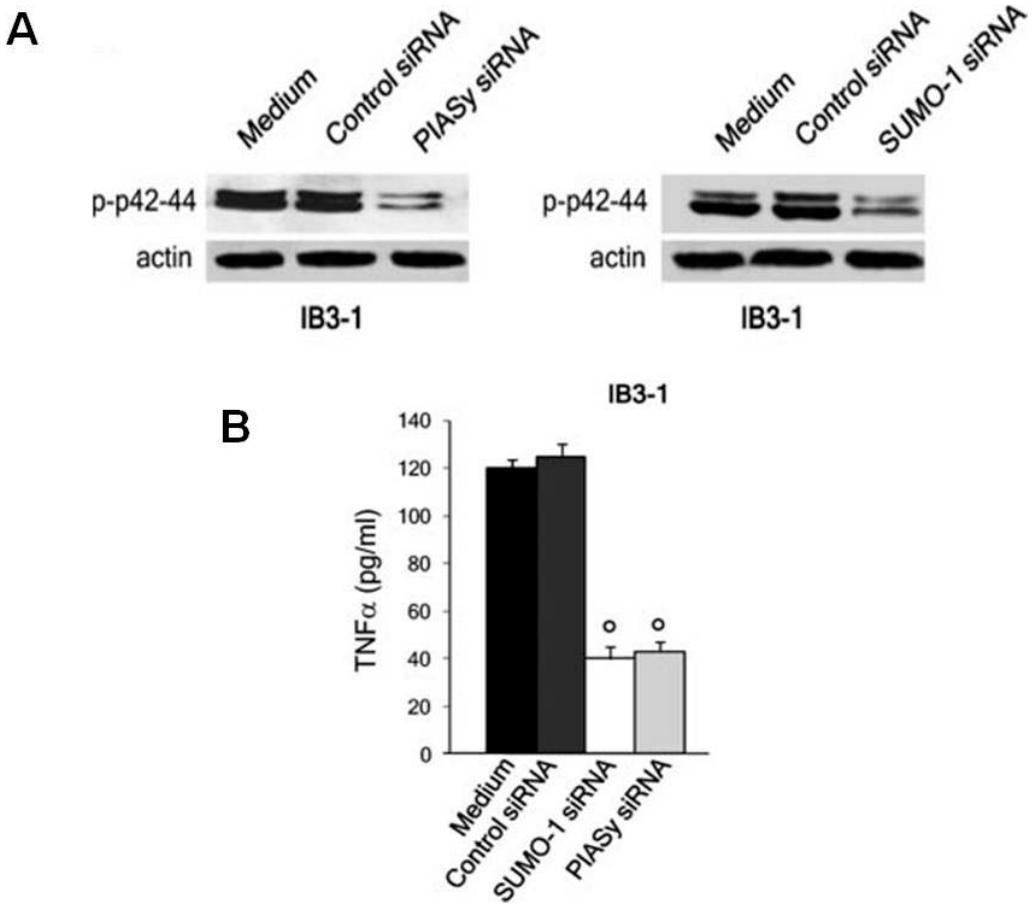

FIGURE 5. SUMO-1 or PIASy gene silencing control inflammation in CF airway epithelial cells

1.3.Imapct of TG2 persistence in CF epithelia

The data underline that CF environment ROS-mediated leads to a persistence of TG2 with strong pro-inflammatory effects and increase of citochine release sucs as TNFα and IL8.
To identify a more effective way to antagonize this pro-inflammatory pathway CFTR-driven, we studied the effect of TG2 persistence in CF epithelia.
TG2 is an enzyme with a vast array of biological functions that mainly catalyzes cross-links or deamidation of target proteins in the presence of high Ca^{2+} levels.
Previously, we shown high TG2 protein level in IB3 cell lines compared to low livel in C38. In these data we demonstrated low levels of 55 kDa Peroxisome Proliferator-Activated Receptor gamma (PPARγ), (Fig 6A) a nuclear hormone receptor expressed in monocytes, macrophages and epithelial cells that negatively regulates inflammatory gene expression by "transrepressing" inflammatory responses (45.).
To unravel the putative link between TG2 and PPARγ, we then performed experiment of Immunoprecipitation (IP) of protein lysates of IB3 vs C38 cell line The IP analysis underline a direct interaction between PPARγ and TG2 shown with band corresponding to reciprocal antibodies of IP, with a strong decrease of interaction in presence of TG2 inhibitor (data not shown).
We, then tested the hypothesis that TG2 might induce posttranslational modifications (cross-linking) of PPARγ in CFTR-defective cells, because the QP and QXXP motifs in the PPARγ sequence could be recognized as specfic sites for TG2 activity (40)
We demonstrated that in IB3 cell TG2 catalizes crosslinking and ubiquitination of PPARγ. After IP of PPARγ, the membrane was blotted for Nε(γ-L-glutamyl)-L-lysine isopeptide antibody that reveled the specific bound between TG2 and target protein. The figure 6A shows high molecular weight corresponding to modification induced by TG2 (130-250 kDa). Exposure of the IB3-1 cells to the irreversible TG2-specific inhibitor R283 or silencing of TG2, induced a significant reduction of high molecular mass PPARγ ,TG2-induced (Fig. 6B) and a significant increase of the normal 55 -kDa PPARγ in the IB3-1 cells (Fig. 6B). This indicated that the crosslinked PPARy was due to increased TG2 activity.

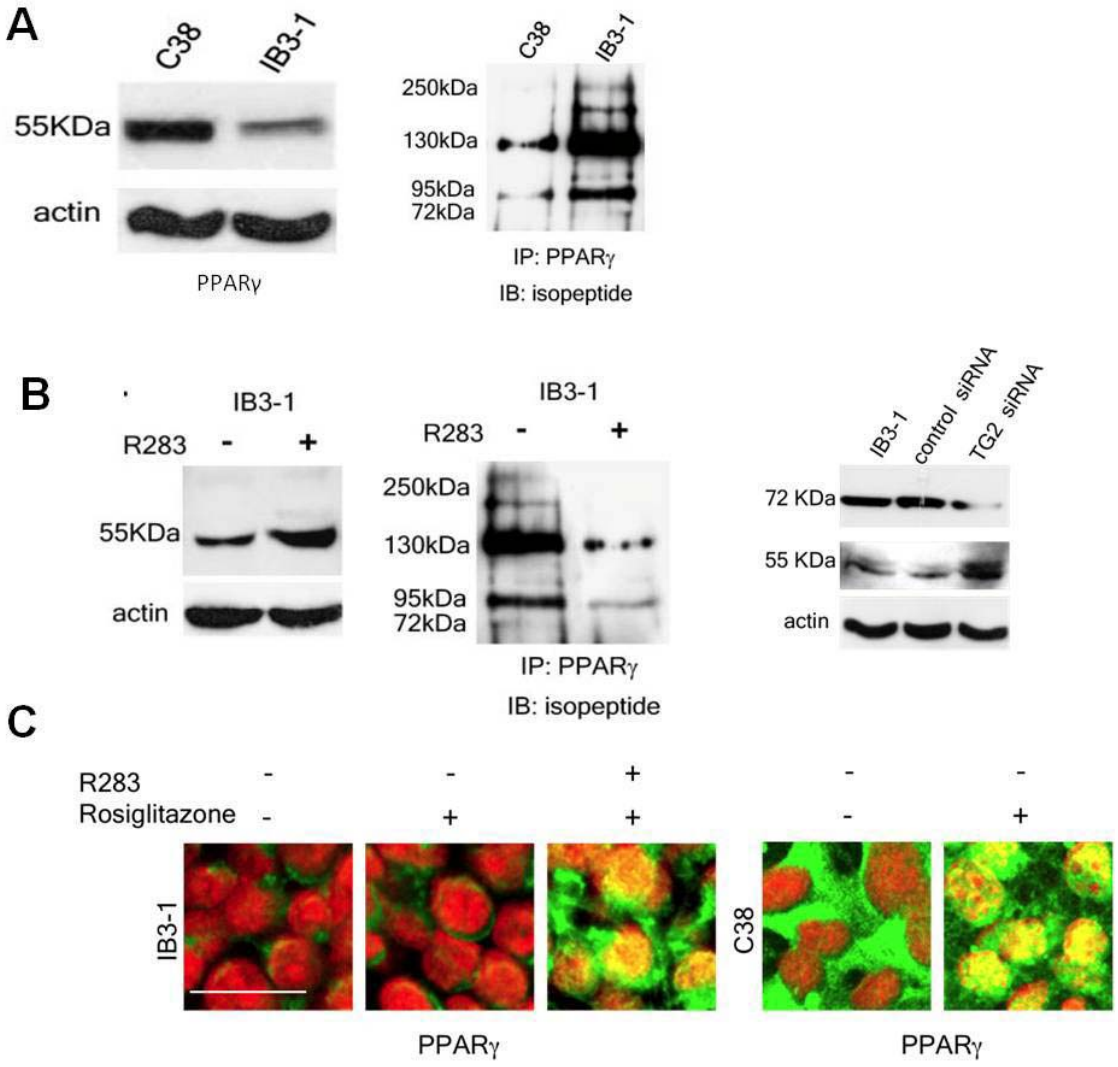

FIGURE 6. Effects of TG2 on PPARϒ protein expression and localization

In IB3-1 cells, PPARϒ nuclear translocation was promoted only by R283, whereas rosiglitazone, a PPARϒ agonist with potent antiinflammatory activity used in clinic (46), induced only a marginal nuclear PPARϒ increase (Fig. 6C). In contrast, rosiglitazone alone was able to induce an impressive PPARϒ nuclear translocation in C38 cells (Fig. 6C).

These results indicate that crosslinking of PPARϒ by TG2 in CFTR-defective cells flavored a pro-inflammatory environment.

As previously described, TG2 SUMOylation may have great relevance in driving CF inflammatory phenotype and release of pro-inflammatory cytokines and chemoattractants. PPARϒ which may be targeted by TG2 to crosslinking, may also be targeted by SUMO-1 and undergo sumoylation in response to a PPARϒ agonists, such as Rosiglitazone (47). Sumoylated PPARϒ interacts with the nuclear-receptor co-repressor (N-CoR)-histone deacetylase 3 (HDAC3) complex and thereby blocks its ubiquitination, thus maintaining a repressor condition (47).
This study shows that sustained TG2 activation inhibits PPARϒ SUMOylation and its interaction with the N-CoR (47) thus favoring inflammation. Moreover TG2 induces crosslinking and degradation of Ik-Bα, a known TG2 substrate (48) and a negative regulator of NF-kB activation, inhibits Ik-Bα SUMOylation and favors NF-kB activation (Figure 7).
Immuprecipitation experiments shown an increased PPARϒ sumoylation (Fig.7A) , blocking TG2 through specific gene silencing or with specific inhibitor cystamine , in response to rosiglitazone (agonist of PPARϒ) in IB3 cell line, ; confocal microscopy images shown an enhanced N-CoR protein and its nuclear localization (Fig. 7*B*), and favored N-CoR- PPARϒ interaction (data not shown). Moreover siRNA of TG2 or cystamine induced increase of Ik-Bα sumoylation and its protein level.(fig. 7C).
TG2 SUMOylation may therefore switch off the intracellular regulatory machinery, preventing PPARy SUMOylation, IkBa stabilization, and leading to an uncontrolled inflammatory response.

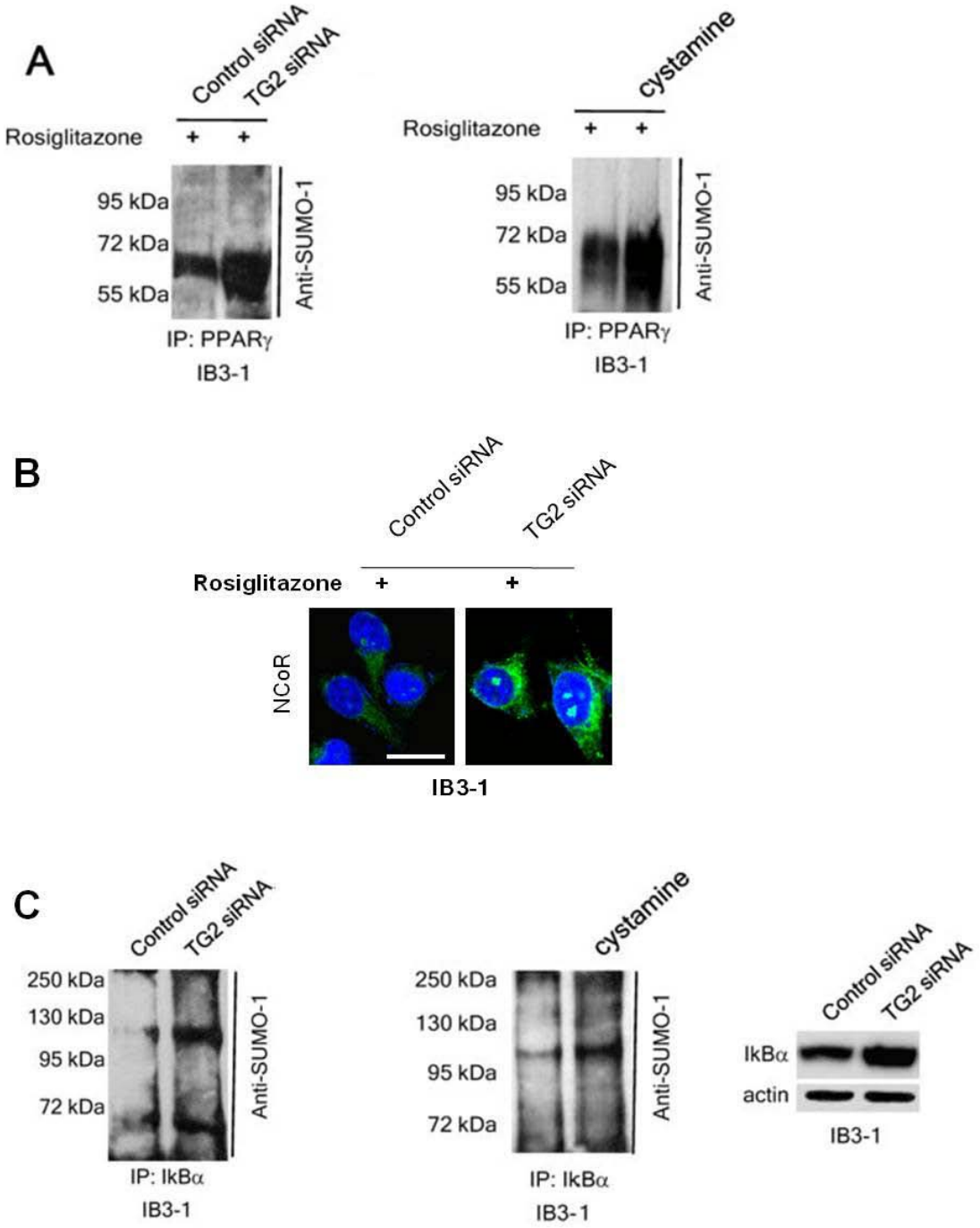

FIGURE 7. TG2 inhibition modulates PPARγ and IkBα pathways in CF airway epithelia.

1.4. *Aggresome: a feature of CF epithelia*

To test whether persistence of PPARγ due to TG2-crosslinkin influenced its proteasome degradation, we performed immuprecipitation of PPARγ upon treatments with MG132 (chemical inhibitor of proteasome), and reveled for Ubiquitin. The figure 8A shows that IB3 cell after treatments with MG132 increased PPARγ protein level and its ubiquitination and microscopy images evidenced that it was mainly limited to perinuclear localization in CFTR-defective IB3-1 cell line .
This perinuclear localization was suggestive of aggresomes, a specific cellular response against accumulation of ubiquitinated misfolded and/or aggregated proteins, which might also result from impaired proteasome function (49). Although aggresomes containing PPARγ have not been described before, aggresomes containing ubiquitinated misfolded MF508 CFTR molecules have been previously observed as result of overexpression of the defective CFTR (49). The aggresomes of CFTR also contain HDAC6, a microtubule-associated deacetylase that interacts with ubiquitin and stabilizes polyubiquitin chains (50). We have shown by confocal microscopy images that in the CFTR-defective IB3-1 cell line, the perinuclear aggregates of PPARγ also colocalize with both HDAC6 and ubiquitin (Fig. 8B); inhibition of proteasome by MG132 increased this colocalization and the level of HDAC6 and Ubiquitin (Fig.8B). The data thus demonstrated the aggresome nature of these aggregates.

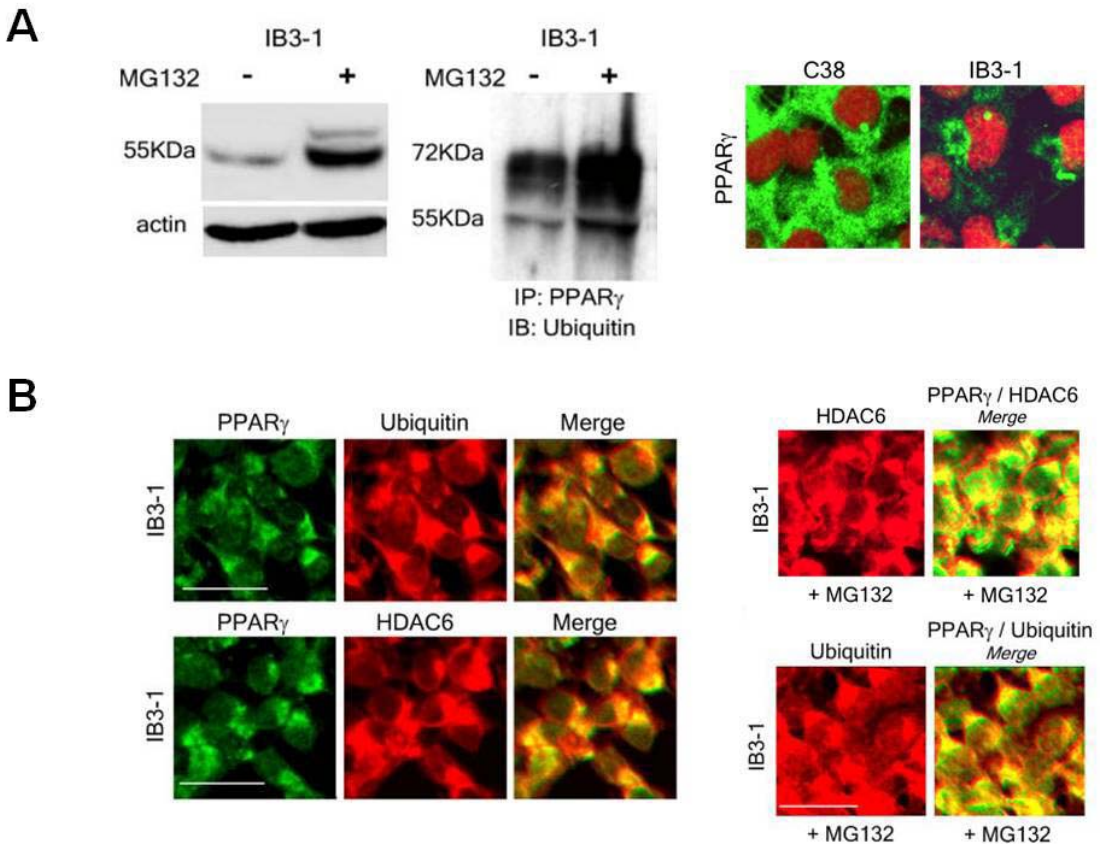

FIGURE 8. Aggresome: a feature of CF epithelia

1.5. Aggresome and autophagy

In previous data we described the presence of peroxisome proliferator activated receptor (PPAR)-ɤ in aggresomes in CF airways (24), and the mutant CFTRF508del has been described as the prototype of a misfolded aggresome-prone protein (51-53) Sequestration of the anti-inflammatory PPAR-ɤ into aggresomes, mediated by the increased TG2 levels, contributes to the lung inflammation in CF (54). This is the result of ROS-mediated TG2 SUMOylation inducing the crosslinking, ubiquitylation and aggresome sequestration of several target proteins (54). Because oxidative stress and accumulation of protein aggregates are features of CF airway epithelia (24,54,55), we speculated that the accumulation of aggresomes in CF is due to defective autophagy.

Autophagy is a cytoprotective mechanism for the degradation of misfolded/ polyubiquitylated proteins and damaged organelles through lysosome mediated self-digestion (56,57).

Autophagy is important in clearing protein aggregates after overload of polyubiquitylated proteins (58,59). Here we demonstrate how defective CFTR drives autophagy inhibition in mouse and human CF airway epithelia by means of the ROS–TG2 pathway, with sequestration of beclin 1 interactome, a key player of autophagosome formation (60-62), in the aggresomes. Rescuing beclin 1 and autophagy restores CFTR trafficking and damps down inflammation.

We cultured human CF airway epithelial IB3-1 or CFBE41o- cells(F508del/F508del), C38, or bronchial epithelial 16HBE14o-cells under nutrient starvation to stimulate autophagy (63,64).

In first analysis we observed, through transmission electron microscopy, the presence of autophagosomes containing mitochondria and cellular organelles in C38 but rarely in IB3-1 cells (Fig. 9A). The western blot analysis shown the accumulation of LC3, a marker of autophagosomes (64) in IB3 and C38 cells line. Increase of LC3 II, the lipidated product of LC3 (63,64), was observed in C38 but not in IB3-1 cells under starvation (Fig. 9B). E64d and pepstatin A, inhibitors of the lysosomal proteases (Fig. 9C), as well as chloroquine, a weak base disrupting lysosomal functions failed to increase LC3-II, thus indicating that reduced LC3 II levels were not due to LC3 lysosomal degradation. Defective autophagy in IB3-1 cells was also revealed by the increased pool of polyubiquitinated proteins, and accumulation of p62 (Fig. 9C,D), a LC3- and ubiquitin-binding protein, that accumulates in intracellular aggregates under defective autophagy (63,64). IB3-1 cells were also resistant to rapamycin, a known autophagy inducer (63,64).

Real-time PCR analysis of several autophagy-related genes(64,65), *ULK1, ULK2, ATG5, ATG6* (beclin 1), *ATG7, ATG14, Bcl-2*, vacuolar protein sorting (*hVps)34*, regulatory myrisoylated kinase *hVps15* and *Ambra1* did not reveal reduced mRNA expression levels in IB3-1 and CFBE41o- as compared to C38 and 16HBE14o-cells(Fig.10A).

Growing evidences indicate that beclin 1, a tumor suppressor gene (60,61), interacts with the class III PI3K, hVps34 (65,66) and ER associated class III PI3K activity is crucial in the initiation of autophagosome formation (67,68). Moreover the dissociation of beclin 1 from Bcl-2 promotes autophagy during stress conditions, such as starvation (67-70).

PI3K core complex binds either to Atg14L or UV-irradiation-resistance-associated gene (UVRAG) (65,71), involved in distinct functional complexes driving either

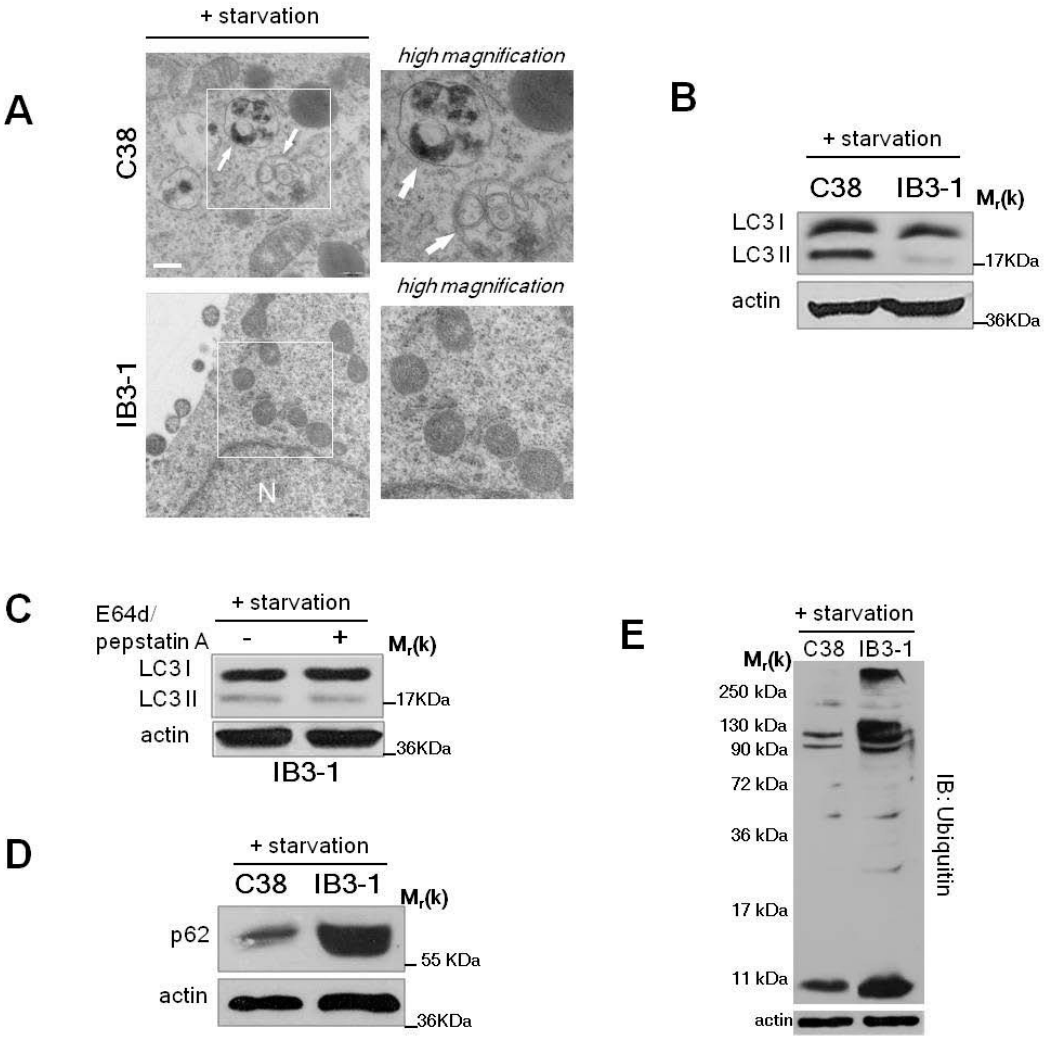

FIGURE 9. Autophagy is defective in human and mice CF airway epithelia

autophagy or endosome-to-Golgi retrograde trafficking (71), and Atg14L appears to divert hVps/Class III PI3K into an autophagic role (71)

We preformed immunoprecipitation of beclin 1 in IB3-1 and C38 cells with or without starvation and reduced Bcl-2 immunoreactivity was observed in IB3-1 with starvation compared to nutrient condition; hVps34, hVps15, Ambra1 and Atg14L immunoreactivities were detected in beclin 1 immunoprecipitates from C38 but also IB3-1 cells and increased upon starvation, thus suggesting an intracellular environment favourable to autophagy induction (Fig.10B). Reduced protein levels of beclin 1, hVps34, hVps15, Ambra1 and Atg14L (Fig.10B), as well as of UVRAG (data not shown), were observed in IB3-1 cells. Western blots of the insoluble protein fraction revealed increased beclin 1 in IB3-1 as compared to C38 cells, this suggesting retention of beclin 1 as an insoluble protein within aggregates in CF epithelia (Fig.10C). Interestingly, hVps34 (Fig. 10D), beclin 1 and the other beclin 1 interacting proteins (data not shown) colocalized with the ER marker calnexin in C38 but not in IB3-1 cells. In CF cells beclin 1 and beclin 1 interacting proteins, are sequestered in perinuclear aggregates, where they co-localized with the aggresome marker HDAC6 (50) (Fig. 10D). The results indicated an essential role of Beclin 1 in autophagy machinery due to aggresome formation.

To test the role of Beclin 1, we overexpressed beclin 1 in IB3-1 cells. HA-tagged beclin induced increased LC3 II and reduced p62 accumulation (Fig. 11A) and increase of autophagosome formation (Fig. 11A); moreover, HA-beclin was detected at the ER level (Fig. 11B, top panel) and restored co-localization of hVps34 (Fig. 11B, bottom panel), hVps15, Ambra1, and Atg14L (data not shown) with calnexin

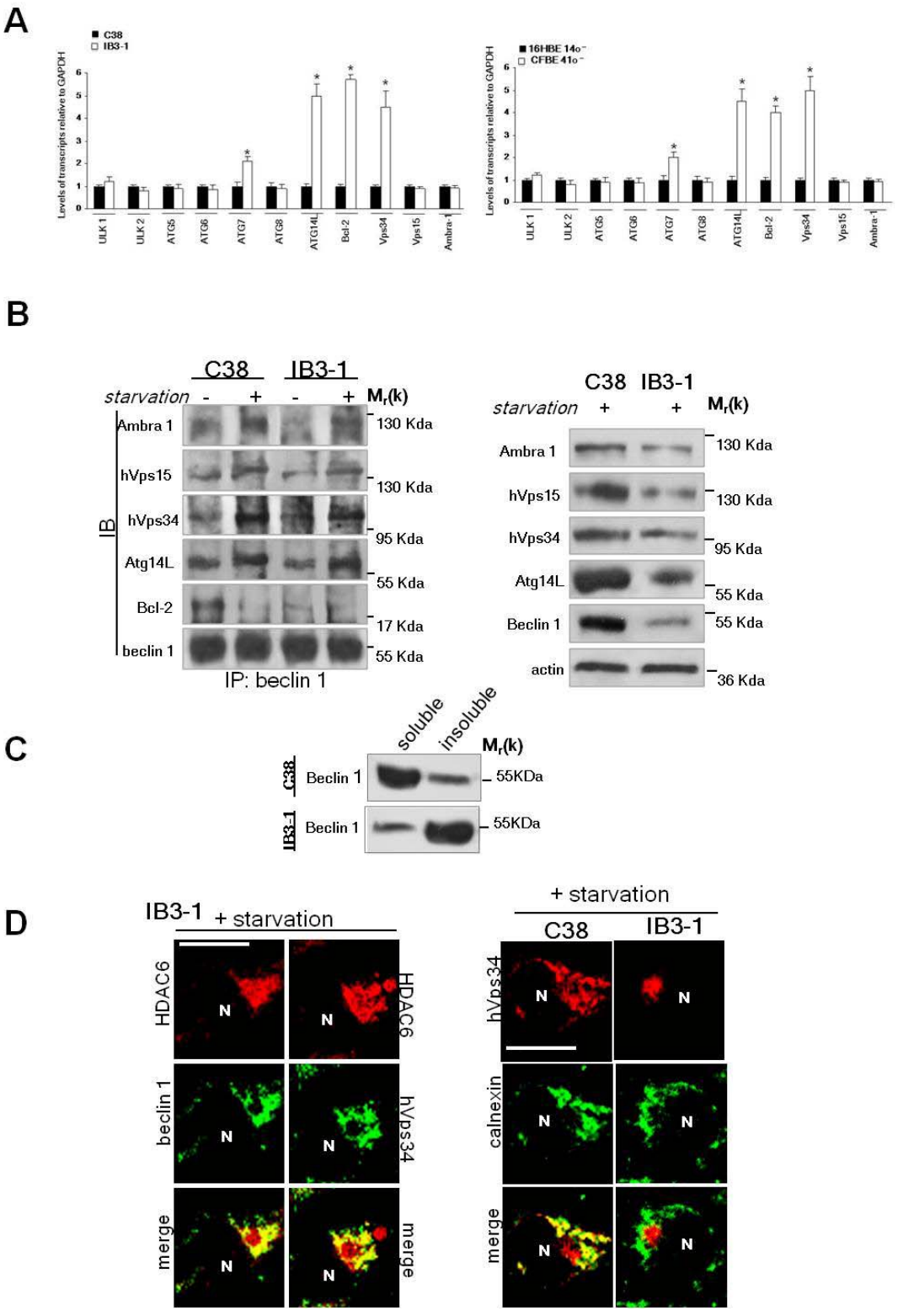

FIGURE 10. Sequestration of beclin 1 interactome in aggresomes drives defective autophagy in CF airway epithelia

.

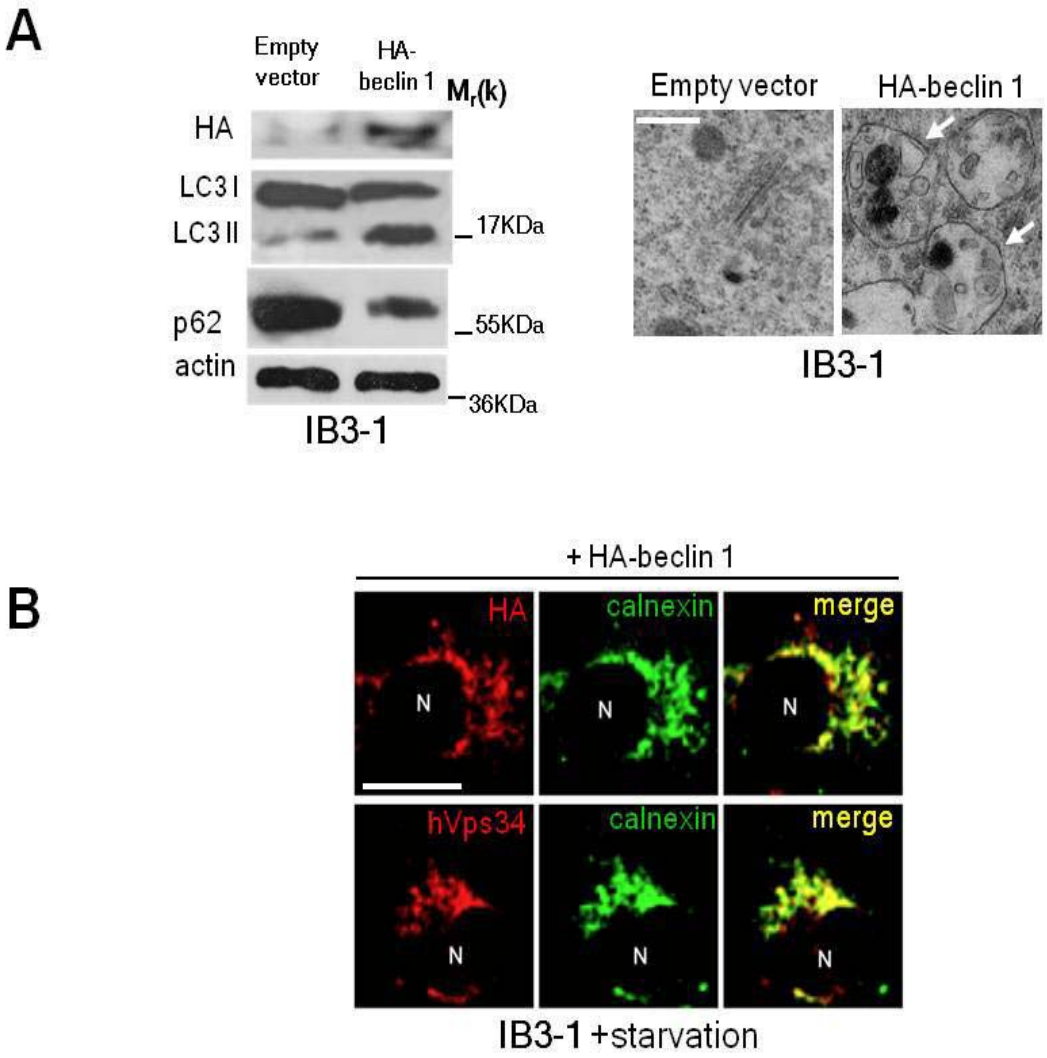

FIGURE 11. Effect of Beclin 1 overexpression

These findings suggest post-transcriptional regulation of beclin 1 expression in CF airways. Since beclin 1 protein sequence contains QP and QXXP motifs, specific target sites for TG2 activity (40), we tested the hypothesis that beclin 1 might undergo TG2-mediated cross-linking and in Beclin 1 immunoprecipitates from IB3-1 cells we observed positive isopeptide immnureactivity that were reduced upon TG2 knock down as well as by the TG2 inhibitor cystamine (40) (Fig.12A) or the calcium chelator BAPTA-AM (24,54). TG2 siRNA or cystamine restored the soluble forms of beclin 1 and beclin 1 interactor proteins (Fig. 12B) and reduced also, beclin 1/HDAC6 co-localization and aggresome sequestration (Fig. 12B). These results indicate that TG2-mediated cross-linking drives defective autophagy in CF epithelial cells.
Because increased ROS sustain high TG2 levels via PIASy-mediated TG2 SUMOylation (54), we incubated IB3-1 cells with EUK-134 (54) and we observed reduced beclin 1 cross-linking and aggresome sequestration (data not shown), autophagosome formation (Fig. 12C), and beclin 1 upregulation 4 or knocked down PIASy (Fig. 12C). CFTR knock down in autophagy-competent C38 cells reduced beclin 1 and LC3 II protein, and p62 (Fig. 12D). These effects were prevented by cystamine as well as by EUK-134 (Fig. 12D) or NAC (data not shown)These results indicate that ROS-mediated TG2 SUMOylation is responsible for defective autophagy in CF epithelia.

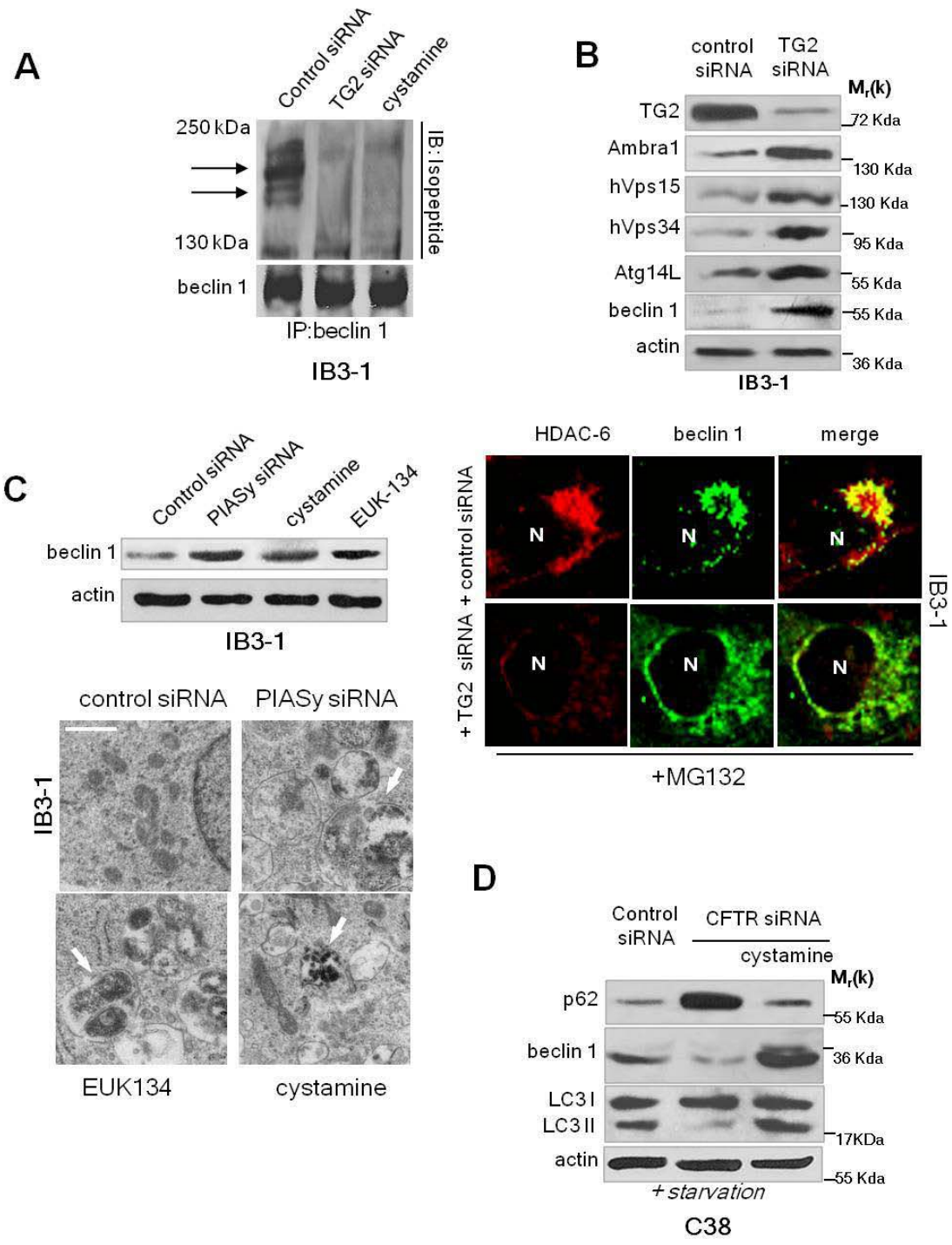

FIGURE 12. TG2-mediated crosslinking of beclin 1 induces aggresome sequestration of beclin 1 interactome and drives defective autophagy in CF airway epithelial cells

These results indicate that defective CFTR plays a pivotal role in driving beclin 1 downregulation and defective autophagy in CF airways via ROS-TG2 pathway.
Next, we investigated whether defective autophagy might play a role in CF inflammation. HA-tagged-beclin 1 rescued pro-inflammatory phenotype of IB3-1 cells as it reduced p42-44 phosphorylation (Fig. 13A), increased 55 kDa PPARγ protein (Fig. 13A), and reduced TNF-α secretion in medium ($p<0.01$) (Fig. 13A). We also investigated whether defective autophagy might in turn sustain TG2 activation. HA-beclin 1 decreased ROS ($p<0.01$) and TG2 SUMOylation (data not shown), PIASy and TG2 proteins (Fig. 13A). Since targeting TG2 restores inflammation in human and mice CF airways, we investigated whether these effects were mediated by rescue of autophagy. The effects of cystamine or antioxidants (data not shown) in controlling p42-44 phosphorylation, and TNF-α secretion (Fig. 13B) were neutralized upon beclin 1 knock down. This indicates that rescue of beclin 1 and autophagy mediates the effects of cystamine and antioxidant molecules in CF epithelia.
These results indicate that targeting ROS-TG2 axis ameliorates human and mouse CF airway phenotype by restoring beclin 1 and autophagy.

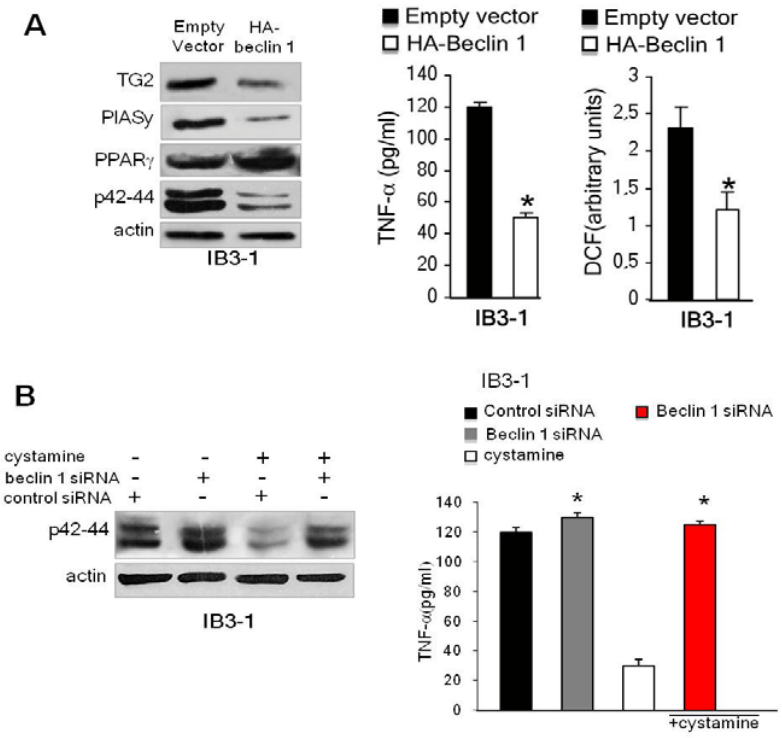

FIGURE 13. Restoring beclin 1 and autophagy rescues CF phenotype in IB3-1 cells.

1.6.In vivo model

The data described above in CFTR-mutated cell line or normal given a strong concept that in CF induced an activation of ROS-TG2 axis that leads to a pro-inflammatory environment. To demonstrate the importance of this pathway in CF, we used others two biological model: ex vivo human nasal polyp mucose and mice model of CF disease.
The first one was the more representative model of human pathology since give a correlation between pathological phenotype and genotype of patient considering the thousand known mutation (divided in six classes). The mice model were the fundamental approaches for therapeutic valence of study.
The data of TG2 high protein level and activity on nasal polyp was shown by confocal microscopy in fig.14A, and the effects of inhibition of TG2 on inflammatory target, p42\44 and Tyr phosphorilation, was shown in fig. 14B. The fig.14C shown the PPARϒ level in control and CF nasal polyp and the effect of R283 (fig 14C).
To investigate whether TG2-PIASy interaction and TG2 SUMOylation may take place in human airways of CF patients and whether it was induced by the oxidative stress, we used a well established tissue culture model of biopsies of human CF nasal polyps (72).

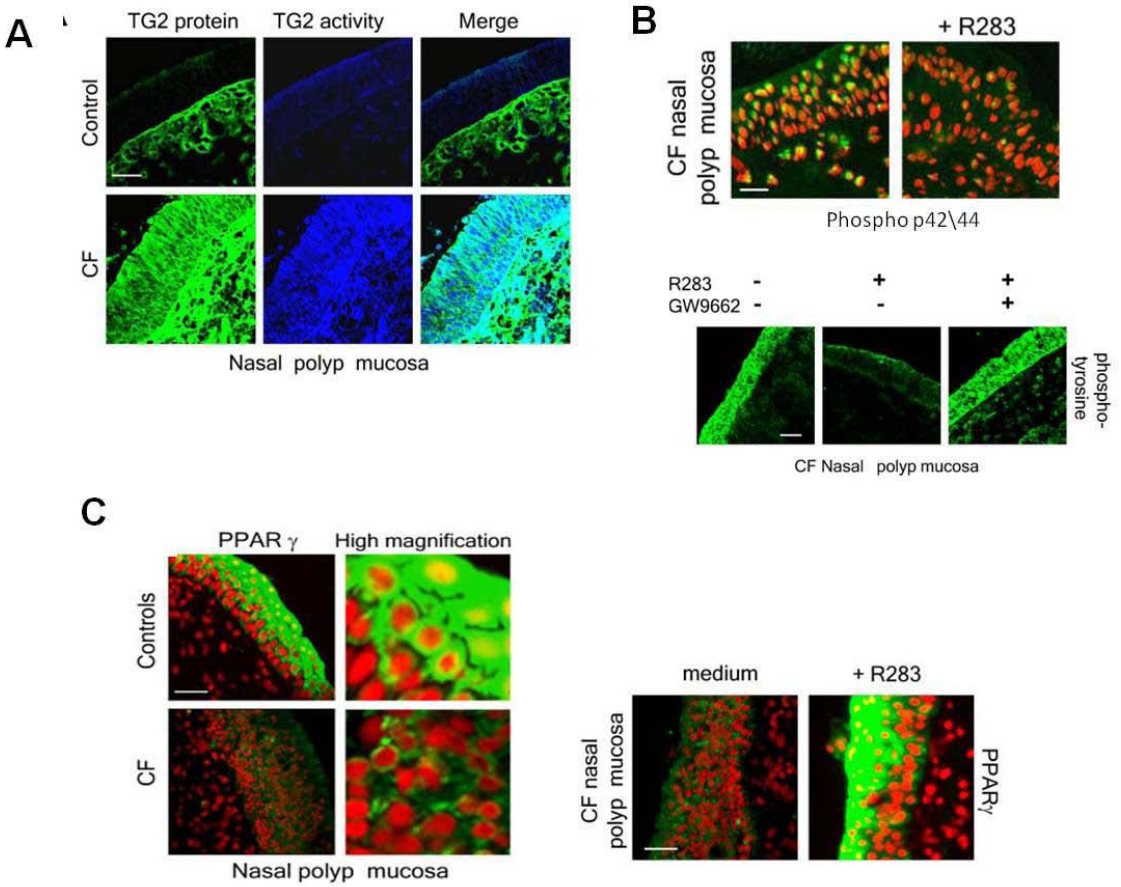

FIGURE 14. TG2 and PPARϒ in "ex vivo" human model

These data allow to validate this experimental model (24,72) and reported that increased TG2 levels are a feature of CF nasal polyp mucosa and that the inhibition of TG2 is effective in controlling mucosal inflammation by restoring normal lev els of PPARγ protein (24). We found that TG2-PIASy colocalized in human CF airways (Fig. 15A) and that this interaction was inhibited upon treatment with the EUK-134 (Fig. 15B). After EUK-134 treatment the distribution of TG2 in CF nasal polyp biopsies was similar to that observed in non-CF controls (24).

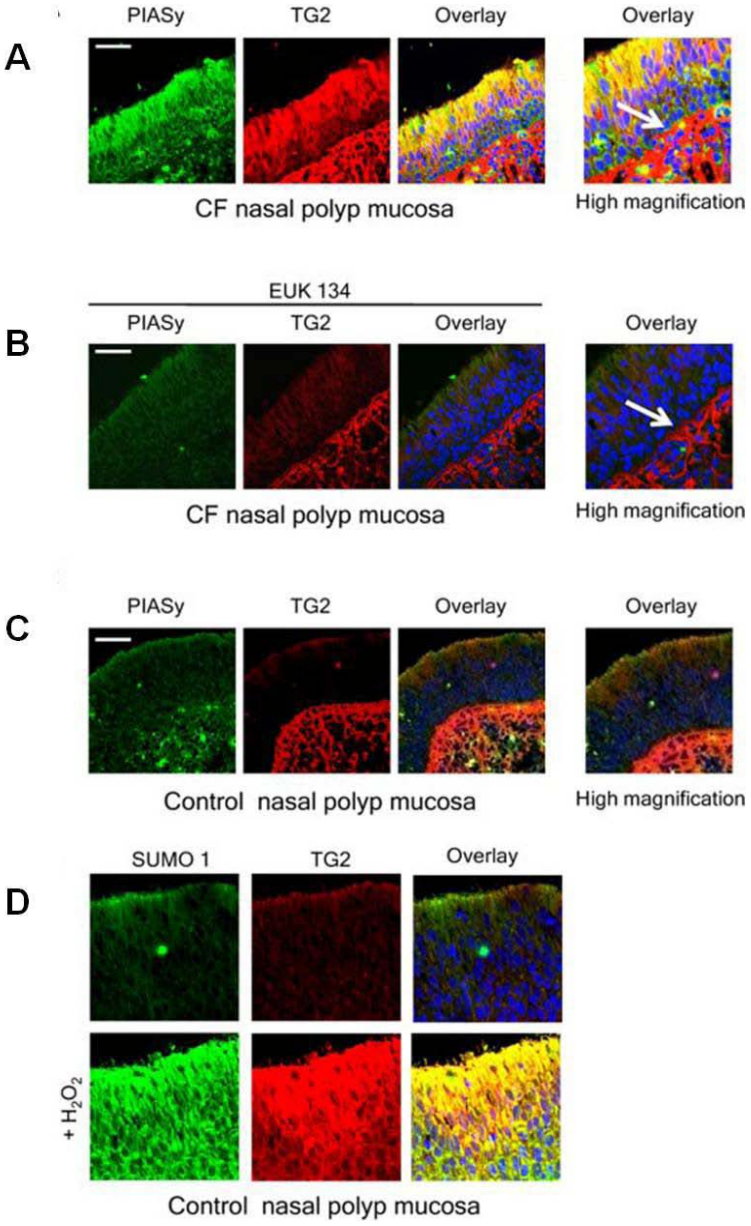

FIGURE 15. ROS-mediated PIASy-TG2 interaction in human nasal polyp mucosa.

This suggests that the inhibition of TG2-PIASy interaction restores the physiological levels and distribution of TG2 in CF airways (22). Furthermore, in CF nasal polyp mucosa TG2 colocalizes with SUMO-1, and the incubation with EUK-134 inhibited TG2-SUMO-1 colocalization (data not shown). Non-CF control nasal polyp mucosa showed very faint TG2, PIASy, or SUMO-1 expression at the epithelial level (Fig. 15C and D).

To test the effects of TG2 inhibition in vivo, we treated CF mutant mice homozygous for F508del-CFTR mutation (73) and their control littermates (36) with cystamine, previously reported to inhibit TG2 and ameliorate disease manifestations in a mouse model of Huntington's disease (38). We treated CF and wild-type mice with a daily injection of cystamine or PBS, for 7 days. After treatment with PBS the expression and distribution of the tested markers remained unaltered as compared with the pattern observed in untreated CF mice. Before treatment, as well as after treatment with PBS, all seven tested CF mice showed increase of ROS (FIG.16A), as well as TG2 activity (Fig. 16B), as compared with control littermates. PPARy was also reduced and sequestered in aggresomes (Fig. 15B), whereas phosphorylation of p42–44 (Fig. 16B) and increase of TNF-a protein were observed (Fig. 16C). Cystamine did not induce any changes in wild-type mice (data not shown).

This cascade of events leads to reduced secretion of inflammatory cytokines as TNF-α and of the neutrophil chemoattractant IL-8.

As above described, targeting ROS-TG2 axis ameliorates human and mouse CF airway phenotype by restoring beclin 1 and autophagy, therefore we used ex-vivo and mouse model to validate the data of CFTR defective cell line, and control.

Defective basal autophagy was also observed in human nasal polyp biopsies from severe CF patients (n=10) and mouse lung tissues from F508del-CFTR homozygous mice (*Cftr*^{F508del}) (73). Reduced beclin 1 protein levels were also observed in CF nasal polyp biopsies (24,54,72) (n=10) and in airway tissues from CftrF508del mice (n=10) (Fig. 17A). To investigate whether rescuing beclin 1 was effective in restoring autophagy in vivo in CF airways, CftrF508del mice (n=3 per group) were administered intranasally with a lentiviral vector encoding beclin 1 (74,75) or a lentiviral vector expressing the GFP. Overexpression of beclin 1 from the lentivirus induced significant increase of LC3 dots ($p<0.001$), reduced p62 accumulation, TG2 protein level and activity as compared to CftrF508del mice treated with LV-GFP (Fig. 17B).

To study the effects of Cystamine or NAC in vivo, we treated CftrF508del mice with daily intraperitoneal injections of NAC (n = 10) or PBS (n = 10). Treated mice showed a pattern similar to cell line.

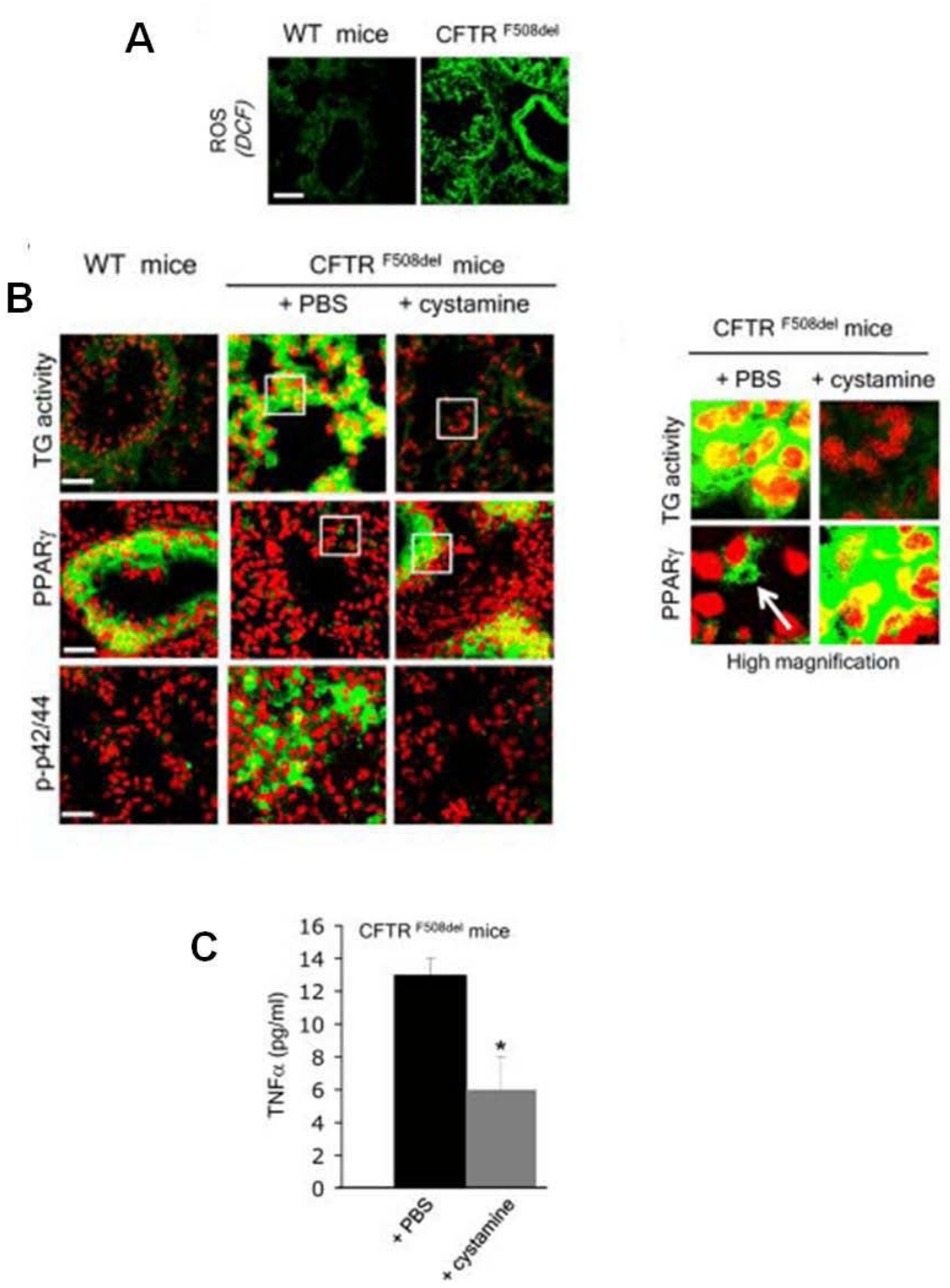

FIGURE 16. TG2 inhibition in mice model

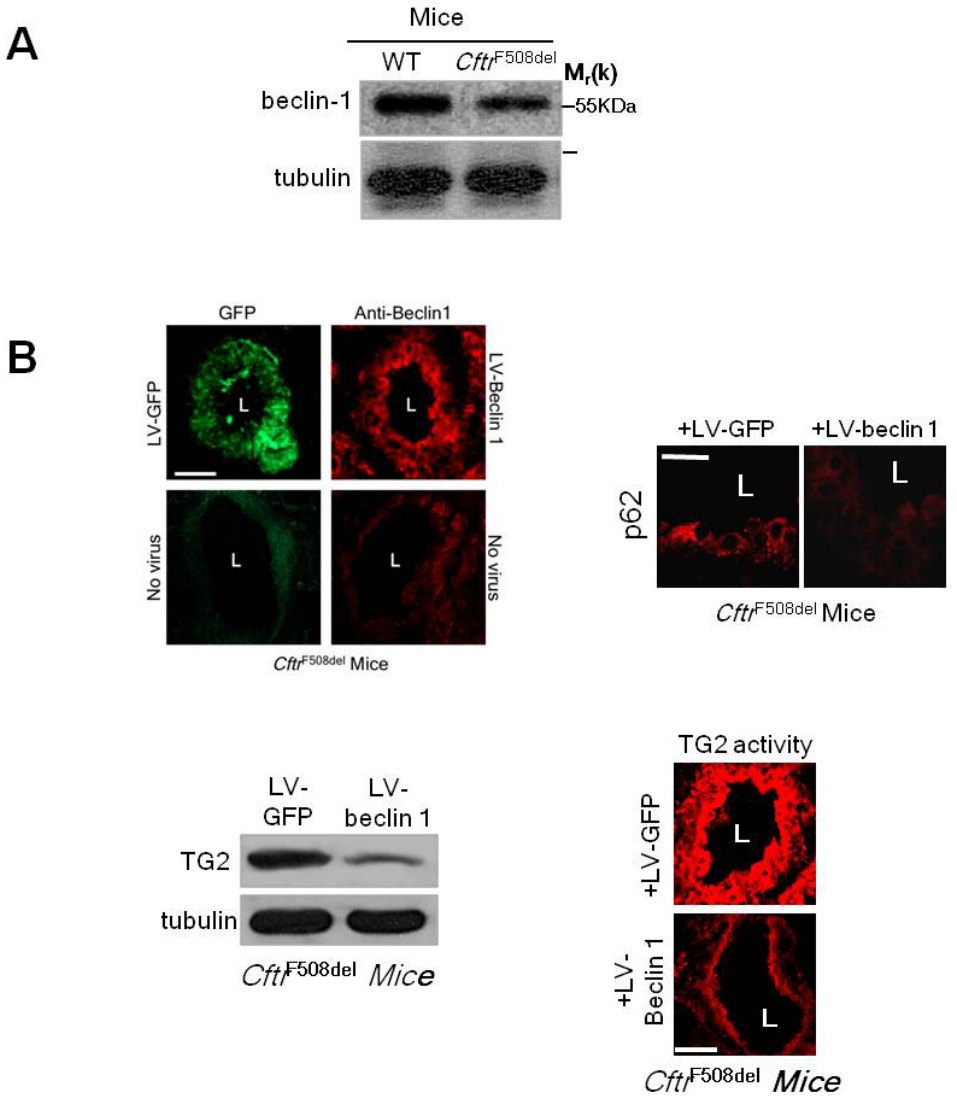

FIGURE 17. Restoring autophagy by cystamine or beclin 1 overexpression rescues CF phenotype in mice CF airways

The data obtained reveled a direct link between the regulation of IL8 and inflammation TG2-ROS driven.
The IL8 was a drive key in neutrophils movements, and the data obtained about its regulation and modulation in inflammatory environment offer a mechanism for the study of migration IL8-induced and can to develop a model for biotechnological application.
For this reason, in second part of activity, we developed a 3D motility model for study of migration driven by chemoattractant molecule, and we employed an important system for screening of potential molecules in therapeuthic application

2.Chemotaxis: Motility model

Cell motility is involved in a number of biological processes, from morphogenesis to inflammation. In spite of its relevance in human physiology the currently available techniques for the characterization of cell motility do not allow clear advantage in quantitative interpretation and application in biotechnology for industrial purposes. Furthermore the automation of measurement and a contemporary analysis of multiple samples are controversial . The application of new technologies, as the time-lapse microscopy (available in our lab) has revealed to be useful in overcoming these limits and allowed quantification of the random or directional (chemotaxis) cell movement as well as haptotaxis or contact guidance phenomena (1) and represents the nearest approach to in vivo assays.
Cell migration is a very complex phenomena that are strictly related to the inflammatory response as well as several processes of cell biology and development. Chronic inflammation is an ideal condition for the study of cell migration and its de-regulation. In this condition several cell populations are recruited in response to the enhanced local release of chemo-attractant molecules (chemokines) that favour the infiltration of circulating leukocytes within a disease-target tissue. This phenomena is known as chemotaxis and the chemical mediators (chemokine, citokine) recall the white cells from blood; the cells must go through different layers (blood vessel, extracellular matrix, epithelia). The formation of chemical gradient (cytokine-chemokine) is an important driving force for cell migration.
The first problem in studying the motility is the creation of physiological habitat for cell. The 2D model or microscopy approaches are not a real condition of organisms where the cells interact with other cells (tissue), matrix or liquid (blood cells). For this reason the generation of a 3D model system is mandatory.
During inflammation, the neutrophils are recruited in the site of injury by chemoattractant molecules that create a gradient flux in tissue; this gradient induce a extravasion of neutrophils from blood vessel and a movement to site of inflammation. These molecules are the chemokines (interleukin 8, IL-8) which react with specific receptor present on cell membranes to activate their movements. After extravasation, the neutrophils need to cross over a 3D structure, rich in fibronectin, collagen, elastin, the extracellular matrix. This structure is very complex and alters the movement of cell and was subjected to continuous modeling. Many membrane proteins interact with it (i.e. integrin) inducing a rearrangement of cytoskeleton.

2.1.The 3D matrix collagen gel

The first experiments were focused on the study of a ideal 3D model to observe neutrophil motility in basal condition, as well as in pathological condition.
The literature offers different models to study motility in 3D such as Boyden assay (76) (a typical indirect assay), that was ideal to perform an initial screening, but the results can be affected by variations in adhesion, motility or spatial orientation. For

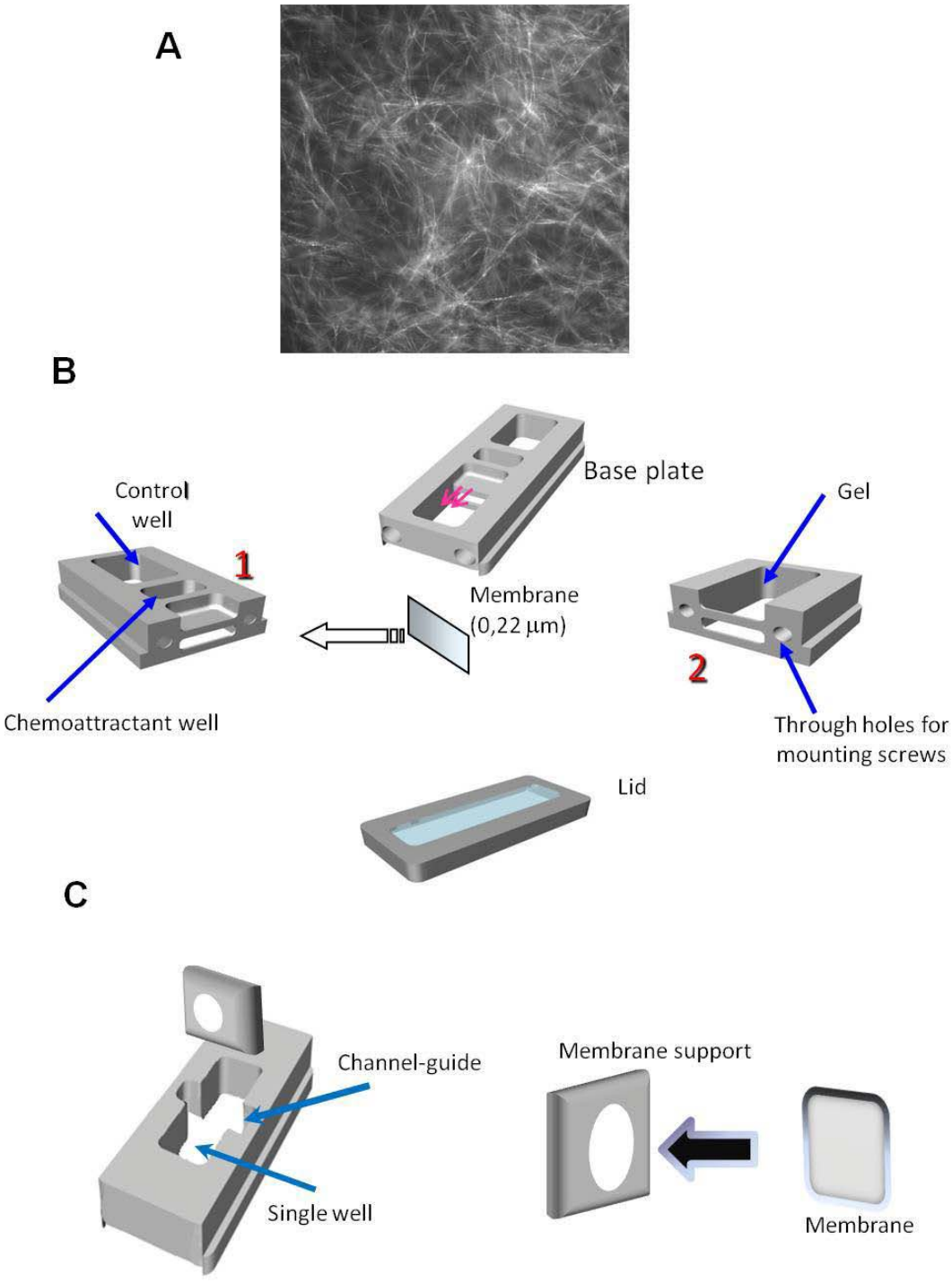

FIGURE 18. Schematic representation of 3D model: matrix collagen gel and chambers

example, an increased motility (chemokinesis) would result in an increased migration of randomly directed cells and might score as chemotaxis in many studies.
To perform 3D motility experiments, we created a matrix gel to mimic the extracellular matrix and to allow a movement of cell without impediments. To prepare the gel we used collagen rat-tail high concentration, to dilute in different percentage. We added in the mix a precise quantity of medium 1X and 10X free, to allow the cell viability, and we used NaOH 0,1 M to stabilize the pH around physiological value (pH 7.2). All components were kept in ice to prevent gelification of mix during preparation. The gelification required 30 minutes in the incubator at 37°C and 5% CO_2.
In first analysis we used a multiwells culture dish to test the polymerization of gel. The confocal microscopy images reveled an auto florescence and a fine structure of collagene fibres (Fig.18A). A fibroblast cell line (HT1080) was used to verify cell vitality and the absence of constriction in movement.
In second analysis, to study the chemotaxis phenomena, we projected and realized a prototype of chamber to surpass the limits of Boyden assay. It is a rectangular and horizontal chamber splits in two compartments by a divisor barrier. It is composed by two aluminum blocks: A) charatterized by one well for the matrix gel with cells, B) have two wells, one for control gel without the cells and other one for gel with chemoattractant; the two blocks are separated by a semipermeable membrane to allow the flux of chemoattractant. The chamber is equipped with a coverslide on the bottom (for microscopy analysis) and a lid to close the chamber (to keep sterile conditions). The two block are united by some screws and a little quantity of silicon grease, to close all slits (Fig.18B). More experiments underline a objective limit in assembling of chamber.
On the basis of these observations, we realized a second prototype of chamber composed by single aluminum block with one single well, in the center; this well is “subsplited” in two wells by a little aluminum block covered with a semi-permeable membrane of 0.22 µm pores (Fig.18C). The assembling processes is more easy. To demonstrate the efficiency of chamber, we performed more experiments of gelification test and cell viability test. We kept the cells in the chambers at 37°C and 5% CO_2 for 24h or more, and observed the viability of the cell with TIME LAPSE microscopy images. The Fig.19 showed the HT1080 cell line in different layers of the gel at time 0h and after 24 hours; these images reveled any alterations of cells morphology and composition of matrix gel.

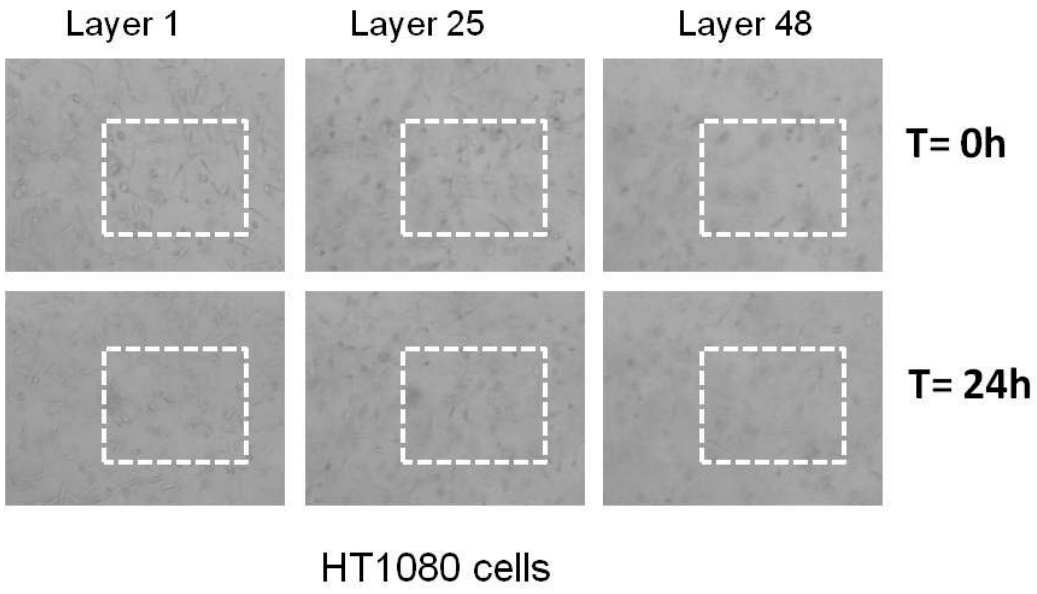

FIGURE 19. HT1080 in collagen gel

2.2. TIME-LAPSE system

To study the 2D cell motility phenomena ,fluorescence microscopy techniques was available on fixed samples, where the examined cells are observed in instants of time that precede and follow the addition of particularly factor, missing the progression of motility event. The advent of technology as time-lapse microscopy has allowed to overcome these limits, being able to follow cell motility from time to time and obtain quantification of the random or directional (chemotaxis) cell movement. Microscopy images give a static moment of processes lacking a intermediate time of phenomena. Therefore to study complex phenomena such the chemotaxis or cell with high motility a system able to follow all time of neutrophils\ cells movements was required, as the time lapse video system.
The TIME LAPSE system was based on an inverted optical microscope, equipped with mercury lamp and epifluorescence reflectors. The microscope was placed on an anti-vibrating table and was equipped with motorized stage and focus, that allowed to automatically position the field of view within the sample under observation. Images are acquired using a monochrome CCD camera and sent to the PC through Firewire interface.
In order to mimic environmental conditions required to run time-lapse experiments, a microscope incubator was used, consisting in a plexiglass box, coated with a

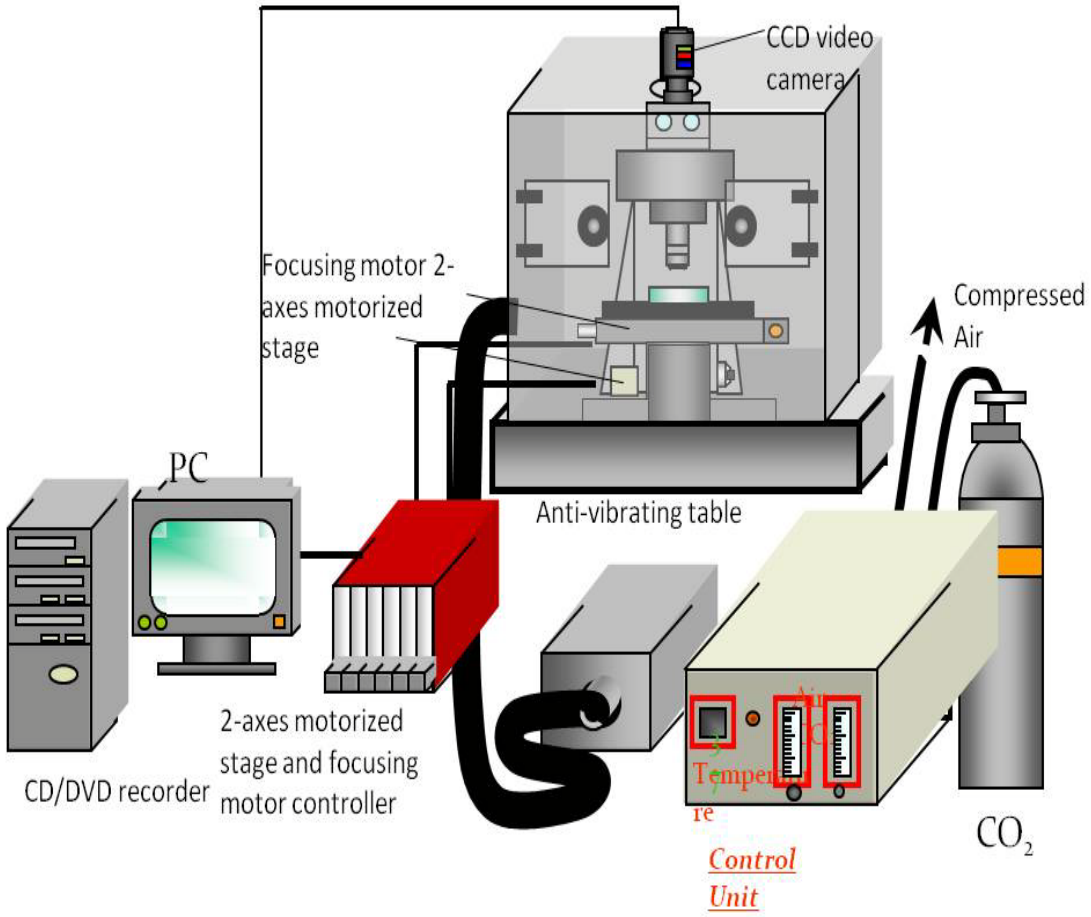

FIGURE 20. TIME-LAPSE work station

polystirol thermal isolator, in the box a radiator and a fan allow heat transfer and temperature uniformity. The temperature in the incubator was monitored by a thermocouple, connected to a PC via serial port. Temperature control was ensured by a software PID control that continuously update the temperature of the radiator. A 5% CO2 air flow is humidified through a bubbling column inside the incubator, and sent in a micro chamber that keeps the sample in a controlled air, constant temperature environment

The system was connected to a video-camera with high solution and velocity to follow the motility of high speed cells, and this was manage by a software on PC. The software allowed to move the table (the sample) on three axis (x,y,z) to follow the sample in all 3 dimension. The x and y axis was controlled by a joystick connect to motor of table, and the z axis was controlled by a system of focus. Using the software we selected a specific object with a defined x, y position and chose a

position in the gel that corresponded to a layer with cell on focus; with specific functions of software we selected the total delta of layer (in μm), the number of layers that const the total delta and the time of acquisition: a Z-stack acquisition. In this way we followed the single cell (of selected object) in 3D for every single instant of time(Fig.20).
Time lapse experiments ran according to the following protocol. Once introduced the samples in the incubators, image acquisition started. A software allowed periodic scanning of marked positions in the sample. Input parameters was the sample positions to image and the acquisition time frequency. Each time cycle the software was then control the microscope stage and focus in order to cyclically place any marked position under the field of view and automatically acquire images, that was stored on hard drive, the software was than wait a pause up to the next acquisition cycle. At the end of the experiment we obtained a number of images for every single layer in single instant of time, and we could create a sequences of images as like a film.
The single cells present in the images were analyzed by a specific software of cell analysis (Image Pro-Plus) provided of a macro to follow the single cell; through a mathematical model we obtained many parameter such as speed, dimension, trajectory, diffusion profile (in presence of chemoattractant molecules).

2.3.Calibration of system

The diffusion profile of chemoattractant was basic to analyze the cell motility in 3D model.
The concentration gradient was studied by measurement of concentration of a fluorescence type of chemoattractant, IL8, or by a component with analogous molecular weight that take bound the fluorescent tag (dextran bound to FITCH). The measurement of fluorescence was perform by means of optic microscopy and images analysis by using the Imege ProPlus software. A preliminary calibration was performed on sample with different concentration of FITCH-dextran without the barrier, in order to have a uniform distribution. The sample exposition at excitant radiation was minimize to avoid the photobleaching of tag. In second time we performed the experiments by using different concentrations of FITCH-dextran. We kept in the well a mix collagen with FITC-dextran and observed the diffusion trough the membrane in control well with gel alone. The emitted fluorescence was proportionally direct to concentration of FITCH-dextran used (Fig.21A). The intensity of fluorescence was expressed as mean of grey level. We calculated the concentration profile of FITCH-dextran during time and in the space, by measuring the emitted intensity of sample light into control well at different distance from membrane, in chancing of time since the adding of FITCH-dextran. The fitting data revealed a diffusion coefficient of $2 \cdot 10^{-6}$ cm^2/sec, according to literature data (Fig.21B).

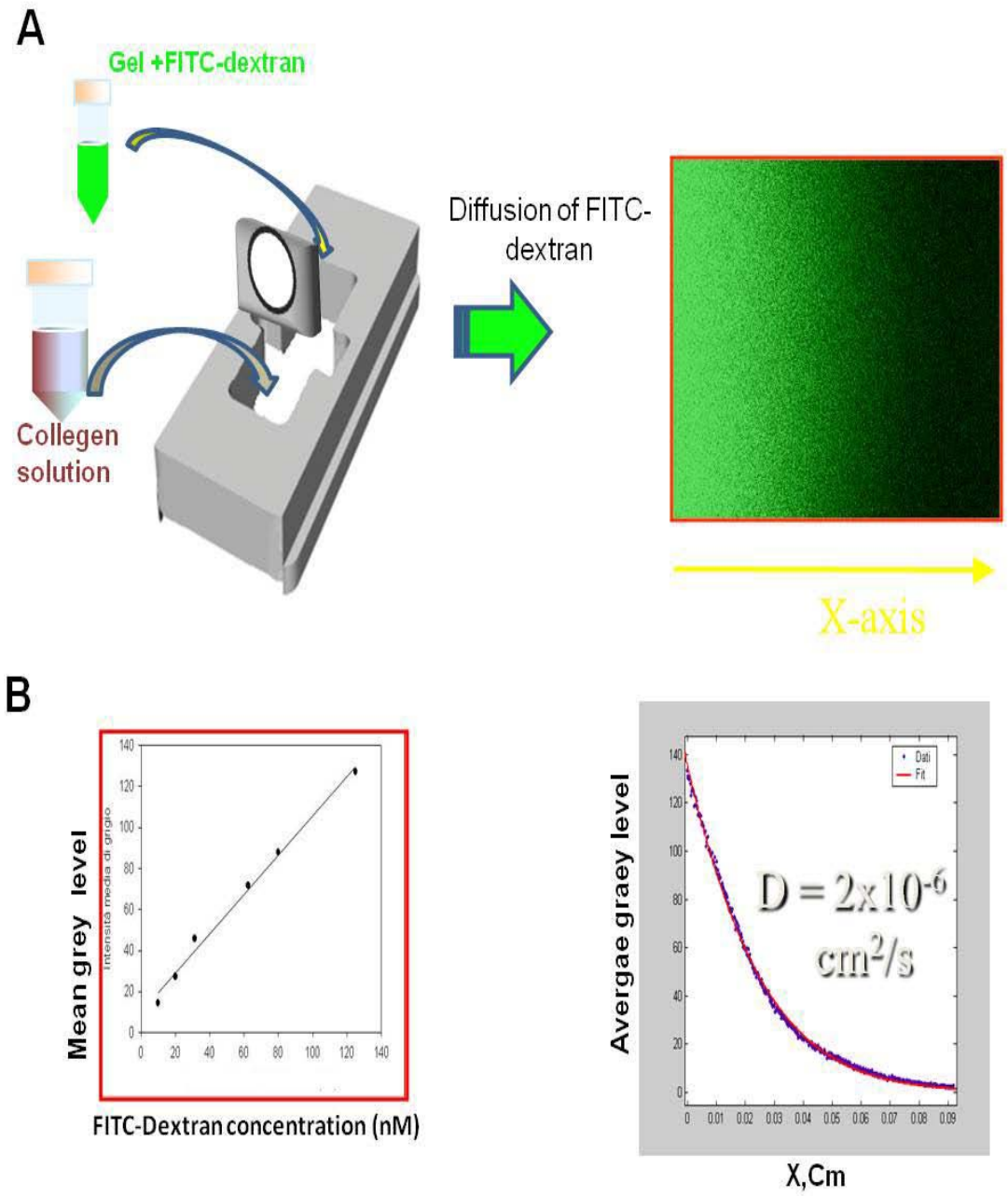

FIGURE 21 Diffusion of FITC-dextran: calibration system

2.4. Neutrophils in collagen gel: 3D model

To test whether the chamber was an ideal condition to study neutrophils as well as other cell line (epithelial, fibroblast, gut, etc.) we performed a experiment with neutrophils isolated from peripheral blood.
The neutrophils were isolated from blood followed a specific protocol with Ficoll-Paque buffer. Ficoll-Paque was normally placed at the bottom of a conical tube, and blood was then slowly layered above Ficoll-Paque. After being centrifuged, the following layers will be visible in the conical tube, from top to bottom: plasma and other constituents, a layer of mono-nuclear cells called buffy coat (PBMC/MNC), Ficoll-Paque, and erythrocytes & granulocytes which should be present in pellet form. This separation allows easy harvest of PBMC's. After washing and Dextran-NaCl lysis, the nutrophils were isolated; an appropriate number of white blood cells($5*10^5$ cell\ml) was counted in Burcker chambers. The mix of collagen was prepared in a conical tube without any cheattractant, and was divided in two mix: one of them was put into control well and other one was mixed with appropriate number of cell. In this way the cells were included in collagen fibres reticulum that block the sedimentation and represent a tridimensional substratum and can partially reproduce the microstructure of extracellular matrix. After gelification at 37°C and 5% CO_2, the chambers was fixed on specific supporter of TIME LAPSE STATION. The cell motility was observed for 24h with Z-stack acquisition images every five minutes (Fig.22A).
The quantitative analysis of single cell performed by Image Pro-Plus software, reveled a random motility in absence of chemokin (Fig.22B). Moreover we performed the experiments in same conditions (number cells, acquisition time) in presence of IL8 (50µg\ml); its diffusion time was very early and neutrophils showed a directional motility. The results were obtained from mathematical analysis of motility parameters.
The qualitative and quantitative data analysis evidenced a directional motility of neutrophils under IL8 diffusion compared to absence of IL8. The results indicated that the prototype chamber was an ideal model to study migration of different cell lines. The qualitative and quantitative analysis of images allow to obtain many information about the “parameters” motility-dependent. Moreover, was more hopeful for application in industrial biotechnological sector.
Furthermore, the system offered a new approaches to study the motility IL8-induced and IL8 modulation (see above data) represented a key strategy for new therapeutic application.

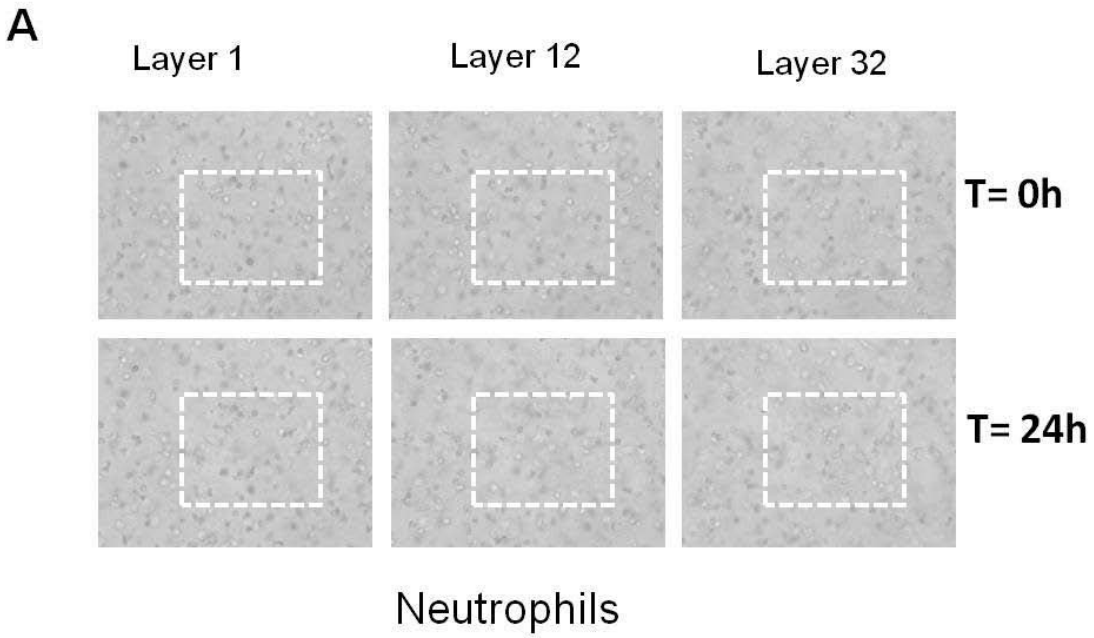

FIGURE 22. Neutrophils in collagen gel

2.5.T84 motility: 2D model

The 3D model was one of many way to study cell movements in a physiological system with a collagen gel to mimic extracellular matrix. the neutrophils migration under chemokine flux offered a valid model to set the system condition, and modulation of chemoattractant factors was the key to study chemotaxis phenomena and develop biotechnological application. CF disease represented the optimal system to study the mechanisms of modulation since it was characterized by a strong recruitment of neutrophil under IL8 diffusive flux CFTR-defective driven. The inflammatory environment was crucial effector of this condition such as for many other patholy as well as Coeliac Disease (CD).
The common characteristic of either CF and CD, besides the inflammation condition, was the presence of high TG2 level. In CD the inflammatory milieu was a response to a persistence attach from its inductor, the gluten, which led to an evident modification of tissue (or cell line model) architecture with consequent re-arrangement of cytoskeleton.
This data offered a valid condition to develop a 2D-motility model to study epithelial cell line in adhesion and view the cytoskeleton modification.
Coeliac disease is a relatively common pathology that affects 1% of the population, and is precipitated by the ingestion of gluten proteins. In predisposed individuals, gliadin acts as leading to a powerful activation of gliadin specific T cells. Several fragments of gliadin have been found to be ‘toxic’ for predisposed individuals and it has also been suggested that different portion(s) of gliadin, ostensibly not those recognised by Tcells, modulates this innate activation of coeliac small intestine. Further studies have indicated that TG2 is the essential “pivot” in the pathogenesis of celiac disease (27) because TG2 operates a crucial posttranslational modification,

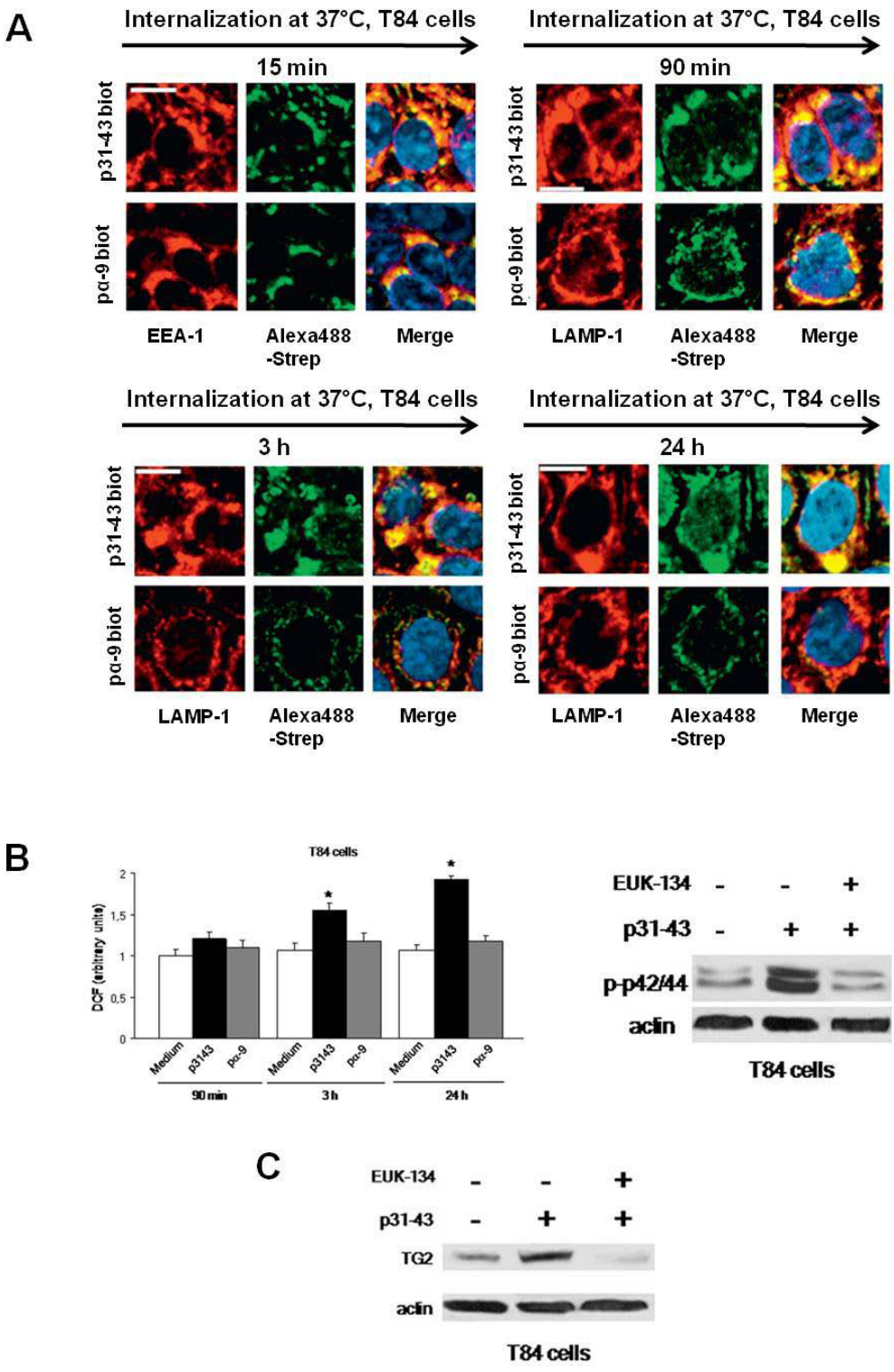

FIGURE 23. Internalization and pro-inflammatory effects of p31-43 and control peptide

the deamidation of strategic glutamine to glutamic acid, within the sequence of immunodominant gliadin epitopes(Subunits of the antigenic determinant that are most easily recognised by the adaptive immune system and thus most effective in the induction of antibody and T-cell responses).
Among toxic peptides , p31-43 induces the expression of early markers of epithelial activation and leads to enterocyte apoptosis (77) both in coeliac intestine and in sensitive intestinal epithelial cell lines. Moreover, p31-43 induces early tissue transglutaminase (TG2) upregulation compared to immunodominant gliadin peptides (35). This indicates that TG2 is not only central to the adaptive response to gliadin as the main deamidating enzyme of the immunodominant epitopes, but is also a key player in the initiation of inflammation in coeliac disease. However, it is still unknown how p31e43 induces early TG2 activation in both coeliac intestine and 'gliadin-sensitive' intestinal epithelial cells (35,79).
We have demonstrated that in cystic fibrosis (CF) airway epithelia (24) sustained TG2 activation is driven by the increased levels of reactive oxygen species (ROS) caused by the CFTR genetic defect. We therefore investigated whether p31-43 was able to drive an intracellular prooxidative environment and demonstrate that p31-43 leads to an increase of ROS levels in celiac duodenum as well as T84 intestinal epithelial cells. To understand how p31-43 challenge induces oxidative stress, we analysed the delivery of this peptide to the intracellular degradation systems.
Recent data demonstrated increased transepithelial translocation of the 33-mer (p56–89) in active coeliac disease compared to healthy controls. Moreover, incomplete degradation of the 33-mer and protected transport of the peptide 31-49 occurs in patients with untreated coeliac disease, thus favouring their respective immunostimulatory and toxic effects (79). Here we show that p31-43 is retained within the lysosomes as compared to the more rapid disappearance of the immunodominant peptides pa-2 or pa-9 from the intracellular compartments. T84 cells were incubated with biotinylated p31-43, p-a2, p-a9 for 15, 30, 60, 90 min, 3 h and 24 h at 378C. Soon after 15 min of challenge, peptides co-localised with EEA-1 (Fig. 23A), a marker of early endosomes; After 90 min the internalized peptides co localised with Lysosomal Associated Membrane Protein-1 (LAMP-1) (Fig. 23A), a marker of lysosomes. No internalisation of peptides or colocalisation with LAMP-1 were observed when T84 cells were pre-incubated with M-β-CD, which inhibits clathrin-mediated endocytosis (80), or filipin, a specific inhibitor of lipid raft- or caveolae-dependent endocytosis (80) (data not shown). This suggests that endocytosis is essential for the delivery of gliadin peptides to the lysosomes for degradation. Increasing appearance of the internalised p31-43 in LAMP-1- positive vesicles, mainly limited to perinucelar localisation, was observed after 3e24 h of challenge (Fig. 23A). At these late time points p-a9 (Fig. 23A) or pa-2 (data not shown) were only faintly detected in LAMP-1-positive structures, thus indicating that p31e43, but not p-a9 or p-a2 is retained within the lysosomes. Moreover, after 90 min of challenge neither p31e43 nor pa-9, induced significant increase of ROS (Fig. 23B). At the later time points (3 e 24 h of challenge), p31-43, but not pa-9 (Fig. 23B), induced a time-dependent significant increase of ROS levels, suggesting that the prolonged persistence of p31-43 in LAMP-1 positive vesicles generates a pro-oxidative environment. Blocking p31-43 endocytosis with M-β-CD, prevents the increase of ROS (data not shown).
The generation of a pro-oxidative environment induces activation of different stress sensitive signalling pathways (78,24); therefore, we investigated whether p31e-43-induced ROS-mediated p42/44 MAPK phosphorylation in T84 cells. We

demonstrated that p42\44 MAPK phosphorylation induced by the challenge with p31e43 was prevented by the incubation with the catalase-superoxide dismutase (SOD) mimetic EUK-134 (Fig.23C). To investigate whether the increased levels of ROS may account for the p31-43-induced increase of TG2 levels,(24)we incubated p31-43-challenged T84 cells with EUK-134. We demonstrated that EUK-134 was effective in controlling the increase of TG2 protein levels (Fig.23C) and TG2 activity (data not shown) induced by p31e43. No increase of TG2 was observed after challenge with p31-43 upon M-b-CD or filipin treatment (data not shown). This indicates that p31-43 internalisation is critical for the induction of ROS-mediated TG2 activation.

The pro-inflammatory environment p31-43-driven induces a strong re-organization of cytoskeleton; as matter of fact the lumen intestinal of CD patients shown atrophy of villi and cryptic hyperplasy due to persistence T-cells infiltration gluten-toxicity induced.

To test whether the p31-43 toxicity could impact on cell motility and interaction of gut epithelial cell line (T84), we used a 2D model.

The T84 cell line was characterized by a typical collective migration where the cell line was organized in a compact structure such as “island”, and their movement was due to movement of total and contemporary motility of single cell that composed the island. During the movements, the cells\islands have interaction either between single cell, either between the island, and we showed a phenomena like “englobetion” of island after their touching.

To demonstrate the role of p31-43 on cell motiliy, we cultured the T84 cell line on multiwells cultur dish; we incubated p31-43-challenged T84 cells with EUK-134 or with TG2 monoclonal antibody, 4G3, to block the toxic effect with specific inhibition of ROS or TG2

We performed a 2D motility experiments using time-lapse workstation and setting the acquisition time every 15 minutes for a total of 48 hours.

The images reveled a visible motility alteration ,evidenced by a strong collective migration of cell and faster “englobetion” of island in presence of p31-43versus the control not treated; moreover, in presence of inhibition the motility rescued its pattern like not treated.(Fig.24A)

To demonstrate whether the alteration of motility p31-43 induced, was due to re-organization of actin, we fixed the samples and used a specific fluorescent molecule, FITCH-phalloidin, to marker the cytoskeleton. The confocal imges reveled a tipical actin structure of T84 in control not treated and a rearrangement of cytoskeleton after p31-43; the actin rescued the structure after inhibition of ROS or TG2.(Fig.24B)

The results indicated that TG2-ROS axis was critical point to regulation in Coelic Disease, and its modulation will be the goal to treatments of pathology; moreover, the 2D model analysis open the way to possible system of screening of molecule with high impact on motility and become a future fast test screening in biotechnological application.

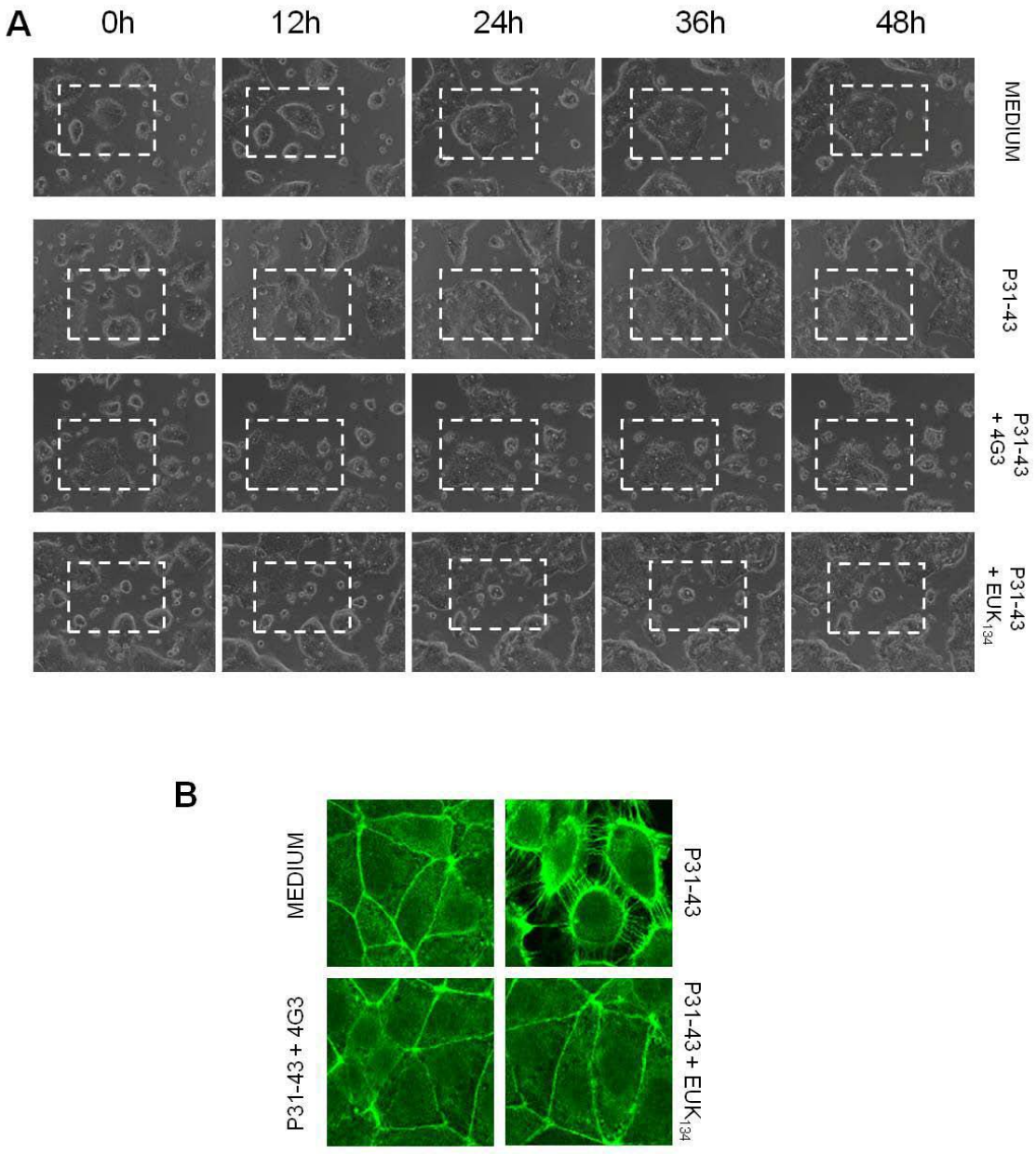

FIGURE 24. T84 motility and cytoskeleton organization: 2D model

CONCLUSIONS

The results of PhD thesis project give an important contribution in defining the pathological mechanisms of airway inflammation in CF and identifying new therapeutic options for patients .
The principal results of the study have been published in four papers on international journals (J. Immuol 2008, J. Immunol 2009; Gut 2010; Nature Cell. Biol. 2010) and underline:

A) the role of TG2 as a new pathogenic factor in Cystic Fibrosis (24).

The novel finding of the study is the demonstration that CFTR mutations lead to an increase of TG2 levels and activity that, in turn, down-regulate the anti-inflammatory effects of PPARy. We have shown that PPARy is not only reduced in CF epithelium and CFTR-defective cell lines, but also sequestered in perinuclear aggresomes, prominent pathological features common to many neurodegenerative conditions such as Huntington and Parkinson's diseases (81). Aggresomes are generated in response to alterations of the ubiquitin proteasome system, the principal cellular mechanism of degradation of misfolded proteins and represent a cytoprotective mechanism that cells adopt to clear mutant/modified aggregate-prone proteins (82). This suggests that the formation of the aggresomes in CF is caused by the accumulation of misfolded proteins fated to final degradation.
TG2 is a pleiotropic enzyme with a calcium-dependent transamidating activity that results in cross-linking of proteins via ε(y-glutamyl) lysine bonds (36,40). Our results demonstrated a significant increase of TG2 protein and enzymatic activity in CF epithelium and CFTR-defective cell lines. TG2 up-regulation was also responsible for the aggresome formation in CF. Importantly, TG2 induced cross-linking of PPARϒ and its sequestration into aggresomes, because the TG2-inhibitor R283 produced a significant reduction of PPARϒ protein aggregates and restored a wider intracellular protein distribution.
Collectively, our study provides a molecular explanation of the reported association between CFTR defective function and sterile inflammation. Highlighting the role of TG2 in CF, we have also indicated novel ways to modulate inflammation, a key component in CF pathogenesis.

B) the role of post-translational modifications of TG2 as a link between genetic defect of CFTR ad inflammation (54)

These data have underpinned the relationship between CFTR defective function, oxidative stress, and chronic airway inflammation in CF. We have identified TG2 SUMOylation as a pivot in driving the pro-inflammatory CF phenotype.
SUMOylation has been defined as a key player of the posttranslational network to regulate key cellular functions. Herein we demonstrate that in CF airway epithelia the increased levels of ROS lead to TG2 SUMOylation via interaction of TG2 with PIASy, an E3 ligase. Oxidative stress increases PIASy protein levels and favors TG2 SUMOylation that leads to the persistence of high TG2 tissue levels by down-regulating TG2 ubiquitination and proteasome degradation. Our results also indicate that TG2 SUMOylation is a general response to oxidative stress. The rheostat role of TG2 makes this enzyme an attractive target to restore cellular homeostasis and dampen chronic inflammation in CF airways. The regulation of the high levels of TG2 protein or the inhibition of sustained TG2 enzyme activation may represent a new attractive approach to control disease evolution in CF patients. To

evaluate whether we can translate our in vitro findings into an appropriate animal model and confirm their biological relevance in vivo we have studied CF mutant mice homozygous for F508del-CFTR. Our results highlight TG2 as an unforeseen unifying link between genetic defect, deregulation of cellular homeostasis, and inflammation. They also indicate TG2 as a candidate target for the design of a pathogenic-based therapy in CF and add to the rationale for attempting inhibition of TG2 in CF patients..

C) the mechanisms of autophagy inhibition via ROS-TG2 axis , in epithelial airway cell line and mice model of CF. For the first time this study defined the CF as an autophagy-related disease (87).

Defective autophagy is a critical mechanism in several chronic human diseases (83) such as neurodegeneration (84) and cancer. Here we show that defective autophagy due to decreased levels of beclin 1 protein, a key molecule involved in autophagosome formation (60,63,66,70), drives lung inflammation in CF.
A common feature between this neurodegeneative disease and CF is the aberrant intracellular accumulation of misfolded proteins within the affected tissues (85,86). In CF airways, misfolded or damaged proteins, such as misfolded CFTR and PPARγ, accumulate into aggresomes. Here we demonstrate that in CF epithelia TG2-mediated crosslinking and sequestration of beclin 1 dislodges PI3K platform from the ER, thus inhibiting initiation of autophagy. TG2-driven defective autophagy in turn increases ROS and TG2 levels, thus generating a vicious cycle leading to a deleterious pro-oxidative and pro-infammatory environment. Autophagy inhibition with p62 accumulation (58) increases the levels of proteasome substrates and compromises the Ubiquitin Proteasome System (UPS) (58), thus favouring aggresome formation. TG2 contributes to proteasome overload and aggresome formation in CF airways by inducing cross-linking and aggregation of several substrate proteins. Therefore, TG2 functions as a rheostat of the post-translational network and UPS under disease conditions and switch off the post-translational regulatory mechanisms. As a consequence of this function, TG2 is involved in the pathogenesis of neurodegenerative diseases due to protein aggregates.
We have previously reported that CFTR inhibition results in the upregulation of ROS and their downstream events leading to inflammation. Here we show that CFTR knock down drives defective autophagy as it occurs in human and mouse epithelia carrying either homozygotes for F508del or compound heterozygotes for two severe CFTR mutations. Our results provide a new mechanism linking CFTR defect and inflammation via ROS-TG2-mediated inhibition of autophagy. Therefore, we have provided a novel rationale and the mechanism of action for both NAC and cystamine in treatment of CF patients.
In conclusion, our study suggests that restoration of beclin 1 and autophagy may be a novel approach to treat CF and may pave the way for the development of a new class of drugs that by enhancing beclin 1 levels could be effective treatments for CF.

D) the development of model for 3D migration assay and 2D motility

The study of mechanisms that regulate the IL8 is mandatory to develop a 3D model for IL8-induced neutrophils migration assay for potential biotechnological application.
The 3D model is a ideal model to study the movements of cell in a 3D matrix of gel where a diffusive flux of molecule induced migration; instead, a useful model to test the cell motility in adhesion condition was the 2D model. The 2D model is ideal condition to study effect of molecule that influenced cell motility due to a organization of cytoskeleton; for this propose, the intestinal epithelial cell (T84), model of Coeliac

Disease, represent an ideal application of 2D the model.
The Coeliac Disease is characterized by sensitive response to A-gliadin peptide fragments, that induce an immune activation with an inflammatory response. Among the gliadin peptide, the p31-43 induces an alteration of inflammation via ROS-TG2 pathway (82), which have many implications in the organization of actins filaments. This pathology is strong linked to TG2 that has a crucial role in the pathogenesis of disease. The 2D model offers a ideal screening test to verify whether the p31-43 toxicity can impact on cell motility and interaction of epithelial cell line (T84).
The results highlight the possibility to use this model as a prototype of fast screening procedures to test the effects of several putative toxic fragments as well as molecules that prevent gluten-induced toxicity.

These data provide the rationale for the development of cell motility and migration assays as ideal instruments to test the efficiency of molecules with potential pharmacological impact.
The use of quantitative and qualitative analysis could also be implemented in the screening of various drugs potentially effective in controlling cancer cell invasiveness and in modulating drugs-resistance. The effects of TG2 and ROS modulation on these dynamic processes could allow the set up of appropriate devices for either research purposes or industrial biotechnological application.

MATERIALS AND METHODS

***Cell lines and cultures*.** Human CF bronchial epithelial cell line IB3-1, carrying F508del/W1282X CFTR mutation and isogenic stably rescued C38 (LGC Promochem, Milan, Italy), were cultured with LHC-8 medium (Invitrogen) supplemented with 5% FBS and the appropriate amount of penicillin/streptomycin. Normal bronchial epithelial 16HBE (LGC Promochem, Milan, Italy) were cultured with MEM Earl's salt medium supplemented with 10% FBS and 1% penicillin/streptomycin, as recommended by American Type Culture Collection. CFBE41o- human CF bronchial epithelial cells (gift from Dr. D. C. Gruenert) were cultured MEM Earl's salt L-Glutamine (200 mM L-Glutamine) medium supplemented with 10% FBS and the appropriate amount of penicillin/streptomycin. Cell lines were incubated for 24 hours with R283 (250 μM), μcystamine (250 μM, Sigma Aldrich), N-acetyl Cysteine (NAC, 10 mM, Vinci Biochem), EUK-134 (50 μg/ml, Vinci Biochem), rapamycin (100 nM, Sigma Aldrich), chloroquine (25μM, Sigma Aldrich), E64d (50 μg/ml for 4 hours) and pepstatin A (50 μg/ml for 4hours), Rosiglitazone (10 μM for 4 hours, Vinci-Biochem); BAPTA-AM (25 μg/ml, Calbiochem, for 4 hours), proteasome inhibitor MG132 (50 μM, Calbiochem, for 6 hours). C38 and 16HBE cells were incubated for 48 hours with CFTRinh172 (20 μM, Calbiochem) followed by cystamine or EUK-134.
Human colon adenocarcinoma T84 were cultured in DMEM:F12 mixture 1:1 medium supplemented with 5% FBS and the appropriate amount of penicillin/streptomycin, as recommended by American Type Culture Collection (ATCC).
The cells were challenged with p31-43 for 24 h in the presence or absence of the ROS scavenger EUK-134 (50 mg/ml; Alexis Biochemicals), or the TG inhibitor cystamine (400 mmol/l; Sigma). To study internalisation of peptides, cells were challenged for 15, 30, 60 or 90 min, 3 or 24 h at 378C with the biotinylated peptides (20 mg/ml). To inhibit endocytosis, the cells were pre-treated with the cholesterol-binding agent methyl-bcyclo-dextrin (M-b-CD, 10 mmol/l; Sigma) or filipin (5 mg/ml; Sigma) and then challenged with biotinylated peptides

***Human subjects and ex vivo cultures of nasal polyp mucosal biopsies*.** Ten CF patients carrying severe CFTR mutations (Table 1) and ten consecutive non-CF patients (mean age 21 years, range 16–32) underwent surgical treatment for non-allergic nasal polyposis were enrolled. Nasal polyp biopsies from seven patients for each group (patients #4-10 of Table 1) were cultured for 4 hours with or without EUK-134 (50 μg/ml) or NAC (10 mM) or cystamine (400 mM) or R283 (250μM). Nasal polyp biopsies from five CF patients (patients #6-10 of Table 1) were also incubated with NAC or Cystamine or PPARyantagonist GW9662 (1 μM; Alexis Biochemical), or R283 for 24 h, followed by GW9662 (1 μM) for 4 h. Informed consent was obtained from all subjects, and the ethical committee of Regione Campania Health Authority approved the study.

***Mice and treatments*.** Young adult female CF mice homozygous for the F508del mutation (abbreviated CftrF508del) in the 129/FVB outbred background (obtained from Bob Scholte, Erasmus Medical Center Rotterdam, The Netherlands), and their wild-type littermates were housed in static isolator cages at the animal care specific pathogen free facility of Charles River (Varese, Italy). To prevent intestinal obstruction CF mice were weaned to a liquid diet (Peptamen; Nestle´ Nutrition). Peptamen was replaced daily. The genotype of each animal was checked at 21 days of age. These studies and procedures were approved by the local Ethics Committee for Animal Welfare and conformed to the European Community regulations for animal use in research (CEE no. 86/609).We treated CftrF508del homozygous mice by intraperitoneal injection (i.p.) with a daily dose of 100 µl of 0.01 M cystamine in PBS solution for 7 days16 (n=7 for each group of treatment) or NAC with a daily dose of 100 mg per Kg (body weight) in PBS solution for 5 days or with PBS solution (n=10 for each group of treatment). Mice were then killed by i.p. injection of 20 mg of sodium pentobarbital (Abbott Laboratories).
Airway administrations of lentiviral vectors expressing the mouse beclin 1 or GFP were performed in anesthetized CftrF508del homozygous mice aged 4-8 weeks as previously described (74). Mice were sacrificed 5 days post-vector administration and lung tissues were collected for analyses.

***Plasmids and transfection*.** The pcDNA3-HA-beclin 1 expression vector (gift from Dr. N. Mizushima) and the corresponding empty expression vectors were used for transfection experiments. IB3 cells were transfected with pcDNA3-HA-beclin 1 and empty vector , as control, using Lipofectamine 2000 (Invitrogen) according to the manufacturer's protocol. Briefly, one day before transfection, we plated cells in growth medium without antibiotics such that they will be 60-70% confluent at the time of transfection; the day of transfection we prepared the complex of DNA and Lipofectamine 2000 (in a ratio of 1µg:3µl, DNA:Lipofectamine) and incubate for 30 minutes at Room Temperature; we added the complex to the cells and incubated at 37°C for 24 h.

RNA interference. Cells were transfected with 50 nM human TG2, SUMO-1,PIASy, beclin 1 and CFTR siRNA (Invitrogen) or scrambled oligonucleotides by using Lipo RnaiMax (Invitrogen) according to the manufacturer's instructions. Briefly, one day before transfection, we plated cells in growth medium without antibiotics such that they will be 30-50% confluent at the time of transfection; the day of transfection we prepared the complex of siRNA oligonucletides and LipoRNAiMAX and incubate for 30 minutes at Room Temperature; we added the complex to the cells and incubated at 37°C for 72 h.
For siRNA oligonucleotides sequences see Supplementary Information, Table 2 .

Adenoviral Vector. Human MnSOD cDNA was cloned into the shuttle vector pAd5CMVK-NpA (gift from Dr. Michael Brownlee). Briefly, one day before infection we plated cells in growth medium without antibiotics; the next day, the cells were infected with MnSOD or control adenovirus for 2 hours at 37°C.

Quantitative RT-PCR. Total RNA was extracted using the RNeasy Mini Kit (Qiagen). The mRNA was reverse transcribed by SuperScriptTM III First Strand Synthesis System (Invitrogen). Quantitative RT-PCR was performed using iCycler iQ Multicolour Real-Time PCR Detector (Bio-Rad) with iQ TM SYBR Green supermix (Bio-Rad). Expression levels of genes were normalized to β-actin levels in the same sample. The sequence of primers is reported in Table 3. The relative amounts of mRNA were calculated by using the comparative CT method.

Western blot analysis. Cells were washed 2 times with ice PBS and then lysed in buffer containg 50 mM Tris- HCl (pH 7.5), 150 mM NaCl, 1% NP-40, 5 mM EDTA, 1 mM phenylmethylsulfonyl fluoride, 50 mM NaF, 10 µg/ml leupeptin and 10 µg/ml apoprotein supplemented with protease inhibitors (Sigma), kept in ice for 40 minutes and centrifuged at 14,000rpm at 4°C for 20 minutes. The amounts of proteins were determined by a Bio-Rad protein assay to ensure equal protein loading before Western blot analysis. Fifty micrograms of cell lysate of each sample was electrophoresed through 10% or 8% polyacrylamide gels (BioRad), transferred onto blotting membranes (Polyscreen PVDF, NEN) and immunobloted for specific primary antibody in agitation at 4°C for 12-18 hours. The primary Abs were counterstained by a HRP-conjugated anti-IgG Ab (Amersham Biosciences) for 60 min at room temperature. Proteins were visualized by chemiluminescence (ECL Plus; Amersham Biosciences) and exposed to X-OMAT film (Eastman Kodak).
The antibodies used for immunoblot analysis are reported in Table 4.
The densitometric analysis was performed by Image J software and each data point is expressed as the mean ± s.d. of three independent experiments.

Immunoprecipitation. Cells were washed 2 times with ice PBS and then lysed in buffer containg 50 mM Tris- HCl (pH 7.5), 150 mM NaCl, 0,5% NP-40, 5 mM EDTA, 1 mM phenylmethylsulfonyl fluoride, 50 mM NaF, 10 µg/ml leupeptin and 10 µg/ml apoprotein supplemented with protease inhibitors (Sigma), kept in ice for 40 minutes and centrifuged at 14,000rpm at 4°C for 20 minutes. Following cell lysis , 500 µg of whole cell-lysates were incubated in agitation at 4°C for 8-12 h with antibody specific primary antibody. After the addition of Protein A/G-agarose beads, the incubation was continued in agitation at 4°C for 1 h. After washing, the immunoprecipitated proteins were electrophoresed through 8% polyacrylamide gels (BioRad), transferred onto blotting membranes (Polyscreen PVDF, NEN) and analyzed.

***Soluble and insoluble fraction*.** Cells were lysed in buffer containg 50 mM Tris- HCl (pH 7.5), 150 mM NaCl, 0.5% NP-40, 5 mM EDTA, 1 mM phenylmethylsulfonyl fluoride, 50 mM NaF, 10 µg ml-1 leupeptin and 10 µg ml-1 apoprotein supplemented with protease inhibitors (Sigma) and centrifuged at 14,000rpm at 4°C for 20 minutes. After centrifugation the soluble (supernatant) and insoluble (pellet) fraction were used in Western blot analysis using anti-Beclin1. The NP-40 insoluble pellet was dissolved in sample buffer 5X, boiled at 95°C for 5' and resolved onto 10% polyacrylammide gel.

Cell fractionation. IB3-1 cells were collected in cold buffer A (20 mM Tris-HCl (pH 7.4), 2 mM EDTA, 20 mM 2-ME, 1X PMSF, 1 {g/ml inhibitor protease cocktail), homogenized in Potter-Elvehjem pestle and glass tube (Sigma-Aldrich), and centrifuged at 2000 rpm for 15 min at 4°C to obtain nuclear pellets. Supernatants were collected as cytoplasmic fractions. Nuclear pellets were washed with buffer A and resuspended in buffer B (2 mM Na3VO4, 400 mM NaCl, 1 mM MgCl2, 1 mM EGTA, HEPES 10 mM (pH 7.9), 1 mM DTT, 1X PMSF, 1 µg/ml inhibitor protease cocktail) and incubated on ice for 50 min with occasional mixing to extract nuclear proteins. Nuclear extracts were cleared by centrifugation (7000 rpm, 15 min, 4°C), and supernatants were collected as nuclear fraction. Then, cytoplasmic and nuclear whole-cell fractions were analyzed by western blot analysis

Confocal microscopy. *Cell lines.* Treated or untreated cells were fixed in ice methanol for five minute at -20°C, washed 3 times with PBS, permeabilized with 0.5% Triton X-100 for ten minutes at room temprature, washed 3 times with PBS and incubated with primary antibodies over night at 4°C.
Human tissue sections. Five-micrometer frozen human lung tissue sections were fixed in acetone for 10 min. The sections were incubated for 2 h at room temperature with primary Abs.
Mice lung tissue. Seven-micrometer frozen lung tissue sections from each mice were fixed in acetone for 10 min. The sections were incubated for 2 h at room temperature with primary Abs.
The primary antibodies were counterstained by a Alexa fluor-conjugated anti-IgG Ab. and an LSM510 Zeiss confocal laser-scanning unit (Carl Zeiss, Germany) was used for detection.
The antibodies used for immunofluorescence analysis are reported in Table 4.

ROS detection. Cell lines were pulsed with 10 µM 5(and 6)-chloromethyl-2'7'-dichlorodihydrofluorescein diacetate acetyl ester (CM-H2DCFDA; Molecular Probes, Invitrogen), according to manufacturer suggestions, and analyzed with Wallac 1420 multilabel counter (PerkinElmer). Tissue sections (5 µm) of nasal mucosa and cells were incubated with 10 µM CMH2DCFDA, according to manufacturer suggestions, and an LSM510 Zeiss confocal laser-scanning unit (Carl Zeiss, Germany) was used for detection.

In situ detection of TG2 activity and protein. TG2 protein and enzyme activity were detected and analyzed by confocal microscopy. Briefly, for detection of TG2 enzyme activity, live cells were preincubated with TG2 assay buffer (965 µl of 100 mM Tris/HCl (pH 7.4), 25 µl of 200 mM CaCl2) for 15 min and then with the same TG2 assay buffer added with 10 µl of 10 mM biotinylated monodansylcadaverine (bio-MDC; Molecular Probes) for 1hat room temperature. The reaction was stopped with 25 mM EDTA for 5 min. The cells were then fixed in 4% paraformaldehyde for 10 min. The incorporation of labeled substrate was visualized by incubation with PE-conjugated streptavidin (Dako-Cytomation; 1:50) for 30 min. Control experiments included the omission of bio-MDC, as well as replacement of 200 mM CaCl2 with 200 mM EDTA. Blocking experiments were also conducted by incubating cells with the active site inhibitor R283 (250 µM) for 1 h before incubation with the substrates (bio-MDC or biotinylated peptides) and detection of TG2 enzymatic activity. Data were analyzed under fluorescence examination by LSM510 Zeiss confocal laser-scanning unit (Carl Zeiss).
The simultaneous detection of TG2 protein and activity was performed by incubating live cells with bio-MDC for1hat room temperature, according to the above described procedure, and then with anti-TG2 CUB 7402 mAb (NeoMarkers; 1:50) for 1hat room temperature. This was followed by simultaneous incubation with PE-conjugated streptavidin (DakoCytomation; 1:50) and FITC-conjugated rabbit anti-mouse Ig F(ab')2 (DakoCytomation; 1:20) for 1 h.
An LSM510 Zeiss confocal laser-scanning unit (Carl Zeiss, Germany) was used for detection. Of TG2 activity and protein on tissue sections

***Electron Microscopy*.** Cell culture monolayers were fixed for 15 min at 4 °C with 4% paraformaldehyde and 2.5% glutaraldehyde in 125 mM cacodylate buffer and stained with uranil and lead citrate and examined in a Leo912 electron microscope. We used Image J software (US National Institutes of Health) to quantify the number of autophagosomes per cell in 15–20 different randomly taken micrographs for each condition

ELISA . Human or murine TNF-a secretion was measured using the BD OptEIA TNF-a ELISA kit II (BD Biosciences). Measurements were performed at least in triplicate. Values were normalized to 10^6 cells; results were expressed as means ± SEM.

***Statistical analysis*.** Data are reported as arithmetic mean ±s.d.. Data distribution was analyzed for normality and statistical analysis performed using the one-way ANOVA. Significant differences are indicated in the figures. All data were obtained from independent measurements. Data were analyzed using SPSS 13 software. Statistical significance was defined as P value of <0.05.

Collagen gel mix. Liquid collagen rat-tail high concentration (9 mg/ml) was diluted to obtain a final concentration of 2mg/ml different percentage. We added in the mix an appropriate amount of medium 1X free and 10X free and we used NaOH 0,1 M to stabilize the pH around physiological value (pH 7.2). The was placed in incubator at 37°C and 5% CO_2 for 30 minutes. We added $2*10^5$ cell/ml of gel, or FITC-dextran (50µg/ml).

Neutrophils isolation. Peripheral blood (10 ml) was taken from healty human donors into BD Vacutainers containing K3EDTA. Neutrophils were freshly isolated by dextran sedimentation and centrifugation on Ficoll-Hypaque. The pellet of a density-gradient centrifugation containing neutrophil granulocytes and erythrocytes was diluted 1:1.3 with a high-molecular-weight dextran solution. After 2h erythrocytes had settled down and the neutrophil granulocytes containing supernatant was separated from the pellet. If necessary, red blood cells in the neutrophil-rich fraction were lysed with hypotonic saline. The neutrophils were washed twice with phosphate buffered saline (PBS) and then resuspended in RPMI 1640 containing 10% heat-treated fetal bovin serum (FBS). The obtained purified neutrophil granulocytes were used immediately after isolation.

Image analysis. The Image Pro Plus software, with a home-made macro tool, was used to analyze single cell motility. Math-lab software was used to fitting data.

Phalloidin staining. Treated or untreated cells were fixed paraforlmadehyde 4% for 15 minute at room temperature, washed 3 times with PBS, permeabilized with 0.5% Triton X-100 for ten minutes at room temperature, washed 3 times with PBS and incubated with FITC-phalloidin (1:100) for 30 minutes at RT. An LSM510 Zeiss confocal laser-scanning unit (Carl Zeiss, Germany) was used for detection.

TABLE 1. Clinical characteristics of Cystic Fibrosis patients

Patients #	1	2	3	4	5	6	7	8	9	10
Sex;	F	M	F	M	F	M	M	F	M	F
Age*	13, 2	14, 3	13,4	13, 1	13, 6	13,3	29	19	11	24
Age at diagnosis*	0, 6	0, 3	0, 8	2, 3	11, 0	1,5	7,2	2,0	0,4	7,0
Genotype	F508del/ F508del	F508del/ W1282X	F508del/ N1303K	F508del/ G542X	F508del/ F508del	F508del/ F508del	F508del/ G542X	F508del/ W1282X	F508del/ F508del	F508del/ W1282X
Pancreatic insufficiency	Yes	Yes	Yes	Yes	Yes	Yes	Yes	Yes	Yes	Yes
Chronic respiratory infection (PA)	Yes	No	No	No	Yes	Yes	No	Yes	Yes	No
Mean FEV1, % predicted	69	78	73	80	69	81	72	64	72	75

TABLE 2. Sequence of siRNA oligonucleotides

GENE NAME	OLIGO-SENSE(5'-3')	OLIGO-ANTISENSE (5'-3')
TG2	GCGUCGUGACCAACUACAAdTdT	UUGUAGUUGGUCACGACGCdGdG
PIASγ oligo#2	CAAGACAGGUGGAGUUGAUUU	pAUCAACUCCACCUGUCUUGUU
PIASγ oligo#4	AAGCUGCCGUUCUUUAAUAUU	pUAUUAAAGAACGGCAGCUUUU
BECLIN-1	AAGAUUGAAGACACAGGAGGC	GCCUCCUGUGUCUUCAAUCUU
CFTR oligo#1	CGUGUGUCUGUAAACUGAUGGCUAA	UUAGCCAUCAGUUUACAGACACAGC
CFTR oligo#2	CCCUUCUGUUGAUUCUGCUGACAAU	AUUGUCAGCAGAAUCAACAGAAGGG
CFTR oligo#3	GGCAUAGGCUUAUGCCUUCUCUUUA	UAAAGAGAAGGCAUAAGCCUAUGCC
SUMO-1 oligo#1	GGAUAGCAGUGAGAUU CACUUCAAA	UUUGAAGUGAAUCUCACUGCUA UCC
SUMO-1 oligo#2	GGUGUUCCAAUGAAUU CACUCAGGU	ACCUGAGUGAAUUCAUUGGAAC ACC
SUMO-1 oligo#3	GGAAGAAGAUGUGAUU GAAGUUUAU	AUAAACUUCAAUCACAUCUUCU UCC

TABLE 3. Sequence of primers used for Quantitative RT-PCR

GENE NAME	***FOWARD*** **PRIMER SEQUENCE (5'-3')**	***REVERSE*** **PRIMER SEQUENCE (5'-3')**
β-actin	ATTGCCGACAGGATGCAGAA	ACATCTGCTGGAAGGTGGACAG
ULK1	GTCCAGCTTTGACAGTCAGT	TCCCAGGACTCAGGATTCCA
ULK2	TGTTTCTAGGGTGTAGCTGG	CACCATCTACCCCAAGACCT
ATG5	AGTATCAGACACGATCATGG	TGCAAAGGCCTGACACTGGT
ATG6\BECLIN1	TGTCACCATCCAGGAACTCA	CTGTTGGCACTTTCTGTGGA
ATG7	CACTGTGAGTCGTCCAGGAC	CGCTCATGTCCCAGATCTCA
ATG8	CGTGGAGTCCGCGAAGATTC	AGGCATGAGGACAATGCACA
ATG14L	ATGAGCGTCTGGCAAATCTT	CCCATCGTCCTGAGAGGTAA
Bcl2	GCTGCTGGAGGCTGGGGAGA	CCCCCACAGGAACCCTCCTC
hVsps34	AAGCAGTGCCTGTAGGAGGA	TGTCGATGAGCTTTGGTGAG
hVsps15	TGGGACTGGCGGTCTGCACT	CGGGACGGGAAAACGCGTCA
Ambra-1	AACCCTCCACTGCGAGTTGA	TCTACCTGTTCCGTGGTTCTCC

TABLE 4. Primary antibody

ANTIBODY	COMPANY
phospho-p42/p44 MAP kinases	CELL SIGNALING
phospho-p65	CELL SIGNALING
β-actin (13E5)	CELL SIGNALING
PPARγ (E8)	SANTA CRUZ BIOTECNOLOGY
PIASγ(H75)	SANTA CRUZ BIOTECNOLOGY
Ubiquitin(FL76)	SANTA CRUZ BIOTECNOLOGY
Nε(γ-L-glutamyl)-L-lysine isopeptide (81DIC2)	COVOLAB
TG2 (H237)	SANTA CRUZ BIOTECNOLOGY
TG2 (CUB7402)	NEOMARKER
IkBα	SANTA CRUZ BIOTECNOLOGY
SUMO-1	SANTA CRUZ BIOTECNOLOGY
BECLIN-1	ABCAM
GFP(FL)	SANTA CRUZ BIOTECNOLOGY
hVps15\p150 (Nterm)	SANTA CRUZ BIOTECNOLOGY
Bcl-2(C2)	SANTA CRUZ BIOTECNOLOGY
HDAC-6	SANTA CRUZ BIOTECNOLOGY
N-Cor	SANTA CRUZ BIOTECNOLOGY
LC3	ABCAM
CFTR	ABCAM
AMBRA-1	ABCAM
p62	BD BIOSCIENCE
HA	BD BIOSCIENCE
αβ-TUBULIN	SIGMA
hVps34	SIGMA
Atg14L	ABCAM
LAMP1	ABCAM
EEA-1	ABCAM

REFERENCES

1. Ridley A, Schwartz M, Burridge K, Firtel R, Ginsberg M, Borisy G, Parsons J, Horwitz A. *Cell migration: integrating signals from front to back*. Science 2003, 302(5651):1704-1709.

2. Friedl P, Gilmour D. *Collective cell migration in morphogenesis, regeneration and cancer*. Nat Rev Mol Cell Biol 2009, 10(7):445-457.

3. Birchmeier C, Birchmeier W, Gherardi E, Vande Woude GF. *Met, metastasis, motility and more*. 2003 Nat Rev Mol Cell Biol.;4(12):915-25

4. Linder S. *The matrix corroded: podosomes and invadopodia in extracellular matrix degradation*. Trends Cell Biol 2007, 17(3):107-117

5. Destaing O, Saltel F, Géminard J, Jurdic P, Bard F. *Podosomes display actin turnover and dynamic self-organization in osteoclasts expressing actin-green fluorescent protein***.** Mol Biol Cell 2003, 14(2):407-416.

6. Hynes R. *Integrins: bidirectional, allosteric signaling machines***.** Cell 2002, 110(6):673-687

7. Friedl P, Bröcker E. *The biology of cell locomotion within three-dimensional extracellular matrix.* Cell Mol Life Sci 2000, 57(1):41-64.

8. Geiger B, Bershadsky A, Pankov R, Yamada K. *Transmembrane crosstalk between the extracellular matrix--cytoskeleton crosstalk***.** Nat Rev Mol Cell Biol 2001, 2(11):793-805.

9. Zamir E, Geiger B. *Molecular complexity and dynamics of cell-matrix adhesions.* J Cell Sci 2001, 114(Pt 20):3583-3590.

10. Legrand C, Gilles C, Zahm J, Polette M, Buisson A, Kaplan H, Birembaut P, Tournier J: *Airway epithelial cell migration dynamics. MMP-9 role in cell-extracellular matrix remodeling***.** J Cell Biol 1999, 146(2):517-529.

11. Golubovskaya V, Cance W: *Focal adhesion kinase and p53 signal transduction pathways in cancer***.** Front Biosci 2010, 15:901-912.

12. McEver RP. *Rolling back neutrophil adhesion*. Nat Immunol. 2010;11(4):282-4

13. Entschladen F, Drell Tt, Lang K, Masur K, Palm D, Bastian P, Niggemann B, Zaenker K: *Analysis methods of human cell migration*. Exp Cell Res 2005, 307(2):418-426.

14. Ratjen, F., and G. Doring.. *Cystic fibrosis*. Lancet 2003. 361: 681–689.

15. Osika, E., J. M. Cavaillon, K. Chadelat, M. Boule, C. Fitting, G. Tournier, and A. Clement. *Distinct sputum cytokine profiles in cystic fibrosis and other chronic inflammatory airway disease*. Eur. Respir. J. 1999, 14: 339–346.

16. Dubin, P. J., F. McAllister, and J. K. Kolls. *Is cystic fibrosis a TH17 disease?* Inflamm. Res. 2007, 56: 221–227.

17. Escotte, S., O. Tabary, D. Dusser, C. Majer-Teboul, E. Puchelle, and J. Jacquot. *Fluticasone reduces IL-6 and IL-8 production of cystic fibrosis bronchial epithelial cells via IKK-f kinase pathway*. Eur. Respir. J. 2003, 21: 574–581.

18. Rottner, M., C. Kunzelmann, M. Mergey, J. M. Freyssinet, and M. C. Martinez. *Exaggerated apoptosis and NF-KB activation in pancreatic and tracheal cystic fibrosis cells*. FASEB J. 2007, 21: 2939–2948.

19. Venkatakrishnan, A., A. A. Stecenko, G. King, T. R. Blackwell, K. Brigham, J. W. Christman, and T. S. Blackwell. *Exaggerated activation of nuclear factor-KB and altered IKB-beta processing in cystic fibrosis bronchial epithelial cells.* Am. J. Respir. Cell Mol. Biol. 2000, 23: 396 –403.

20. Becker, M. N., M. S. Sauer, M. S. Muhlebach, A. J. Hirsh, Q. Wu, M. W. Verghese, and S. H. Randell. *Cytokine secretion by cystic fibrosis airway epithelial cells*. Am. J. Respir. Crit. Care Med. 2004, 169: 645–653.

21. Hybiske, K., Z. Fu, C. Schwarzer, J. Tseng, J. Do, N. Huang, and T. E. Machen. *Effects of cystic fibrosis transmembrane conductance regulator and bF508CFTR on inflammatory response, ER stress, and* Ca^{2+} *of airway epithelia*. Am. J. Physiol 2007,. 293: L1250–L1260.

22. Perez, A., A. C. Issler, C. U. Cotton, T. J. Kelley, A. S. Verkman, and P. B. Davis. *CFTR inhibition mimics the cystic fibrosis inflammatory profile*. Am. J. Physiol. 2007, 292: L383–L395.

23. Verhaeghe, C., C. Remouchamps, B. Hennuy, A. Vanderplasschen, A. Chariot, S. Tabruyn, C. Oury, and V. Bours.. *Role of IKK and ERK pathways in intrinsic inflammation of cystic fibrosis airways*. Biochem. Pharmacol. 2007, 73: 1982–1994.

24. Maiuri, L., A. Luciani, I. Giardino, V. Raia, V. R. Villella, M. D'Apolito, M. Pettoello-Mantovani, S. Guido, C. Ciacci, M. Cimmino,Cexus ON, Londei M, Quaratino S. *Tissue transglutaminase activation modulates inflammation in cystic fibrosis via PPARy down-regulation*. J. Immunol. 2008, 180: 7697–7705.

25. Vij, N., S. Mazur, and P. L. Zeitlin. *CFTR is a negative regulator of NFKB mediated innate immune response*. PLoS ONE 2009, 4: e4664.

26. Sollid LM. *Coeliac disease: dissecting a complex inflammatory disorder*. Nat Rev Immunol 2002;2:647e55.

27. Sollid LM. *Molecular basis of coeliac disease*. Annu Rev Immunol 2000;18:53e81.

28. Shan L, Molberg O, Parrot I,. *Structural basis for gluten intolerance in celiac sprue*. Science 2002;297:2275e79.

29. Arentz-Hansen H, Korner R, Molberg O, Quarsten H, Vader W, Kooy YM, Lundin KE, Koning F, Roepstorff P, Sollid LM, McAdam SN. *The intestinal T cell response to alpha-gliadin in adult celiac disease is focused on a single deamidated glutamine targeted by tissue transglutaminase*. J Exp Med 2000;191:603–612.

30. van de Wal Y, Kooy Y, Van Veelen P, Pena S, Mearin L, Papadopoulos G, Koning F. *Selective deamidation by tissue transglutaminase strongly enhances gliadin-specific T cell reactivity*. J Immunol 1998;161:1585–1588.

31. Kim CY, Quarsten H, Bergseng E, Khosla C, Sollid LM. *Structural basis for HLA-DQ2-mediated presentation of gluten epitopes in celiac disease*. Proc Natl Acad Sci U S A 2004;101:4175–4179.

32. Reinke Y, Zimmer KP, Naim HY *Toxic peptides in Frazer's fraction interact with the actin cytoskeleton and affect the targeting and function of intestinal proteins*. Exp Cell Res. 2009;15;315(19):3442-52.

33. Malorni, W., M. G. Farrace, C. Rodolfo, and M. Piacentini. *Type 2 trans-glutaminase in neurodegenerative diseases: the mitochondrial connection*. Curr. Pharm. Des. 2008; 14: 278–288.

34. Beninati S, Piacentini M. *The transglutaminase family: an overview*: minireview article Amino Acids. 2004;26(4):367-72

35. Maiuri, L., C. Ciacci, I. Ricciardelli, L. Vacca, V. Raia, A. Rispo, M. Griffin, T. Issekutz, S. Quaratino, and M. Londei. *Unexpected role of surface transglutaminase type II in celiac disease*. Gastroenterology 2005;129: 1400 – 1413.

36. Siegel, M., and C. Khosla. *Transglutaminase 2 inhibitors and their therapeutic role in disease states.* Pharmacol. Ther. 2007;115: 232–245.

37. Skill, N. J., T. S. Johnson, I. G. Coutts, R. E. Saint, M. Fisher, L. Huang, A. M. El Nahas, R. J. Collighan, and M. Griffin. *Inhibition of transglutaminase activity reduces extracellular matrix accumulation induced by high glucose levels in proximal tubular epithelial cells*. J. Biol. Chem. 2004; 279: 47754 – 47762.

38. Yi, S. J., K. H. Kim, H. J. Choi, J. O. Yoo, H. I. Jung, J. A. Han, Y. M. Kim, I. B. Suh, and K. S. Ha. *[$Ca^{(2+)}$]-dependent generation of intracellular reactive oxygen species mediates maitotoxin-induced cellular responses in human umbilical vein endothelial cells*. Mol. Cells 2006; 21: 121–128.

39. Starosta, V., E. Rietschel, K. Paul, U. Baumann, and M. Griese. *Oxidative changes of bronchoalveolar proteins in cystic fibrosis*. Chest 2006; 129: 431–437.

40. Lorand, L., and R. M. Graham. *Transglutaminases: crosslinking enzymes with pleiotropic functions*. Nat. Rev. Mol. Cell Biol. 2003; 4: 140–156.

41. Meulmeester, E., and F. Melchior. *Cell biology: SUMO*. 2008; Nature 452: 709–711.

42. Geiss-Friedlander, R., and F. Melchior. *Concepts in sumoylation: a decade on*. Nat. Rev. Mol. Cell Biol. 2007; 8: 947–956

43. Mabb, A. M., and S. M. Wuerzberger-Davis. *PIASy mediates NEMO sumoylation and NF-KB activation in response to genotoxic stress.* Nat. Cell Biol. 2006; 8: 986–993.

44. Mu¨ller, S., and C. Hoege. *SUMO-1, ubiquitin's mysterious cousin*. Nat. Rev. Mol. Cell Biol. 2001; 2: 202–210.

45. Daynes, R. A., and D. C. Jones. *Emerging roles of PPARs in inflammation and immunity*. Nat. Rev. Immunol. 2002; 2: 748–759.

46. Belvisi, M. G., D. J. Hele, and M. A. Berrel.. *Peroxisome proliferatoractivated receptor y agonists as therapy for chronic airway inflammation.* Eur. J. Pharmacol. 2006; 533: 101–109.

47. Pascual, G., A. L. Fong, S. Ogawa, A. Gamliel, A. C. Li, V. Perissi, D. W. Rose, T. M. Willson, M. G. Rosenfeld, and C. K. Glass. *A SUMOylation-dependent pathway mediates transrepression of inflammatory response genes by PPAR-γ*. Nature 2005; 437: 759–763

48. Kim, D. S., S. S. Park, B. H. Nam, I. H. Kim, and S. Y. Kim. *Reversal of drug resistance in breast cancer cells by transglutaminase 2 inhibition and nuclear factor-KB inactivation.* Cancer Res. 2006; 66: 10936–10943

49. Kopito, R. R. *Aggresomes, inclusion bodies and protein aggregation.* Trends Cell Biol. 2000; 10: 524–530.

50. Kawaguchi, Y., J. J. Kovacs, A. McLaurin, J. M. Vance, A. Ito, and T. P. Yao. *The deacetylase HDAC6 regulates aggresome formation and cell viability in response to misfolded protein stress.* Cell 2003; 115: 727–738.

51. Sha, Y., Pandit, L., Zeng, S. & Eissa, N. T. *A critical role of CHIP in the aggresome pathway*. Mol. Cell. Biol. 2009; 29, 116–128.

52. Bence, N. F., Sampat, R. M. & Kopito, R. R. *Impairment of the ubiquitin-proteasome system by protein aggregation*. Science 2001; 292, 1552–1555.

53. Fu, L. & Sztul, E. *ER-associated complexes (ERACs) containing aggregated cystic fibrosis transmembrane conductance regulator (CFTR) are degraded by autophagy*. Eur. J. Cell Biol. 2009; 88, 215–226.

54. Luciani A, Villella VR, Vasaturo A, Giardino I, Raia V, Pettoello-Mantovani M, D'Apolito M, Guido S, Leal T, Quaratino S, Maiuri L. *SUMOylation of tissue transglutaminase as link between oxidative stress and inflammation*. J. Immunol. 2009; 183, 2775–2784.

55. Trudel S, Kelly M, Fritsch J, Nguyen-Khoa T, Thérond P, Couturier M, Dadlez M, Debski J, Touqui L, Vallée B, Ollero M, Edelman A, Brouillard F. *Peroxiredoxin 6 fails to limit phospholipid peroxidation in lung from Cftr-knockout mice subjected to oxidative challenge*. PLoS One 2009; 4, e6075.

56. Mizushima, N., Levine, B., Cuervo, A. M. & Klionsky, D. J. *Autophagy fights disease through cellular self-digestion*. Nature 2008; 28, 1069–1075.

57. Moreau, K., Luo, S. & Rubinsztein, D. C. *Cytoprotective roles for autophagy*. Curr. Opin. Cell Biol. 2010; 22, 206–211.

58. Korolchuk, V. I., Mansilla, A., Menzies, F. M. & Rubinsztein, D. C. *Autophagy inhibition compromises degradation of ubiquitin–proteasome pathway substrates*. Mol. Cell 2009; 33, 517–527.

59. Kirkin, V., McEwan, D. G., Novak, I. & Dikic, I. *A role for ubiquitin in selective autophagy*. Mol. Cell 2009; 34, 259–269.

60. Sinha, S. & Levine, B. *The autophagy effector Beclin 1: a novel BH3-only protein*. Oncogene 2008; 27, S137–S148.

61. Maiuri, M. C., Criollo, A. & Kroemer, G. *Crosstalk between apoptosis and autophagy within the Beclin 1 interactome*. EMBO J. 2010; 29, 515–516.

62. He, C. & Levine, B. *The Beclin 1 interactome*. Curr. Opin. Cell Biol. 2010; 22, 140–149.

63. Klionsky, D. J., Abeliovich, H., Agostinis, P., Agrawal, D. K. & Aliev, G. *Guidelines for the use and interpretation of assays for monitoring autophagy in higher eukaryotes*. Autophagy 2008; 4,151–175.

64. Mizushima, N., Yoshimori, T. & Levine, B. *Methods in mammalian autophagy research*. Cell 2010; 140, 313–326.

65. Matsunaga, K., Saitoh T, Tabata K, Omori H, Satoh T, Kurotori N, Maejima I, Shirahama-Noda K, Ichimura T, Isobe T, Akira S, Noda T, Yoshimori I. *Two Beclin 1-binding proteins, Atg14L and Rubicon, reciprocally regulate autophagy at different stages*. Nature Cell Biol. 2009; 11, 385–396.

66. Zhong, Y., Wang QJ, Li X, Yan Y, Backer JM, Chait BT, Heintz N, Yue Z. *Distinct regulation of autophagic activity by Atg14L and Rubicon associated with Beclin 1-phosphatidylinositol-3-kinase complex*. Nature Cell Biol. 2009; 11, 468–476.

67. Axe EL, Walker SA, Manifava M, Chandra P, Roderick HL, Habermann A, Griffiths G, Ktistakis NT. *Autophagosome formation from membrane compartments enriched in phosphatidylinositol 3-phosphate and dynamically connected to the endoplasmic reticulum*. J. Cell Biol. 2008; 182, 685–701

68. Hayashi-Nishino, M., Fujita N, Noda T, Yamaguchi A, Yoshimori T, Yamamoto A. *A subdomain of the endoplasmic reticulum forms a cradle for autophagosome formation.* Nature Cell Biol. 2009; 11, 1433–1437.

69. Maiuri MC, Le Toumelin G, Criollo A, Rain JC, Gautier F, Juin P, Tasdemir E, Pierron G, Troulinaki K, Tavernarakis N, Hickman JA, Geneste O, Kroemer G. *Functional and physical interaction between Bcl-XL and a BH3-like domain in Beclin-1*. EMBO J. 2007; 26, 2527–2539.

70. Pattingre S, Tassa A, Qu X, Garuti R, Liang XH, Mizushima N, Packer M, Schneider MD, Levine B *Bcl-2 antiapoptotic proteins inhibit Beclin 1-dependent autophagy*. Cell 2005; 23, 927–939 .

71. Liang, C., Lee JS, Inn KS, Gack MU, Li Q, Roberts EA, Vergne I, Deretic V, Feng P, Akazawa C, Jung JU. *Beclin1-binding UVRAG targets the class C Vps complex to coordinate autophagosome maturation and endocytic trafficking*. Nature Cell Biol. 2008; 10, 776–787.

72. Raia V, Maiuri L, Ciacci C, Ricciardelli I, Vacca L, Auricchio S, Cimmino M, Cavaliere M, Nardone M, Cesaro A, Malcolm J, Quaratino S, Londei M. *Inhibition of p38 mitogen activated protein kinase controls airway inflammation in cystic fibrosis*. Thorax 2005; 60: 773–780.

73. Legssyer, R., F. Huaux, J. Lebacq, M. Delos, E. Marbaix, P. Lebecque, D. Lison, B. J. Scholte, P. Wallemacq, and T. Leal. 2006. *Azithromycin reduces spontaneous and induced inflammation in bF508 cystic fibrosis mice*. Respir. Res. 7: 134

74. Spencer, B., Potkar R, Trejo M, Rockenstein E, Patrick C, Gindi R, Adame A, Wyss-Coray T, Masliah E. *Beclin 1 gene transfer activates autophagy and ameliorates the neurodegenerative pathology in α-synuclein models of Parkinson's and Lewy body diseases.* J. Neurosci. 2009; 29, 13578–13588.

75. Stocker, A. G., Kremer KL, Koldej R, Miller DS, Anson DS, Parsons DW. *Single-dose lentiviral gene transfer for lifetime airway gene expression.* J. Gene Med. 11, 861–867 (2009).

76. Stark HJ, Szabowski A, Fusenig NE, Maas-Szabowski N. *Organotypic cocultures as skin equivalents: A complex and sophisticated in vitro system.* 2004 Biol Proced Online.;6:55-60.

77. Maiuri L, Ciacci C, Ricciardelli I, Vacca L, Raia V, Auricchio S, Picard J, Osman M, Quaratino S, Londei M. *Association between innate response to gliadin and activation of pathogenic T cells in coeliac disease*. Lancet 2003;362:30e7

78. Barone MV, Gimigliano A, Castoria G, Paolella G, Maurano F, Paparo F, Maglio M, Mineo A, Miele E, Nanayakkara M, Troncone R, Auricchio S. *Growth factor-like activity of gliadin, an alimentary protein: implications for coeliac disease*. Gut 2007;56:480e8

79. Matysiak-Budnik T, Candalh C, Dugave C, et al. Alterations of the intestinal transport and processing of gliadin peptides in celiac disease. Gastroenterology 2003;125:696e707.

80. Lu A, Tebar F, Alvarez-Moya B, et al. *A clathrin-dependent pathway leads to KRas signaling on late endosomes en route to lysosomes.* J Cell Biol 2009;6:863e79.

81. Taylor, J. P., F. Tanaka, J. Robitschek, C. M. Sandoval, A. Taye, S. Markovic-Plese, and K. H. Fischbeck. *Aggresomes protect cells by enhancing the degradation of toxic polyglutamine containing protein*. Hum. Mol. Genet. 2003; 12: 749- 757.

82. Johnston, J. A., C. L. Ward, and R. R. Kopito. *Aggresomes: a cellular response to misfolded proteins*. J. Cell Biol. 1998*;*143: 1883–1898.

83. Maiuri, C., Zalckvar, E., Kimchi, A. & Kroemer, G. *Self-eating and self-killing: crosstalk between autophagy and apoptosis.* Nature Rev Mol. Cell. Biol. 2007; 8, 741–752.

84. Hara, T., Nakamura K, Matsui M, Yamamoto A, Nakahara Y, Suzuki-Migishima R, Yokoyama M, Mishima K, Saito I, Okano H, Mizushima N. *Suppression of basal autophagy in neural cells causes neurodegenerative disease in mice*. Nature 2006; 441, 885–889.

85. Tebbenkamp, A. T. & Borchel, D. R. *Protein aggregate characterization in models of neurodegenerative disease.* Methods Mol. Biol. 2009; 566, 85–91.

86. Martínez, A, Portero-Otin, M., Pamplona, R. & Ferrer, I. *Protein targets of oxidative damage in human neurodegenerative diseases with abnormal protein aggregates*. Brain Pathol. 2010; 20, 281–297.

87. Luciani A, Villella VR, Esposito S, Brunetti-Pierri N, Medina D, Settembre C, Gavina M, Pulze L, Giardino I, Pettoello-Mantovani M, D'Apolito M, Guido S, Masliah E, Spencer B, Quaratino S, Raia V, Ballabio A, Maiuri L. *Defective CFTR induces aggresome formation and lung inflammation in cystic fibrosis through ROS-mediated autophagy inhibition*. Nat Cell Biol. 2010;12(9):863-75

88. Luciani A, Villella VR, Vasaturo A, Giardino I, Pettoello-Mantovani M, Guido S, Cexus ON, Peake N, Londei M, Quaratino S, Maiuri L. *Lysosomal accumulation of gliadin p31-43 peptide induces oxidative stress and tissue transglutaminase-mediated PPARgamma downregulation in intestinal epithelial cells and coeliac mucosa.* Gut. 2010;59(3):311-9.

APPENDIX

Publications

- Luciani A & Villella VR, Esposito S, Brunetti-Pierri N, Medina D, Settembre C, Gavina M, Pulze L, Giardino I, Pettoello-Mantovani M, D'Apolito M, Guido S, Masliah E, Spencer B, Quaratino S, Raia V, Ballabio A, Maiuri L. *Defective CFTR induces aggresome formation and lung inflammation in cystic fibrosis through ROS-mediated autophagy inhibition*. Nat Cell Biol. 2010;12(9):863-75

- Luciani A, Villella VR, Vasaturo A, Giardino I, Pettoello-Mantovani M, Guido S, Cexus ON, Peake N, Londei M, Quaratino S, Maiuri L. *accumulation of gliadin p31-43 peptide induces oxidative stress and tissue transglutaminase-mediated PPARgamma downregulation in intestinal epithelial cells and coeliac mucosa.* Gut. 2010;59(3):311-9.

- Luciani A, Villella VR, Vasaturo A, Giardino I, Raia V, Pettoello-Mantovani M, D'Apolito M, Guido S, Leal T, Quaratino S, Maiuri L. *SUMOylation of tissue transglutaminase as link between oxidative stress and inflammation*. J. Immunol. 2009; 183, 2775–2784.

- Maiuri, L., A. Luciani, I. Giardino, V. Raia, V. R. Villella, M. D'Apolito, M. Pettoello-Mantovani, S. Guido, C. Ciacci, M. Cimmino,Cexus ON, Londei M, Quaratino S. *Tissue transglutaminase activation modulates inflammation in cystic fibrosis via PPARy down-regulation*. J. Immunol. 2008, 180: 7697–7705.

Experiences in foreign laboratories

- University of Southampton School of Medicine, Cancer Science Division, General Hospital, Southampton, UK. Scientific collaboration for my PhD project, under supervision of Prof.ssa Sonia Quaratino and Dott. Nick Peake and in collaboration with Prof. Luigi Maiuri of European Institute for Research in Cystic Fibrosis and Prof. S. Guido of the University of Naples (Oct 2009-Jan 2010).

nature cell biology

Defective CFTR induces aggresome formation and lung inflammation in cystic fibrosis through ROS-mediated autophagy inhibition

Alessandro Luciani[1,2,11], Valeria Rachela Villella[2,11], Speranza Esposito[2,3], Nicola Brunetti-Pierri[4,5], Diego Medina[4], Carmine Settembre[4], Manuela Gavina[1], Laura Pulze[1], Ida Giardino[6], Massimo Pettoello-Mantovani[3], Maria D'Apolito[3], Stefano Guido[2], Eliezer Masliah[7], Brian Spencer[7], Sonia Quaratino[8], Valeria Raia[9,12], Andrea Ballabio[4,10,12] and Luigi Maiuri[1,3,12]

Accumulation of unwanted/misfolded proteins in aggregates has been observed in airways of patients with cystic fibrosis (CF), a life-threatening genetic disorder caused by mutations in the gene encoding the cystic fibrosis transmembrane conductance regulator (CFTR). Here we show how the defective CFTR results in defective autophagy and decreases the clearance of aggresomes. Defective CFTR-induced upregulation of reactive oxygen species (ROS) and tissue transglutaminase (TG2) drive the crosslinking of beclin 1, leading to sequestration of phosphatidylinositol-3-kinase (PI(3)K) complex III and accumulation of p62, which regulates aggresome formation. Both CFTR knockdown and the overexpression of green fluorescent protein (GFP)-tagged-CFTR^{F508del} induce beclin 1 downregulation and defective autophagy in non-CF airway epithelia through the ROS–TG2 pathway. Restoration of beclin 1 and autophagy by either beclin 1 overexpression, cystamine or antioxidants rescues the localization of the beclin 1 interactome to the endoplasmic reticulum and reverts the CF airway phenotype *in vitro*, *in vivo* in *Scnn1b*-transgenic and *Cftr*^{F508del} homozygous mice, and in human CF nasal biopsies. Restoring beclin 1 or knocking down p62 rescued the trafficking of CFTR^{F508del} to the cell surface. These data link the CFTR defect to autophagy deficiency, leading to the accumulation of protein aggregates and to lung inflammation.

Autophagy is a cytoprotective mechanism for the degradation of misfolded/polyubiquitylated proteins and damaged organelles through lysosome-mediated self-digestion[1,2]. Autophagy is important in clearing protein aggregates after overload of polyubiquitylated proteins[3–5]. The accumulation of unwanted/misfolded protein aggregates has been described in several human disorders, such as neurodegenerative diseases[6,7], myopathies[8] and cancer[9]. Recently we described the presence of peroxisome proliferator-activated receptor (PPAR)-γ in aggresomes in CF airways[10]. CF is caused by mutations in the *CFTR* gene[11] and the mutant CFTR^{F508del} has been described as the prototype of a misfolded aggresome-prone protein[12–14].

Sequestration of the anti-inflammatory PPAR-γ into aggresomes, mediated by the increased TG2 levels, contributes to the lung inflammation in CF[15]. This is the result of ROS-mediated TG2 SUMOylation inducing the crosslinking, ubiquitylation and aggresome sequestration of several target proteins[15]. Because oxidative stress and accumulation of protein aggregates are features of CF airway epithelia[10,15,16], we speculated that the accumulation of aggresomes in CF is due to defective autophagy.

Here we demonstrate how defective CFTR drives autophagy inhibition in mouse and human CF airway epithelia by means of the ROS–TG2 pathway, with sequestration of beclin 1 interactome, a key player of autophagosome formation[17–19], in the aggresomes. Rescuing beclin 1 and autophagy restores CFTR trafficking and damps down inflammation. Our results provide evidence that defective autophagy has a critical function in CF pathogenesis and suggest that drugs restoring beclin 1 and autophagy are potentially effective in the treatment of CF.

RESULTS

Human and mouse CF airway epithelia have defective autophagy

We cultured human CF airway epithelial IB3-1 or CFBE41o$^-$ cells, carrying F508del/W1282X and F508del/F508del mutations, respectively,

[1]European Institute for Research in Cystic Fibrosis, San Raffaele Scientific Institute, Milan 20132, Italy. [2]Department of Chemical Engineering, Federico II University, Naples 80125, Italy. [3]Institute of Pediatrics, University of Foggia, Foggia 71100, Italy. [4]Telethon Institute of Genetics and Medicine (TIGEM), Naples 80131, Italy. [5]Department of Pediatrics, Federico II University, Naples 80131, Italy. [6]Department of Laboratory Medicine, University of Foggia, Foggia 71100, Italy. [7]Departments of Neurosciences, University of California, San Diego, La Jolla, CA 92093-0624, USA. [8]Cancer Research UK Oncology Unit, University of Southampton, Southampton, SO16 6YD, U.K. [9]Cystic Fibrosis Unit, Department of Pediatrics, Federico II University, Naples 80131, Italy. [10]Medical Genetics, Department of Pediatrics, Federico II University, Naples 80131, Italy.
[11]These authors contributed equally to this work
[12]Correspondence should be addressed to L.M., A.B. or V.R. (email: maiuri@unina.it; ballabio@tigem.it; raia@unina.it)

Received 6 May 2010; accepted 29 July 2010; published online 15 August 2010; DOI:10.1038/ncb2090.

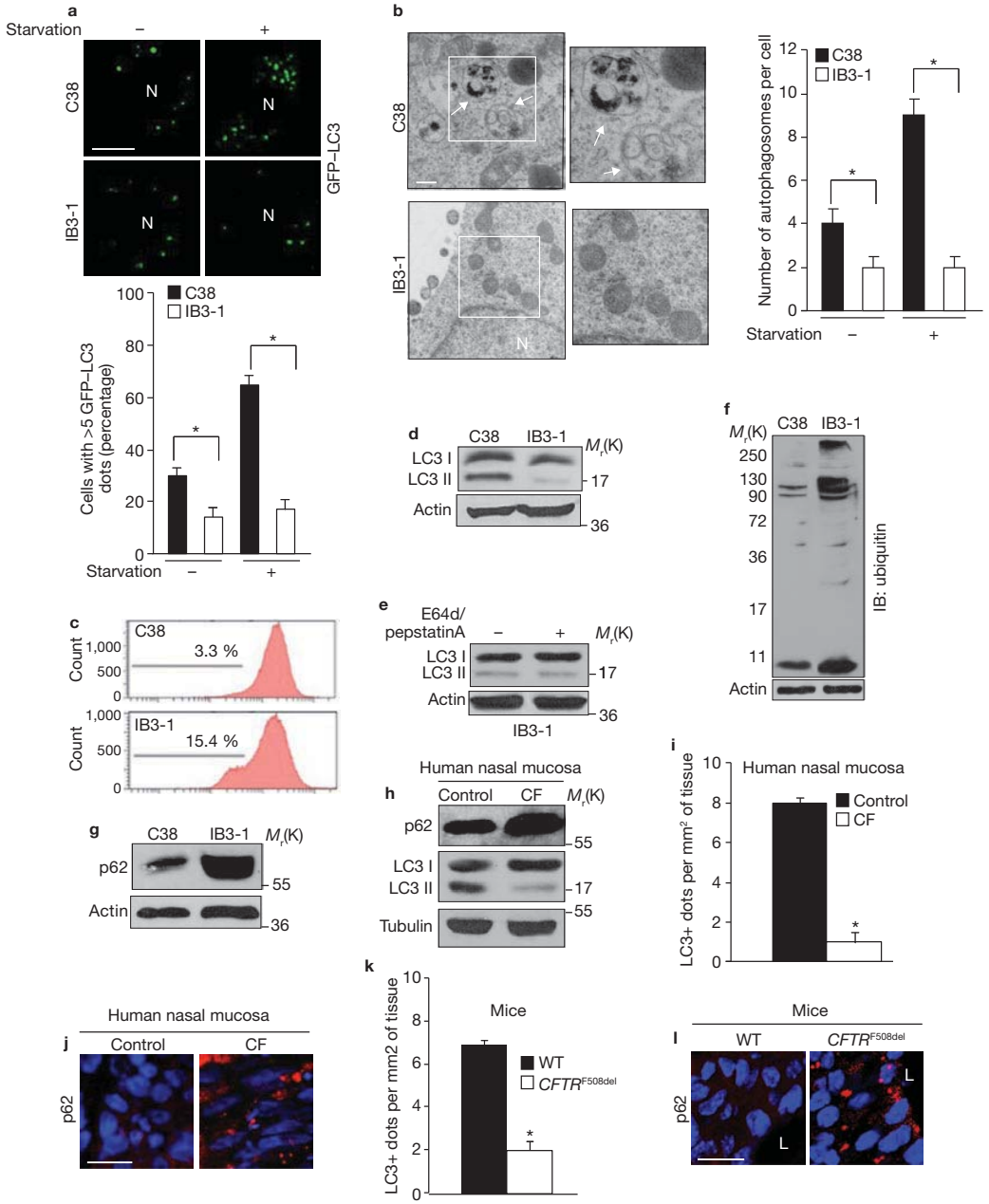

Figure 1 Autophagy is defective in human and mice CF airway epithelia. C38 and IB3-1 cells transfected with GFP–LC3 plasmid in nutrient-rich or starvation medium. (**a**) Top: confocal microscopy of GFP. N, nucleus. Scale bar, 10 μm. Bottom: percentage of cells containing more than five GFP–LC3 punctate dots per cell. Means ± s.d. ($n = 5$). Asterisk, $P < 0.001$ versus C38 cells; analysis of variance (ANOVA). (**b**) Left: electron microscopy of starved C38 and IB3-1 cells. The right-hand images are higher magnifications showing areas enriched in autophagosomes in C38 cells (arrows) and perinuclear mitochondria in IB3-1 cells. N, nucleus. Scale bar, 250 nm. Right: numbers of autophagosomes per cell counted in 20 cells per experiment. Means ± s.d. for three independent experiments. Asterisk, $P < 0.001$ versus C38 cells; ANOVA. (**c**) Fluorescence-activated cell sorting (FACS) analysis after staining with fluorescent dye $DiOC_6$ in starved C38 and IB3-1 cells. (**d**, **e**) Immunoblot of LC3 in starved C38 and IB3-1 cells (**d**) and IB3-1 cells (**e**) after incubation with E64d and pepstatin A. (**f**, **g**) Immunoblots (IB) of polyubiquitin (**f**) and p62 (**g**) in starved C38 and IB3-1 cells. Uncropped images of blots are shown in Supplementary Information, Fig. S10. (**h**) Immunoblot of LC3 and p62 in control ($n = 10$) and CF ($n = 10$) human nasal mucosa. (**i**) Number of LC3-positive dots (per 10^4 mm^{-2} of mucosa) in control ($n = 10$) and CF ($n = 10$) human nasal mucosa. Means ± s.d. Asterisk, $P < 0.01$ versus controls; ANOVA. (**j**) Confocal microscopy of p62 in control and CF human nasal mucosa. Representative images from ten patients with CF. Nuclei counterstained with 4′,6-diamidino-2-phenylindole (DAPI; blue). Scale bar, 10 μm. (**k**) Number of LC3-positive dots in lung tissues from wild-type (WT) and *Cftr*^{F508del} mice. Means ± s.d. for lung tissues from ten mice per group. Asterisk, $P < 0.001$ versus WT mice; ANOVA. (**l**) Confocal microscopy of p62 in WT and *Cftr*^{F508del} homozygous mice. Representative staining from at least five airway epithelial areas per mouse ($n = 10$ mice per group). L, lumen. Nuclei counterstained with DAPI (blue). Scale bar, 10 μm. β-Actin was used as loading control for immunoblot analysis of cells, and αβ-tubulin for nasal mucosa. All expreriments were repeated three times. Densitometric analysis of blots is shown in Supplementary Information, Fig. S9.

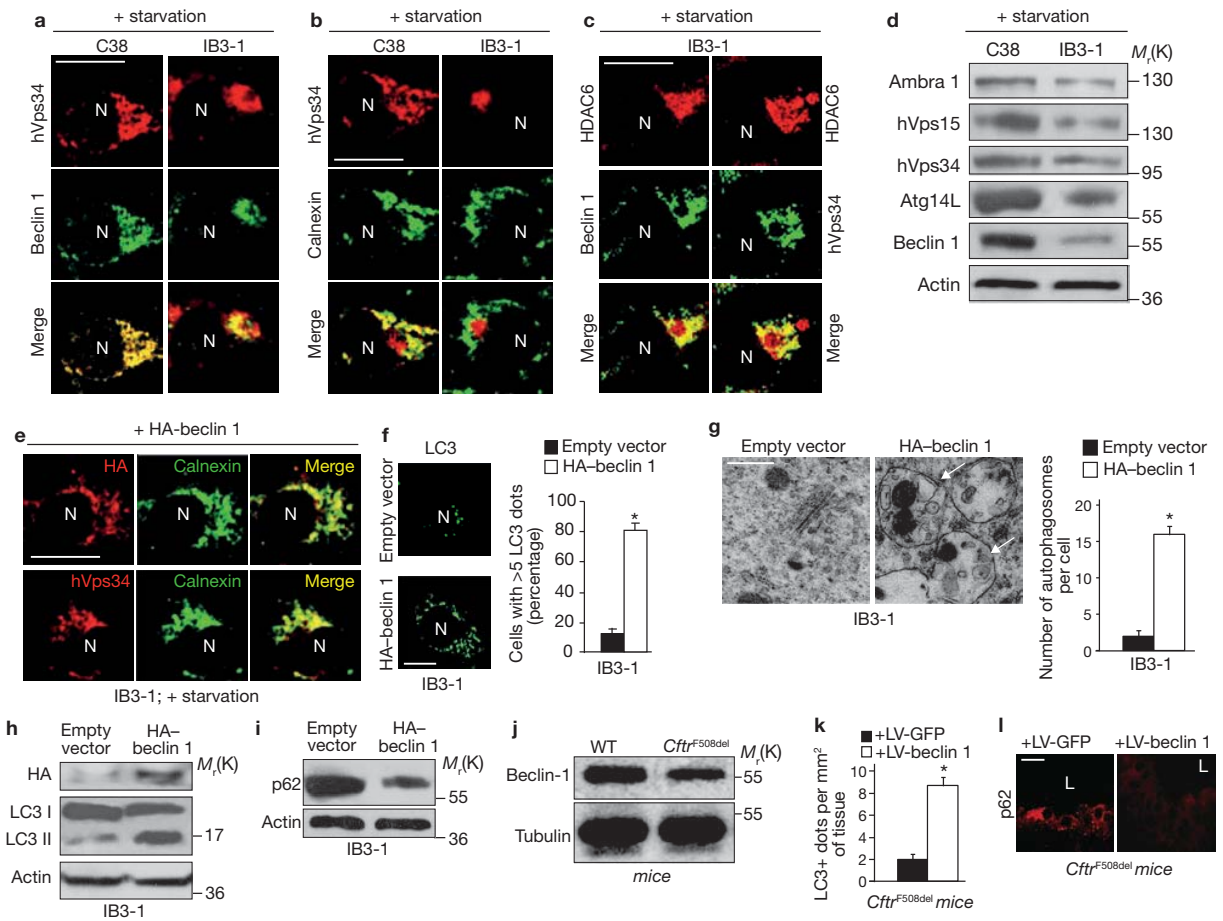

Figure 2 Sequestration of beclin 1 interactome in aggresomes drives defective autophagy in CF airway epithelia. (**a**–**d**) Starved C38 and IB3-1 cells. (**a**–**c**) Confocal microscopy images of beclin 1 (green) and hVps34 (red) (**a**), calnexin (green) and hVps34 (red) (**b**), and beclin 1 (green) and HDAC6 (red) (**c**, left) or hVps34 (green) and HDAC6 (red) (**c**, right). N, nucleus. Scale bar, 10 μm. Yellow indicates co-localization. (**d**) Immunoblot of Ambra1, hVps15, hVps34, Atg14L and beclin 1. Uncropped images of blots are shown in Supplementary Information, Fig. S10. (**e**–**i**) Starved IB3-1 cells transfected with either HA-tagged human beclin 1 or the empty vector. (**e**) Confocal microscopy images of HA (red) and calnexin (green) (top) or hVps34 (red) and calnexin (green) (bottom). Yellow indicates co-localization. N, nucleus. Scale bar, 10 μm. (**f**) Left: confocal images of LC3-positive dots. N, nucleus. Scale bar, 10 μm. Right: percentage of cells containing more than five LC3-positive dots. At least 60 cells were counted in each experiment. Means ± s.d. for three independent experiments. Asterisk, $P < 0.001$ versus cells transfected with the empty vector; ANOVA. (**g**) Left: electron microscopy of HA–beclin 1-transfected IB3-1 cells shows areas enriched in autophagosomes (arrows). Scale bar, 250 nm. Right: number of autophagosomes per cell; 20 cells were counted in each experiment. Means ± s.d. for three independent experiments. Asterisk, $P < 0.001$ versus cells transfected with the empty vector; ANOVA. (**h**) Immunoblot of HA and LC3. (**i**) Immunoblot of p62. Uncropped images of blots are shown in Supplementary Information, Fig. S10. (**j**) Immunoblot of beclin 1 in WT and *Cftr*^{F508del} mice. Representative of seven mice for each group. (**k**, **l**) *Cftr*^{F508del} mice ($n = 3$ per group) were administered intranasally with a lentiviral vector encoding beclin 1 (LV-beclin 1) or GFP (LV-GFP). (**k**) LC3-positive dots per mm^2 of lung tissues. Means ± s.d. for lung tissues from three mice per group. (**l**) Confocal microscopy micrographs of p62. L, lumen. Representative stainings from at least five airway epithelial areas per mouse. Scale bar, 10 μm. β-Actin was used as loading control for immunoblot analysis of cells, and αβ-tubulin for mouse tissue. Densitometric analysis of blots and quantitative measurement of co-localizations are shown in Supplementary Information, Fig. S9.

and the isogenic stably rescued C38, S9 (refs 10, 15) or bronchial epithelial 16HBE14o$^-$ cells[10,15], under nutrient starvation to stimulate autophagy[20,21]. Transfection of GFP–LC3, a marker of autophagosomes[21], revealed a larger number of GFP–LC3 puncta in C38 cells than in IB3-1 cells ($P < 0.001$) (Fig. 1a). Transmission electron microscopy showed autophagosomes containing mitochondria and cellular organelles in C38 cells but rarely in IB3-1 cells (Fig. 1b; Supplementary Information, Fig. S1a). Increased mitochondrial membrane depolarization was observed in IB3-1 cells but not in C38 cells (Fig. 1c).

An increase in LC3 II, the lipidated product of LC3 (refs 20, 21), was observed in C38 cells but not in IB3-1 cells under starvation (Fig. 1d). E64d and pepstatin A, inhibitors of the lysosomal proteases (Fig. 1e), and also chloroquine, a weak base disrupting lysosomal functions[21] (Supplementary Information, Fig. S1b), failed to increase LC3 II, thus indicating that decreased LC3 II levels were not due to lysosomal degradation of LC3.

Defective autophagy in IB3-1 cells was also revealed by the increased pool of polyubiquitylated proteins (Fig. 1f) and the accumulation of p62 (Fig. 1g; Supplementary Information, Fig. S1c), a LC3-binding and ubiquitin-binding protein, that accumulates in intracellular aggregates under defective autophagy[3,20,21]. IB3-1 cells were also resistant to rapamycin, a known inducer of autophagy[20,21] (Supplementary Information,

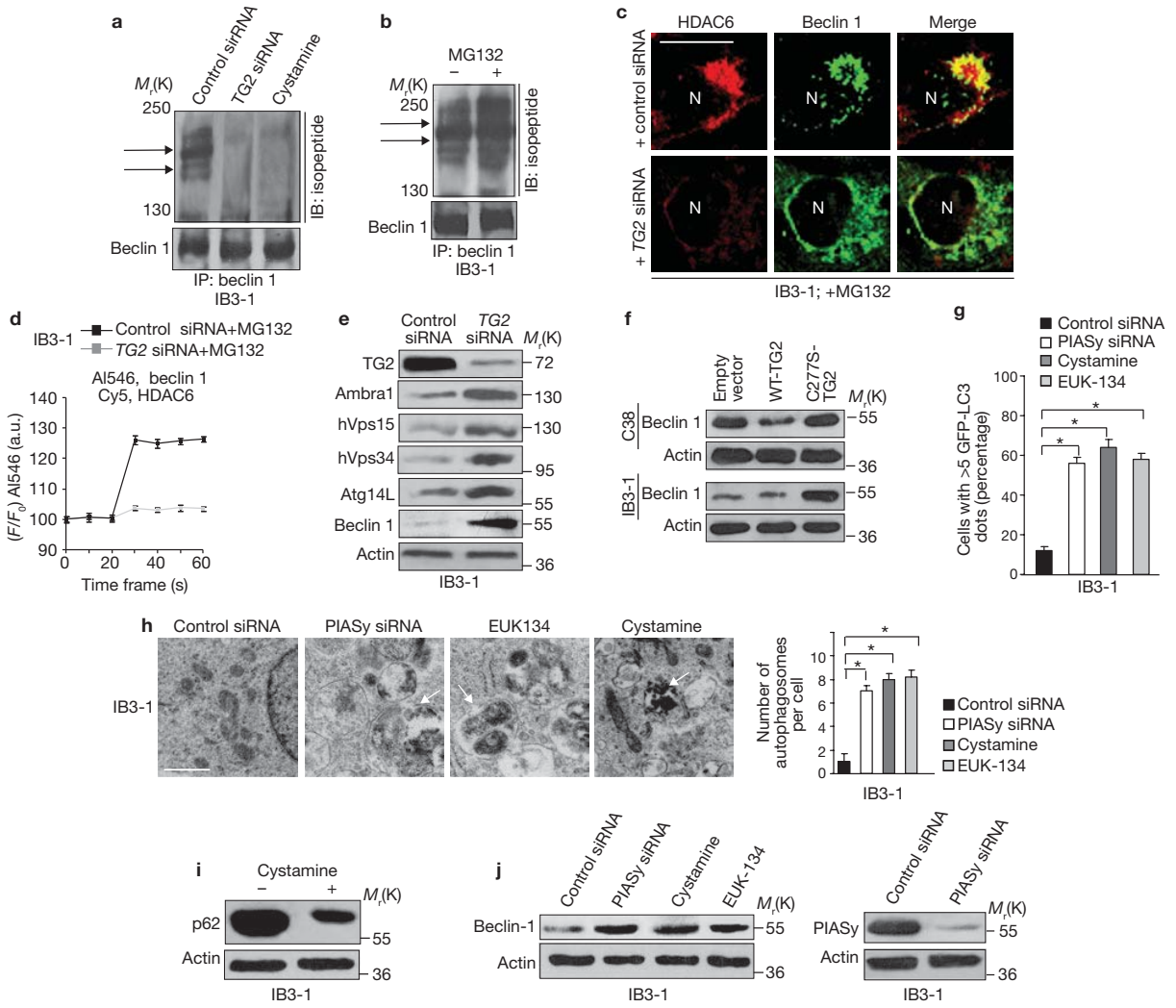

Figure 3 TG2-mediated crosslinking of beclin 1 induces aggresome sequestration of beclin 1 interactome and drives defective autophagy in CF airway epithelial cells. (**a**) IB3-1 cells cultured with 250 μM cystamine or transfected with either 50 nM human TG2 siRNA or scrambled oligonucleotides. IP, immunoprecipitation; IB, immunoblot. (**b**) IB3-1 cells cultured with the proteasome inhibitor MG132 (50 μM). (**c**, **d**) IB3-1 cells transfected with either human TG2 siRNA or scrambled oligonucleotides followed by incubation with MG132. (**c**) Cells immunostained with anti-beclin 1 (green) and anti-HDAC-6 (red) antibodies. Yellow indicates co-localization. N, nucleus. Scale bar, 10 μm. (**d**) FRET analysis of beclin 1-Alexa 546 (Al546) fluorescence after HDAC6-Cy5 photobleaching. F/F_0 indicates the post-bleaching/pre-bleaching fluorescence ratio of Al546/Cy5. (**e**) IB3-1 cells were transfected with either human TG2 siRNA or scrambled oligonucleotides. Immunoblot of TG2, Ambra-1, hVps15, hVps34, Atg14L and beclin 1 in IB3-1 cells grown in starvation. Uncropped images of blots are shown in Supplementary Information, Fig. S10. (**f**) IB3-1 and C38 cells were transfected with either 1 μg of pLPCX-WT-TG or pLPCX-Cys277Ser-TG or the empty vector. Immunoblot of beclin 1. Uncropped images of blots are shown in Supplementary Information, Fig. S10. (**g**, **h**) IB3-1 cells were treated with cystamine or 10 mM EUK-134 or transfected with either 50 nM human PIASy siRNA or scrambled oligonucleotides. (**g**) Percentage of cells containing more than five GFP–LC3 punctate dots. Means ± s.d. for three independent experiments. Asterisk, $P < 0.001$ versus control; ANOVA. (**h**) Left: electron micrographs of IB3-1 cells showing areas enriched in autophagosomes (arrows) on PIASy gene silencing, EUK-134 or cystamine. Scale bar, 100 nm. Right: number of autophagosomes per cell counted in 20 cells per experiment. Means ± s.d. for three independent experiments. Asterisk, $P < 0.001$ versus control; ANOVA. (**i**) IB3-1 cells treated with cystamine. Immunoblot of p62. (**j**) IB3-1 cells treated with cystamine or EUK-134 or transfected with human PIASy siRNA or scrambled oligonucleotides. Immunoblot of beclin 1 (left) and PIASy (right). Uncropped images of blots are shown in Supplementary Information, Fig. S10. The experiments were repeated three times. β-actin was used as loading control for all blots. Densitometric analysis of blots and quantitative measurement of co-localizations are shown in Supplementary Information, Fig. S9.

Fig. S1d). CFBE41o$^-$ cells behaved in a similar manner to IB3-1 cells, whereas both S9 and 16HBE14o$^-$ cells behaved in a similar manner to the C38 cell line (data not shown).

Defective basal autophagy was observed in human and mouse CF airways. Nasal polyp biopsies from patients with severe CF ($n = 10$) (Supplementary Information, Table S1)[10,15,22], showed decreased levels of LC3 II protein and LC3 dots (per 10^4 mm^{-2} of mucosa, $P < 0.01$) (Fig. 1h, i), an increased pool of polyubiquitylated proteins (data not shown), and increased levels of p62 with accumulation in intraepithelial aggregates in comparison with non-CF controls ($n = 10$) (Fig. 1h, j). A decrease in LC3 dots (per mm^2 of tissue, $P < 0.001$), an increased pool of polyubiquitylated proteins (data not shown) and intraepithelial

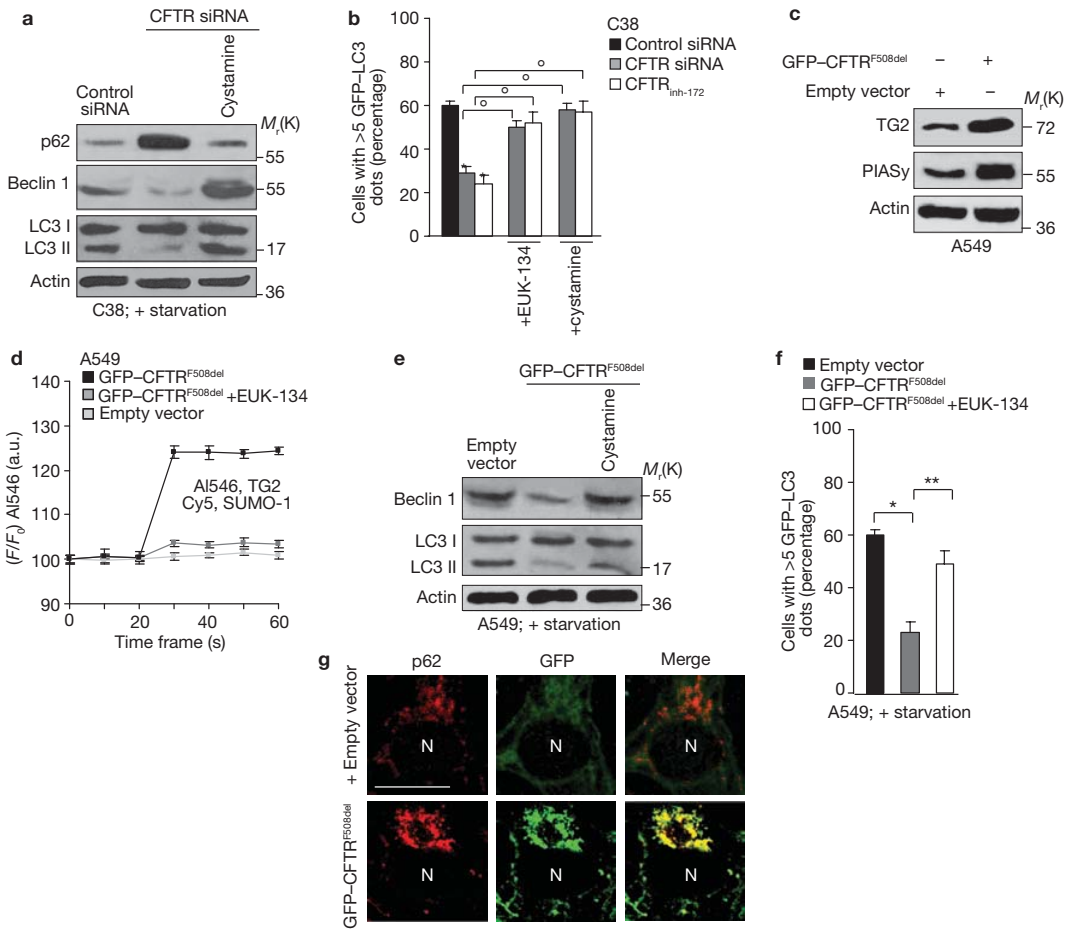

Figure 4 Defective CFTR drives inhibition of autophagy by means of ROS-mediated TG2 SUMOylation in airway epithelial cells. (**a**, **b**) C38 cells were transfected with either 50 nM human CFTR siRNA or scrambled oligonucleotides (**a**, **b**) or cultured with CFTR$_{inh-172}$ (**b**) in the presence or absence of cystamine (250 μM) or EUK-134 (10 mM). (**a**) Immunoblot of beclin 1, LC3 and p62 in C38 cells on starvation. Uncropped images of blots are shown in Supplementary Information, Fig. S10. (**b**) Percentage of cells containing more than five GFP–LC3 punctate dots per cell. Means ± s.d. for three independent experiments. Asterisk, $P < 0.001$ versus scrambled oligonucleotides; circle, $P < 0.01$ versus CFTR siRNA or CFTR$_{inh-172}$; ANOVA. (**c**–**g**) A549 cells were transfected with 1 μg of pGFP—CFTR^{F508del} or pGFP (empty vector), in the presence or absence of 10 mM EUK-134 or 250 μM cystamine. (**c**) Immunoblot of TG2 and PIASy. (**d**) FRET analysis of TG2-Alexa 546 fluorescence after SUMO-1 Cy5 photobleaching. (**e**) Immunoblot of beclin 1 and LC3 in A549 cells after starvation. Uncropped images of blots are shown in Supplementary Information, Fig. S10. (**f**) Percentage of cells containing more than five GFP–LC3 punctate dots per cell. Means ± s.d. for three independent experiments. Asterisk, $P < 0.001$; two asterisks, $P < 0.01$; ANOVA. (**g**) Immunostaining with anti-p62 (red) and anti-GFP (green) antibodies in starved A549 cells. Yellow indicates co-localization. N, nucleus. Scale bar, 10 μm. Each experiment was repeated three times. β-Actin was used as loading control for immunoblot. Densitometric analysis of blots and quantitative measurement of co-localizations are shown in Supplementary Information, Fig. S9.

accumulation of p62 aggregates were observed in lung tissues from CFTR^{F508del} homozygous (*Cftr*^{F508del}) mice[23] ($n = 10$) compared with their control littermates ($n = 10$) (Fig. 1k, l).

Sequestration of beclin 1 interactome in aggresomes drives defective autophagy in CF airway epithelia

We analysed the expression levels of several autophagy-related genes[21,24], including *ULK1*, *ULK2*, *ATG5*, *ATG6* (encoding beclin 1), *ATG7*, *ATG14*, *Bcl-2*, *hVps34* (encoding vacuolar protein sorting 34), *hVps15* (encoding regulatory myristoylated kinase) and *Ambra1*, a beclin 1-interacting WD40-domain protein[19]. Real-time PCR did not reveal decreased messenger RNA expression levels of any of the tested genes in IB3-1 and CFBE41o$^-$ cells in comparison with C38 and 16HBE14o$^-$ cells. In contrast, significant increased expression of *ATG7*, *ATG14*, *Bcl-2* and *hVps34* was observed in CF epithelia (Supplementary Information, Table S2; Supplementary Information, Fig. S1e, f).

A growing body of evidence indicates that beclin 1, a tumour suppressor gene[17–19], interacts with the class III PI(3)K hVps34 (refs 24, 25), and endoplasmic-reticulum-associated class III PI(3)K activity is crucial in the initiation of autophagosome formation[26,27]. Moreover, dissociation of beclin 1 from Bcl-2 promotes autophagy during stress conditions such as starvation[18,26–29].

We immunoprecipitated beclin 1 from IB3-1 and C38 cells under nutrient-rich conditions or starvation. Decreased Bcl-2 immunoreactivity was observed in IB3-1 cells under basal conditions and was negligible under starvation (Supplementary Information, Fig. S2a). Fluorescence resonance energy transfer (FRET) analysis confirmed decreased interaction between beclin 1 and Bcl-2 (Supplementary Information, Fig. S2b),

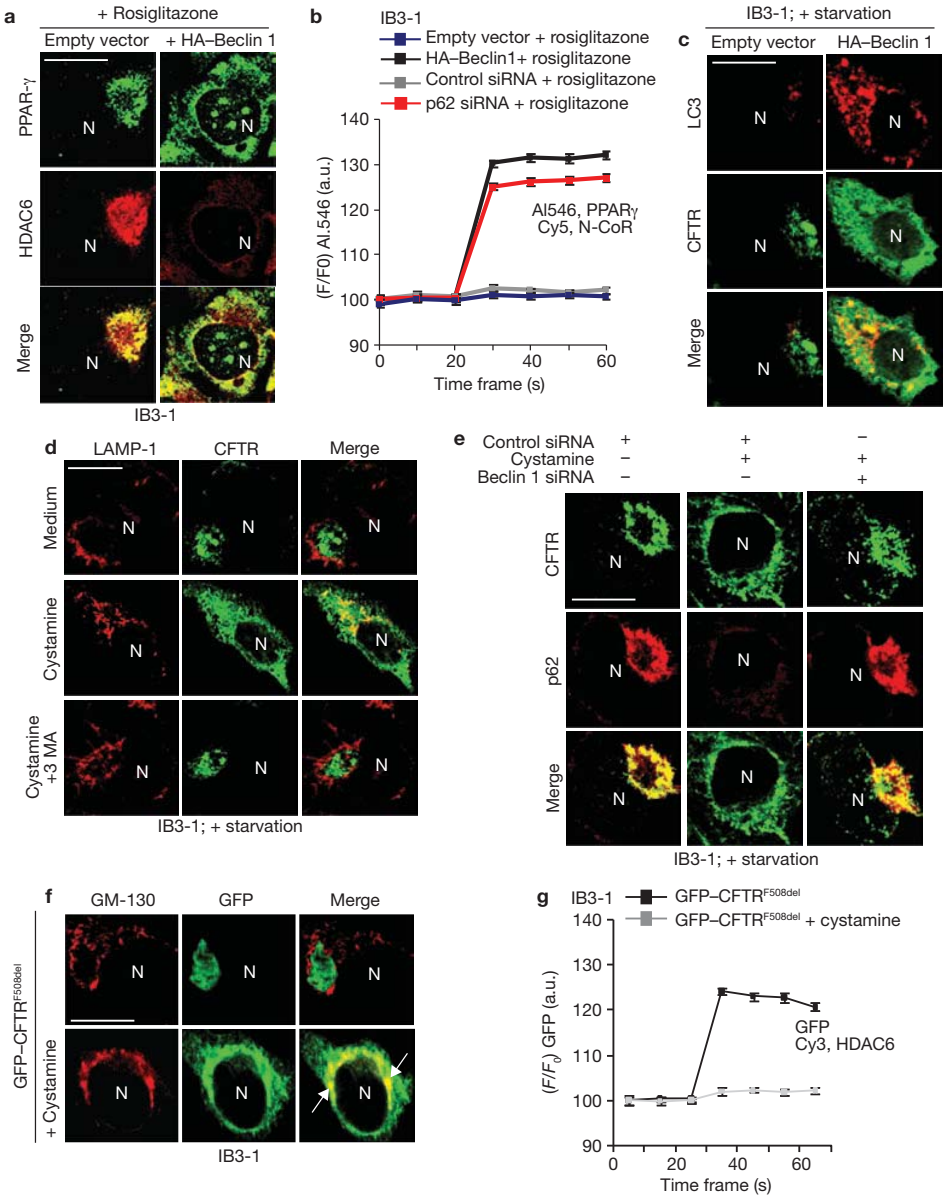

Figure 5 Restoring beclin 1 and autophagy decreases aggresome accumulation in CF epithelia. (**a**, **b**) IB3-1 cells were transfected with either HA-tagged human beclin 1, empty vector, p62 siRNA or scrambled oligonucleotides followed by rosiglitazone (10 μM). (**a**) Cells were immunostained with anti-HDAC6 (red) and anti-PPAR-γ (green) antibodies. Yellow indicates co-localization. N, nucleus. Scale bar, 10 μm. (**b**) FRET analysis of increase in PPAR-γ–Alexa 546 fluorescence after N-CoR Cy5 photobleaching. (**c**) IB3-1 cells were transfected with either HA-tagged human beclin 1 or the empty vector under nutrient starvation. Cells were immunostained with anti-LC-3 (red) and anti-CFTR (green). Yellow indicates co-localization. N, nucleus. Scale bar, 10 μm. (**d**) IB3-1 cells were cultured under nutrient starvation with cystamine (250 μM) in the presence or absence of the PI(3)K inhibitor 3-MA. Immunostaining was with anti-LAMP-1 (red) and anti-CFTR (green). Yellow indicates co-localization. N, nucleus. Scale bar, 10 μm. (**e**) IB3-1 cells were transfected with either 50 nM human beclin 1 siRNA or scrambled oligonucleotides in the presence or absence of 250 μM cystamine under nutrient starvation. Cells were immunostained with anti-p62 (red) and anti-CFTR (green) antibodies. Yellow indicates co-localization. N, cell nucleus. Scale bar, 10 μm. (**f**, **g**) IB3-1 cells were transfected with 1 μg of pGFP–CFTR^{F508del} or the empty vector, in the presence or absence of 250 μM cystamine. (**f**) Cells were immunostained with anti-GM-130 (red) and anti-GFP (green) antibodies. Yellow indicates co-localization (arrows). Scale bar, 10 μm. (**g**) FRET analysis of GFP fluorescence after HDAC6 Cy3 photobleaching. Each experiment was repeated three times. Quantitative measurement of co-localizations is shown in Supplementary Information, Fig. S9.

suggesting an intracellular environment favourable to the induction of autophagy.

Immunoreactivities to hVps34, hVps15 and Ambra1 were detected in beclin 1 immunoprecipitates from both C38 and IB3-1 cells and increased on starvation (Supplementary Information, Fig. S2a). Because the PI(3)K core complex binds to either Atg14L or the ultraviolet-irradiation-resistance-associated gene (UVRAG)[24,30], involved in distinct functional complexes driving either autophagy or endosome-to-Golgi retrograde

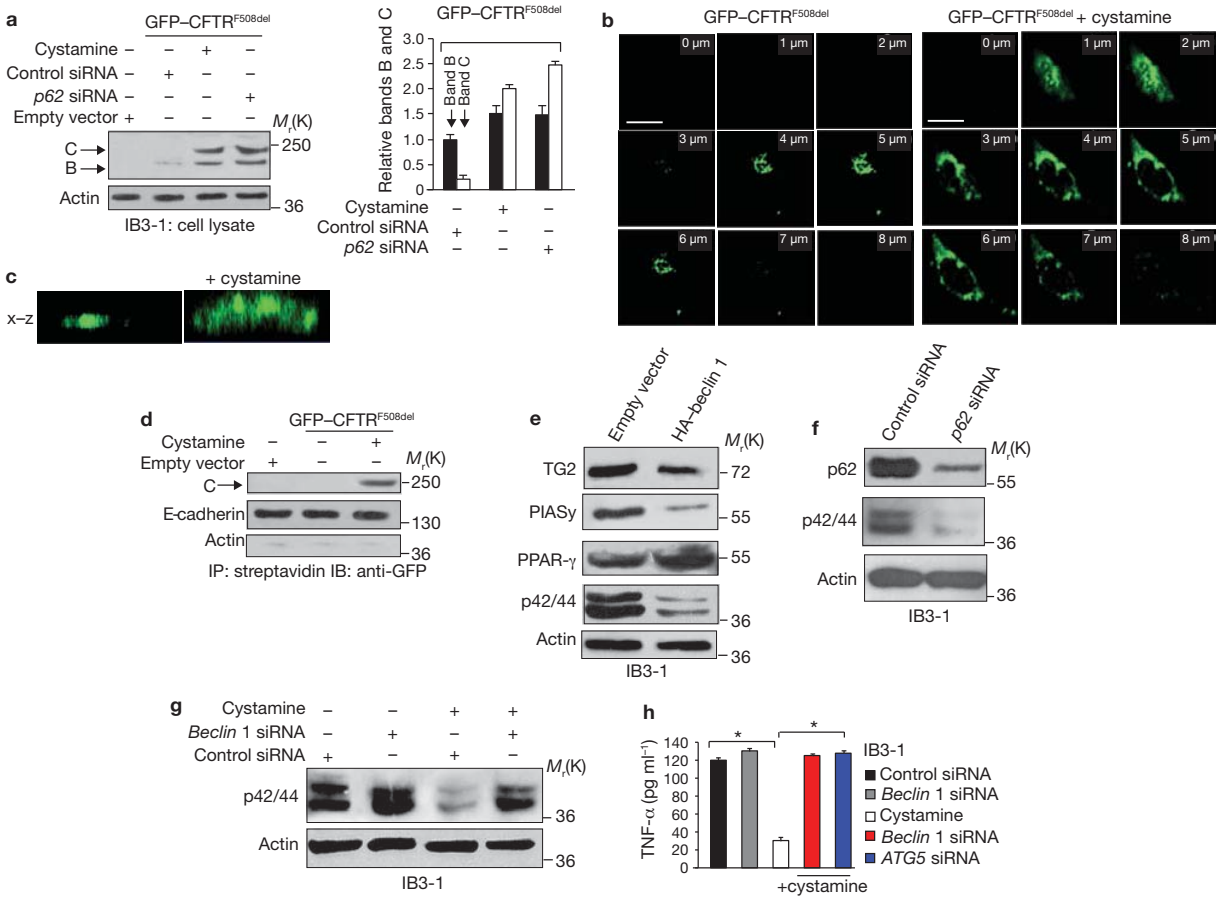

Figure 6 Restoring beclin 1 and autophagy rescues CF phenotype in IB3-1 cells. (**a**–**d**) IB3-1 cells transfected for 24 h at 37 °C with 1 μg of pGFP–CFTR^{F508del} or empty vector in the presence or absence of 250 μM cystamine or with either 50 nM human p62 siRNA or scrambled oligonucleotides. (**a**) Left: CFTR revealed with anti-GFP primary antibody in IB3-1 cell lysate. Top arrow, complex-glycosylated form (apparent M_r of band C about 170K, revealed as 210K with GFP tag); bottom arrow, core-glycosylated form (apparent M_r of band B about 150K, revealed as 190K with GFP tag). Uncropped images of blots are shown in Supplementary Information, Fig. S10. Right: quantification of bands B (black) and C (white) normalized to β-actin levels. Values are means ± s.d. for three independent experiments. (**b**) Cells immunostained with an anti-GFP antibody under non-permeabilizing conditions. Serial confocal sections were collected from top to bottom of cell. (**c**) Side view (X–Z) of a z-stack of confocal images taken in **b**. (**d**) Surface biotinylation assays was performed with membrane-impermeable sulpho-NHS-LC-biotin. The cells were fractioned to obtain the plasma membrane fraction, and biotinylated proteins were precipitated with streptavidin beads. Immunoblot of GFP to reveal the C form. E-cadherin and β-actin were used as positive and negative controls, respectively. (**e**) IB3-1 cells transfected with either HA-tagged human beclin 1 or empty vector. Immunoblot of PIASy, TG2, phospho-p42/44 and PPAR-γ proteins. (**f**) IB3-1 cells transfected with either 50 nM human p62 siRNA or scrambled oligonucleotides. Immunoblot of p62 and phospho-p42/44. Uncropped images of blots are shown in Supplementary Information, Fig. S10. (**g**) IB3-1 cells transfected with either 50 nM human beclin 1 siRNA or scrambled oligonucleotides in the presence or absence of cystamine. Immunoblot of phospho-p42/44. (**h**) IB3-1 cells transfected with either 50 nM human beclin 1 siRNA or 50 nM human ATG5 siRNA or scrambled oligonucleotides in the presence or absence of cystamine. TNF-α secretion. Each bar represents the mean ± s.d. for $n = 3$ experiments. Asterisk, $P < 0.01$; ANOVA. Each experiment was repeated three times. β-Actin was used as loading control. Densitometric analysis of blots and quantitative measurement of co-localizations are shown in Supplementary Information, Fig. S9.

trafficking[30], and Atg14L seems to divert hVps/class III PI(3)K into an autophagic role[30], we investigated the interaction between Atg14L and beclin 1. Atg14L immunoreactivity was detected on beclin 1 immunoprecipitates and increased after starvation in both C38 and IB3-1 cells (Supplementary Information, Fig. S2a). Confocal microscopy and FRET analysis revealed co-localization of beclin 1 with hVps34, hVps 15, Ambra 1 and Atg14L (Fig. 2a; Supplementary Information, Fig. S2c, d) in both C38 and IB3-1 cells. hVps34 (Fig. 2b), beclin 1 and the other beclin 1-interacting proteins (data not shown) co-localized with the endoplasmic reticulum marker calnexin in C38 cells but not in IB3-1 cells. In CF cells, beclin 1 and beclin 1-interacting proteins are sequestered in perinuclear aggregates, where they co-localize with the aggresome marker HDAC6 (ref. 31) (Fig. 2c; Supplementary Information, Fig. S2d) and also with γ-tubulin and are associated with the collapse of the vimentin cage (data not shown)[12,31]. The absence of the beclin 1 interactome at the endoplasmic reticulum level[18,19] might have functional relevance in autophagy deficiency of CF epithelia, because PI(3)K complex III is a specialized endoplasmic reticulum membrane platform for the assembly of a phagosomal initiation complex[18,19].

Decreased protein levels of beclin 1, hVps34, hVps15, Ambra1 and Atg14L (Fig. 2d), and also of UVRAG (data not shown), were observed in IB3-1 cells. Western blots of the insoluble protein fraction

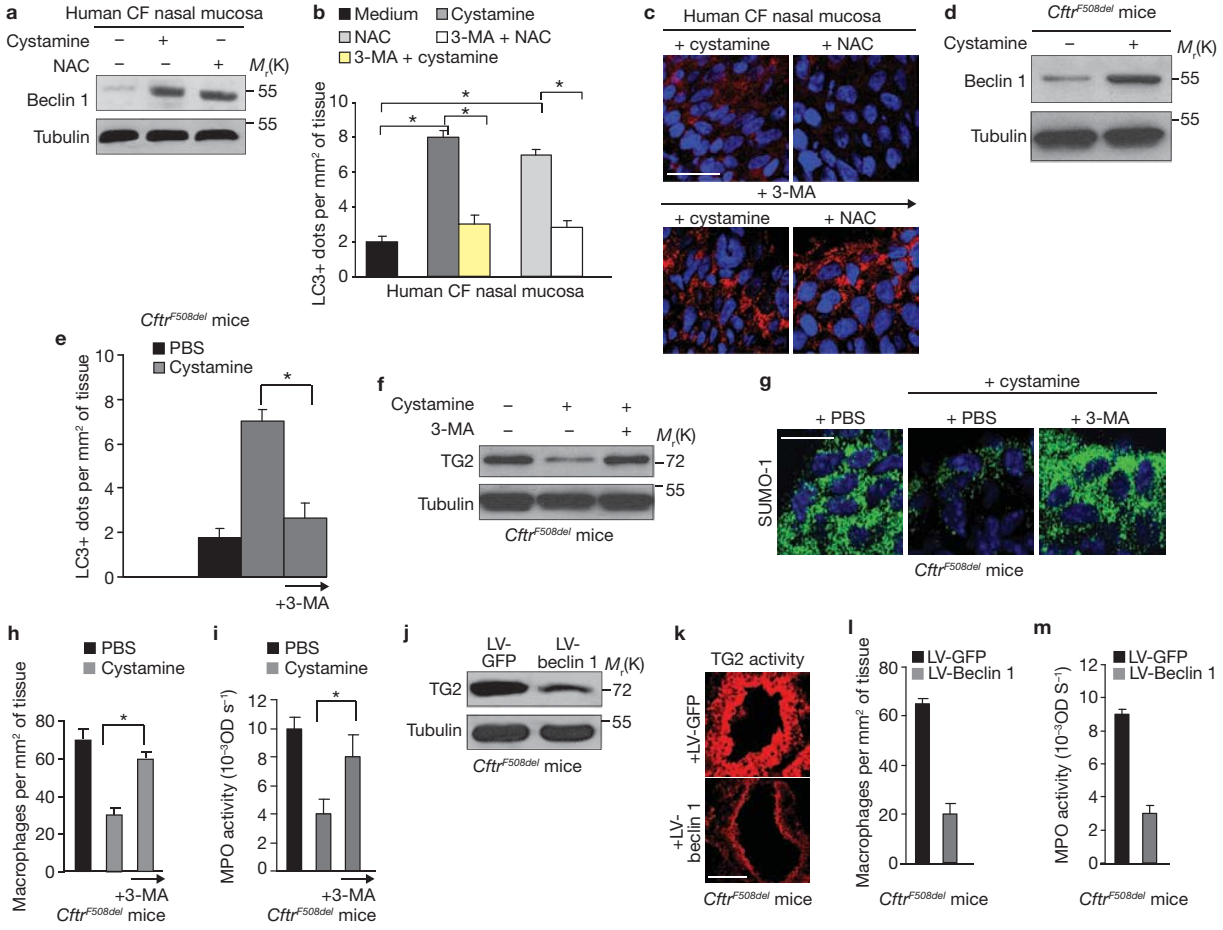

Figure 7 Restoring autophagy by cystamine or beclin 1 overexpression rescues CF phenotype in human and mice CF airways. CF human nasal mucosae cultured with cystamine or NAC (patients 4–10 in Supplementary Information, Table S1) (**a**–**c**) in the presence or absence of 3-MA (patients 6–10 in Supplementary Information, Table S1) (**b**, **c**). (**a**) Immunoblot of beclin 1. (**b**) Fluorescence microscopy quantification of LC3-positive dots. Results represent means ± s.d. Asterisk, $P < 0.05$ between groups of treatment; ANOVA. (**c**) Confocal microscopy micrographs of p62. Nuclei counterstained with DAPI (blue). Scale bar, 10 μm. Representative of five patients per group. (**d**–**i**) *Cftr*^{F508del} mice treated with cystamine or PBS in the presence or absence of 3-MA (**e**–**i**) ($n = 7$ per group). (**d**) Immunoblot of beclin 1. (**e**) Quantification of LC3 dots (per mm^2 of lung tissue). Means ± s.d. Asterisk, $P < 0.01$; ANOVA. (**f**) Immunoblot of TG2. Uncropped images of blots are shown in Supplementary Information, Fig. S10. (**g**) Confocal microscopy of SUMO-1 in lung tissues. Nuclei counterstained with DAPI (blue). Scale bar, 10 μm. (**h**) Number of CD68+ macrophages counted in 15–20 different randomly taken sections. Means ± s.d. per mm^2 of lung tissue from seven mice in each group. Asterisk, $P < 0.01$; ANOVA. (**i**) MPO activity in lung homogenates (expressed as 10^{-3} × optical density (OD) s^{-1}). Means ± s.d. for lung tissues from seven mice in each group. Asterisk, $P < 0.05$; ANOVA. (**j**–**m**) *Cftr*^{F508del} mice ($n = 3$ per group) administered intranasally with a lentiviral vector encoding beclin 1 (LV-beclin 1) or GFP (LV-GFP). (**j**) TG2 Immunoblot in lung tissues. Uncropped images of blots are shown in Supplementary Information, Fig. S10. (**k**) Confocal microscopy of TG2 activity. Representative stainings from at least five airway epithelial areas per mouse from three mice per group. L, lumen. Scale bar, 10 μm. (**l**) Number of CD68+ macrophages counted in 15–20 different randomly taken sections. Means ± s.d. per mm^2 of lung tissue. Asterisk, $P < 0.01$; ANOVA. (**m**) MPO activity in lung homogenates (expressed as 10^{-3} × OD s^{-1}). Means ± s.d. for lung tissues. Asterisk, $P < 0.05$; ANOVA. Anti-β-Tubulin was used as loading control for immunoblot analysis. Densitometric analysis of blots is shown in Supplementary Information, Fig. S9.

revealed increased beclin 1 levels in IB3-1 cells in comparison with C38 cells, suggesting the retention of beclin 1 as an insoluble protein within aggregates in CF epithelia (Supplementary Information, Fig. S2e).

Next we overexpressed beclin 1 in IB3-1 cells. Haemagglutinin (HA)-tagged beclin 1 was detected at the endoplasmic reticulum level (Fig. 2e, top panel) and restored co-localization of hVps34 (Fig. 2e, bottom panel), hVps15, Ambra1 and Atg14L (data not shown) with calnexin. Moreover, HA–beclin induced an increase in LC3 dots ($P < 0.001$) (Fig. 2f) and autophagosome formation (Fig. 2g), increased LC3 II levels and decreased p62 accumulation (Fig. 2h, i).

Decreased beclin 1 protein levels were also observed in CF nasal polyp biopsies[10,15,22] ($n = 10$) (Supplementary Information, Table S1 and Fig. S2f) and in airway tissues from *Cftr*^{F508del} mice ($n = 10$) (Fig. 2j), even though *beclin 1* mRNA levels were similar to those in controls (data not shown). To investigate whether rescuing beclin 1 was effective in restoring autophagy *in vivo* in CF airways, *Cftr*^{F508del} mice ($n = 3$ per group) were administered intranasally with a lentiviral vector

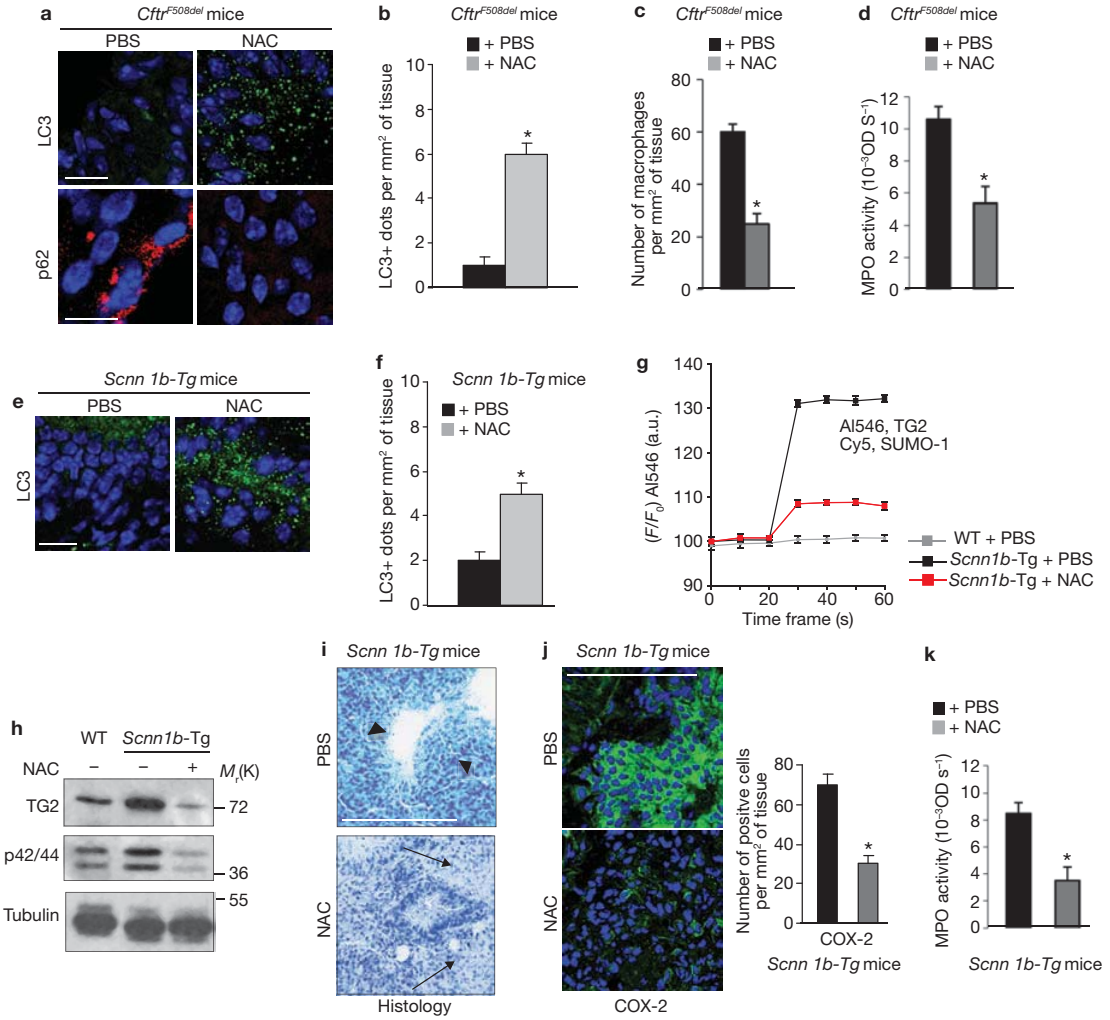

Figure 8 NAC restores autophagy and ameliorates CF lung phenotype in CF mice. *Cftr*^{F508del} mice (**a**–**d**) and *Scnn1b*-Tg mice (**e**–**k**) treated with NAC or PBS ($n = 10$ per group). (**a**) Confocal microscopy of LC3 (top) and p62 (bottom) in lung tissues from *Cftr*^{F508del} mice. Nuclei counterstained with DAPI (blue). Scale bar, 10 μm. Representative images of ten PBS-treated and ten NAC-treated mice. (**b**) Quantification of LC3 dots (per mm^2 of tissue) in lung tissues from *Cftr*^{F508del} mice. Means ± s.d. Asterisk, $P < 0.001$ versus PBS-treated mice; ANOVA. (**c**) Number of macrophages per mm^2 of lung tissue from *Cftr*^{F508del} mice (CD68-positive cells in 15–20 different randomly taken sections for each mouse lung for each condition); means ± s.d. for three separate experiments. Asterisk, $P < 0.05$ versus PBS-treated mice; ANOVA. (**d**) MPO activity in lung homogenates from *Cftr*^{F508del} mice (expressed as $10^{-3} \times$ OD s^{-1}). Means ± s.d. Asterisk, $P < 0.05$ versus PBS-treated mice; ANOVA. (**e**) Confocal microscopy of LC3-positive dots in lung tissues from PBS-treated or NAC-treated *Scnn1b*-Tg mice. Nuclei counterstained with DAPI (blue). Scale bar, 10 μm. (**f**) Number of LC3-positive dots in lung tissues from *Scnn1b*-Tg mice. Means ± s.d. Asterisk, $P < 0.01$ versus PBS-treated mice; ANOVA. (**g**) FRET analysis of TG2-Alexa 546 fluorescence after SUMO-1 Cy5 photobleaching in lung tissues from PBS-treated WT mice and PBS-treated or NAC-treated *Scnn1b*-Tg mice. (**h**) Immunoblot of TG2 and phospho-p42/44 in lung tissues from PBS-treated WT mice and PBS-treated or NAC-treated *Scnn1b*-Tg mice. αβ-Tubulin was used as loading control. (**i**) Lung histology of PBS-treated and NAC-treated *Scnn1b*-Tg mice. Haematoxylin staining. Scale bar, 150 μm. Black arrows indicate decrease in lung infiltration in NAC-treated in comparison with PBS-treated mice (arrowheads). (**j**) Left: confocal microscopy of COX-2 staining (left) in PBS-treated and NAC-treated *Scnn1b*-Tg mice. Nuclei counterstained with DAPI (blue). Scale bar, 150 μm. Right; number of COX-2-positive cells per mm^2 of lung tissue in PBS-treated and NAC-treated *Scnn1b*-Tg mice. Means ± s.d. Asterisk, $P < 0.05$ versus PBS-treated mice; ANOVA. (**k**) MPO activity in lung homogenates from PBS-treated and NAC-treated *Scnn1b*-Tg mice (expressed as $10^{-3} \times$ OD s^{-1}). Means ± s.d. Asterisk, $P < 0.05$ versus PBS-treated mice; ANOVA. Densitometric analysis of the blot is shown in Supplementary Information, Fig. S9.

encoding beclin 1 under the control of the ubiquitous CMV promoter[32,33] or a lentiviral vector expressing GFP under the control of the same promoter (LV-GFP) (Supplementary Information, Fig. S2g). Overexpression of beclin 1 from the lentivirus induced a significant increase in LC3 dots ($P < 0.001$) and decreased p62 accumulation in comparison with *Cftr*^{F508del} mice treated with LV-GFP (Fig. 2k, l).

TG2-mediated crosslinking induces sequestration of beclin 1 in aggresomes and drives defective autophagy in CF airway epithelial cells

These findings suggest that there is post-transcriptional regulation of beclin 1 expression in CF airways. Because the beclin 1 protein sequence contains QP and QXXP motifs, which are specific target sites

for TG2 activity[34] (Supplementary Information, Fig. S3a), and TG2 is an autophagy inhibitor in pancreatic adenocarcinoma cells[35], we tested the hypothesis that beclin 1 might undergo TG2-mediated crosslinking. Immunoprecipitates of beclin 1 from IB3-1 cells were blotted with an N^{ε}(γ-L-glutamyl)-L-lysine isopeptide crosslink catalysed by TG2 (ref. 34). We observed high-molecular-mass bands in the M_r 130,000–250,000 (130K–250K) range that were decreased by knockdown of TG2 as well as by the TG2 inhibitor cystamine[34] (Fig. 3a; Supplementary Information, Fig. S3b) or the calcium chelator bis-(*o*-aminophenoxy)ethane-*N*,*N*,*N*′,*N*′-tetra-acetic acid acetoxymethyl ester (BAPTA-AM)[10,15] (data not shown) and enhanced by the proteasome inhibitor MG132 (Fig. 3b).

TG2 short interfering RNA (siRNA) or cystamine decreased beclin1/HDAC6 co-localization and aggresome sequestration (Fig. 3c, d), restored the soluble forms of beclin 1 and beclin 1 interactor proteins (Fig. 3e), decreased the amount of beclin 1 in the insoluble protein fraction (Supplementary Information, Fig. S3c) and increased the number of Atg16L-positive puncta (Supplementary Information, Fig. S3d), which associate transiently with the surface of forming autophagosomes[24,36]. They also increased LC3 dots ($P < 0.001$) and autophagosome formation (Fig. 3g, h; Supplementary Information, Fig. S3e) and decreased the accumulation of p62 in IB3-1 cells (Fig. 3i). To prove the role of TG2 further, we transfected autophagy-competent C38 cells with pLPCX-TG2, a plasmid expressing wild-type TG2 or mutant Cys277Ser-TG2 including the amino-acid substitution Cys277Ser in the catalytic site. Wild-type TG2 induced a decrease in beclin 1 protein in C38 cells, whereas mutant TG2 did not (Fig. 3f). Overexpression of mutant TG2 restored beclin 1 protein levels in IB3-1 cells (Fig. 3f).

These results indicate that TG2-mediated crosslinking drives defective autophagy in CF epithelial cells.

ROS-mediated TG2 SUMOylation is responsible for defective autophagy in CF epithelia

Because increased ROS sustain high TG2 levels through TG2 SUMOylation mediated by PIASy (protein inhibitor of activated STAT γ)[15], we incubated IB3-1 cells with superoxide dismutase (SOD)–catalase mimetic EUK-134 or knocked-down PIASy[15]. We observed decreased beclin 1 crosslinking and aggresome sequestration (data not shown), increased LC3 dots ($P < 0.001$) (Fig. 3g), autophagosome formation (Fig. 3h) and beclin 1 upregulation (Fig. 3j); overexpression of manganese superoxide dismutase (MnSOD)[15] and the ROS scavenger *N*-acetylcysteine (NAC) showed similar effects to those of EUK-134 (data not shown). NAC, EUK-134 or PIASy knockdown were all as effective as TG2 knockdown in restoring protein levels of soluble beclin 1, Atg14L, hVps34, hVps15 and Ambra1 (data not shown). These results indicate that ROS-mediated TG2 SUMOylation is responsible for defective autophagy in CF epithelia.

Defective CFTR inhibits autophagy through ROS-mediated TG2 SUMOylation

We tested whether defective autophagy is a consequence of the CF genetic defect, because ROS-mediated TG2 SUMOylation is induced on inhibition of CFTR[10,15]. CFTR knockdown (Supplementary Information, Fig. S4a) in autophagy-competent C38 cells decreased beclin 1 and LC3 II protein levels (Fig. 4a), LC3 dots ($P < 0.001$) (Fig. 4b) and increased p62 levels (Fig. 4a). Similar effects were observed on inhibition of CFTR by the small molecule CFTR inhibitor-172 ($CFTR_{inh\text{-}172}$)[10,15] ($P < 0.001$) (Fig. 4b). These effects were prevented by cystamine and by EUK-134 ($P < 0.01$) (Fig. 4a, b) or NAC (data not shown). Transfection of C38 cells with HA–beclin on CFTR inhibition abrogated the effects on autophagy of $CFTR_{inh\text{-}172}$ (data not shown). 16HBE14o$^-$ cells behaved similarly to C38 cells (data not shown).

Overexpression of GFP–$CFTR^{F508del}$ in A549 lung adenocarcinoma cell lines[31] increased intracellular ROS and Ca^{2+} concentrations and eIF-2α phosphorylation (Supplementary Information, Fig. S4b–d), thus indicating $CFTR^{F508del}$-induced activation of the unfolded protein response and endoplasmic reticulum stress[36,37]. GFP–$CFTR^{F508del}$ also increased PIASy and TG2 levels (Fig. 4c) and TG2 SUMOylation (Fig. 4d), and decreased beclin 1 and LC3 II protein levels (Fig. 4e) and LC3 dots ($P < 0.001$) (Fig. 4f). EUK-134 and cystamine (Fig. 4d–f) or NAC (data not shown) prevented these effects. Overexpression of mutant CFTR also induced p62 accumulation and co-localization of p62 with GFP–$CFTR^{F508del}$ in aggregates (Fig. 4g). These results indicate that defective CFTR has a pivotal role in driving beclin 1 downregulation and defective autophagy in CF airways through the ROS–TG2 pathway.

Restoring beclin 1 and autophagy decreases aggresome accumulation in CF epithelia

Next we investigated whether restoring beclin 1 levels might influence the aggresome-prone behaviour of CF epithelia. HA–beclin 1 decreased the aggresome sequestration of PPAR-γ (Fig. 5a; Supplementary Information, Fig. S5a) and allowed PPAR-γ to interact with the nuclear co-repressor (N-CoR)[15] in response to the PPAR-γ agonist rosiglitazone (Fig. 5b). Both HA–beclin 1 and cystamine induced CFTR co-localization with LC3 (Fig. 5c) and with the lysosomal marker LAMP-1 (Fig. 5d). They also decreased CFTR/HDAC-6 co-localization and 3-MA (3-methyl adenine) prevented the effects of cystamine (Fig. 5d; Supplementary Information, Fig. S5b). Both beclin 1 knockdown and 3-MA also inhibited the effects of cystamine in decreasing CFTR (Fig. 5e) and PPAR-γ (data not shown) sequestration in aggresomes and co-localization with p62 (Fig. 5e). These results suggest that the effects of cystamine are due to its ability to rescue beclin 1 and autophagy.

We investigated the role of p62 in driving aggresome formation in CF epithelia. p62 is a regulator of packing and targeting polyubiquitylated proteins and aggregates to autophagosomes for lysosomal degradation[3,4] and is involved in the formation of protein aggregates in cancer cells[38,39]. p62 knockdown in autophagy-deficient IB3-1 cells decreased PPAR-γ and the inhibitory protein IkB-α aggresomes (data not shown), restored the interaction between PPAR-γ and N-CoR[15] (Fig. 5b), decreased the accumulation of CFTR aggregates (Supplementary Information, Fig. S5c) and decreased the co-localization of CFTR with HDAC6 (data not shown). This suggests that, in CF epithelia, p62 mediates the effects of defective autophagy in driving aggresome accumulation of misfolded or modified proteins.

Defective autophagy with p62 accumulation compromises the delivery of ubiquitylated substrates to the proteasome[40]. However, upregulation of autophagy has been reported as a compensatory response to proteasome inhibition[40], thus revealing crosstalk between the proteasome-based and the autophagy-based degradasomes[40]. We incubated IB3-1 cells with the proteasome inhibitor MG132 and demonstrated that MG132 was not effective in enhancing soluble beclin 1 protein or increasing LC3 dots, but enhanced beclin 1 sequestration in HDAC6-positive aggregates (Supplementary Information, Fig. S5d–f).

Rescuing beclin 1 and autophagy restores CFTR trafficking in CF epithelia

These results indicate that HA–beclin 1, cystamine and p62 knockdown all favoured the clearance of CFTR^{F508del} aggregates. They also raise the question of whether rescuing beclin 1 and autophagy in IB3-1 cells might restore mutant CFTR maturation and trafficking to the Golgi and ultimately to the cellular surface.

The F508del mutation results in a temperature-sensitive folding defect of CFTR and premature degradation by the endoplasmic-reticulum-associated degradation system (ERAD)[41,42]. Functional CFTR can be increased by growth at a lower temperature or incubation with chemical chaperones, which favour the escape of CFTR^{F508del} from ERAD[41–47].

We transfected autophagy-deficient IB3-1 cells for 24 h with GFP–CFTR^{F508del} in the presence or absence of cystamine at 37 °C or p62 knockdown. Either cystamine or p62 knockdown (data not shown) induced an increase in GFP–CFTR^{F508del} co-localization with the Golgi marker GM-130 (Fig. 5f) and decreased the sequestration of CFTR in aggresomes (Fig. 5g). Western blotting of the whole protein extracts revealed increased mature complex-glycosylated CFTR^{F508del} (band C, apparent M_r about 170K)[46] after treatment with cystamine or p62 knockdown in comparison with cells transfected with GFP–CFTR^{F508del} alone (Fig. 6a), with an increased ratio between the complex-glycosylated band C and its core-glycosylated counterpart band B (apparent M_r about 150K)[46], the predominant form in untreated cells[46] (Fig. 6a). These results also revealed a greater increase in band B in cystamine-treated cells or after p62 knockdown (Fig. 6a). Western blots of the insoluble protein fraction revealed higher amounts of CFTR^{F508del} band B that were decreased after treatment with cystamine or p62 knockdown (Supplementary Information, Fig. S6a), indicating the sequestration of CFTR^{F508del} within insoluble aggregates.

Confocal microscopy revealed an increase in GFP–CFTR^{F508del} at the plasma membrane after treatment with cystamine (Fig. 6b, c) as well as on p62 knockdown (data not shown) in comparison with IB3-1 cells transfected with GFP–CFTR^{F508del} alone (Fig. 6b, c). To confirm the presence of complex-glycosylated CFTR at the cell surface, plasma membrane fractions were isolated from GFP–CFTR^{F508del}-transfected IB3-1 cells by biotinylation assay and streptavidin pull-down, as reported previously[47]. Band C of GFP–CFTR^{F508del} was pulled down specifically on streptavidin beads after cystamine treatment (Fig. 6d, Supplementary Information, Fig. S6b) or p62 knockdown (data not shown).

These results indicate that restoring intracellular homeostasis by rescuing beclin 1 and autophagy by cystamine or reducing p62 accumulation inhibits sequestration of mutant CFTR in aggresomes and allows its maturation and trafficking to the cell membrane.

Restoring beclin 1 rescues the CF inflammatory phenotype

Next we investigated whether defective autophagy might have a function in inflammation in CF. HA–beclin 1 rescued pro-inflammatory phenotype of IB3-1 cells as it decreased p42/44 phosphorylation (Fig. 6e), increased the levels of M_r 55K PPAR-γ protein (Fig. 6e) and decreased tumour necrosis factor (TNF)-α secretion in medium ($P < 0.01$) (Supplementary Information, Fig. S6c). We also investigated whether defective autophagy might in turn sustain TG2 activation. HA–beclin 1 decreased ROS ($P < 0.01$) and TG2 SUMOylation (Supplementary Information, Fig. S6d, e), and also PIASy and TG2 protein levels (Fig. 6e). Moreover, p62 knockdown in autophagy-deficient IB3-1 cells decreased p42/44 phosphorylation (Fig. 6f) and TG2 SUMOylation (Supplementary Information, Fig. S6f) and increased the levels of M_r 55K PPAR-γ protein (data not shown). In contrast, MG132 did not decrease TNF-α secretion in medium ($P < 0.01$) (Supplementary Information, Fig. S5g) or p42/44 phosphorylation (data not shown).

Because targeting TG2 restores inflammation in human and mice CF airways[15], we investigated whether these effects were mediated by the rescue of autophagy. We incubated IB3-1 cells with cystamine or the antioxidants EUK-134 and NAC in the presence or absence of beclin 1 knockdown. The effects of cystamine or antioxidants (data not shown) in controlling p42/44 phosphorylation (Fig. 6g) and TNF-α secretion (Fig. 6h) were neutralized on beclin 1 knockdown (Fig. 6g, h; Supplementary Information, Fig. S6g). The effects of cystamine on TG2 SUMOylation and inflammation were also neutralized by either 3-MA[48] (data not shown) or ATG5 knockdown (Fig. 6i, Supplementary Information, Fig. S6h).

This indicates that rescue of beclin 1 and autophagy mediates the effects of cystamine and antioxidant molecules in CF epithelia.

Targeting the ROS–TG2 pathway ameliorates the CF phenotype through restoration of autophagy in human and mouse CF airways

To validate these results in human CF airways, we cultured nasal polyp biopsies with cystamine or EUK-134 (refs 10, 15, 22). In all CF biopsies tested ($n = 7$) (Supplementary Information, patients #4-10 of Supplementary Information, Table S1), both NAC and cystamine increased beclin 1 protein and LC3 dots ($P < 0.05$), decreased p62 aggregates (Fig. 7a–c, top panel, Supplementary Information, Fig. S7a), decreased TG2 SUMOylation and enhanced PPAR-γ/N-CoR interaction; these effects were prevented by 3-MA[48] (Fig. 7b, c; Supplementary Information, Fig. S7b, c).

To confirm the biological relevance of these findings *in vivo*, we treated *Cftr*^{F508del} homozygous mice with cystamine[15] in the presence or absence of 3-MA or PBS ($n = 7$ for each group). Cystamine has been proved to be effective *in vivo* in a mouse model of Huntington's disease[49], and also to control inflammation in *Cftr*^{F508del} homozygous mice [15,23]. In all mice tested, cystamine increased beclin 1 protein (Fig. 7d) and LC3 dots ($P < 0.01$) (Fig. 7e), thus indicating rescue of autophagy. These effects were neutralized in lung homogenates by 3-MA (Fig. 7e), which also prevented the effects of cystamine in reducing TG2 protein (Fig. 7f), SUMO-1 protein expression[15] (Fig. 7g), TG2 SUMOylation (Supplementary Information, Fig. S7d), macrophage lung infiltration (per mm^2 of tissue, versus PBS-treated mice; $P < 0.01$) (Fig. 7h) and myeloperoxidase (MPO) activity, a marker of neutrophilic recruitment and activation status[23] (Fig. 7i). On its own, 3-MA did not induce changes in lung phenotype in *Cftr*^{F508del} homozygous mice (data not shown).

To investigate whether beclin 1 overexpression was effective in damping down CF lung inflammation *in vivo*, we evaluated inflammation markers in LV-beclin 1-treated *Cftr*^{F508del} homozygous mice. Intranasal administration of LV-beclin 1 was effective in restoring autophagy in *Cftr*^{F508del} homozygous mice, as shown in Fig. 2. We demonstrate that LV-mediated beclin 1 overexpression induced a decrease in TG2 protein and activity (Fig. 7j, k) and decreased macrophage lung infiltration and MPO activity in lung homogenates (Fig. 7l, m), in comparison with LV-GFP-treated mice (Fig. 7j–m).

These results indicate that targeting ROS–TG2 axis ameliorates the human and mouse CF airway phenotype by restoring beclin 1 and autophagy.

Antioxidant treatment restores autophagy and ameliorates the CF lung phenotype in mouse CF airways

To study the effects of NAC *in vivo*, we treated *Cftr*^{F508del} mice with daily intraperitoneal injections of NAC[50] ($n = 10$) or PBS ($n = 10$). NAC-treated mice showed an increase in LC3-positive vesicles (Fig. 8a) and punctate dots ($P < 0.001$) (Fig. 8b), and a decrease in p62 accumulation (Fig. 8a), macrophage infiltration ($P < 0.05$) (Fig. 8c) and MPO activity ($P < 0.05$) in the lungs (Fig. 8d).

We tested the effects of NAC in *Scnn1b*-Tg mice, another well-established mouse model of CF, with overexpression of the β-ENaC subunit[51] and Na^+ hyperabsorption, which induce a severe CF-like lung disease including inflammation[51,52]. Similarly to the *Cftr*^{f508del} mice, *Scnn1b*-Tg show a spontaneous lung inflammatory phenotype regardless of the presence of bacterial infections[15,23,51,52]. *Scnn1b*-Tg lung tissues showed decreased LC3-positive vesicles and LC3 dots and p62 accumulation, and increased TG2 activity, in comparison with their control littermates (Supplementary Information, Fig. S7e–g). NAC-treated *Scnn1b*-Tg mice ($n = 10$) showed increased LC3-positive vesicles and LC3 dots ($P < 0.01$) (Fig. 8e, f) with decreased p62 aggregates (data not shown) and a decrease in TG2 SUMOylation (Fig. 8g), TG2 protein levels and p42/44 phosphorylation (Fig. 8h) in comparison with PBS-treated mice. Treatment with NAC also decreased lung infiltration by leukocytes (Fig. 8i), decreased the number of cyclo-oxygenase-1 (COX-2)-positive cells (per mm^2 of tissue, $P < 0.05$ versus PBS-treated mice) (Fig. 8j) and decreased MPO activity in lung homogenates ($P < 0.05$ vs. PBS-treated mice) (Fig. 8k).

Finally, we found that cystamine increased LC3 dots and decreased inflammatory lung infiltration (data not shown) in *Scnn1b*-Tg mice. Neither cystamine nor NAC induced changes in wild-type mice (data not shown).

These results indicate that NAC rescues beclin 1 and autophagy and ameliorates the airway phenotype *in vivo* in CF mouse models.

DISCUSSION

Defective autophagy is a critical mechanism in several chronic human diseases[53] such as neurodegeneration[54] and cancer[55]. Here we have shown that defective autophagy due to decreased levels of beclin 1 protein, a key molecule involved in autophagosome formation[17,19,24,25,30], drives lung inflammation in CF.

Decreased beclin 1 expression has been described in the affected brain regions in early Alzheimer's disease, and defective autophagy has been linked to amyloid-β accumulation[56]. A feature that is common to this neurodegenerative disease and CF is the aberrant intracellular accumulation of misfolded proteins within the affected tissues[57,58]. In CF airways, misfolded or damaged proteins such as misfolded CFTR[31] and PPAR-γ[10] accumulate in aggresomes. Here we demonstrate that in CF epithelia TG2-mediated crosslinking and sequestration of beclin 1 dislodge the PI(3)K platform from the endoplasmic reticulum, thus inhibiting the initiation of autophagy. TG2-driven defective autophagy in turn increases ROS and TG2 levels, thus generating a cycle leading to a deleterious pro-oxidative and pro-inflammatory environment (Supplementary Information, Fig. S8a, b).

Autophagy inhibition with p62 accumulation[3,4,5,38,39] increases the levels of proteasome substrates[3] and compromises the ubiquitin proteasome system[3,59], thus favouring aggresome formation[4,5]. TG2 contributes to proteasome overload and aggresome formation in CF airways by inducing the crosslinking and aggregation of several substrate proteins[10,15]. TG2 therefore functions as a rheostat of the post-translational network and the ubiquitin proteasome system under disease conditions and switches off the post-translational regulatory mechanisms. As a consequence of this function, TG2 is involved in the pathogenesis of neurodegenerative diseases due to protein aggregates[60].

Our study highlights an unpredicted role of p62 in CF. p62 is a stress-induced protein that also regulates the formation and disposal of the intracellular aggregates[3,4,5,38–40]. Either restoring beclin 1 by cystamine or reducing p62 levels allows CFTR^{F508del} maturation and trafficking to the cell surface, probably interrupting the cycle that disregulates the intracellular chaperone system.

CF airway tissues are characterized by a pro-inflammatory phenotype with constitutive ceramide accumulation[61] and activation of NF-κB secondary to defective CFTR function[62]. We have previously reported that CFTR inhibition results in the upregulation of ROS and their downstream events, leading to inflammation[10,15]. Here we show that CFTR knockdown drives defective autophagy, as it occurs in human and mouse epithelia that are either homozygotes for F508del or compound heterozygotes for two severe CFTR mutations. Because under the latter conditions negligible amounts of functional CFTR are detected at the cell surface[45,63,64], our results highlight an unforeseen role of CFTR in the regulation of autophagy in CF.

We show that targeting TG2 SUMOylation with antioxidant molecules as well as inhibiting TG2 with cystamine rescue the CF lung phenotype by means of autophagy induction in both human and mouse CF airways. Our results provide a new mechanism linking the CFTR defect with inflammation, through the ROS–TG2-mediated inhibition of autophagy (Supplementary Information, Fig. S8a, b). We have therefore provided a novel rationale and a mechanism of action for both NAC[65] and cystamine in the treatment of patients with CF.

Our study suggests that the restoration of beclin 1 and autophagy may be a novel approach to the treatment of CF and may pave the way for the development of a new class of drugs that, by enhancing beclin 1 levels, could be effective treatments for CF.

METHODS

Methods and any associated references are available in the online version of the paper at http://www.nature.com/naturecellbiology/

Note: Supplementary Information is available on the Nature Cell Biology website.

ACKNOWLEDGEMENTS

We thank Noboru Mizushima for the gift of the pEGFP–LC3 and pcDNA3-HA–beclin 1 expression vectors; Ron Kopito for the gift of the pGFP–F508del-CFTR expression vector; Michael Bownlee for the gift of the adenoviral vectors; Gian Maria Fimia for the gift of the TG2 plasmid; Dieter C. Gruenert for the gift of CFBE41o$^-$ and 16HBE14o$^-$ cell lines; Maria Carla Panzeri for support in electron microscopy and in the analysis of the data; Rosarita Tatè for technical support in confocal microscopy; and Ilaria Russo for technical support in histology. Cftrtm1EUR (F508del (FVB/129) mice were obtained from Bob Scholte under European Economic Community European Coordination Action for Research in Cystic Fibrosis program EU FP6 LSHM-CT-2005-018932. This work was supported by the European Institute for Research in Cystic Fibrosis, Cancer Research UK, Rothschild Trust, Coeliac UK and Regione Campania (L. 229/99).

AUTHOR CONTRIBUTIONS

A.L. co-designed the research concept, planned the overall experimental design, performed organ culture and confocal microscopy studies and wrote the manuscript. V.R.V. co-designed the research concept, planned the overall experimental design and performed immunoblot and immunoprecipitation experiments, cell cultures and transfections. S.E. contributed to the study design, interpretation and analysis of the data and performed immunoblot and immunoprecipitation experiments, cell cultures and transfections. N.B. contributed to the study design, provided scientific knowledge, contributed to the interpretation and analysis of the data, performed experiments on mice and wrote the manuscript. D.M. contributed to the study design, provided scientific knowledge, contributed

to the interpretation and analysis of the data and performed the analysis of mitochondrial function. C.S. provided expression vectors and scientific knowledge and contributed to the analysis of the data. M.G. and L.P. performed experiments on mice and contributed to the interpretation and analysis of the data. I.G., M.P.M. and M.D. performed PCR and contributed to the interpretation and analysis of the data. S.G. contributed to the discussion of the data. E.M. and B.S. provided the lentiviral vectors and scientific knowledge. S.Q. contributed to the interpretation and analysis of the data and provided scientific knowledge. A.B. co-designed the research concept and co-supervised the project. V.R. and L.M. designed the research concept, planned the overall experimental design, supervised the study and wrote the manuscript.

COMPETING FINANCIAL INTERESTS

The authors declare no competing financial interests.

Published online at http://www.nature.com/naturecellbiology
Reprints and permissions information is available online at http://npg.nature.com/reprintsandpermissions/

1. Mizushima, N., Levine, B., Cuervo, A. M. & Klionsky, D. J. Autophagy fights disease through cellular self-digestion. *Nature* **28,** 1069–1075 (2008).
2. Moreau, K., Luo, S. & Rubinsztein, D. C. Cytoprotective roles for autophagy. *Curr. Opin. Cell Biol.* **22,** 206–211 (2010).
3. Korolchuk, V. I., Mansilla, A., Menzies, F. M. & Rubinsztein, D. C. Autophagy inhibition compromises degradation of ubiquitin–proteasome pathway substrates. *Mol. Cell* **33,** 517–527 (2009).
4. Kirkin, V., McEwan, D. G., Novak, I. & Dikic, I. A role for ubiquitin in selective autophagy. *Mol. Cell* **34,** 259–269 (2009).
5. Bjørkøy, G. *et al.* p62/SQSTM1 forms protein aggregates degraded by autophagy and has a protective effect on huntingtin-induced cell death. *J. Cell Biol.* **171,** 603–614 (2005).
6. Dohm, C. P., Kermer, P. & Bahr, M. Aggregopathy in neurodegenerative diseases: mechanisms and therapeutic implication. *Neurodegen. Dis.* **5,** 321–338 (2008).
7. Williams, A. *et al.* Aggregate-Prone proteins are cleared from the cytosol by autophagy: Therapeutic Implications. *Curr. Top. Dev. Biol.* **76,** 89–101 (2006).
8. Schessl, J., Zou, Y., McGrath, M. J., Cowling, B. S. & Maiti, B. Proteomic identification of FHL1 as the protein mutated in human reducing body myopathy. *J. Clin. Invest.* **118,** 904–912 (2008).
9. Rodriguez-Gonzalez, A. *et al.* Role of the aggresome pathway in cancer: targeting histone deacetylase 6-dependent protein degradation. *Cancer Res.* **68,** 2557–2560 (2008).
10. Maiuri, L. *et al.* Tissue transglutaminase activation modulates inflammation in cystic fibrosis via PPARγ down-regulation. *J. Immunol.* **180,** 7697–7705 (2008).
11. Ratjen, F. & Doring, G. Cystic fibrosis. *Lancet* **361,** 681–689 (2003).
12. Sha, Y., Pandit, L., Zeng, S. & Eissa, N. T. A critical role of CHIP in the aggresome pathway. *Mol. Cell. Biol.* **29,** 116–128 (2009).
13. Bence, N. F., Sampat, R. M. & Kopito, R. R. Impairment of the ubiquitin–proteasome system by protein aggregation. *Science* **292,** 1552–1555 (2001).
14. Fu, L. & Sztul, E. ER-associated complexes (ERACs) containing aggregated cystic fibrosis transmembrane conductance regulator (CFTR) are degraded by autophagy. *Eur. J. Cell Biol.* **88,** 215–226 (2009).
15. Luciani, A. *et al.* SUMOylation of tissue transglutaminase as link between oxidative stress and inflammation. *J. Immunol.* **183,** 2775–2784 (2009).
16. Trudel, S. *et al.* Peroxiredoxin 6 fails to limit phospholipid peroxidation in lung from Cftr-knockout mice subjected to oxidative challenge. *PLoS One* **4**, e6075 (2009).
17. Sinha, S. & Levine, B. The autophagy effector Beclin 1: a novel BH3-only protein. *Oncogene* **27**, S137–S148 (2008).
18. Maiuri, M. C., Criollo, A. & Kroemer, G. Crosstalk between apoptosis and autophagy within the Beclin 1 interactome. *EMBO J.* **29,** 515–516 (2010).
19. He, C. & Levine, B. The Beclin 1 interactome. *Curr. Opin. Cell Biol.* **22,** 140–149 (2010).
20. Klionsky, D. J., Abeliovich, H., Agostinis, P., Agrawal, D. K. & Aliev, G. Guidelines for the use and interpretation of assays for monitoring autophagy in higher eukaryotes. *Autophagy* **4**,151–175 (2008).
21. Mizushima, N., Yoshimori, T. & Levine, B. Methods in mammalian autophagy research. *Cell* **140,** 313–326 (2010).
22. Raia, V. *et al.* Inhibition of p38 mitogen activated protein kinase controls airway inflammation in cystic fibrosis. *Thorax* **60,** 773–780 (2005).
23. Legssyer, R. *et al.* Azithromycin reduces spontaneous and induced inflammation in DF508 cystic fibrosis mice. *Respir. Res.* **7,** 134 –136 (2006).
24. Matsunaga, K. *et al.* Two Beclin 1-binding proteins, Atg14L and Rubicon, reciprocally regulate autophagy at different stages. *Nature Cell Biol.* **11,** 385–396 (2009).
25. Zhong, Y. *et al.* Distinct regulation of autophagic activity by Atg14L and Rubicon associated with Beclin 1-phosphatidylinositol-3-kinase complex. *Nature Cell Biol.* **11,** 468–476 (2009).
26. Axe, E. L. *et al.* Autophagosome formation from membrane compartments enriched in phosphatidylinositol 3-phosphate and dynamically connected to the endoplasmic reticulum. *J. Cell Biol.* **182,** 685–701 (2008).
27. Hayashi-Nishino, M. *et al.* A subdomain of the endoplasmic reticulum forms a cradle for autophagosome formation. *Nature Cell Biol.* **11,** 1433–1437 (2009).
28. Maiuri, M. C. *et al.* Functional and physical interaction between Bcl-X_L and a BH3-like domain in Beclin-1. *EMBO J.* **26,** 2527–2539 (2007).
29. Pattingre, S. *et al.* Bcl-2 antiapoptotic proteins inhibit Beclin 1-dependent autophagy. *Cell* **23,** 927–939 (2005).
30. Liang, C. *et al.* Beclin1-binding UVRAG targets the class C Vps complex to coordinate autophagosome maturation and endocytic trafficking. *Nature Cell Biol.* **10,** 776–787 (2008).
31. Kawaguchi, Y. *et al.* The deacetylase HDAC6 regulates aggresome formation and cell viability in response to misfolded protein stress. *Cell* **115,** 727–738 (2003).
32. Spencer, B. *et al.* Beclin 1 gene transfer activates autophagy and ameliorates the neurodegenerative pathology in α-synuclein models of Parkinson's and Lewy body diseases. *J. Neurosci.* **29,** 13578–13588 (2009).
33. Stocker, A. G. *et al.* Single-dose lentiviral gene transfer for lifetime airway gene expression. *J. Gene Med.* **11,** 861–867 (2009).
34. Lorand, L. & Graham, R. M. Transglutaminases: crosslinking enzymes with pleiotropic functions. *Nature Rev. Mol. Cell Biol.* **4,** 140–156 (2003).
35. Akar, U. *et al.* Tissue transglutaminase inhibits autophagy in pancreatic cancer cells. *Mol. Cancer Res.* **5,** 241–249 (2007).
36. Ron, D. & Walter, P. Signal integration in the endoplasmatic reticulum unfolded protein response. *Nature Rev. Mol. Cell Biol.* **8,** 519–529 (2007).
37. Bartoszewski, R. *et al.* Activation of the unfolded protein response by ΔF508 CFTR. *Am. J. Respir. Cell Mol. Biol.* **39,** 448–457 (2008).
38. Moscat, J. & Diaz-Meco, M. T. p62 at the crossroads of autophagy, apoptosis, and cancer. *Cell* **137,** 1001–1004 (2009).
39. Mathew, R. *et al.* Autophagy suppresses tumorigenesis through elimination of p62. *Cell* **137,** 1062–1075 (2009).
40. Komatsu, M. *et al.* Homeostatic levels of p62 control cytoplasmic inclusion body formation in autophagy-deficient mice. *Cell* **131,** 1149–1163 (2007).
41. Riordan, J. R. CFTR function and prospects for therapy. *Annu. Rev. Biochem.* **77,** 701–726 (2008).
42. Wang, X. *et al.* Hsp90 cochaperone Aha1 downregulation rescues misfolding of CFTR in cystic fibrosis. *Cell* **127,** 803–815 (2006).
43. Wang, X., Koulov, A. V., Kellner, W. A., Riordan, J. R. & Balch, W. E. Chemical and biological folding contribute to temperature-sensitive ΔF508 CFTR trafficking. *Traffic* **11,** 1878–1893 (2008).
44. Skach, W. R. CFTR: new members join the fold. *Cell* **127,** 673–675 (2006).
45. Amaral, M. D. CFTR and chaperones: processing and degradation. *J. Mol. Neurosci.* **23,** 41–48 (2004).
46. Pedemonte, N. *et al.* Small-molecule correctors of defective ΔF508-CFTR cellular processing identified by high-throughput screening. *J. Clin. Invest.* **115,** 2564–2571 (2005).
47. Caohuy, H., Jozwik, C. & Pollard, H. B. Rescue of ΔF508-CFTR by the SGK1/Nedd4-2 signaling pathway. *J. Biol. Chem.* **284,** 25241–25253 (2009).
48. Ghavami, S. *et al.* S100A8/A9 induces autophagy and apoptosis via ROS-mediated cross-talk between mitochondria and lysosomes that involves BNIP3. *Cell Res.* **20,** 314–331 (2010).
49. Karpuj, M. V. *et al.* Prolonged survival and decreased abnormal movements in transgenic model of Huntington disease, with administration of the transglutaminase inhibitor cystamine. *Nature Med.* **8,** 143–149 (2002).
50. Sablina, A. A., Budanov, A. V., Ilyinskaya, G. V., Agapova, L. S. & Kravchenko, J. E. The antioxidant function of the p53 tumor suppressor. *Nature Med.* **11,** 1306–1313 (2005).
51. Mall, M., Grubb, B. R., Harkema, J. R., O'Neal, W. K. & Boucher, R. C. Increased airway epithelial Na^+ absorption produces cystic fibrosis-like lung disease in mice. *Nature Med.* **10,** 487–493 (2004).
52. Frizzell, R. A. & Pilewski, J. M. Finally, mice with CF lung disease. *Nature Med.* **10,** 452–454 (2004).
53. Maiuri, C., Zalckvar, E., Kimchi, A. & Kroemer, G. Self-eating and self-killing: crosstalk between autophagy and apoptosis. *Nature Rev Mol. Cell. Biol.* **8,** 741–752 (2007).
54. Hara, T. *et al.* Suppression of basal autophagy in neural cells causes neurodegenerative disease in mice. *Nature* **441,** 885–889 (2006).
55. Takahashi, Y. *et al.* Bif-1 interacts with Beclin 1 through UVRAG and regulates autophagy and tumorigenesis. *Nature Cell Biol.* **9,** 1142–1151 (2007).
56. Pickford, F. *et al.* The autophagy-related protein beclin 1 shows reduced expression in early Alzheimer disease and regulates amyloid beta accumulation in mice. *J. Clin. Invest.* **118,** 2190–2199 (2008).
57. Tebbenkamp, A. T. & Borchel, D. R. Protein aggregate characterization in models of neurodegenerative disease. *Methods Mol. Biol.* **566,** 85–91 (2009).
58. Martínez, A, Portero-Otin, M., Pamplona, R. & Ferrer, I. Protein targets of oxidative damage in human neurodegenerative diseases with abnormal protein aggregates. *Brain Pathol.* **20,** 281–297 (2010).
59. Korolchuk, V. I., Menzies, F. M. & Rubinsztein, D. C. Mechanisms of cross-talk between the ubiquitin–proteasome and autophagy–lysosome systems. *FEBS Lett.* **584,** 1393–1398 (2010).
60. Muma, N. A. Transglutaminase is linked to neurodegenerative disease. *J. Neuropathol. Exp. Neurol.* **66,** 258–263 (2007).
61. Teichgräber, V. *et al.* Ceramide accumulation mediates inflammation, cell death and infection susceptibility in cystic fibrosis. *Nature Med.* **14,** 382–391 (2008).
62. Vij, N., Mazur, S. & Zeitlin, P. L. CFTR is a negative regulator of NFκB mediated innate immune response. *PLoS One* **4**, e4664 (2009).
63. Farinha, C. M. & Amaral, M. D. Most F508del-CFTR is targeted to degradation at an early folding checkpoint and independently of calnexin. *Mol. Cell. Biol.* **25,** 5242–5252 (2005).
64. Scott-Ward, T. S. & Amaral, M. D. Deletion of Phe508 in the first nucleotide-binding domain of the cystic fibrosis transmembrane conductance regulator increases its affinity for the heat shock cognate 70 chaperone. *FEBS J.* **276,** 7097–7109 (2009).
65. Rochat, T., Lacroix, J. S. & Jornot, L. N-acetylcysteine inhibits Na^+ absorption across human nasal epithelial cells. *J. Cell Physiol.* **201,** 106–116 (2004).

DOI: 10.1038/ncb2090

METHODS

Cell lines. IB3-1 human CF bronchial epithelial, C38 or S9 cells, normal bronchial epithelial 16HBE14o$^-$ or lung carcinoma A549 cell lines (LGC Promochem, Milan, Italy) were cultured as recommended by the American Type Culture Collection. CFBE41o$^-$ human CF bronchial epithelial cells (a gift from D. C. Gruenert) were cultured in MEM Earl's salt L-glutamine (200 mM L-glutamine) medium supplemented with 10% FBS and the appropriate amount of penicillin/streptomycin. Cell lines were incubated for 24 h with cystamine (250 μM; Sigma Aldrich), NAC (10 mM; Vinci Biochem), EUK-134 (50 μg ml^{-1}; Vinci Biochem), rapamycin (100 nM; Sigma Aldrich), chloroquine (25 μM; Sigma Aldrich), E64d (50 μg ml^{-1} for 4 h) and pepstatin A (50 μg ml^{-1} for 4 h), rosiglitazone (10 μM for 4 h; Vinci Biochem); BAPTA-AM (25 μg ml^{-1} for 4 h; Calbiochem) and proteasome inhibitor MG132 (50 μM for 6 h; Calbiochem). IB3-1 cells were also incubated for 24 h with 3-MA (20 mM; Calbiochem) followed by cystamine. C38 and 16HBE cells were incubated for 48 h with $CFTR_{inh\text{-}172}$ (20 μM; Calbiochem)[10,15] followed by cystamine or EUK-134.

Human subjects and *ex vivo* cultures of nasal polyp mucosal biopsies. Ten patients with CF carrying severe CFTR mutations (Supplementary Information, Table S1) and ten consecutive patients without CF (mean age 21 years, range 16–32 years) undergoing surgical treatment for non-allergic nasal polyposis were enrolled. Nasal polyp biopsies from seven patients in each group (patients 4–10 in Supplementary Information, Table S1) were cultured for 4 h with or without EUK-134 (50 μg ml^{-1}), NAC (10 mM) or cystamine (400 μM). Nasal polyp biopsies from five patients with CF (patients 6–10 in Supplementary Information, Table S1) were also incubated with NAC or cystamine in the presence or absence of 3-MA (3 mM)[20], followed by incubation wth rosiglitazone (10 mM for 4 h).

Mice and treatments. Young adult female CF mice homozygous for the F508del mutation (abbreviated $Cftr^{F508del}$)[23] in the 129/FVB outbred background (obtained from Bob Scholte, Erasmus Medical Center Rotterdam, The Netherlands), young adult *Scnn1b*-Tg mice[51] and their wild-type littermates were housed in static isolator cages at the animal care specific pathogen-free facility of Charles River (Varese, Italy). We treated $Cftr^{F508del}$ homozygous mice and *Scnn1b*-Tg mice by intraperitoneal injection with a daily dose of 100 μl of 0.01 M cystamine in PBS solution for 7 days (ref. 16) ($n = 7$ for each group of treatment) or NAC with a daily dose of 100 mg per kg body weight in PBS solution for 5 days or with PBS solution ($n = 10$ for each group of treatment). $Cftr^{F508del}$ mice were also treated with cystamine in the presence or absence of 3-MA (intraperitoneal injection of 50 mg kg^{-1} in 100 μl of PBS for 7 days) or 3-MA alone ($n = 7$ for each group of treatment). Airway administrations of lentiviral vectors expressing mouse beclin 1 or GFP[32] were performed in anaesthetized $Cftr^{F508del}$ homozygous mice aged 4–8 weeks, as described previously[33]. In brief, mice received a single dose of 4 μl of 1% L-α-lysophosphatidylcholine (LPC; Sigma) in PBS into the nasal airway by inhalation-driven instillation 1 h before delivery of the GFP or beclin 1 lentiviral vectors at a dose of 1.2×10^7 transducing units per mouse delivered into the nose (two 10-μl aliquots over several minutes). Mice were killed 5 days after vector administration, and lung tissues were collected for analyses.

Histology. We excised and immediately fixed mouse lungs in buffered 4% paraformaldehyde; they were then embedded in paraffin and sectioned to a thickness of 5 μm. We performed haematoxylin staining on serial sections.

Plasmids. The pGFP–$CFTR^{F508del}$ expression vector (provided by Ron R. Kopito), pEGFP–LC3 and pcDNA3-HA–beclin 1 expression vector (a gift from N. Mizushima), pLPCX-TG and pLPCX-TGCys277Ser (a gift from G. M. Fimia) and the corresponding empty expression vectors were used for transfection experiments.

Transfection and RNA interference. Cells were transfected with TG2 (ref. 15), PIASy (ref. 15), beclin 1 and p62 (Oligonucleotide Synthesis Core Facility, CEINGE s.c.a.r.l. Naples, Italy), CFTR and ATG5 siRNA (Invitrogen) or scrambled oligonucleotides by using Lipo RnaiMax (Invitrogen) in accordance with the manufacturer's instructions. siRNA oligonucleotide sequences are shown in Supplementary Information, Table S2a. Cell lines were also transfected with pcDNA3-HA–beclin 1 expression vectors, pEGFP–LC3, human TG2 or Cys277Ser TG2 or antisense cDNAs in pLPCLX vector and GFP–$CFTR^{F508del}$, by using Lipofectamine 2000 (Invitrogen) in accordance with the manufacturer's instructions.

Lentiviruses. The lentiviral vectors expressing mouse beclin 1 or GFP have been described previously[33].

Adenoviral vector. Human MnSOD cDNA was cloned into the shuttle vector pAd5CMVK-NpA (a gift from Michael Brownlee). Cell lines were infected for 2 h with MnSOD or control adenovirus (ref. 15).

Quantitative RT–PCR. Total RNA was extracted with the RNeasy Mini Kit (Qiagen). The mRNA was reverse transcribed with a SuperScriptTM III First Strand Synthesis System (Invitrogen). Quantitative RT–PCR was performed with an iCycler iQ Multicolour Real-Time PCR Detector (Bio-Rad) with iQ TM SYBR Green supermix (Bio-Rad). Expression levels of genes were normalized to β-actin levels in the same sample. The sequence of primers is reported in Supplementary Information, Table S2b. The relative amounts of mRNA were calculated by using the comparative *Ct* method.

Immunoblot analysis. Immunoblot analysis was performed as described previously[10,15]. The antibodies used for immunoblot analysis are reported in Supplementary Information, Table S3. Densitometric analysis was performed with Image J software; each data point is expressed as a mean ± s.d. for three independent experiments. The data are shown in Supplementary Information.

Immunoprecipitation. Whole-cell lysates were incubated at 4 °C for 8–12 h with antibody anti-beclin 1 (Santa Cruz Biotechnology). After the addition of Protein A/G-agarose beads, the incubation was continued for 1 h. After being washed, the immunoprecipitated proteins were subjected to electrophoresis through 8% polyacrylamide gels (Bio-Rad), transferred to blotting membranes (Polyscreen poly(vinylidene difluoride); NEN) and analysed.

Soluble and insoluble fractions. Cells were lysed in buffer containg 50 mM Tris-HCl pH 7.5, 150 mM NaCl, 0.5% Nonidet P40, 5 mM EDTA, 1 mM phenylmethylsulphonyl fluoride, 50 mM NaF, 10 μg ml^{-1} leupeptin and 10 μg ml^{-1} apoprotein supplemented with protease inhibitors (Sigma) and centrifuged at 16,000*g* at 4 °C for 20 min. After centrifugation the soluble (supernatant) and insoluble (pellet) fraction were used in western blot analysis with anti-beclin 1 or anti-GFP antibody. The pellet insoluble in Nonidet P40 was dissolved five times in sample buffer, boiled at 95 °C for 5 min and resolved on a 10% polyacrylamide gel.

Cell-surface biotinylation assay. Cell-surface proteins were biotinylated with sulphosuccinimidyl-6-(biotinamido) hexanoate (sulpho-NHS-LC-biotin, 1 mg ml^{-1} in PBS, pH 8.2; Pierce), as described[47]. IB3-1 cells were homogenized in a Potter–Elvehjem pestle and glass tube (Sigma) and centrifuged at 2,300*g* for 15 min at 4 °C to obtain nuclear pellets. Supernatants containing the cytoplasmic fractions and plasma membrane were centrifuged for 1 h at 16,000*g* at 4 °C; the pellet was the intact membrane and was solubilized in buffer A containing 1% Triton X-100. This was then centrifuged for 1 h at 60,000*g* in the ultracentrifuge. The supernatants were collected as the plasma membrane fraction. Equivalent amounts of protein (500 μg) were used for streptavidin–agarose pull-down (Pierce). Biotinylated proteins were immunoblotted against GFP or E-cadherin or β-actin antibodies. Incubation without biotin was used as control.

Immunofluorescence analysis. Immunofluorescence analysis was performed as described previously[10,15]. Cell or tissue sections were incubated with primary antibodies. The antibodies used for immunofluorescence analysis are reported in Supplementary Information, Table S3. TG2 enzymatic activity in human or mice lung sections was detected by incubating unfixed sections with biotin-mono-dansyl cadaverine for 1 h at room temperature, as described previously[10,15]. Image J software (US National Institutes of Health) was used to quantify the number of GFP–LC3-positive cells containing more than five GFP–LC3 puncta or cells with more than LC3 dots per cell. At least 60 cells were counted in each experiment and the values are means ± s.d. for five independent experiments. Correlation coefficient analysis was used as value of co-localization as described previously[66].

FRET microscopy. For acceptor photobleaching, FRET microscopy analysis was performed as described previously[10,15]. The antibodies used for FRET microscopy are reported in Supplementary Information, Table S3. Cy5 was bleached at not

more than 10% of its initial fluorescence, by 200 2.56-ms pulses of 5-mW 633-nm laser per pixel, sampling 0.01 mm^2 of the specimen. Alexa 546 fluorescence was detected before and after Cy5 photobleaching.

Electron microscopy. Cell culture monolayers were fixed for 15 min at 4 °C with 4% paraformaldehyde and 2.5% glutaraldehyde in 125 mM cacodylate buffer and stained with uranyl acetate and lead citrate and examined in a Leo912 electron microscope. We used Image J software (US National Institutes of Health) to quantify the number of autophagosomes per cell in 15–20 different randomly taken micrographs for each condition.

Mitochondrial membrane potential measurements. We incubated 10^6 PBS-washed cells in 40 nM $DiOC_6$ (Sigma) and 1 mg ml^{-1} propidium iodide (Sigma) for 15 min at 37 °C. After being washed, cells were suspended in 1 ml of PBS (pH 7.4) and were subsequently analysed by flow cytometry.

MPO activity. MPO activity in lung homogenates was assessed at 490 nm over 10 min and expressed as $10^{-3} \times OD\ s^{-1}$, as described previously[24].

ROS detection. Cells were pulsed with 10 μM 5-(and-6)-chloromethyl-2′,7′-dichlorodihydrofluorescein diacetate acetyl ester (CM-H2DCFDA; Molecular Probes) and analysed with a Wallac 1420 multilabel counter as described previously[10,15].

Calcium imaging. We loaded A549 cells transfected with $CFTR^{F508del}$ or vector control with Fura-2 (30 min at 37 °C) in calcium imaging buffer in accordance with the manufacturer's instructions (Invitrogen, Molecular probes).

Enzyme-linked immunosorbent assay (ELISA). Human TNF-α secretion was measured with a BD OptEIATM TNF-α ELISA kit II (BD Biosciences, NJ, USA). Values were normalized to 10^6 cells; results are expressed as means ± s.d.

Statistical analysis. Data are reported as arithmetic means ± s.d. The data distribution was analysed for normality and statistical analysis was performed with a one-way ANOVA. Significant differences are indicated in the figures. All data were obtained from independent measurements. Data were analysed with SPSS 13 software. Statistical significance was defined as $P < 0.05$.

66. Luciani, A. *et al.* Lysosomal accumulation of gliadin p31-43 peptide induces oxidative stress and tissue transglutaminase-mediated PPARγ downregulation in intestinal epithelial cells and coeliac mucosa. *Gut* **59,** 311–319 (2010).

nature cell biology

DOI: 10.1038/ncb2090

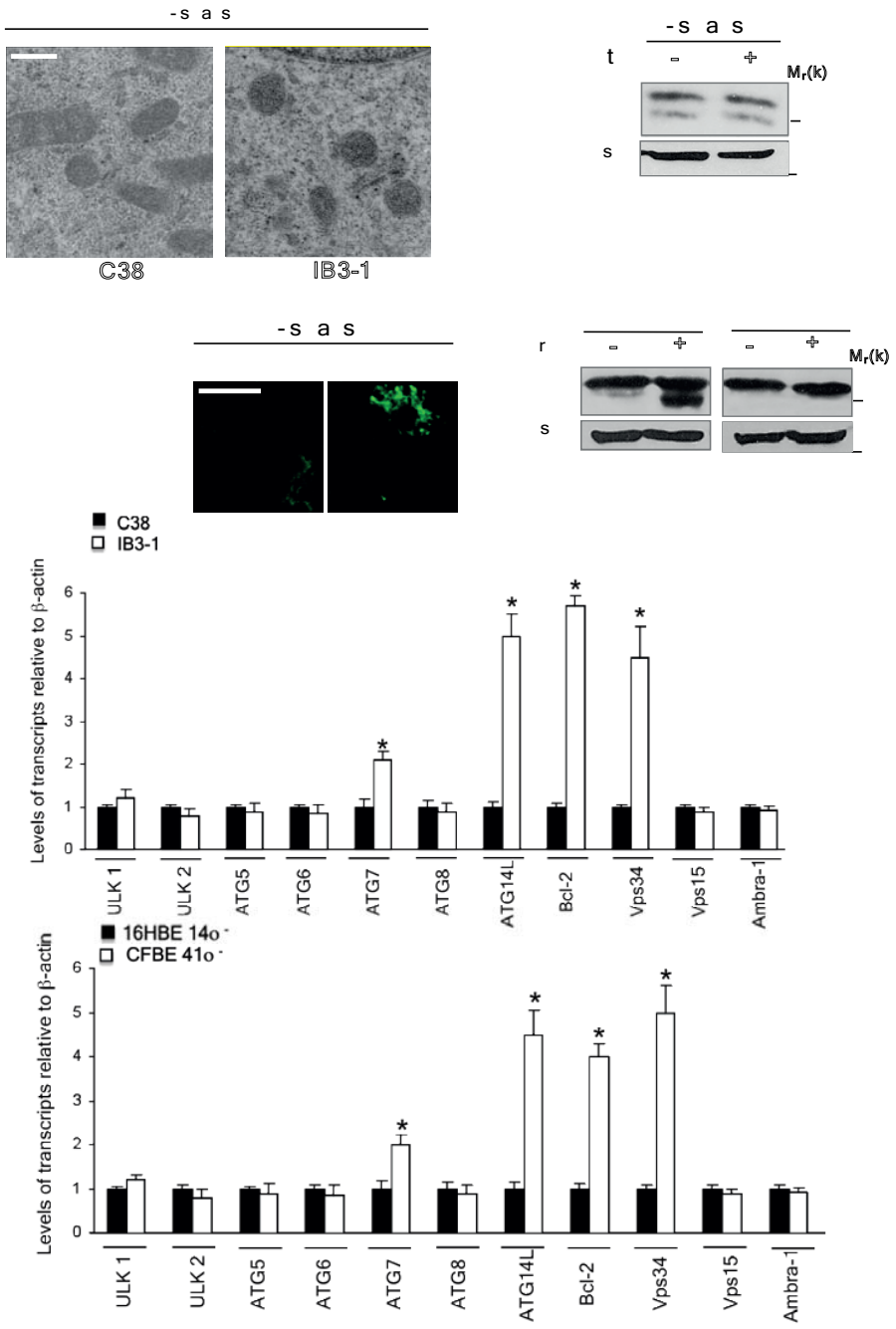

Figure S1 Defective autophagy in human CF airway epithelia. (**a**) Electron microscopy analysis of non-starved C38 and IB3-1 cells. Bar, 250 nm. (**b**) Immunoblot of LC3 in starved IB3-1 cells in the presence or absence of chloroquine. β-actin was used as loading control. (**c**) Confocal microscopy micrographs of p62 in starved C38 and IB3-1 cells. N, nucleus. Scale bar, 10 m. (**d**) Immunoblot of LC3 in C38 and IB3-1 cells in the presence or absence of rapamycin. β-actin was used as loading control. (**e-f**) Real-time PCR of ULK-1, ULK-2, ARTG5, ATG6, ATG7, ATG8, ATG14L, BCL-2, Vps34, Vps15 and Ambra-1 mRNA in C38 and IB3-1 cells (**e**) or 16HBE14 and CFBE 41 (**f**).

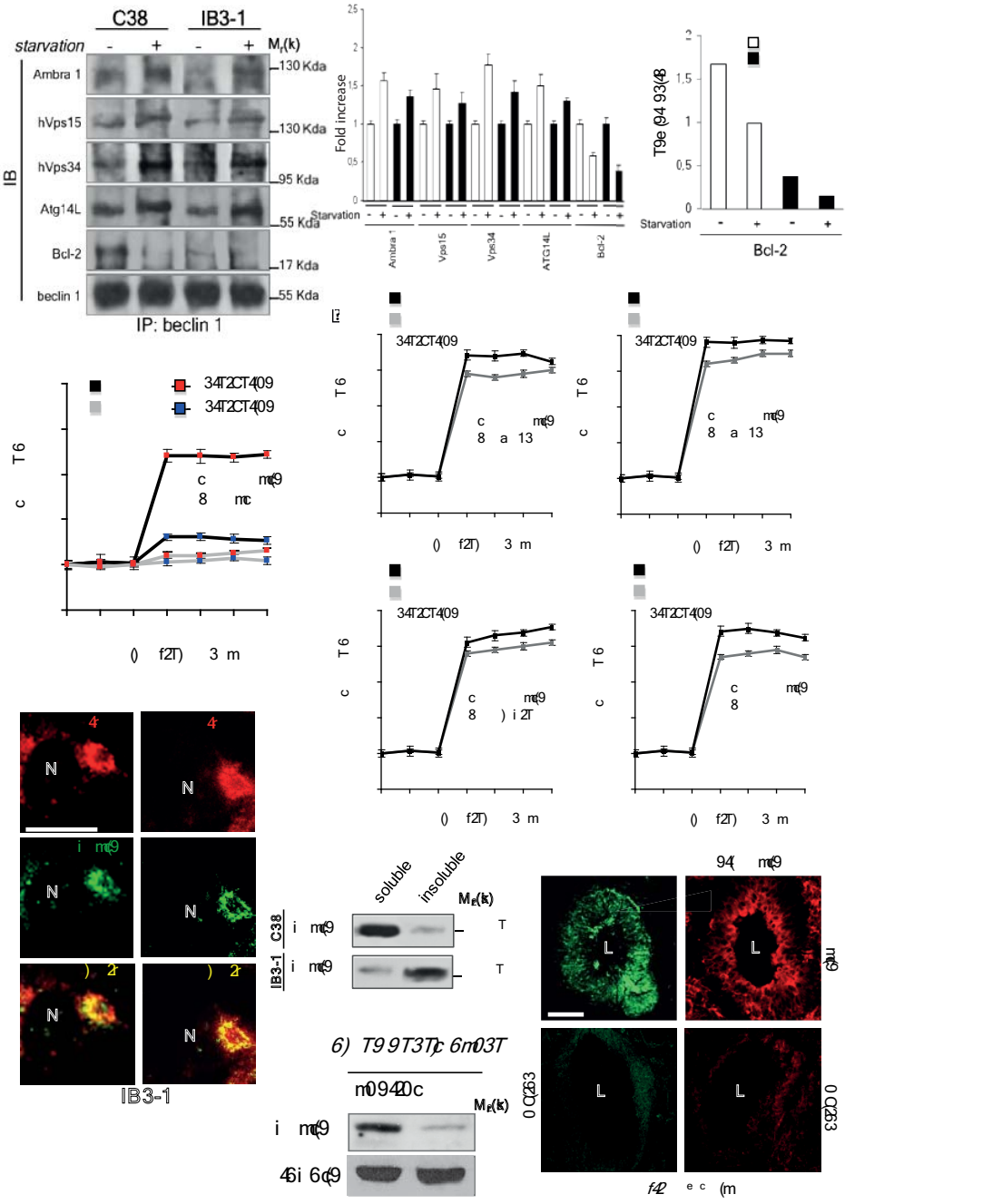

Figure S2 Beclin 1 and beclin 1 interactor proteins in CF airways.–(**a,b**) IB3-1 and C38 cells were grown in nutrient-rich or starvation medium. **(a,** left) Immunoprecipitated (IP) beclin 1 species from whole cell extracts from IB3-1 or C38 cells were subjected to immunoblotting with the antibodies against Ambra 1, hVps15, hVps34, Atg14L, Bcl-2, and beclin1. For full scan see Supplemtary Information, Fig.S10. (a, right) Densitometric analysis of the band intensity (mean ± s.d. of three independent experiments): fold increase after starvation versus cells cultured in nutrient-rich conditions. (**b**) FRET analysis of beclin 1-Alexa 546 fluorescence after Bcl-2-Cy5 photobleaching. F/F0 indicates post-bleaching/pre-bleaching fluorescence ratio of Al546/ Cy5. (**c**) Starved IB3-1 and C38 cells. FRET analysis of beclin 1-Alexa 546 fluorescence after hVps34-Cy5, hVps15-Cy5, Ambra-1-Cy5 and ATG14L-Cy5 photobleaching. F/F0 indicates post-bleaching/pre-bleaching fluorescence ratio of Al546/Cy5. (**d**) Confocal microscopy micrographs of IB3-1 cells of ATG14L (red) and beclin 1 (green) (left panel) or ATG14L (red) and HDAC-6 (green) (right panel) antibodies. Yellow indicates co-localization. N, nucleus. Scale bar, 10 µm. **(e)** Immunoblot of Beclin1 of soluble and insoluble detergent (NP-40) fractions in starved C38 and IB3-1. (**f**) Beclin 1 immunoblot in control and CF human nasal mucosa. αβ-tubulin was used as loading control. **(g)** GFP and mouse beclin 1 expression in airway tissues from *Cftr*^{F508del} homozygous mice after intranasal administration of a lentiviral vector encoding beclin 1(LV-beclin1) or expressing the GFP (LV-GFP). L, Lumen. Scale bar, 10 µm.

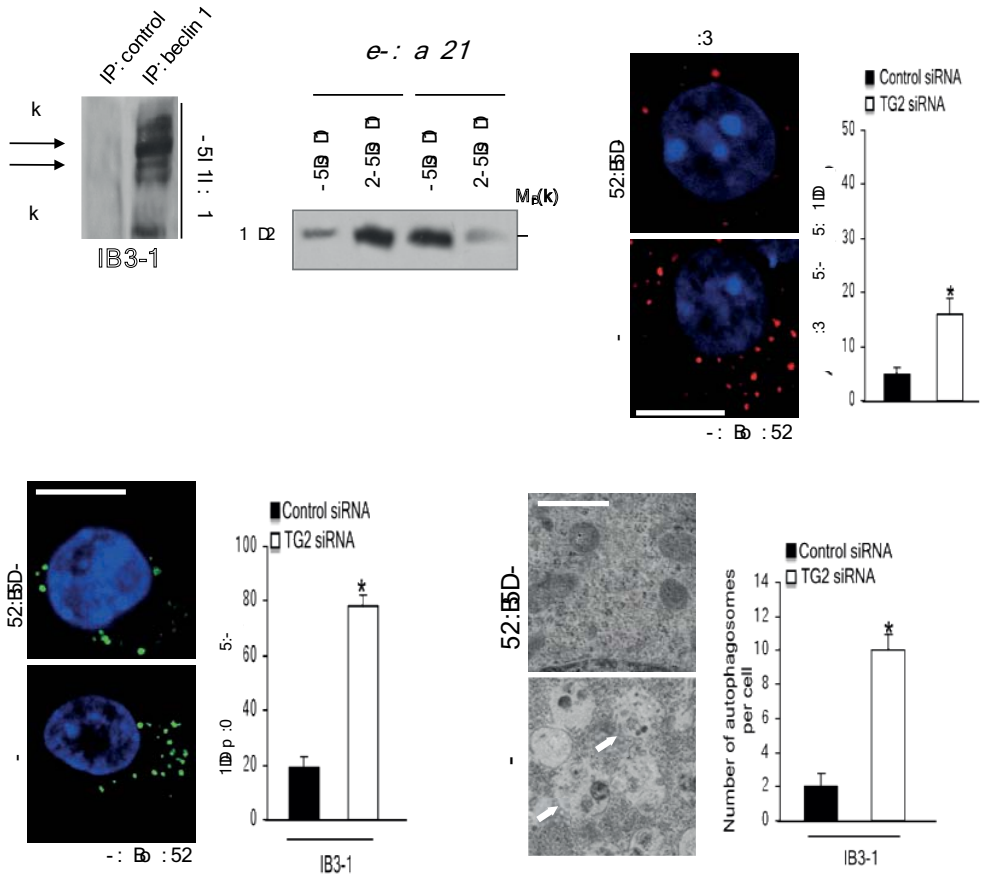

Figure S3 Effects of TG on autophagy in airway epithelia. (**a**) Sites for TG2 activity on beclin 1 sequence. **(b)** Immunoprecipitated (IP) beclin 1 species from whole cell extracts of IB3-1 is immunoreactive for the anti-isopeptide antibody. Immunoprecipitated (IP) without antibody from whole cell extracts of IB3-1 was used as control **(c)** Immunoblot analysis of beclin1 of soluble and insoluble detergent (NP-40) fractions in starved IB3-1 in presence or absence of cystamine. **(d-f)** IB3-1 cells were transfected with either TG2 siRNA or scrambled oligonucleotides upon starvation. (**d**) left panel, confocal microscopy micrographs Atg16L (red). DAPI (blue), nuclear counterstaining. Scale bar, 10 μm. right panel, quantification of the number of Atg16L dots/cell. Mean ± s.d. of three independent experiments (*,p<0.01 vs cells transfected with control siRNA; ANOVA). (**e**) left panel, confocal microscopy micrographs of LC3 (green). DAPI (blue), nuclear counterstaining. Scale bar, 10 μm. right panel, percentage of cells containing more than five LC3 positive punctate dots. Mean ± s.d. of three independent experiments (*, p<0.001 vs cells transfected control siRNA; ANOVA). (**f**) left panel, electron micrographs of starved IB3-1 cells showing areas enriched in autophagosomes (arrow) upon TG2 siRNA. Scale bar, 100 nm. righ panel, number of autophagosomes per cell, counted in 20 cells per experiment. Mean ± s.d. of three independent experiments. (*, p<0.001 vs siRNA control cells; ANOVA).

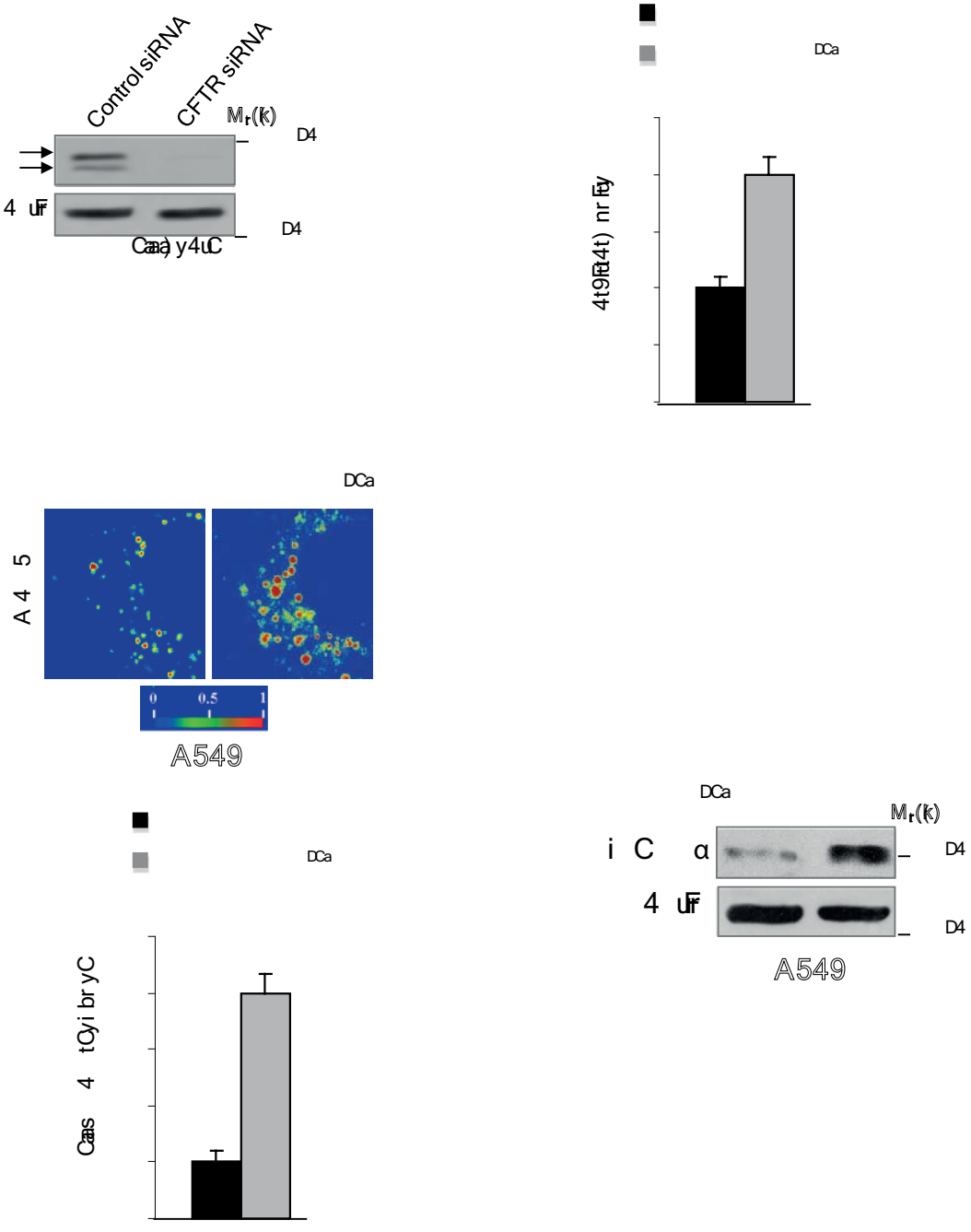

Figure S4 GFP-F508del-CFTR increases ROS and Calcium levels and activates UPR in A549 cells. (**a**). Immunoblot analysis of CFTR in C38 cells transfected with either human CFTR siRNA or scrambled oligonucleotides. β-actin was used as loading control. (**b-d**) A549 cells were transfected with 1 g of pGFP-F508del-CFTR, or pGFP. (**b**) Increase of intracellular ROS in GFP-F508del CFTR transfected A549 cells (each bar represents the mean±s.d. of three indipendent experiments). *, p<0.001 vs empty vector. DCF, 5-(and-6)-chloromethyl-2'7'-dichlorodihydrofluorescein diacetate acetyl ester (CM-H2DCFDA). **(c)** Ca^{2+} imaging of GFP-F508del CFTR transfected A549 cells loaded with FURA-2. Pseudocolor ratiometric images. Colors correspond to the scale of $[Ca^{2+}]_i$ increase. Red, high $[Ca^{2+}]_i$ contents. Quantification of results from three indipendent experiments is shown in the histogram. *, p<0.001 vs empty vector. N, nuclei. (**d**) Immunoblot analysis of p-eIF-2 in GFP-F508del CFTR transfected A549 cells. β-actin was used as loading control.

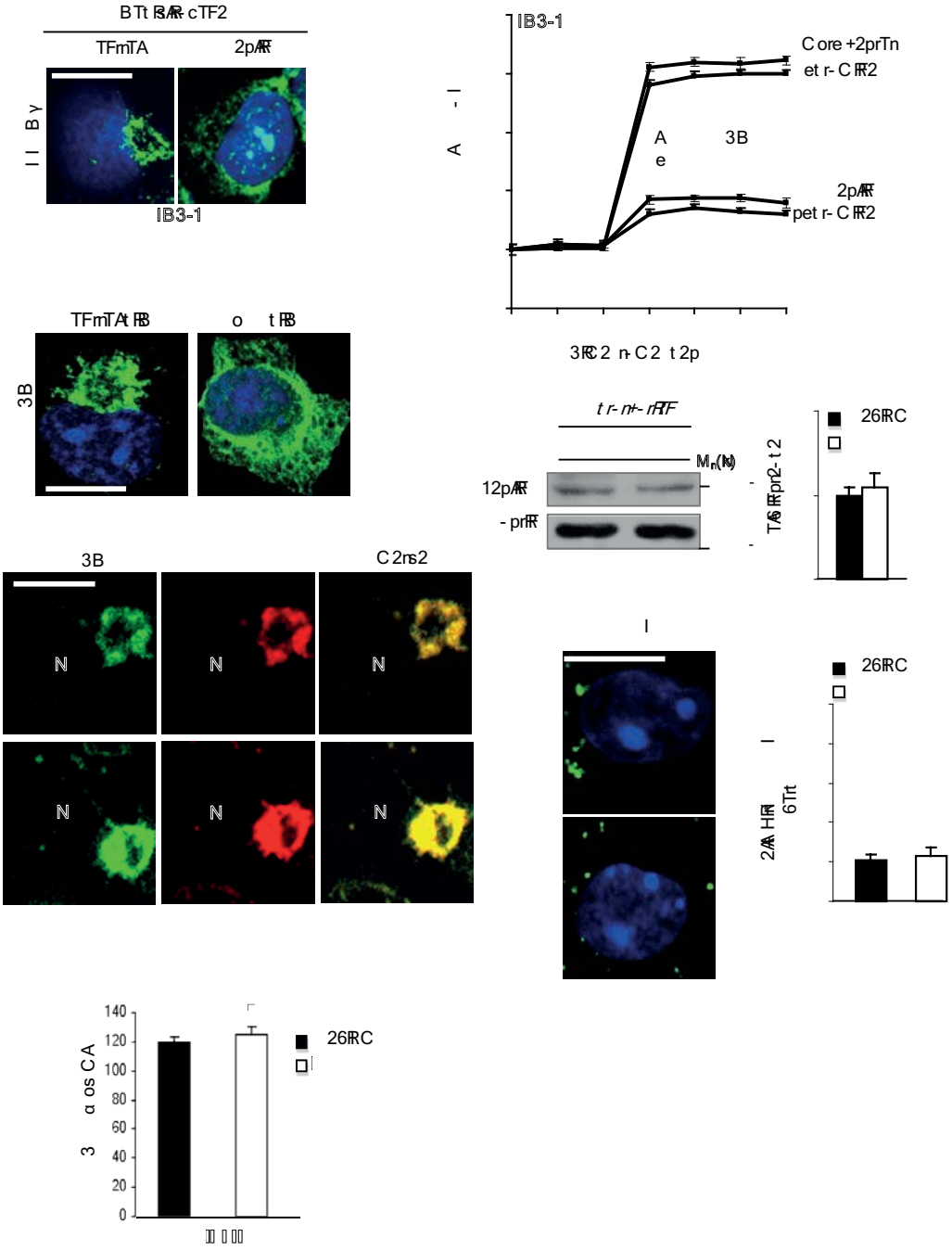

Figure S5 Beclin 1 overexpression and p62 knock down rescue aggresome formation. (**a**) IB3-1 cells transfected with either HA-tagged human beclin 1 or empty vector or with p62 siRNA or scrambled oligonucleotides followed by rosiglitazone. Confocal microscopy analysis of PPAR (green). DAPI (blue), nuclear counterstaining. Scale bar, 10 m (**b**) IB3-1 cells transfected with HA-beclin 1, or empty vector, or with cystamine in presence or absence of 3-MA. FRET analysis of CFTR-Alexa 546 fluorescence after HDAC6 -Cy5 photobleaching. F/F0 indicates post-bleaching/pre-bleaching fluorescence ratio of Al546/Cy5. (**c**) IB3-1 cells transfected with 50 nM human p62 siRNA or scrambled oligonucleotudes. Confocal microscopy analysis CFTR (green). DAPI (blue), nuclear counterstaining. Scale bar, 10 m. (**d**) Starved IB3-1 cells cultured with MG132. top panel, immunoblot of Beclin1. bottom panel, densitometric analysis normalized to β-actin (mean ± s.d. of three independent experiments). (**e**) Confocal microscopy analysis of CFTR (green) and HDAC-6 (red). Yellow colour indicates co-localization. N, nucleus. Scale bar, 10 m. (**f**) IB3-1 cells transfected with plasmid expressing GFP-LC3. left panel, confocal laser microscopy. Scale bar, 10 m. right panel, percentage of cells containing more than five GFP-LC3 punctate dots per cell. Mean ± s.d. of five independent experiments. (**g**) TNF- secretion in IB3-1 cells after MG132 treatment. Each bar represents the mean ± s.d. of three independent experiments. *, p<0.01 vs control ANOVA.

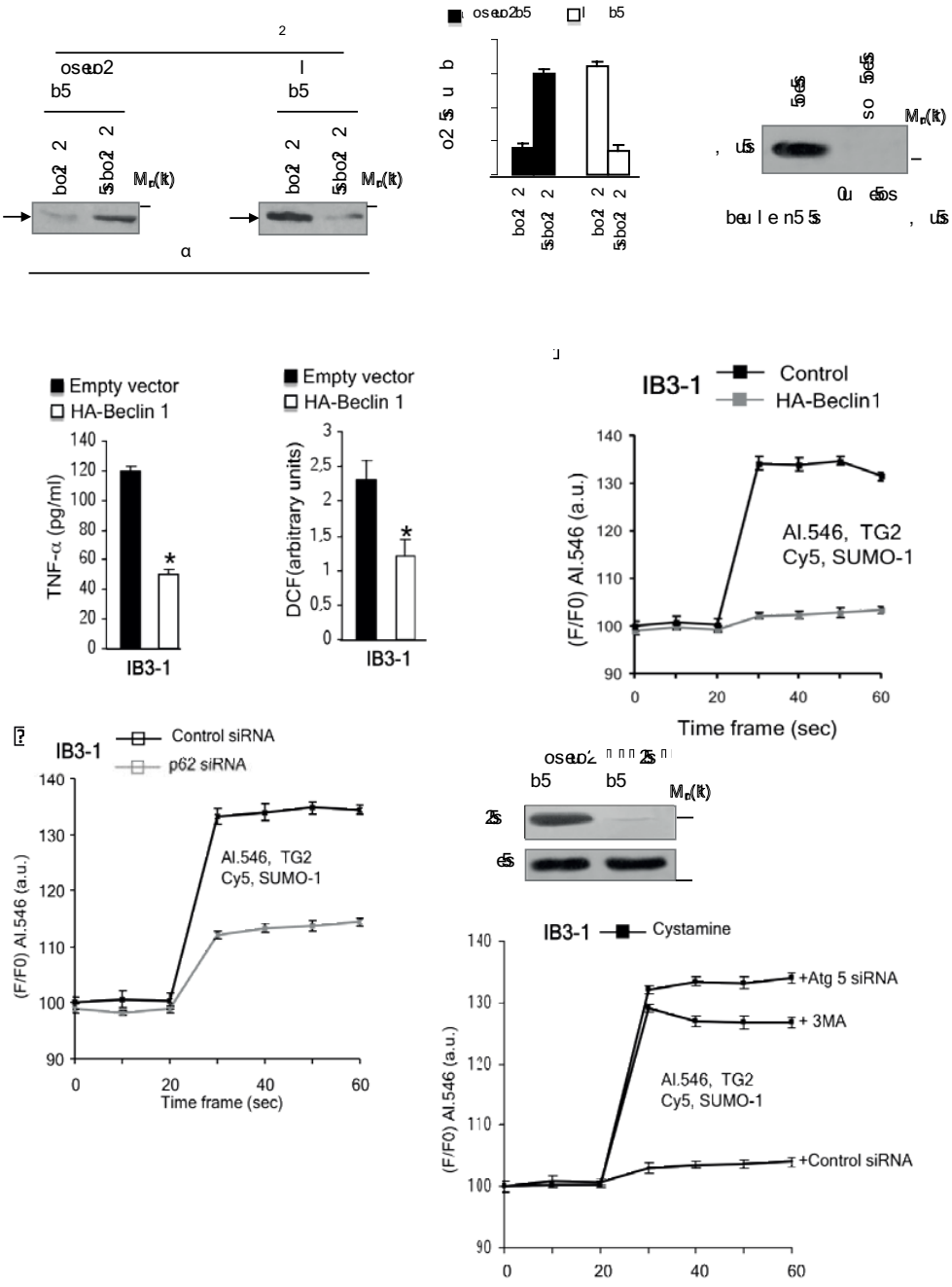

Figure S6 Cystamine and p62 knock down restores F508del-CFTR trafficking and inflammatory phenotype in CF airway epithelia(**a**) IB3-1 cells were transfected with 1μg of pGFP-F508del-CFTR in presence of either human p-62 siRNA or scrambled oligonucleotides. The cells were lyzed with detergent (NP-40) to obtain soluble and insoluble fractions. left panel, immunoblot analysis of GFP. B: core-glycosylated form (MW approximately 150 kDa, revealed as 190kDa as GFP-tagged). right panel, densitometric analysis (mean ± s.d. of three independent experiments). (**b**) Immunoblot of E-cadherin as control of membrane fractioning. **(c-d)** IB3-1 cells transfected with either human HA-tagged-beclin 1 or empty vector. (**c**) TNF-α secretion. Each bar represents the mean ± s.d. of three independent experiments. *, p<0.01 vs the empty vector, ANOVA. (**d**) Intracellular ROS content [CM-H2DCFDA (DCF) detection by a Wallac 1420 multilabel counter]. Each bar represents the mean ± s.d. of three independent experiments.*, p<0.01 compared to the empty vector **(e)** IB3-1 cells transfected with either human p62 siRNA or scrambled oligonucleotides. FRET analysis of TG2-Alexa 546 fluorescence after SUMO-1-Cy5 photobleaching. F/F0 indicates post-bleaching/pre-bleaching fluorescence ratio of Al546/Cy5. **(f)** IB3-1 cells were transfected with either human HA-tagged-beclin 1 or empty vector. FRET analysis of TG2-Alexa 546 fluorescence after SUMO-1 Cy5 photobleaching. (**g**) IB3-1 cells were transfected with either human Beclin 1 or scrambled oligonucleotides. Immunoblot analysis of beclin1. β-actin was used as loading control. (**h**) IB3-1 cells transfected with 50 nM human ATG5 siRNA or scrambled oligonucleotides or cultured with cystamine in presence or absence of 3MA. FRET analysis of TG2-Alexa 546 fluorescence after SUMO-1-Cy5 photobleaching. F/F0 indicates post-bleaching/pre-bleaching fluorescence ratio of Al546/Cy5.

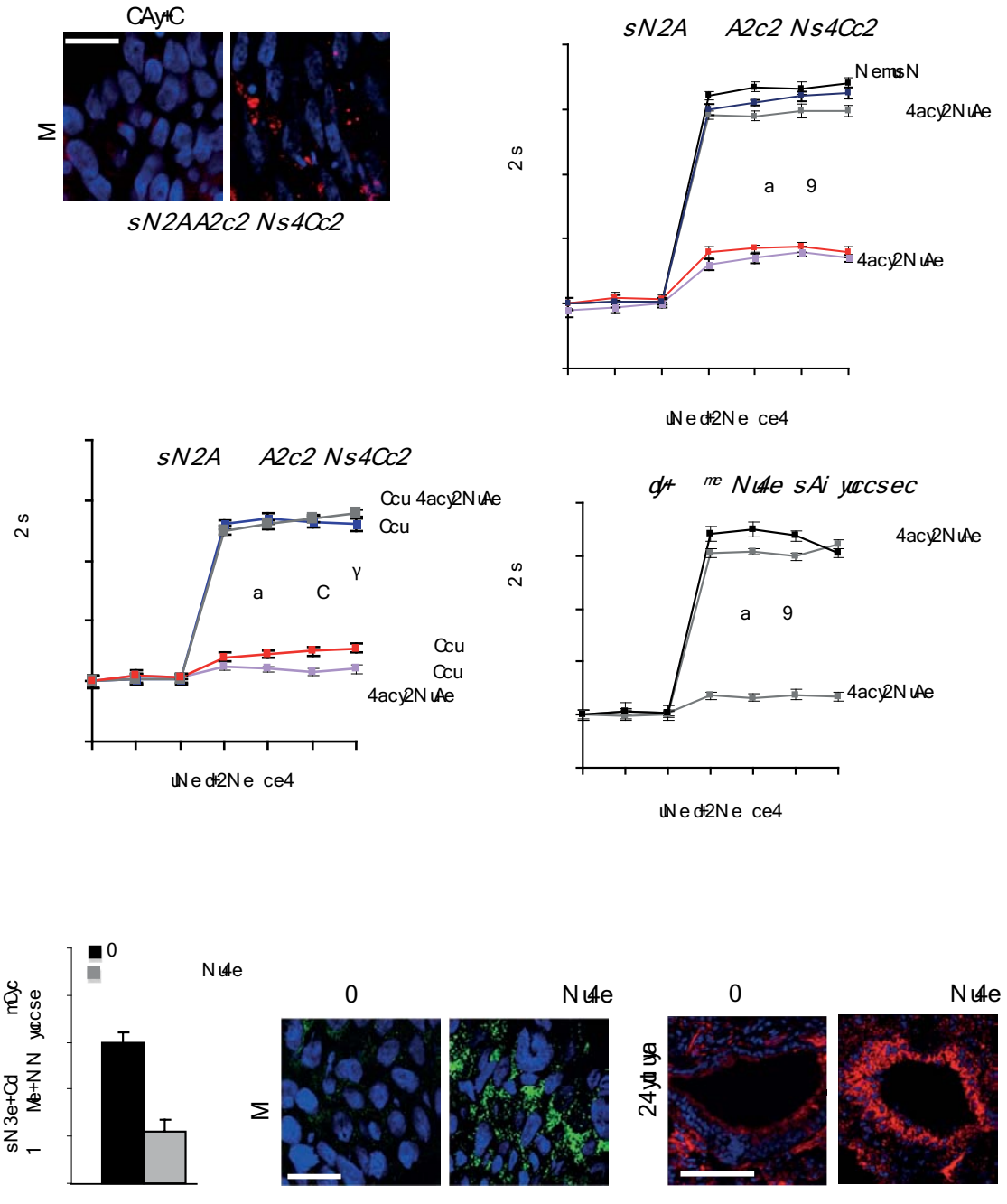

Figure S7 Defective autophagy in human nasal mucosa and in CF mouse models. (**a**) Confocal microscopy micrographs of p62 in control and CF human nasal polyp mucosa. DAPI (blue), nuclear counterstaining. Scale bar, 10 m. Representative of five control and five CF patients (**b**) FRET analysis of TG2-Alexa 546 fluorescence after SUMO-1 Cy5 photobleaching in human nasal mucosae treated with cystamine or NAC in presence or absence of 3-MA. Representative of five cultured CF human nasal polyp mucosa (patients #6-10, **Supplementary Table 1** online). (**c**) FRET analysis of PPAR -Alexa 546 fluorescence after N-CoR-Cy5 photobleaching in in human nasal mucosae treated with cystamine or NAC in presence or absence of 3-MA followed by rosiglitazone (**d**) FRET analysis of TG2-Alexa 546 fluorescence after SUMO-1 Cy5 photobleaching in lung tissues from *Cftr*^{F508del} homozygous mice treated with cystamine or PBS in presence or absence of 3-MA (representative of seven *Cftr*^{F508del} mice). (**e**) Fluorescence-microscopy quantitation of LC3 dots in lung tissues from WT and *Scnn1b*-Tg mice (10 mice per group). Mean ±s.d. *, p<0.01 compared to WT mice. (**f**) Confocal microscopy micrographs of p62 in WT and *Scnn1b*-Tg mice. DAPI (blue), nuclear counterstaining. Scale bar, 10 m. **(g)** Confocal microscopy micrographs of TG2 activity in WT and *Scnn1b*-Tg mice. DAPI (blue), nuclear counterstaining. Scale bar, 100 m.

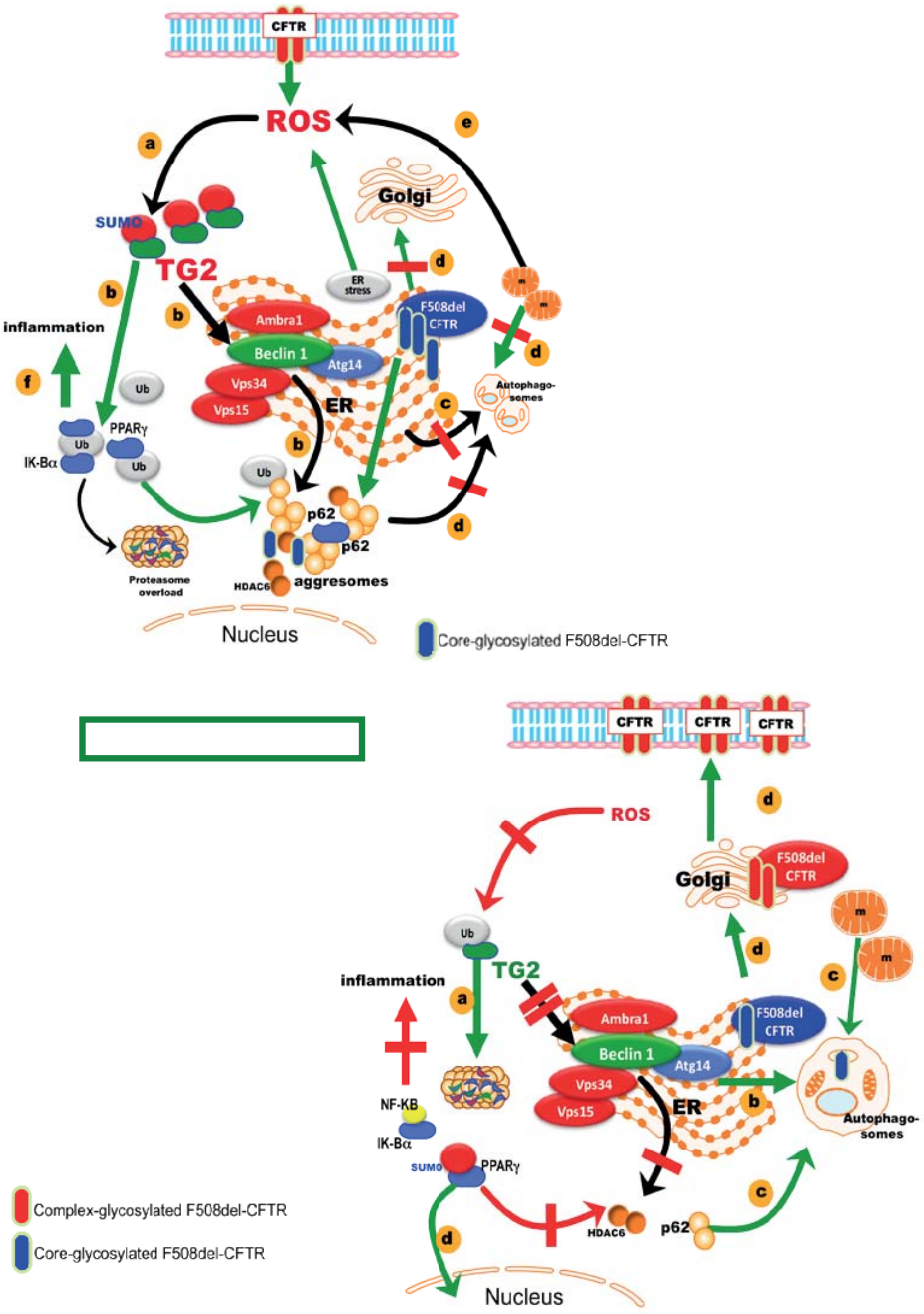

Figure S8 Schematic representation of the main findings of the study. **a:** Defective autophagy in CF airway epithelia. (**a**) Defetive CFTR and mutant CFTR-induced ER stress both increase ROS levels and drive TG2 SUMOylation and persistence of high TG2 protein levels. (**b**) ROS-driven TG2 SUMOylation induces cross-linking, ubiquitination, and aggresome sequestration of PPAR and IK-B . TG2 also cross-links beclin 1 and favours its sequestration in aggresomes. Cross-linked beclin 1 dislocates PI3K complex III away from the Endoplasmic Reticulum (ER) leading to sequestration of beclin 1 interactome into aggresomes. (**c**) This leads to inhibition of autophagy. (**d**) Defective autophagy induces accumulation of damaged mitochondria and p62 accumulation that leads to proteasome overload, favours the formation of protein aggregates, impairs CFTR trafficking leading to sequestration of F508del-CFTR in HDAC6+/p62+ aggresomes. (**e**) Defective autophagy generates a vicious cycle (black arrows) with increasing ROS and TG2 levels and (**f**) inflammation. **b:** Effects of cystamine treatment. (**a**) Cystamine inhibits TG2 cross-linking activity and also decreases TG2 SUMOylation, by reducing ROS levels, favouring TG2 ubiquitination and proteasome degradation. (**b**) This avoids cross-linking of beclin 1 leading to restoration of beclin 1 interactome at the ER levels and allows autophagosome formation and autophagy upon starvation. (**c**) Restoration of beclin 1 and autophagy decreases p62 and aggresome formation and also leads to (**d**) restoration of PPAR and IK-B , thus dampening inflammation. The inhibition of aggresome sequestration of misfolded/modified proteins also allows F508delCFTR to traffic to the Golgi network and plasma membrane.

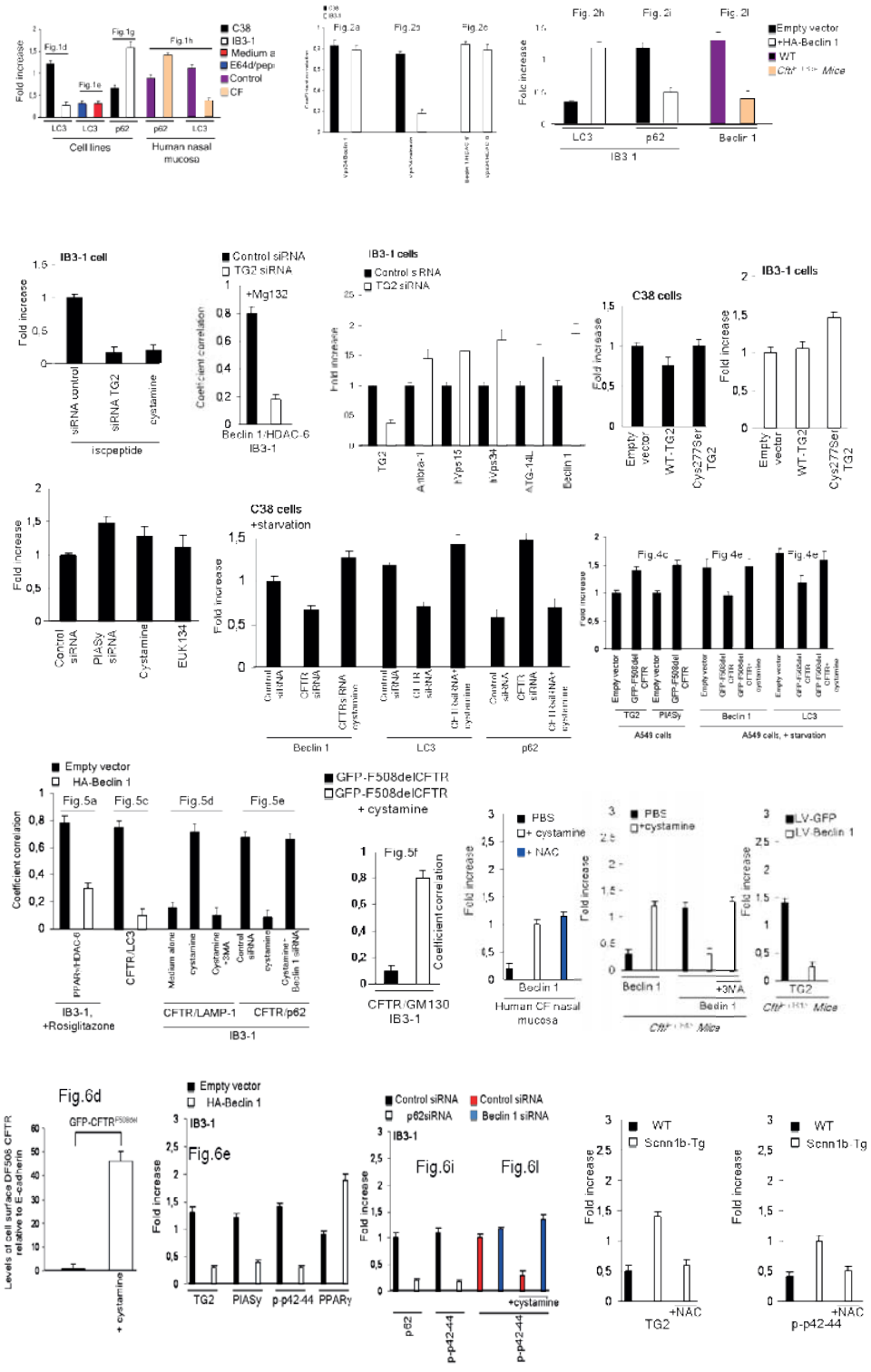

Figure S9 Densitometric analysis of blot experiments and quantitation of confocal microscopy micrographs.

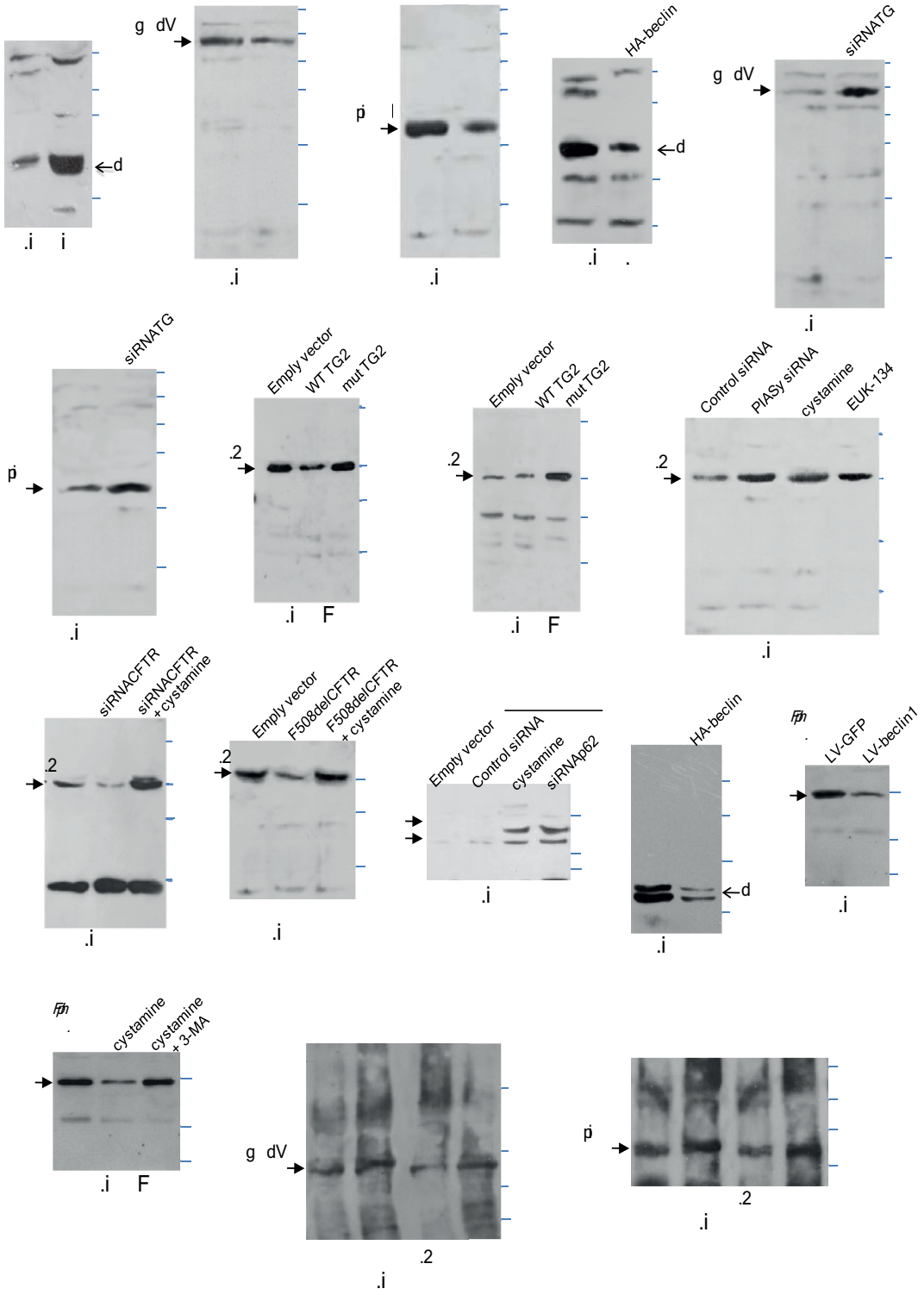

Figure S10 Full scan of key blot experiments

Supplementary Tables

Supplementary Table 1: Clinical characteristics of Cystic Fibrosis patients.

Supplementary Table 2: Sequence of primers used for Quantitative RT-PCR and sequence of siRNA oligonucleotides

Supplementary Table 3: Primary antibodies

Supplementary Table 1: Clinical characteristics of Cystic Fibrosis patients.

Patients #	**1**	**2**	**3**	**4**	**5**	**6**	**7**	**8**	**9**	**10**
Sex; Age*	F 13, 2	M 14, 3	F 13,4	M 13, 1	F 13, 6	M 13,3	M 29	F 19	M 11	F 24
Age at diagnosis*	0, 6	0, 3	0, 8	2, 3	11, 0	1,5	7,2	2,0	0,4	7,0
Genotype	F508del/ F508del	F508del/ W1282X	F508del/ N1303K	F508del/ G542X	F508del/ F508del	F508del/ F508del	F508del/ G542X	F508del/ W1282X	F508del/ F508del	F508del/ W1282X
Pancreatic insufficiency	Yes	Yes	Yes	Yes	Yes	Yes	Yes	Yes	Yes	Yes
Chronic respiratory infection (*PA*)	Yes	No	No	No	Yes	Yes	No	Yes	Yes	No
Mean FEV1, % predicted	69	78	73	80	69	81	72	64	72	75

patient's number; *, (years,months)

Supplementary Table 2:

Sequence of primers used for Quantitative RT-PCR

GENE NAME	*FOWARD* PRIMER SEQUENCE (5'-3')	*REVERSE* PRIMER SEQUENCE (5'-3')
β-actin	ATTGCCGACAGGATGCAGAA	ACATCTGCTGGAAGGTGGACAG
ULK1	GTCCAGCTTTGACAGTCAGT	TCCCAGGACTCAGGATTCCA
ULK2	TGTTTCTAGGGTGTAGCTGG	CACCATCTACCCCAAGACCT
ATG5	AGTATCAGACACGATCATGG	TGCAAAGGCCTGACACTGGT
ATG6\BECLIN1	TGTCACCATCCAGGAACTCA	CTGTTGGCACTTTCTGTGGA
ATG7	CACTGTGAGTCGTCCAGGAC	CGCTCATGTCCCAGATCTCA
ATG8	CGTGGAGTCCGCGAAGATTC	AGGCATGAGGACAATGCACA
ATG14L	ATGAGCGTCTGGCAAATCTT	CCCATCGTCCTGAGAGGTAA
Bcl2	GCTGCTGGAGGCTGGGGAGA	CCCCCACAGGAACCCTCCTC
hVsps34	AAGCAGTGCCTGTAGGAGGA	TGTCGATGAGCTTTGGTGAG
hVsps15	TGGGACTGGCGGTCTGCACT	CGGGACGGGAAAACGCGTCA
Ambra-1	AACCCTCCACTGCGAGTTGA	TCTACCTGTTCCGTGGTTCTCC

Sequence of siRNA oligonucleotides

GENE NAME	OLIGO-SENSE(5'-3')	OLIGO-ANTISENSE (5'-3')
Control	UACCGUCUCCACUUGAUCGdTdT	CGAUCAAGUGGAGACGGUAdTdT
TG2	GCGUCGUGACCAACUACAAdTdT	UUGUAGUUGGUCACGACGCdGdG
PIASγ oligo#2	CAAGACAGGUGGAGUUGAUUU	pAUCAACUCCACCUGUCUUGUU
PIASγ oligo#4	AAGCUGCCGUUCUUUAAUAUU	pUAUUAAAGAACGGCAGCUUUU
BECLIN-1	AAGAUUGAAGACACAGGAGGC	GCCUCCUGUGUCUUCAAUCUU
p62	UACAAAUUUAACAGGAUGGdTdT	CCAUCCUGUUAAAUUUGUAdTdT
CFTR oligo#1	CGUGUGUCUGUAAACUGAUGGCUAA	UUAGCCAUCAGUUUACAGACACAGC
CFTR oligo#2	CCCUUCUGUUGAUUCUGCUGACAAU	AUUGUCAGCAGAAUCAACAGAAGGG
CFTR oligo#3	GGCAUAGGCUUAUGCCUUCUCUUUA	UAAAGAGAAGGCAUAAGCCUAUGCC
ATG5 oligo#1	GGUUUGGACGAAUUCCAACUUGUUU	AAACAAGUUGGAAUUCGUCCAAACC
ATG5 oligo#2	GAUCACAAGCAACUCUGGAUGGGAU	AUCCCAUCCAGAGUUGCUUGUGAUC
ATG5 oligo#3	CAAAGAAGUUUGUCCUUCUGCUAUU	AAUAGCAGAAGGACAAACUUCUUUG

Supplementary Table 3: Primary Antibodies

ANTIBODY	COMPANY	APPLICATION
phospho-p42/p44 MAP kinases	CELL SIGNALING	IB
E-cadherin	CELL SIGNALING	IB
β-actin (13E5)	CELL SIGNALING	IB
PPARγ (E8)	SANTA CRUZ BIOTECNOLOGY	IB
PIASγ(H75)	SANTA CRUZ BIOTECNOLOGY	IB
Ubiquitin(FL76)	SANTA CRUZ BIOTECNOLOGY	IB, IF
TG2 (H237)	SANTA CRUZ BIOTECNOLOGY	IB
TG2 (CUB7402)	NEOMARKER	IB
GFP(FL)	SANTA CRUZ BIOTECNOLOGY	IB, IF
hVps15\p150 (Nterm)	SANTA CRUZ BIOTECNOLOGY	IB, IF
Bcl-2(C2)	SANTA CRUZ BIOTECNOLOGY	IB, IF
HDAC-6	SANTA CRUZ BIOTECNOLOGY	IF
SUMO-1	SANTA CRUZ BIOTECNOLOGY	IF
COX-2	SANTA CRUZ BIOTECNOLOGY	IF
BECLIN-1	ABCAM	IB,IF
LC3	ABCAM	IB,IF
phospho-eIF2α	ABCAM	IB
CFTR	ABCAM	IB,IF
AMBRA-1	ABCAM	IB
p62	BD BIOSCIENCE	IB,IF
HA	BD BIOSCIENCE	IB
αβ-TUBULIN	SIGMA	IB
hVps34	SIGMA	IB,IF
Atg14L	SIGMA	IB,IF
LAMP1	SIGMA	IF
Nε(γ-L-glutamyl)-L-lysine isopeptide (81DIC2)	COVOLAB	IB
CD68	ACRIS	IF
Alexa 546anti-TG2 / Cy5-anti anti-SUMO-1	(Molecular Probes, INVITROGEN)	FRET
Alexa 546anti-beclin 1 / Cy5-anti anti-HDAC6	(Molecular Probes, INVITROGEN)	FRET
Alexa 546anti-PPARγ/ Cy5-anti anti-N-CoR	(Molecular Probes, INVITROGEN)/SANTA CRUZ	FRET
Alexa 546anti-Bcl-2/ Cy5-anti anti-Beclin	(Molecular Probes, INVITROGEN)	FRET
Alexa 546anti-Beclin 1 / Cy5-anti Vps34	(Molecular Probes, INVITROGEN)	FRET
Alexa 546anti-Beclin 1 / Cy5-anti Vps34	(Molecular Probes, INVITROGEN)	FRET
Alexa 546anti-Beclin 1 / Cy5-anti Vps15	(Molecular Probes, INVITROGEN)	FRET
Alexa 546anti-Beclin 1 / Cy5-anti Ambra-1	(Molecular Probes, INVITROGEN)	FRET
Alexa 546anti-Beclin 1 / Cy5-anti ATG14L	(Molecular Probes, INVITROGEN)	FRET
Alexa 546anti-CFTR / Cy5-anti HDAC-6	(Molecular Probes, INVITROGEN)	FRET
Alexa 546-anti GFP / Cy5-anti HDAC-6	(Molecular Probes, INVITROGEN)	FRET

Lysosomal accumulation of gliadin p31–43 peptide induces oxidative stress and tissue transglutaminase-mediated PPARγ downregulation in intestinal epithelial cells and coeliac mucosa

Luigi Maiuri, Alessandro Luciani, Valeria Rachela Villella, et al.

Gut 2010 59: 311-319 originally published online December 1, 2009
doi: 10.1136/gut.2009.183608

Lysosomal accumulation of gliadin p31—43 peptide induces oxidative stress and tissue transglutaminase-mediated PPARγ downregulation in intestinal epithelial cells and coeliac mucosa

Luigi Maiuri,[1] Alessandro Luciani,[1,2] Valeria Rachela Villella,[3] Angela Vasaturo,[3] Ida Giardino,[4] Massimo Pettoello-Mantovani,[1] Stefano Guido,[2,3] Olivier N Cexus,[5] Nick Peake,[5] Marco Londei,[6] Sonia Quaratino[5]

See Commentary, p 286

► Supplementary methods and figures are published online only at http://gut.bmj.com/content/vol59/issue3

[1]Institute of Pediatrics, University of Foggia, Foggia, Italy
[2]Dynamic Imaging Microscopy, CEINGE, Naples, Italy
[3]Department of Chemical Engineering, University Federico II of Naples, Naples, Italy
[4]Department of Biomedical Science, University of Foggia, Foggia, Italy
[5]Cancer Research UK Oncology Unit, University of Southampton, Southampton, UK
[6]Novartis Pharma AG Translational Medicine, Basel, Switzerland

Correspondence to
Professor Luigi Maiuri, Institute of Pediatrics, University of Foggia, viale Pinto 1, Foggia 71100, Italy; maiuri@unina.it

Revised 13 July 2009
Accepted 1 September 2009
Published Online First 1 December 2009

ABSTRACT

Background An unresolved question in coeliac disease is to understand how some toxic gliadin peptides, in particular p31—43, can initiate an innate response and lead to tissue transglutaminase (TG2) upregulation in coeliac intestine and gliadin sensitive epithelial cell lines.

Aim We addressed whether the epithelial uptake of p31—43 induces an intracellular pro-oxidative envoronment favouring TG2 activation and leading to the innate immune response.

Methods The time course of intracellular delivery to lysosomes of p31—43, pα-2 or pα-9 gliadin peptides was analysed in T84 and Caco-2 epithelial cells. The effects of peptide challenge on oxidative stress, TG2 and peroxisome proliferator-activated receptor (PPAR)γ ubiquitination and p42/44—mitogen activated protein (MAP) kinase or tyrosine phosphorylation were investigated in cell lines and cultured coeliac disease biopsies with/without anti-oxidant treatment or TG2 gene silencing by immunoprecipitation, western blot, confocal microscopy and Fluorenscence Transfer Resonance Energy (FRET) analysis.

Results After 24 h of challenge p31—43, but not pα-2 or pα-9, is still retained within LAMP1-positive perinuclear vesicles and leads to increased levels of reactive oxygen species (ROS) that inhibit TG2 ubiquitination and lead to increases of TG2 protein levels and activation. TG2 induces cross-linking, ubiquitination and proteasome degradation of PPARγ. Treatment with the antioxidant EUK-134 as well as TG2 gene silencing restored PPARγ levels and reversed all monitored signs of innate activation, as indicated by the dramatic reduction of tyrosine and p42/p44 phosphorylation.

Conclusion p31—43 accumulation in lysosomes leads to epithelial activation via the ROS—TG2 axis. TG2 works as a rheostat of ubiquitination and proteasome degradation and drives inflammation via PPARγ downregulation.

INTRODUCTION

Coeliac disease is a relatively common pathology that affects 1% of the population, and is precipitated by the ingestion of gluten proteins.[1—3] In predisposed individuals, gliadin acts as a stimulator of innate responses, in turn setting the type and intensity of the adaptive immune response[4] leading to a powerful activation of lamina propria gliadin-specific T cells.[5—7] Several fragments of gliadin have been found to be 'toxic' for predisposed individuals and it has also been suggested that different portion(s) of gliadin, ostensibly not those recognised by T cells, modulates this innate activation of coeliac small intestine.[7 8] Among these, p31—43 induces the expression of early markers of epithelial activation and leads to enterocyte apoptosis[4] both in coeliac intestine and in sensitive intestinal epithelial cell lines.[4]

The mechanisms by which p31—43 initiates an innate immune response in coeliac duodenum are, however, still elusive. It has been reported that p31—43 can delay epidermal growth factor receptor (EGFR) inactivation through interference with the endocytic pathway,[9] this suggesting that gliadin fragments could amplify the effects of trace amounts of EGF. Moreover, p31—43 induces early tissue transglutaminase (TG2) upregulation compared to immunodominant gliadin peptides.[10] This indicates that TG2 is not only central to the adaptive response to gliadin as the main deamidating enzyme of the immunodominant epitopes, but is also a key player in the initiation of inflammation in coeliac disease.[10] However, it is still unknown how p31—43 induces early TG2 activation in both coeliac intestine and 'gliadin-sensitive' intestinal epithelial cells.[9 10]

TG2 expression is regulated by retinoids, steroid hormones, peptide growth factors and cytokines, which also lead to a time-dependent decrease in TG2 ubiquitination,[11] indicating that post-translational control mechanisms also play a role in TG2 regulation. We have demonstrated that in cystic fibrosis (CF) airway epithelia,[12] sustained TG2 activation is driven by the increased levels of reactive oxygen species (ROS) caused by the CFTR genetic defect.[12] We therefore investigated whether p31—43 was able to drive an intracellular pro-oxidative environment and demonstrate that p31—43 leads to an increase of ROS levels in coeliac duodenum as well as T84 and Caco-2 intestinal epithelial cells.

To understand how p31—43 challenge induces oxidative stress, we analysed the delivery of this peptide to the intracellular degradation systems. It has been reported that the epithelial translocation of the gliadin immunostimulatory peptide 33-mer occurs by transcytosis after partial degradation through a rab5 endocytic compartment.[13] Increased transepithelial

translocation of the 33-mer was demonstrated in active coeliac disease compared to healthy controls. Moreover, incomplete degradation of the 33-mer and protected transport of the peptide 31–49 occurs in patients with untreated coeliac disease, thus favouring their respective immunostimulatory and toxic effects.[14] Here we show that p31–43 is retained within the lysosomes as compared to the more rapid disappearance of the immunodominant peptides pα-2 or pα-9 from the intracellular compartments. Blocking p31–43 endocytosis prevents the increase of ROS.

We have previously reported that in CF airways sustained TG2 activation drives inflammation by inducing cross-linking, ubiquitination and proteasome degradation, of the anti-inflammatory peroxisome proliferator-activated receptor (PPAR)γ,[12] a negative regulator of inflammatory gene expression.[15 16] Blocking TG2 through specific gene silencing[12] or the specific TG2 inhibitors restores a physiological control of inflammation in CF airways.[12]

We therefore addressed whether the p31–43-induced innate response was mediated by the ROS–TG2 axis via PPARγ downregulation.

METHODS

Peptide preparation

Biotinylated gliadin peptides p31–43, pα-9 (57–68) or pα-2 (62–75), control human thyroid peroxidase pTPO (535–551) and pTPO (536–547), peptide LGQQQPFAAVQPY (referred to below as pZ), and scrambled peptides with amino acid composition similar to p31–43 (QQGQPFPQPQLQY (referred to below as pX), GLQQFQPPPPQQY (referred to below as pY)) were synthesised by Primm (Milan, Italy) and the purity was determined by reverse-phase HPLC.

Cell lines

Human colon adenocarcinoma T84 or human colorectal carcinoma Caco-2 cell lines were cultured as recommended by American Type Culture Collection (ATCC).

Cell cultures

The cells were challenged with p31–43 for 24 h in the presence or absence of the ROS scavenger EUK-134 (50 μg/ml; Alexis Biochemicals, Florence, Italy), glutathione (GSH) (10 mmol/l; Sigma, Milan, Italy)[17] or the TG inhibitor cystamine (400 μmol/l; Sigma). To study internalisation of peptides, cells were challenged for 15, 30, 60 or 90 min, 3 or 24 h at 37°C with the biotinylated peptides (20 μg/ml). To inhibit endocytosis, the cells were pre-treated with the cholesterol-binding agent methyl-β-cyclo-dextrin (M-β-CD, 10 mmol/l; Sigma) or filipin (5 μg/ml; Sigma) and then challenged with biotinylated peptides. Cell lines were also incubated for 6 h with the PPARγ agonist rosiglitazone (10 μmol/l; Alexis Biochemicals) and then challenged with p31–43. The PPARγ antagonist GW9662 (1 μmol/l; Alexis Biochemicals) was added for 24 h to p31–43 in the presence or absence of TG2 siRNA oligos. The proteosome inhibitor MG132 (50 μmol/l; Calbiochem, Milan, Italy) was added 6 h before p31–43 in the presence or absence of TG2 siRNA oligos or EUK134.

Patients

Duodenal multiple endoscopic biopsies were performed for diagnostic purposes in seven treated patients with coeliac disease (mean age, 25 years; range, 16–41 years), and five non-coeliac controls affected by oesophagitis (22.4 years; range, 18–29 years). Informed consent was obtained from all individuals, and the study was performed according to the Ethics Committee of Regione Campania Health Authority. One specimen from each patient was used for diagnosis; the other samples were cultured in vitro as described.[4]

In vitro organ culture of biopsy specimens from patients with coeliac disease and from controls

Duodenal biopsy specimens were cultured as previously reported[4] for 3 or 24 h with medium alone, p31–43, pα-9, pα-2, pTPO (20 μg/ml) in the presence or absence of cystamine (400 μmol/l). Duodenal biopsy specimens were also incubated for 6 h with the PPARγ agonist rosiglitazone (10 μmol/l; Alexis Biochemicals) and then re-challenged for 3 h with p31–43.

RNA interference

The cells were transfected with 50 nmol/l human TG2 and scrambled small interfering RNAs (siRNAs) duplex using Hiperfect Transfection Reagent (Qiagen, Milan, Italy) at 37°C for 72 h as previously described.[12]

Adenoviral vector

Human manganese superoxide dismutase (MnSOD) cDNA was cloned into the shuttle vector pAd5CMVK-NpA.[18] MnSOD adenovirus was a gift from Michael Brownlee (Albert Einstein College of Medicine, New York). T84 cell lines were infected with MnSOD or the control adenovirus for 2 h, as previously described.[18]

Immunolocalisations

Tissue sections were individually incubated with the antibodies anti-phospho-tyrosine (PY99 mAb, 1:80, mouse IgG2b; Santa Cruz Biotechnology, Santa Cruz, California, USA), anti-PPARγ (clone E8, sc-7273, 1:100, mouse IgG1; clone H100, sc-7196, 1:100, rabbit polyclonal IgG; Santa Cruz Biotechnology) and control antibodies.[4 12] Cell lines were incubated with the antibodies against phospho-tyrosine, Early Endosome Antigen-1 (EEA-1; 1:100, rabbit polyclonal IgG; Abcam, Cambridge, UK), Rab7 (1:200, rabbit polyclonal IgG; Abcam), ARF-1 (1:100, rabbit polyclonal IgG; Abcam), LAMP-1 (1:100, rabbit polyclonal IgG; Abcam). Two-colour and indirect immunofluorescence were used for the detection of the tested markers by using an LSM510 Zeiss confocal laser scanning unit (Zeiss, Jena, Germany).[12] The correlation coefficient analysis was used as value of co-localisation between peptides and EEA-1 or LAMP-1 as described.[19]

In situ detection of TG2 enzymatic activity

The detection of in situ TG2 activity was performed by detection of biotinylated mono-dansyl-cadaverine (MDC) incorporation by Alexa-546 streptavidin as previously described.[4 12]

FRET microscopy

For acceptor photobleaching 4-μm frozen tissue sections of biopsy samples were fixed with buffered 2% paraformaldehyde and permeabilised with 0.5% Triton X-100. Upon fixation, tissues were immunostained with Alexa 546/anti-PPARγ (Santa Cruz Biotechnology, Santa Cruz, California, USA) and Cy5/anti-*N*ε(γ-L-glutamyl)-L-lysine isopeptide (Covolab, Cambridge, UK). Alexa 546 fluorescence was detected before and after Cy5 photobleaching.

Immunoblot and immunoprecipitation

Blots were incubated with anti-phospho-tyrosine (PY99 mAb, 1:500), anti-phospho-p42/p44 MAP kinases (Cell Signaling Technology, Danvers, Massachusetts, USA), PPARγ (clone E8 sc-7273; Santa Cruz Biotechnology, Santa Cruz, California, USA),

TG2 (clone CUB7402, 1:100; NeoMarkers, Fremont, California, USA), *N*ε(γ-L-glutamyl)-L-lysine isopeptide (clone 81DIC2; Covalab), ubiquitin (1:100 clone FL-76, rabbit polyclonal IgG; Santa Cruz Biotechnology), as previously described.[12]

Immunoprecipitations with anti-TG2 CUB 7402 mAb, anti-phospho-tyrosine and anti-PPARγ were carried out as previously described.[12]

ROS detection

Cell lines were pulsed with 10 μmol/l 5-(and-6)-chloromethyl-2′,7′-dichlorodihydrofluorescein diacetate acetyl ester (CM-H2DCFDA) (Molecular Probes, Invitrogen, Milan, Italy) and analysed as previously described.[12]

Statistical analysis

Cells challenged with peptides were compared with those cultured in medium alone, and with those cultured in the presence of the tested inhibitors. All experiments were performed at least in triplicate. Data distribution was analysed, and statistical differences were evaluated using ANOVA Tukey–Kramer test and SPSS 12 software. A p value of <0.05 was considered significant.

Detailed methods are described in the online supplementary information section.

RESULTS

p31–43 is retained within the lysosomes in T84 epithelial cells

T84 cells were incubated with biotinylated p31–43, p-α2, p-α9 (20 μg/ml) for 15, 30, 60, 90 min, 3 h and 24 h at 37°C. The peptides were rapidly detected (upon 15 min) in intracellular vesicles (figure 1A). Prolonged incubation (after 90 min to 24 h) increased the amount of p31–43 (figure 1A), but not of p-α9 (figure 1A) or p-α2 (data not shown), which resided in perinuclear vesicles. Soon after 15 min of challenge, peptides co-localised with EEA-1 (figure 1B), a marker of early endosomes,[13] whereas after 60 min they co-localised with Rab7-positive late endosomes (data not shown).[20] These data are in agreement with those described for the gliadin peptide 33-mer.[13] Co-staining with antibody against Arf1 (data not shown) did not reveal translocation of the peptides to the Golgi complex. After 90 min the internalised peptides co-localised with Lysosomal Associated Membrane Protein-1 (LAMP-1) (figure 1C), a marker of lysosomes.[20] The peptide/EEA-1 or peptide/LAMP-1 correlation coefficients of the spatial intensity distributions yielded a fairly high correlation coefficient (figure 1D), indicating that gliadin peptides are internalised and transported through early and late endocytic endosomes to lysosomes. No internalisation of peptides or co-localisation with LAMP-1 were observed when T84 cells were pre-incubated with M-β-CD, which inhibits clathrin-mediated endocytosis,[20] or filipin, a specific inhibitor of lipid raft- or caveolae-dependent endocytosis[20] (data not shown). This suggests that endocytosis is essential for the delivery of gliadin peptides to the lysosomes for degradation.

Increasing appearance of the internalised p31–43 in LAMP-1-positive vesicles, mainly limited to perinucelar localisation, was observed after 3–24 h of challenge (figure 1E,F). At these late time points p-α9 (figure 1E,F) or pα-2 (data not shown) were only faintly detected in LAMP-1-positive structures. The coefficients of p-α2 or p-α9 co-localisation with LAMP-1 were significantly lower compared to p31–43 (figure 1G), thus indicating that p31–43, but not p-α9 or p-α2 is retained within the lysosomes. Caco-2 cells showed the same behaviour as T84 after peptide challenge (data not shown). The control pTPO (535–551) (data not shown), pTPO (536–547) and pZ, as well as scrambled pX and pY peptides, behaved like pα-9 and pα-2 in both T84 (supplementary figure 1) and Caco-2 cell lines (data not shown).

p31–43 induces increase of ROS in T84 epithelial cells

T84 cells were pulsed with 10 μmol/l CM-H2DCFDA in the presence of the tested peptides and the levels of ROS were monitored after 90 min, 3 h and 24 h of challenge. The intracellular transport of gliadin peptides through early and late endocytic endosomes did not induce ROS generation (data not shown). Moreover, after 90 min of challenge neither p31–43 nor pα-9, both detected in LAMP-1 positive vesicles (figure 1C), induced significant increase of ROS (figure 2A). At the later time points (3–24 h of challenge), p31–43, but not pα-9 (figure 2A), pα-2, pTPO (535–551) (data not shown) or peptides pTPO (536–547), pX, pY and pZ (supplementary figure 1) induced a time-dependent significant increase of ROS levels, suggesting that the prolonged persistence of p31–43 in LAMP-1 positive vesicles (figure 1E,F) generates a pro-oxidative environment. No increase of ROS was observed after challenge with p31–43 upon M-β-CD or filipin treatment (figure 2B).

The generation of a pro-oxidative environment induces activation of different stress sensitive signalling pathways.[9 12 21] Since the challenge with p31–43 induces phosphorylation of the extracellular signal-regulated kinases 1/2 (Erk1/2, p42/44 mitogen-activated protein kinases, MAPK),[9] we investigated whether p31–43-induced ROS-mediated p42/44 MAPK phosphorylation in T84 cells. We demonstrated that p42–44 MAPK phosphorylation induced by the challenge with p31–43 was prevented by the incubation with the catalase–superoxide dismutase (SOD) mimetic EUK-134[12] (figure 2C), as well as by GSH[17] or by MnSOD over-expression[18] (supplementary figure 2). This further indicates that the generation of a pro-oxidative environment is critical to p31–43 biological activity in T84 cells.

p31–43 induces ROS-dependent inhibition of TG2 ubiquitination

To investigate whether the increased levels of ROS may account for the p31–43-induced increase of TG2 levels,[12] we incubated p31–43-challenged T84 cells with EUK-134. We demonstrated that EUK-134 was effective in controlling the increase of TG2 protein levels (figure 3A) and TG2 activity (data not shown) induced by p31–43. The same effects as EUK-134 were observed after incubation with GSH or upon MnSOD over-expression (supplementary figure 2). No increase of TG2 was observed after challenge with p31–43 upon M-β-CD or filipin treatment (data not shown). This indicates that p31–43 internalisation is critical for the induction of ROS-mediated TG2 activation.

Since post-translational modifications of TG2, such as ubiquitination, play a role in regulating the levels of TG2 protein[11] we investigated whether TG2 ubiquitination was influenced by ROS generation induced by p31–43. We incubated T84 cells with p31–43 in the presence or absence of EUK-134 upon inhibition of proteasome function by MG132,[12] then immunoprecipitated TG2 protein and detected ubiquitin co-reactivity. The ubiquitin immunoreactivity on TG2 immunoprecipitates was enhanced upon treatment with EUK-134 (figure 3B). No effects of p31–43 on TG2 ubiquitination were observed when T84 cells were pre-treated with M-β-CD or filipin (data not shown).

p31–43-induced TG2 drives PPARγ cross-linking and proteasome degradation in T84 cells

We investigated whether the p31–43-induced TG2 activation was effective in inducing PPARγ cross-linking and proteasome degradation as we have reported in CF airways.[12]

We immunoprecipitated PPARγ species from T84 cell lysates after challenge with p31–43 and detected the immunoreactivity

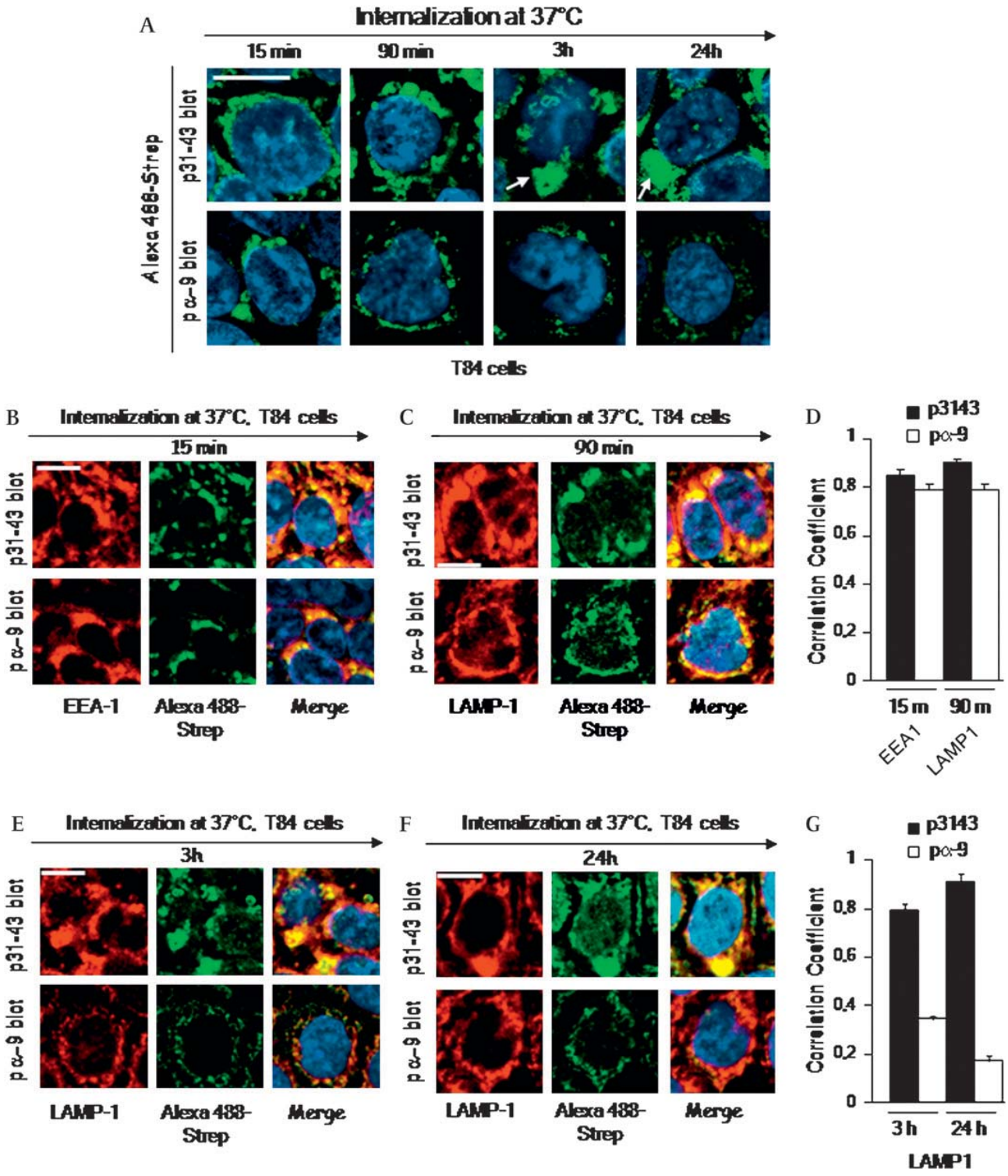

Figure 1 p31—43, but not pα-9, accumulates within the lysosomes in T84 cells. (A) Incubation of T84 cells with biotinylated p31—43 and pα-9 from 15 min to 24 h at 37°C and detection by confocal microscopy upon incubation with Alexa 488-conjugated streptavidin. After 15 min both p31—43 and p-α9 were detected in intracellular peripheral vesicles. Prolonged incubation (90 min to 24 h) increased the amount of p31—43, but not of p-α9, in perinuclear vesicles. (B) Co-localisation of p31—43 and p-α9 (green) with EEA-1 (red) in T84 cells upon 15 min of challenge. Both peptides were detected in EEA1-positive vesicles (yellow). (C) Co-localisation of p31—43 and p-α9 (green) with LAMP-1 (red) in T84 cells after 90 min of challenge. Both peptides were detected in LAMP1-positive vesicles (yellow). (D) Quantitative measurement of peptides/EEA-1 or peptides/LAMP-1 co-localisations shown in B and C, respectively. Each bar represents the mean plus SEM of three independent experiments. (E—F) Co-localisation of p31—43 and p-α9 (green) with LAMP-1 (red) in T84 cells after 3 h and 24 of challenge. p31—43, but not pα-9, was detected in LAMP-1 positive vesicles (yellow). (G) Quantitative measurement of peptides/LAMP-1 co-localisations shown in E and F, respectively. Each bar represents the mean plus SEM of three

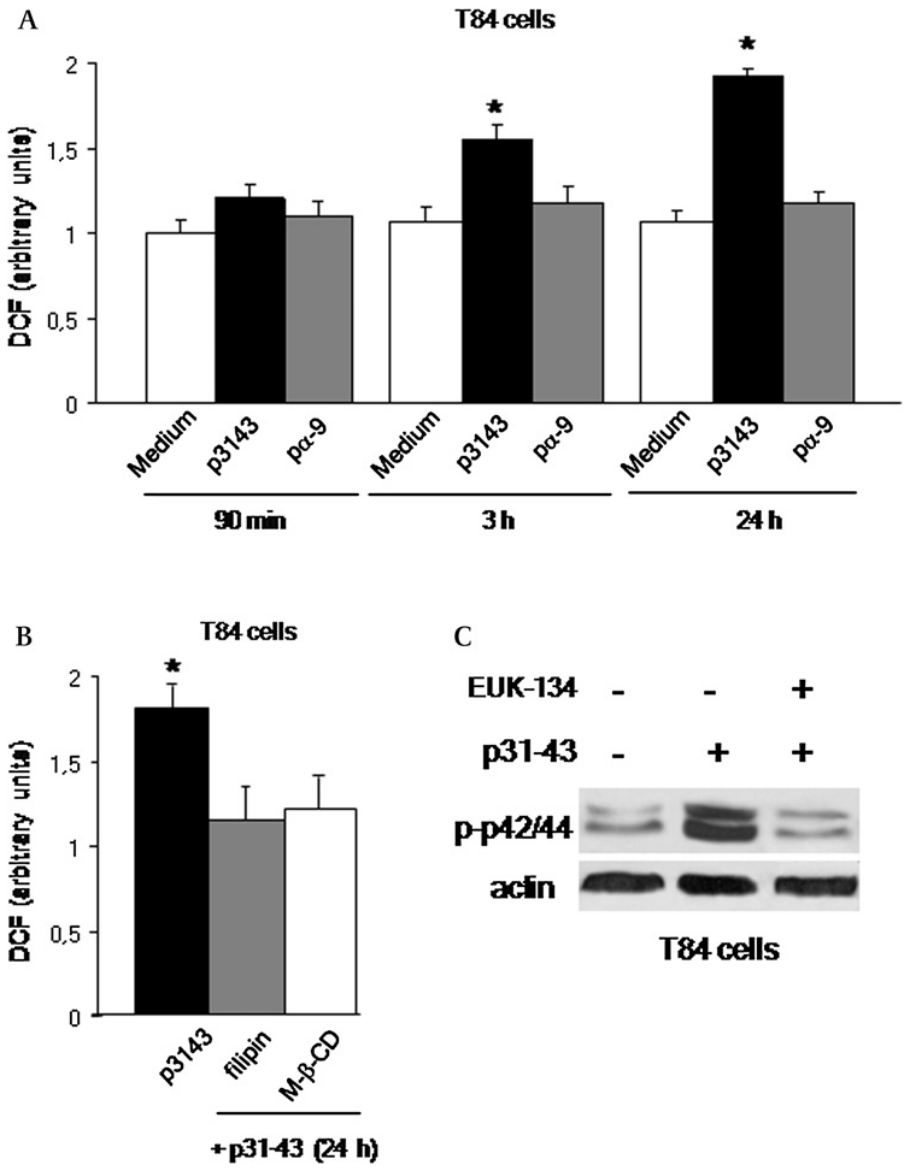

Figure 2 p31—43 induces increase of ROS levels in T84 cells. (A) Increase of intracellular ROS in p31—43 stimulated T84 cells. Each bar represents the mean plus SEM of three independent experiments. *$p<0.01$ versus samples cultured with medium or with p-α9. (B) Inhibition of p31—43 endocytosis by methyl-β-cyclo-dextrin or filipin inhibited p31—43-induced increase of ROS. Each bar represents the mean plus SEM of three independent experiments. *$p<0.017$ versus samples cultured with p31—43. (C) Immunoblot analysis showed a decrease of p31—43-induced p42/p44 phosphorylation upon treatment with the ROS scavenger EUK-134. Representative result of three different experiments. DCF, 5-(and-6)-chloromethyl-2′,7′ -dichlorodihydrofluorescein diacetate acetyl ester; ROS, reactive oxygen species.

with an isopeptide cross-link specifically catalysed by TG2.[22] We observed isopeptide immunoreactivity in PPARγ immunoprecipitates (figure 4A). No PPARγ cross-linking was observed in T84 cells challenged with pα-9 or pα-2 (data not shown). TG2 siRNA[12] was highly effective in preventing PPARγ cross-linking upon p31—43 exposure (figure 4A). Moreover, pre-treatment with the TG2 inhibitor cystamine,[23] as well as with the EUK-134, also prevented TG2-mediated cross-linking of PPARγ (data not shown). These results indicate that p31—43 induces post-translational modifications of PPARγ via the ROS—TG2 axis.

We also investigated whether the cross-linking of PPARγ might favour ubiquitination and PPARγ proteasome degradation with reduction of the 55 kDa PPARγ form. Indeed, a striking increase of ubiquinated PPARγ was observed in p31—43-stimulated T84 cells treated with the proteasome inhibitor MG132 (figure 4B). Negligible amounts of ubiquitinated PPARγ were observed in p31—43-stimulated T84 cells upon TG2 gene silencing (figure 4B) as well as after TG2 inhibition by cystamine or after treatment with EUK-134 (data not shown). Moreover, a reduction of the 55-kDa PPARγ form was observed in T84 cells upon p31—43 challenge (figure 4C) and TG2 siRNA was highly effective in preventing p31—43-induced PPARγ downregulation (figure 4C and supplementary figure 3). The incubation with the TG2 inhibitor cystamine (400 μmol/l), showed the same effects as TG2 knock-down (figure 4C). No PPARγ cross-linking or proteasome degradation was observed in T84 cells upon inhibition of p31—43 endocytosis by M-β-CD or filipin (data not shown). These results indicate that the internalisation and lysosomal delivery of p31—43 induces PPARγ downregulation via the ROS—TG2 axis.

independent experiments. (A—C,E,F), representative results of three independent experiments. Confocal microscopy, DAPI (blue) nuclear counterstaining. Scale bar, 10 μm. DAPI, 4′-diamidine-2′-phenylindol dihydrochloride; EEA-1, Early Endosome Antigen 1; LAMP-1, Lysosomial Associated Membrane Protein 1.

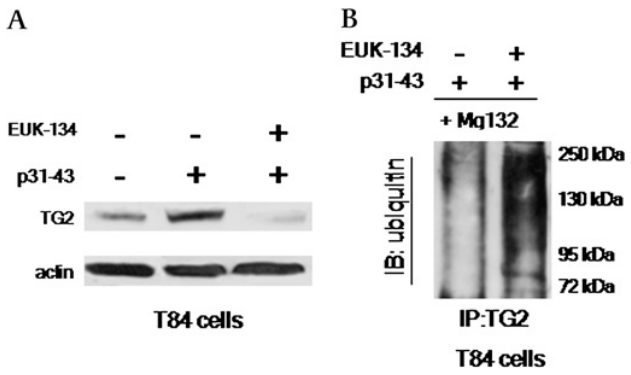

Figure 3 ROS-mediated inhibition of TG2 ubiquitination in T84 cells upon p31–43 challenge. (A) Immunoblot analysis of TG2 protein. ROS scavenger EUK-134 inhibited p31–43-induced increase of TG2 protein in T84 cells. (B) Ubiquitin immunoreactivity in TG2 immunoprecipitates. Incubation with EUK-134 increased TG2 ubiquitination upon MG132 treatment in T84 cells. Immunoprecipitation (IP): anti-TG2 antibody; immunoblot (IB): anti-ubiquitin antibody Representative results of three independent experiments. ROS, reactive oxygen species; TG2, tissue transglutaminase.

The ROS–TG2–PPARγ axis is a master regulator of the epithelial activation to gliadin peptides

To demonstrate that the biological activity of p31–43 was mediated by the downregulation of PPARγ, we pre-incubated T84 cells with the PPARγ agonist rosiglitazone[12] for 6 h and then challenged with p31–43. As a matter of fact, PPARγ ligation by agonists favours PPARγ interaction with the nuclear receptor co-repressor (N-CoR) histone deacetylase 3 (HDAC3) complex and thereby blocks its ubiquitination, thus maintaining a repressor condition.[23] We monitored the effects of p31–43 on epithelial tyrosine phosphorylation, as revealed by PY-99 antibody, a well-established marker of epithelial activation in T84 cells and in human coeliac disease intestinal mucosa.[4] We found that the pre-incubation with rosiglitazone antagonised p31–43-induced tyrosine phosphorylation in T84 cells (figure 4D).

Moreover we incubated p31–43-challenged T84 cells with the PPARγ antagonist GW9662[12] upon TG2 siRNA. The incubation with GW9662 antagonised the downregulatory effect of the TG2 siRNA on tyrosine phosphorylation induced by p31–43, as detected by immunoprecipitation studies (figure 4E) and confocal microscopy (figure 4F). These data indicate that p31–43 may induce epithelial activation via the ROS–TG2–PPARγ axis.

p31–43 induces TG2-mediated PPARγ cross-linking and reduced protein expression in coeliac duodenum

To investigate whether TG2-mediated PPARγ cross-linking and downregulation occurs in human coeliac intestine, we challenged coeliac biopsies with p31–43, pα-2 or pα-9 in presence or absence of cystamine, a well known TG2 inhibitor already used in vivo in a mouse model of Huntington's disease to control TG2-related manifestations.[23] FRET analysis showed that PPARγ interacted with the isopeptide cross-link also in human coeliac disease biopsies (figure 5A). Confocal microscopy showed that PPARγ protein was reduced in coeliac biopsies after challenge with p31–43 (figure 5B) but not with pα-2 or pα-9 (data not shown). Moreover treatment of cultured biopsies with cystamine was highly effective in preventing p31–43-induced PPARγ downregulation (figure 5B). No PPARγ–isopeptide interaction (data not shown) or p31–43 induced PPARγ downregulation was observed in non-coeliac control biopsies (figure 5C), in agreement with our previous data showing that p31–43 fails to induce TG2 upregulation in non-coeliac duodenum.[10] Moreover, upon challenge with p31–43 coeliac biopsies showed intense immunoreactivity to the anti-phospho-tyrosine antibody PY99 (figure 5D). Pretreatment with rosiglitazone completely reversed the p31–43-induced phospho-tyrosine immunoreactivity (figure 5D).

DISCUSSION

An innate response triggered by several 'toxic' gliadin fragments[4 7 8] is involved in both modulating mucosal damage[24–26] as well as in setting the type and intensity of the adaptive immune response in coeliac disease.[4] Furthermore, a series of studies has indicated that several gliadin fragments activate, in a non-disease-specific manner, both mouse and human DC cells,[27 28] a specific type of DC detected in the intestines of patients with coeliac disease[29] and some epithelial cells lines derived from different species.[30 31 10] These results have raised a series of questions and the most pressing is to understand why only CD tissues react to this non-T-cell antigenic portion of gliadin.[4]

Here we demonstrate that 'gliadin sensitive' epithelial cells upregulate intracellular ROS upon challenge with p31–43 but not with immunodominant gliadin peptides. These results indicate that p31–43 induces cellular stress. Among the factors able to trigger cellular stress is the accumulation of improperly handled substances within the intracellular compartments.[32–35] A string of studies has suggested that some α-gliadin peptides, in particular p31–43(9)[13] as well as 33-mer,[14] possess the ability to penetrate cells.[13] It has been demonstrated that gliadin peptides may be internalised by endocytic uptake and activate some signal transduction pathways.[9] Here we demonstrate that p31–43 is delivered to the lysosomes but is retained as late as 24 h after challenge in LAMP1-positive vesicles mainly located in the perinuclear region. The engulfment of lysosomes with p31–43 may induce cellular stress with the generation of a pro-oxidative environment. The relationship between lysosomal garbage and the perturbation of cellular homeostasis has been described in a number of human pathologies such as lysosomal storage diseases,[33 36 37] neurodegenerative diseases[32 34] and even in ageing.[35] However, in T84 or Caco-2 cells as well as in coeliac intestine, the lysosomal machinery of peptide degradation is not generally perturbed since other peptides, such as pTPO and even the gliadin immunodominant pα-2 or pα-9 peptides, are no longer detectable within intracellular organelles after 90 min of challenge. Whatever the mechanism involved in such a puzzling interaction between some gliadin peptides and 'sensitive' epithelia, these results further indicate that a complex alteration of the cross-talk between the intestine and its local environment is crucial for the development of coeliac disease.

Our results demonstrate that p31–43 induces TG2 activation via ROS generation. The increased levels of ROS reduce TG2 degradation by the ubiquitin–proteasome system, thus leading to increased TG2 protein levels. TG2 is a multifunctional enzyme with a vast array of biological functions.[38] Increased tissue levels of TG2 have been described in a number of human diseases, such as neurodegenerative diseases,[39 40] CF[12] and even in cancers.[41] The upregulation of TG2 has recently been associated with an increased metastatic activity[41] or drug resistence.[41] One of the TG2 effects is the cross-linking, with consequent functional sequestration and proteasome degradation of several intracellular proteins such as α-synuclein in Parkinson's disease,[39] huntingtin in Huntington's disease.[42] We have previously reported that in

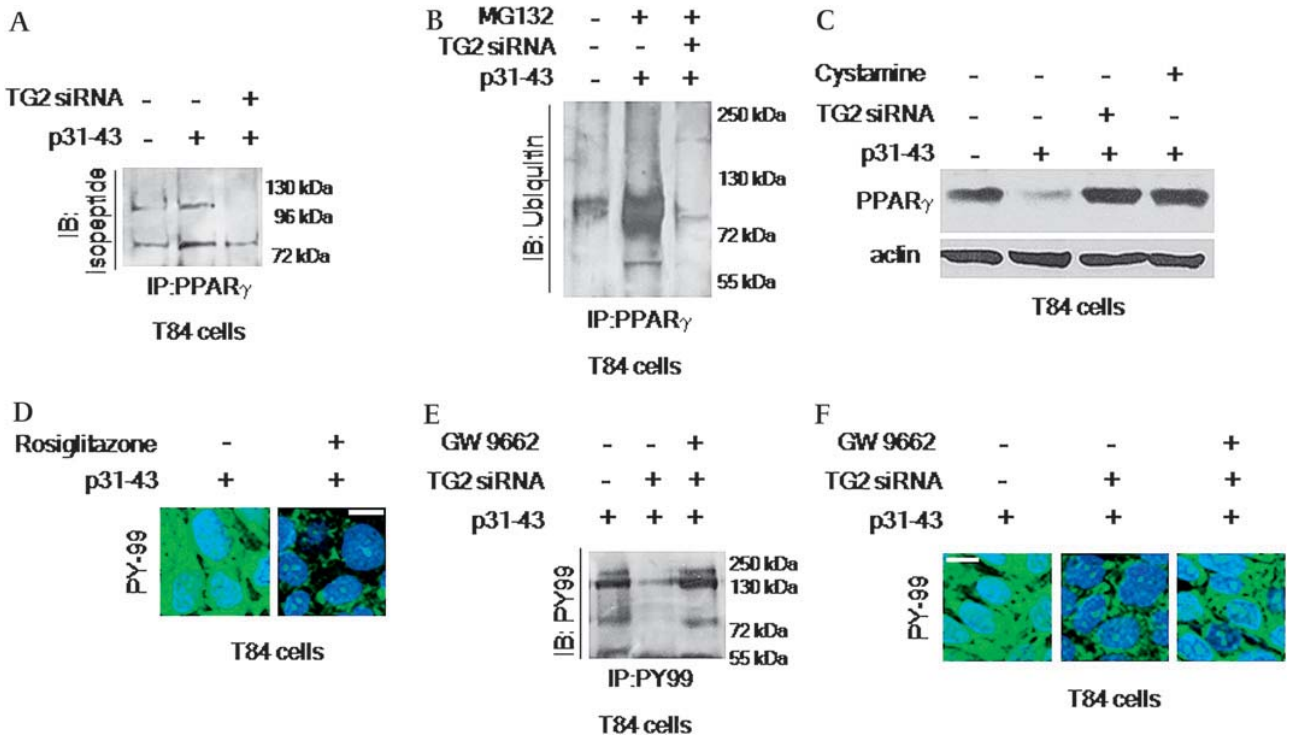

Figure 4 p31—43 challenge induces TG2-mediated PPARγ cross-linking and proteasome degradation in T84 cells. (A) Immunoprecipitates of PPARγ species from whole-cell extracts of T84 cells after challenge with p31—43 were immunoreactive for the anti-isopeptide cross-link antibody. High MW bands ranging from 72 to 130 kDa are evident after p31—43 challenge and significantly reduced upon TG2 siRNA treatment. Immunoprecipitation (IP): anti-PPARγ antibody; immunoblot (IB): anti-isopeptide antibody. (B) Effect of the MG132 treatment on PPARγ ubiquitination upon TG2 siRNA in p31—43-challenged T84cells. Immunoprecipitated PPARγ species from whole-cell extracts of T84 cells immunoreactive for the anti-ubiquitin antibody were evident after challenge with p31—43 upon MG132 treatment. The simultaneous incubation with TG2 siRNA oligos induced a pronounced decrease of ubiquitinated PPARγ protein. Immunoprecipitation (IP): anti-PPARγ antibody; immunoblot (IB): anti-ubiquitin antibody. (C) Immunoblot analysis of PPARγ protein in p31—43-challenged T84 cells. TG2 siRNA as well as cystamine inhibited p31—43-induced PPARγ downregulation. Quantitative analysis (mean, SD) of three different experiments is reported in supplementary figure 3. (D) Confocal microscopy showed a decrease of p31—43-induced tyrosine phosphorylation in T84 cells upon rosiglitazone pre-treatment. (E) Phospho-tyrosine immunoreactivity of PY-99 immunoprecipitates of T84 cells after incubation with p31—43 upon TG2 siRNA in the presence or absence of GW9662. Decrease of PY99 immunoreactivity upon TG2 gene silencing. GW9662 inhibits TG2 siRNA-induced decrease of tyrosine phosphorylation. (F) Confocal microscopy shows an increase of p31—43-induced tyrosine phosphorylation in T84 cells upon TG2 gene silencing followed by GW9662. (D,E) Confocal microscopy, phospho-tyrosine (PY-99 antibody, green), DAPI (blue) nuclear counterstaining. Scale bar, 10 μm (A—F), are the results of three reproducible experiments. DAPI, 4′-diamidine-2′-phenylindol dihydrochloride; PPARγ, peroxisome proliferator-activated receptor γ; TG2, tissue transglutaminase.

CF TG2 drives the characteristic chronic inflammation via PPARγ downregulation.[12]

Here we demonstrate that in T84 cells, as well as in coeliac duodenum, p31—43 induces PPARγ downregulation via ROS-mediated TG2. Therefore, an uncontrolled activation of the ROS—TG2 axis, either constitutive, as a consequence of genetic alterations as in CF,[12] or induced by triggering factors such as p31—43 in a susceptible target (coeliac mucosa and T84 epithelial cells), leads to PPARγ downregulation with a derangement of the appropriate control of inflammation. PPARγ is a hormone receptor produced by several cell types, including epithelial cells, which negatively regulates inflammatory gene expression by 'transrepressing' inflammatory responses[15] and even by modulating oxidative stress.[43 44] PPARγ has been identified as a major functional receptor mediating the aminosalicylate activity[45 46] and PPARγ agonists have been exploited in therapeutic approaches to control inflammation in chronic intestinal inflammatory diseases such as ulcerative colitis[47 48] and in experimental models of colitis.[49] PPARγ plays a key role in the regulation of the intestinal 'inflammatory' homeostasis since is activated by dietary ligands,[50] as well as commensal bacteria.[51] In this paper we provide the first evidence that TG2-mediated PPARγ downregulation plays a key role in the pathogenesis of coeliac disease. The effects of p31—43 are specific for coeliac intestine and 'gliadin-sensitive' cell lines.[30 31 10] This might be related to a coeliac disease-specific peptide internalisation or reflect a still unknown coeliac disease-specific perturbation of the machinery of peptide degradation.

The activation of the ROS—TG2 axis is therefore a key pathway of inflammation. TG2 works as a rheostat of ubiquitination and proteasome degradation in inflammation, particularly in the context of coeliac disease. Indeed, in one case, increased PPARγ ubiquitination and degradation leads to increased inflammation, whilst increased TG2 ubiquitination and degradation leads to a reduced inflammatory response. A derangement of TG2 regulation may lead to the amplification of the effects of the stress. The induction of an epithelial pro-inflammatory phenotype may alter the first mucosal defence against 'toxic' agents and lead to a wide perturbation of the regulatory mechanisms at the mucosal surface. The increased secretion of

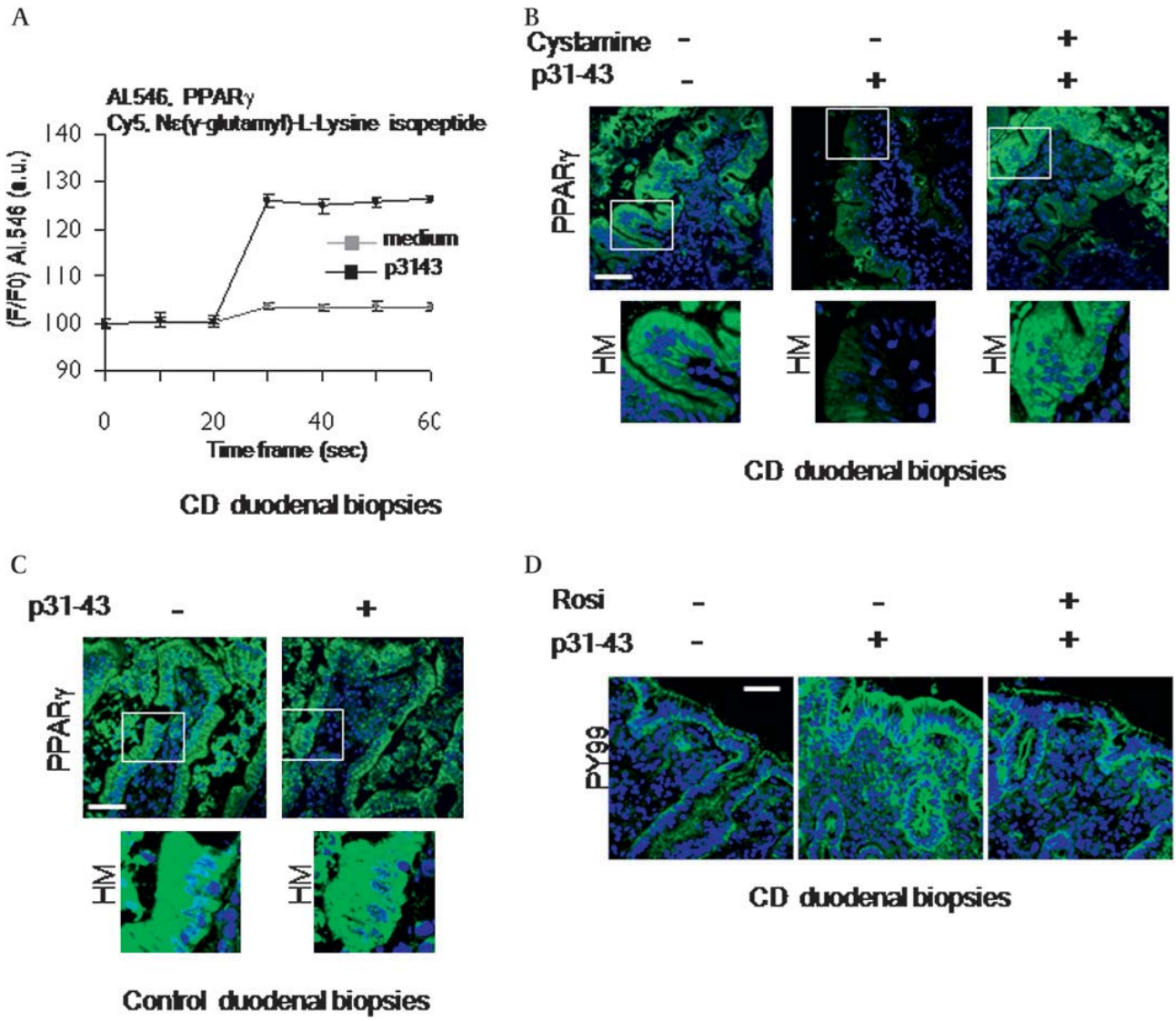

Figure 5 The challenge with p31—43 induces PPARγ cross-linking and reduced PPARγ protein in coeliac duodenum. (A) FRET analysis of celiac duodenal mucosa challenged for 3 h with p31—43. The increase of PPARγ—Alexa-546 fluorescence after *N*ε-(γ-glutamyl)-L-lysine isopeptide—Cy5 photobleaching in enterocytes of p31—43-challenged coeliac biopsies revealed PPARγ—*N*ε-(γ-glutamyl)-L-lysine isopeptide interaction. (B,C) p31—43 challenge for 3 h induced a marked reduction of PPARγ protein (green) in the enterocytes of duodenal mucosa from celiac patients (B) but not controls (C). The incubation with cystamine prevented p31—43 induced PPARγ downregulation (B). (D) p31—43 challenge for 3 h induced high PY99 immunoreactivity (green) in the enterocytes of coeliac duodenal biopsies which was prevented by treatment with rosiglitazone. (B—D), Confocal microscopy, DAPI (blue) nuclear counterstaining. Scale bar, 10 μm. DAPI, 4′-diamidine-2′-phenylindol dihydrochloride; FRET, Fluorescence Resonance Energy Transfer; HM, high magnification; PPARγ, peroxisome proliferator-activated receptor γ.

inflammatory cytokines may, in turn, derange intestinal permeability[52] and enhance the toxic effects of environmental triggers. TG2 may be considered as a main player of the innate response to stress inducers, thus setting the tone of whole mucosal response. Targeting the ROS—TG2 axis might represent a new pathogenic-based approach to antagonise the unwanted effects of gluten in coeliac disease.

Acknowledgements The authors wish to thank Fabio Formiggini (Dynamic Imaging Microscopy, CEINGE, Naples, Italy) for the technical support in FRET analysis.

Funding This work was supported by the Coeliac UK and the Rothschild Trust Corporation and Associazione Italiana Celiachia Regione Puglia (# 1400/07, Del. Reg.502 — 08/04/2008).

Competing interests None.

Ethics approval This study was conducted with the approval of the Regione Campania Health Authority.

Provenance and peer review Not commissioned; externally peer reviewed.

REFERENCES

1. **Sollid LM.** Coeliac disease: dissecting a complex inflammatory disorder. *Nat Rev Immunol* 2002;**2**:647—55.
2. **Sollid LM.** Molecular basis of coeliac disease. *Annu Rev Immunol* 2000;**18**:53—81.
3. **Shan L,** Molberg O, Parrot I, *et al*. Structural basis for gluten intolerance in celiac sprue. *Science* 2002;**297**:2275—79.
4. **Maiuri L,** Ciacci C, Ricciardelli I, *et al*. Association between innate response to gliadin and activation of pathogenic T cells in coeliac disease. *Lancet* 2003;**362**:30—7.

5. **Anderson RP,** Degano P, Godkin AJ, *et al*. In vivo antigen challenge in celiac disease identifies a single transglutaminase-modified peptide as the dominant A-gliadin T-cell epitope. *Nat Med* 2000;**6**:337—42.
6. **Gianfrani C,** Levings MK, Sartirana C, *et al*. Gliadin-specific type 1 regulatory T cells from the intestinal mucosa of treated celiac patients inhibit pathogenic T cells. *J Immunol* 2006;**177**:4178—86.
7. **Meresse B,** Ripoche J, Heyman M, *et al*. Celiac disease: from oral tolerance to intestinal inflammation, autoimmunity and lymphomagenesis. *Mucosal Immunol* 2009;**2**:8—23.
8. **Meresse B,** Chen Z, Ciszewski C, *et al*. Coordinated induction by IL15 of a TCR-independent NKG2D signaling pathway converts CTL into lymphokine-activated killer cells in celiac disease. *Immunity* 2004;**21**:357—66.
9. **Barone MV,** Gimigliano A, Castoria G, *et al*. Growth factor-like activity of gliadin, an alimentary protein: implications for coeliac disease. *Gut* 2007;**56**:480—8.
10. **Maiuri L,** Ciacci C, Ricciardelli I, *et al*. Unexpected role of surface transglutaminase type II in celiac disease. *Gastroenterology* 2005;**129**:1400—13.
11. **Esposito C,** Marra M, Giuberti G, *et al*. Ubiquitination of tissue transglutaminase is modulated by interferon alpha in human lung cancer cells. *Biochem J* 2003;**370**:205—12.
12. **Maiuri L,** Luciani A, Giardino I, *et al*. Tissue Transglutaminase activation modulates inflammation in Cystic Fibrosis via PPARγ downregulation. *J Immunol* 2008;**180**:7697—705.
13. **Schumann M,** Richter JF, Wedell I, *et al*. Mechanisms of epithelial translocation of the α2-gliadin-33mer in coeliac sprue. *Gut* 2008;**57**:747—54.
14. **Matysiak-Budnik T,** Candalh C, Dugave C, *et al*. Alterations of the intestinal transport and processing of gliadin peptides in celiac disease. *Gastroenterology* 2003;**125**:696—707.
15. **Daynes RA,** Jones DC. Emerging roles of PPARs in inflammation and immunity. *Nat Rev Immunol* 2002;**2**:748—59.
16. **Bailey ST,** Ghosh S. 'PPAR'ting ways with inflammation. *Nat Immunol* 2005;**6**:966—7.
17. **Chamberlain CG,** Mansfield KJ, Cerra A. Glutathione and catalase suppress TGFβ-induced cataract-related changes in cultured rat lenses and lens epithelial explants. *Mol Vis* 2009;**15**:895—905.
18. **Du X,** Edelstein D, Obici S, *et al*. Insulin resistance reduces arterial prostacyclin synthase and eNOS activities by increasing endothelial fatty acid oxidation. *J Clin Invest* 2006;**116**:1071—9.
19. **Vereb G,** Matkó J, Vámosi G, *et al*. Cholesterol-dependent clustering of IL-2Ralpha and its colocalization with HLA and CD48 on T lymphoma cells suggest their functional association with lipid rafts. *Proc Natl Acad Sci U S A* 2000;**97**:6013—18.
20. **Lu A,** Tebar F, Alvarez-Moya B, *et al*. A clathrin-dependent pathway leads to KRas signaling on late endosomes en route to lysosomes. *J Cell Biol* 2009;**6**:863—79.
21. **El Bekay R,** Moises A, Javier M, *et al*. Oxidative stress is a critical mediator of the angiotensin II signal in human neutrophils: involvement of mitogen-activated protein kinase, calcineurin, and the transcription factor NF-kB. *Blood* 2003;**102**:662—9.
22. **Andringa G,** Lam KY, Chegary M, *et al*. Tissue transglutaminase catalyzes the formation of α-synuclein cross-links in Parkinson's disease. *FASEB J* 2004;**18**:932—4.
23. **Karpuj MV,** Becher MW, Springer JE, *et al*. Prolonged survival and decreased abnormal movements in transgenic model of Huntington disease, with administration of the transglutaminase inhibitor cystamine. *Nat Med* 2002;**8**:143—9.
24. **Maiuri L,** Picarelli A, Boirivant M, *et al*. Definition of the initial immunologic modifications upon in vitro gliadin challenge in the small intestine of celiac patients. *Gastroenterology* 1996;**110**:1368—78.
25. **Maiuri L,** Ciacci C, Auricchio S, *et al*. Interleukin 15 mediates epithelial changes in celiac disease. *Gastroenterology* 2000;**119**:996—1006.
26. **Shidrawi RG,** Day P, Przemioslo R, *et al*. In vitro toxicity of gluten peptides in coeliac disease assessed by organ culture. *Scand J Gastroenterol* 1995;**30**:758—63.
27. **Palova Jelikova L,** Rozkova D, Pecharova B, *et al*. Gliadin fragments induce phenotypic and functional maturation of human dendritic cells. *J Immunol* 2005;**175**:7038—45.
28. **Thomas KE,** Sapone A, Fasano A, *et al*. Gliadin stimulation of murine macrophage inflammatory gene expression and intestinal permeability are MyD88-dependent: role of the innate immune response in Celiac disease. *J Immunol* 2006;**176**: 2512—21.
29. **Raki M,** Tollefsen S, Molberg O, *et al*. A unique dendritic cell subset accumulates in the celiac lesion and efficiently activates gluten-reactive T cells. *Gastroenterology* 2006;**131**:428—38.
30. **Clemente MG,** De VS, Kang JS, *et al*. Early effects of gliadin on enterocyte intracellular signalling involved in intestinal barrier function. *Gut* 2003;**52**:218—23.
31. **Giovannini C,** Matarrese P, Scazzocchio E, *et al*. Wheat gliadin induces apoptosis of intestinal cells via an autocrine mechanism involving FAS-FAS ligand pathway. *FEBS Lett* 2003;**540**:117—24.
32. **Jeyakumar M,** Dwek RA, Butters TD, *et al*. Storage solutions: treating lysosomal disorders of the brain. *Nat Rev Neurosci* 2005;**6**:713—25.
33. **Verheijen FW,** Verbeek E, Aula N, *et al*. A new gene, encoding an anion transporter, is mutated in sialic acid storage diseases. *Nat Genet* 1999;**23**:462—5.
34. **Futerman AH,** van Meer G. The cell biology of lysosomal storage disorders. *Nat Rev Mol Cell Biol* 2004;**5**:554—65.
35. **Terman A.** Catabolic insufficiency and aging. *Ann N Y Acad Sci* 2006;**1067**: 27—36.
36. **Settembre C,** Fraldi A, Jahreiss L, *et al*. A block of autophagy in lysosomal storage disorders. *Hum Mol Genet* 2008;**17**:119—29.
37. **Diez-Roux G,** Ballabio A. Sulfatases and human disease. *Annu Rev Genomics Hum Genet* 2005;**6**:355—79.
38. **Lorand L,** Graham RM. Transglutaminases: crosslinking enzymes with pleiotropic functions. *Nat Rev Mol Cell Biol* 2003;**4**:140—56.
39. **Juun E,** Ronchetti RD, Quezado MM, *et al*. Tissue transglutaminase-induced aggregation of alpha synuclein: implication for Lewy body formation in Parkinson's disease and dementia with Lewy bodies. *Proc Natl Acad Sci U S A* 2003;**100**:2047—52.
40. **Zainelli GM,** Ross CA, Troncoso JC, *et al*. Calmodulin regulates transglutaminase 2 cross-linking of hungtingtin. *J Neurosci* 2004;**24**:1954—61.
41. **Verna A,** Wang H, Manavathi B, *et al*. Increased expression of tissue transglutaminase in pancreatic ductal adenocarcinoma and its implications in drug resistance and metastasis. *Cancer Res* 2006;**66**:10525—33.
42. **Bailey CD,** Johnson GV. Tissue transglutaminase contributes to disease progression in the R6/2 Huntington's disease mouse model via aggregate-independent mechanisms. *J Neurochem* 2005;**92**:83—92.
43. **Rizzo G,** Fiorucci S. PPARs and other nuclear receptors in inflammation. *Curr Opin Pharmacol* 2006;**6**:421—7.
44. **Collino M,** Aragno M, Mastrocola R, *et al*. Modulation of the oxidative stress and inflammatory response by PPAR-gamma agonists in the hippocampus of rats exposed to cerebral ischemia/reperfusion. *Eur J Pharmacol* 2006;**530**:70—80.
45. **Liang HL,** Ouyang Q. A clinical trial of combined use of rosiglitazone and 5-aminosalicylate for ulcerative colitis. *World J Gastroenterol* 2008;**14**:114—19.
46. **Rousseaux C,** Lefebvre B, Dubuquoy L, *et al*. Intestinal antiinflammatory effect of 5- aminosalicylic acid is dependent on peroxisome proliferator-activated receptor-gamma. *J Exp Med* 2005;**201**:1205—15.
47. **Dubuquoy L,** Jansson EA, Deeb S, *et al*. Impaired expression of peroxisome proliferatoractivated receptor gamma in ulcerative colitis. *Gastroenterology* 2003;**124**:1265—76.
48. **Ramakers JD,** Verstege MI, Thuijls G, *et al*. The PPARgamma agonist rosiglitazone impairs colonic inflammation in mice with experimental colitis. *J Clin Immunol* 2007;**27**:275—83.
49. **Bassaganya-Riera J,** Reynolds K, Martino-Catt S, *et al*. Activation of PPAR gamma and delta by conjugated linoleic acid mediates protection from experimental inflammatory bowel disease. *Gastroenterology* 2004;**127**:777—91.
50. **Marion-Letellier R,** Déchelotte P, Iacucci M, *et al*. Dietary modulation of peroxisome proliferator-activated receptor gamma. *Gut* 2009;**58**:586—93.
51. **Dubuquoy L,** Rousseaux C, Thuru X, *et al*. PPARgamma as a new therapeutic target in inflammatory bowel diseases. *Gut* 2006;**55**:1341—9.
52. **Lammers KM,** Lu R, Brownley J, *et al*. Gliadin induces an increase in intestinal permeability and zonulin release by binding to the chemokine receptor CXCR3. *Gastroenterology* 2008;**135**:194—204.

approved clinical trial and registry. However, it is a fact and needs to be pointed out, that only one third of our identified IAR (80 of 205) participated in the recommended screening programme. A pilot study on 32 of these IAR using standard questionnaires and interviews (Beck Depression Inventory (BDI) and Brief Symptom Inventory (BSI)) around counselling (days −7, 0, +30) conducted by a psychiatrist revealed, that these IAR were critically biased by cognitive coping strategies (unpublished data). Pancreatic cancer (PC) screening is clearly different from other cancer screening programmes, given the disastrous prognosis of PC, the unknown true penetrance in the different settings of hereditary PC, the lack of a major gene defect, the lack of reliable imaging or biomarkers, the lack of evidence to improve prognosis or to save lives by any screening, and the high risk of morbidity and mortality of potential preventive surgery. Some authors even advocate that at present 'doing nothing' provides the greatest remaining quality of life-adjusted years and the lowest costs.[6]

We fully agree that we need to gain much more knowledge about hereditary PC to draw a definite conclusion about the true value of PC screening in IAR. However, based on our data, we strongly believe, in accordance with the recommendations of the Fourth International Symposium of Inherited Diseases of the Pancreas,[5] that all screening procedures should be performed as part of peer-reviewed protocols combined with a scientific appraisal of the screening methods and human subject protection. At present there is no data, that would justify a general PC screening even of high risk individuals outside of such protocols as suggested by Harinck *et al*. In contrast, it has to be feared that uncritical use and interpretation of screening results obtained with the presently available tools on a healthcare basis may cause unnecessary physical harm and psychological distress. On the other hand over-estimation of the power of our present screening tools may lead to a deceptive, unjustified and potentially dangerous level of safety, if done uncritically and uncontrolled. The message of our paper thus is not 'to do nothing', but to carefully evaluate screening methods for IAR from familial pancreatic cancer (FPC) families in the setting of board approved clinical trials, to continuously improve our knowledge and strategies.

P Langer,[1] TM Gress,[2] DK Bartsch[1]

[1]Department of General Surgery, Philipps-University Marburg, Germany; [2]Department of Gastroenterology, Philipps-University Marburg, Germany

Correspondence to Dr D K Bartsch, Department of Visceral-, Thoracic and Vascular Surgery, Philipps University Marburg, Germany; bartsch@med.uni-marburg.de

Competing interests None.

Provenance and peer review Not commissioned; not externally peer reviewed.

Gut 2010;**59**:1006–1007. doi:10.1136/gut.2010.214163

REFERENCES

1. **Harinck F,** Canto MI, Schulick R, *et al*. Surveillance in individuals at high risk of pancreatic cancer; too early to tell? *Gut* 2010;**59**:1005–6.
2. **Langer P,** Kann PH, Fendrich V, *et al*. Five years of prospective screening of high-risk individuals from families with familial pancreatic cancer. *Gut* 2009;**58**:1410–18.
3. **Canto MI,** Goggins M, Hruban RH, *et al*. Screening for early pancreatic neoplasia in high-risk individuals: a prospective controlled study. *Clin Gastroenterol Hepatol* 2006;**4**:766–81. quiz 665.
4. **Poley JW,** Kluijt I, Gouma DJ, *et al*. The yield of first-time endoscopic ultrasonography in screening individuals at a high risk of developing pancreatic cancer. *Am J Gastroenterol* 2009;**104**:2175–81.
5. **Brand R,** Rubinstein C, Lerch MM, *et al*. Advances in counselling and surveillance of patients at risk for pancreatic cancer. *Gut* 2007;**56**:1460–9.
6. **Rubenstein JH,** Scheiman JM, Anderson MA. A clinical and economic evaluation of endoscopic ultrasound for patients at risk for familial pancreatic adenocarcinoma. *Pancreatology* 2007;**7**:514–25.

CORRECTIONS

doi:10.1136/gut.2009.208975ecorr1

Safety and comfort for colonoscopy in the over seventies-time to achieve a balance? *Gut* 2010;**59**(Suppl 1):A23. The correct author list should have been Hancock J, Ali F, Sarkar A, Parr J.

doi:10.1136/gut.2009.190439corr1

Ibeakanma C, Vanner S. *Gut* 2010;**59**:612–21. TNFα is a key mediator of the pronociceptive effects of mucosal supernatant from human ulcerative colitis on colonic DRG neurons. The figures were ordered incorrectly in the print version of the paper. The latest online pdf and full text have been corrected. The journal apologises for the error.

doi:10.1136/gut.2009.180182corr1

Long-term outcome of endoscopic dilatation in patients with Crohn's disease is not affected by disease activity or medical therapy. *Gut* 2010;**59**:320–4. The correct author list should have been Thienpont C, D'Hoore A, Vermeire S, Demedts I, Bisschops R, Coremans G, Rutgeerts P, Van Assche G. The latest online pdf and full text have been corrected. The journal apologises for the error.

doi:10.1136/gut.2008.155226corr1

De-Xin Zhang, Peng-Tao Zhao, Lin Xia, *et al*. *Gut* 2010;**59**:292–9. Potent inhibition of human gastric cancer by HER2-directed induction of apoptosis with anti-HER2 antibody and caspase-3 fusion protein. Panels E–H were missing in figure 5. The latest online pdf and full text have been corrected. The journal apologises for this error.

doi:10.1136/gut.2008.174904corr1

Yue H-Y, Yin C, Hou J-L, *et al*. *Gut* 2010;**59**:236–46. Hepatocyte nuclear factor 4α attenuates hepatic fibrosis in rats. Professor Lin Yong and Dr Weifen Xie should have been co-corresponding authors on this paper. The latest online pdf and full text have been corrected.

doi:10.1136/gut.2008.155853corr1

Park DH, Kim M-H, Chari S T. *Gut* 2009;**58**:1680–9. Recent advances in autoimmune pancreatitis. M-H Kim and S T Chari should have been co-corresponding authors on this paper. The latest online pdf and full text have been corrected.

doi:10.1136/gut.2009.179606corr1

Mangia A, Andriulli A. Tailoring the length of antiviral treatment for Hepatitis C. *Gut* 2010;**59**:1–5. There were several errors in table 1 which have now been corrected online.

doi:10.1136/gut.2008.174607corr1

Cahill RA, Lindsey I, Cunningham C. *Gut* 2009;**58**:1168–9. NOTES for colorectal neoplasia—surgery through the looking glass. The surname of the third author should be spelt Cunningham, not Cunnigham. The latest online pdf and full text have been corrected.

doi:10.1136/gut.2009.183608corr1

Lysosomal accumulation of gliadin p31e43 peptide induces oxidative stress and tissue transglutaminase-mediated PPARγ down-regulation in intestinal epithelial cells and coeliac mucosa. *Gut* 2010;**59**:311–9. The correct author list should have been Luciani A, Rachela Villella V, Vasaturo A, Giardino I, Pettoello-Mantovani M, Guido S, Cexus O N, Peake N, Londei M, Quaratino S, Maiuri L as it appeared in the online first version. We have replaced the latest online pdf and full text. The journal apologises for the error.

Published July 22, 2009, doi:10.4049/jimmunol.0900993

SUMOylation of Tissue Transglutaminase as Link between Oxidative Stress and Inflammation[1]

Alessandro Luciani,*† Valeria Rachela Villella,‡ Angela Vasaturo,‡ Ida Giardino,§ Valeria Raia,¶ Massimo Pettoello-Mantovani,* Maria D'Apolito,* Stefano Guido,†‡ Teresinha Leal,‖ Sonia Quaratino,# and Luigi Maiuri[2]*·***

Cystic fibrosis (CF) is a monogenic disease caused by mutations in the CF transmembrane conductance regulator (CFTR) gene. CF is characterized by chronic bacterial lung infections and inflammation, and we have previously reported that tissue transglutaminase (TG2), a multifunctional enzyme critical to several diseases, is constitutively up-regulated in CF airways and drives chronic inflammation. Here, we demonstrate that the generation of an oxidative stress induced by CFTR-defective function leads to protein inhibitor of activated STAT (PIAS)y-mediated TG2 SUMOylation and inhibits TG2 ubiquitination and proteasome degradation, leading to sustained TG2 activation. This prevents peroxisome proliferator-activated receptor (PPAR)γ and IkBα SUMOylation, leading to NF-κB activation and to an uncontrolled inflammatory response. Cellular homeostasis can be restored by small ubiquitin-like modifier (SUMO)-1 or PIASy gene silencing, which induce TG2 ubiquitination and proteasome degradation, restore PPARγ SUMOylation, and prevent IkBα cross-linking and degradation, thus switching off inflammation. Manganese superoxide dismutase overexpression as well as the treatment with the synthetic superoxide dismutase mimetic EUK-134 control PIASy-TG2 interaction and TG2 SUMOylation. TG2 inhibition switches off inflammation in vitro as well as in vivo in a homozygous F508del-CFTR mouse model. Thus, TG2 may function as a link between oxidative stress and inflammation by driving the decision as to whether a protein should undergo SUMO-mediated regulation or degradation. Targeting TG2-SUMO interactions might represent a new option to control disease evolution in CF patients as well as in other chronic inflammatory diseases, neurodegenerative pathologies, and cancer. *The Journal of Immunology,* **2009, 183: 0000–0000.**

Cystic fibrosis (CF)[3] is the most common life-threatening inherited disease among the Caucasian population worldwide with considerable morbidity and reduced life expectancy (1). The birth prevalence of CF is estimated to be in 3500–4500, with 200–300 new cases each year in single geographic areas (1). CF is caused by mutations in the CF transmembrane conductance regulator (CFTR) gene, which encodes a cAMP-regulated chloride channel expressed at the apical membrane of epithelial cells in the airways, pancreas, testis, and other tissues (Online Mendelian Inheritance in Man no. 219700) (1, 2). The most common CFTR mutation producing CF is deletion of phenylalanine at residue 508 (F508del) in its amino acid sequence (1, 2). The misfolded F508del-CFTR protein is degraded and fails to reach the cell membrane, leading to defective chloride channel function (3–6).

As a prototype of a monogenic disease, gene therapy is ideally placed to treat CF patients, although this approach has so far not proved to be beneficial (7). Alternative therapeutic approaches have therefore been considered, such as small-molecule correctors of defective F508del-CFTR folding/cellular processing ("correctors") and channel gatings ("potentiators") (8, 9).

Although CF is a systemic disease, the main cause of death is due to chronic airway inflammation and persistent and untreatable pulmonary infections, with *Pseudomonas aeruginosa* colonizing most of the patients (10–12). As inflammation has a central role in the pathogenesis of CF (13), new antiinflammatory drugs provided some encouraging results in recent clinical trials. However, conflicting results have been reported on whether CF airways undergo proinflammatory response in the absence of bacterial infections (14–16). Several studies have shown that both cytokine profile secretion and NF-κB activation are similar in CF and normal cells (17, 18). However, mounting evidence suggests that inflammation may occur before infection, and CFTR-defective cells have an intrinsically proinflammatory phenotype (19–23). Recently, it has been shown that CFTR is a negative regulator of NF-κB-mediated innate immune response, and its localization to lipid rafts is involved in control of inflammation (24).

We have previously investigated the molecular mechanisms that regulate this "intrinsic" proinflammatory profile and made a link between CFTR-defective function and inflammation (22). We have shown that nasal polyp mucosa from CF patients as well as human

*Institute of Pediatrics, University of Foggia, Foggia, Italy; †Dynamic Imaging Microscopy, Centro di Ingegneria Genetica, Naples, Italy; ‡Department of Chemical Engineering, University Federico II of Naples, Naples, Italy; §Department of Laboratory Medicine, University of Foggia, Foggia, Italy; ¶Department of Pediatrics, University Federico II of Naples, Naples, Italy; ‖Clinical Chemistry, Université Catholique de Louvain, Brussels, Belgium; #Cancer Research UK Oncology Unit, University of Southampton, Southampton, United Kingdom; and **European Institute for Research in Cystic Fibrosis, San Raffaele Scientific Institute, Milan, Italy

Received for publication March 30, 2009. Accepted for publication June 21, 2009.

The costs of publication of this article were defrayed in part by the payment of page charges. This article must therefore be hereby marked *advertisement* in accordance with 18 U.S.C. Section 1734 solely to indicate this fact.

[1] This work was supported by the European Institute for Research in Cystic Fibrosis, Cancer Research UK, Rothschild Trust, Coeliac UK, and Regione Campania (L.229/99) and Associazione Italiana Celiachia Puglia (N.1400/07).

[2] Address correspondence and reprint requests to Prof. Luigi Maiuri, European Institute for Research in Cystic Fibrosis, San Raffaele Scientific Institute, 20132 Milan, Italy. E-mail address: maiuri@unina.it

[3] Abbreviations used in this paper: CF, cystic fibrosis; CFTR, CF transmembrane conductance regulator; F508del, deletion of phenylalanine at residue 508; TG2, tissue transglutaminase; PPAR, peroxisome proliferator-activate receptor; ROS, reactive oxygen species; SUMO, small ubiquitin-like modifier; PIAS, protein inhibitor of activated STAT; NEMO, NF-κB essential modulator; siRNA, small interfering RNA; MnSOD, manganese superoxide dismutase; FRET, fluorescence resonance energy transfer; N-CoR, nuclear co-repressor.

CFTR-defective cell lines constitutively up-regulate tissue transglutaminase (TG2), a multifunctional protein expressed in several tissues (25). The increased TG2 activity drives inflammation through down-regulation of the antiinflammatory peroxisome proliferator-activated receptor (PPAR)γ, a negative regulator of inflammatory gene expression (26).

TG2 is an enzyme with a vast array of biological functions (27). It catalyzes cross-links or deamidation of target proteins in the presence of high Ca^{2+} levels (27), whereas at low Ca^{2+} concentrations it may function as a G protein or a protein disulfide isomerase (27), thus contributing to the functionality of the mithocondrial respiratory chain complexes. We have shown that in CF airways high levels of reactive oxygen species (ROS) lead to an increase of TG2 activity, TG2-mediated PPARγ cross-linking, ubiquitination, and proteasome degradation, thus driving inflammation (22). Blocking TG2 through specific gene-silencing or TG2 inhibitors increases PPARγ protein and reverses inflammation (22). The mechanisms by which the genetic CF defect leads to TG2 up-regulation and inflammation, however, are still unknown.

TG2 is regulated by retinoids, steroid hormones, peptide growth factors, and cytokines that also lead to a time-dependent decrease in TG2 ubiquitination (25). Increased TG2 tissue levels have been observed in neurodegenerative diseases (28), including Alzheimer's, Huntington's, and Parkinson's diseases, as well as in chronic inflammatory conditions such as celiac disease (29). Increased tissue levels of TG2 have also been detected in cancer such as glioblastomas, malignant melanomas, and pancreatic ductal adenocarcinomas (30), and they are often associated with an increased metastatic activity or acquisition of drug resistance (30).

In this paper we investigated whether posttranslational modifications result in the persistence of high levels of TG2 protein in CF airways. We focused on small ubiquitin like-modifier (SUMO) posttranslational modification, since this has been defined as a central way of regulating key cellular functions and stability of proteins (31, 32). Since protein inhibitor of activated STAT (PIAS)y, a member of the PIAS family (33), has recently been defined as the first SUMO ligase for NF-κB essential modulator (NEMO) (33), and PIASy-NEMO interaction is mediated by ROS (33), we also investigated whether PIASy-TG2 interaction could mediate ROS-driven posttranslational modifications of TG2. We demonstrate that in CF airway epithelia the pro-oxidative intracellular milieu leads to PIASy-mediated TG2 SUMOylation and uncontrolled TG2 activation. This prevents PPARγ and IkBα SUMOylation, leading to NF-κB activation and persistent inflammation. Moreover SUMO-1 or PIASy gene silencing can switch off inflammation, favoring TG2 degradation and restoring cellular homeostasis.

We demonstrate increased ROS levels and TG2 SUMOylation also in vivo, in a mouse model homozygous for the F508del-CFTR mutation, and show that TG2 inhibition blocks lung inflammation in vivo.

These results indicate TG2 as a missing link between oxidative stress and inflammation and flag TG2 as a new attractive target to control the evolution of chronic airway inflammation in CF.

Materials and Methods

Cell lines and cultures

Human CF bronchial epithelial cell line IB3-1, carrying F508del/W1282X CFTR mutation, isogenic stably rescued C38, normal bronchial epithelial 16HBE, or lung carcinoma A549 cell lines (LGC Standards) were cultured as recommended by American Type Culture Collection. IB3-1 cell lines were incubated for 24 h with EUK-134 (50 μg/ml; Alexis Biochemicals), TG inhibitor R283 (250 μM), KCC009 (250 μM), or cystamine (400 μM; Sigma-Aldrich) followed or not by rosiglitazone for 6 h (10 μM; Alexis Biochemicals). A549 and 16HBE cell lines were incubated for 1 h with H_2O_2 (33) (2 mM; Sigma-Aldrich) and for 24 h with rotenone (1 μM; Sigma-Aldrich) or buthionine sulfoximine (10 μM; Sigma-Aldrich) in the presence or absence of EUK-134 as well as with CFTR-inh172 (20, 22) (20 μM; Calbiochem). A549 and 16HBE cell lines were also cultured under hypoxic conditions in a humidified hypoxia chamber (Cop Laboratories) for 1 h at 1% O_2 (5% CO_2 balance N_2), and temperature was maintained at 37°C (34).

RNA interference

IB3-1 cells were transfected with 50 nM human SUMO-1 or scrambled small interfering RNA (siRNA) duplex using Lipofectamine RNAiMAX at 37°C for 72 h. The SUMO-1 duplex siRNA was a pool of three sequences: siRNA no. 1, SUMO-1, sense, 5′-GGAUAGCAGUGAGAUU CACUUCAAA-3′, antisense, 5′-UUUGAAGUGAAUCUCACUGCUA UCC-3; siRNA no. 2, SUMO-1, sense, 5′-GGUGUUCCAAUGAAUU CACUCAGGU-3′, antisense, 5′-ACCUGAGUGAAUUCAUUGGAAC ACC-3′; siRNA no. 3, SUMO-1, sense, 5′-GGAAGAAGAUGUGAUU GAAGUUUAU-3′, antisense 5′-AUAAACUUCAAUCACAUCUUCU UCC-3′. siRNA-mediated knockdown of PIASy was performed using specific siRNA oligos, as previously described (33). TG2 gene silencing was performed as previously reported (22).

Adenoviral vector

Human manganese superoxide dismutase (MnSOD) cDNA was cloned into the shuttle vector pAd5CMVK-NpA (35). MnSOD adenovirus was a gift from Michael Brownlee (Albert Einstein College of Medicine, New York, NY). IB3-1, A549, and 16HBE cell lines were infected with MnSOD or control adenovirus for 2 h, as previously described (35).

TG2 overexpression

A549 cells were transfected with wild-type TG2 cloned into the pLPCX vector (pLPCX-TG2) (a gift from Dr. G. M. Fimia, National Institute for Infectious Diseases, Istituto di Ricovero e Cura a Carattere Scientifico,"L. Spallanzani", Rome, Italy) and empty vector (pLPCX), as control, using Lipofectamine 2000 (Invitrogen) according to the manufacturer's protocol, and incubated at 37°C for 48 h.

Cell fractionation

IB3-1 cells were collected in cold buffer A (20 mM Tris-HCl (pH 7.4), 2 mM EDTA, 20 mM 2-ME, 1× PMSF, 1 μg/ml inhibitor protease cocktail), homogenized in Potter-Elvehjem pestle and glass tube (Sigma-Aldrich), and centrifuged at 2000 rpm for 15 min at 4°C to obtain nuclear pellets. Supernatants were collected as cytoplasmic fractions. Nuclear pellets were washed with buffer A and resuspended in buffer B (2 mM Na_3VO_4, 400 mM NaCl, 1 mM $MgCl_2$, 1 mM EGTA, HEPES 10 mM (pH 7.9), 1 mM DTT, 1× PMSF, 1 μg/ml inhibitor protease cocktail) and incubated on ice for 50 min with occasional mixing to extract nuclear proteins. Nuclear extracts were cleared by centrifugation (7000 rpm, 15 min, 4°C), and supernatants were collected as nuclear fraction. Then, cytoplasmic and nuclear whole-cell fractions were analyzed by immunoblotting.

Immunoblot

The blots were incubated with anti-phospho-p42/p44 MAP kinases (rabbit polyclonal IgG, 1/500; Cell Signaling Technology), PPARγ (clone E8 sc-7273, mouse monoclonal IgG1, 1/500; Santa Cruz Biotechnology), TG2 (clone CUB7402, mouse monoclonal IgG1, 1/500; NeoMarkers), ubiquitin (clone FL-76 sc9133, rabbit polyclonal IgG, 1/500; Santa Cruz Biotechnology), SUMO-1 (clone FL-101 sc9060, 1/500; Santa Cruz Biotechnology), phopsho-p65(Ser^{536}) (rabbit polyclonal, 1/500; Cell Signaling Technology), PIASy (clone H75 sc50437, rabbit polyclonal IgG, 1/1000; Santa Cruz Biotechnology), IκBα (clone H4 sc1643, mouse monoclonal IgG1, 1/1000; Santa Cruz Biotechnology), β-actin (clone 13E5, rabbit polyclonal IgG, 1/2000; Cell Signaling Technology), and $\alpha\beta$-tubulin (rabbit polyclonal IgG, 1/2000; Cell Signaling Technology). The primary Abs were counterstained by a HRP-conjugated anti-IgG Ab (Amersham Biosciences) for 60 min at room temperature. Proteins were visualized by chemiluminescence (ECL Plus; Amersham Biosciences) and exposed to X-OMAT film (Eastman Kodak). The amounts of proteins were determined by a Bio-Rad protein assay to ensure equal protein loading before Western blot analysis. Fifty micrograms of cell lysate was loaded in each lane.

Immunoprecipitation

Treated and untreated cells were harvested, lysed, and 500 μg of cell lysate was immunoprecipitated by overnight incubation at 4°C on a mixer with an appropriate dilution of specific Ab (anti-TG2 CUB 7402 mAb, anti-PIASy, anti-PPARγ, anti-IκBα) in cold lysis buffer. The samples were then incubated with protein G-Sepharose at 4°C for 2 h with constant mixing. After

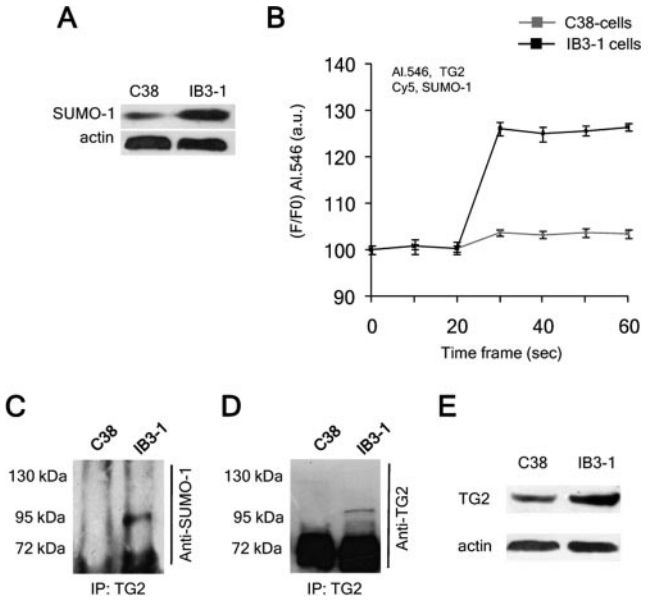

FIGURE 1. TG2 SUMOylation in CF airway epithelial cells. *A*, Immunoblot analysis of SUMO-1 expression in CF IB3-1 and C38 cells. β-actin levels were used as loading control. *B*, FRET analysis of SUMO-1-TG2 interaction in IB3-1 and C38 cells. *C*, Immunoprecipitated (IP) TG2 species from whole-cell extracts of IB3-1 cells are immunoreactive for the anti-SUMO-1 Ab. *D*, Immunoblot analysis of TG2 immunoprecipitates with anti-TG2 Abs. Two TG2 bands are detected in IB3-1 cells. *E*, Immunoblot analysis of TG2 expression in CF IB3-1 and C38 cells. β-actin levels were used as loading control.

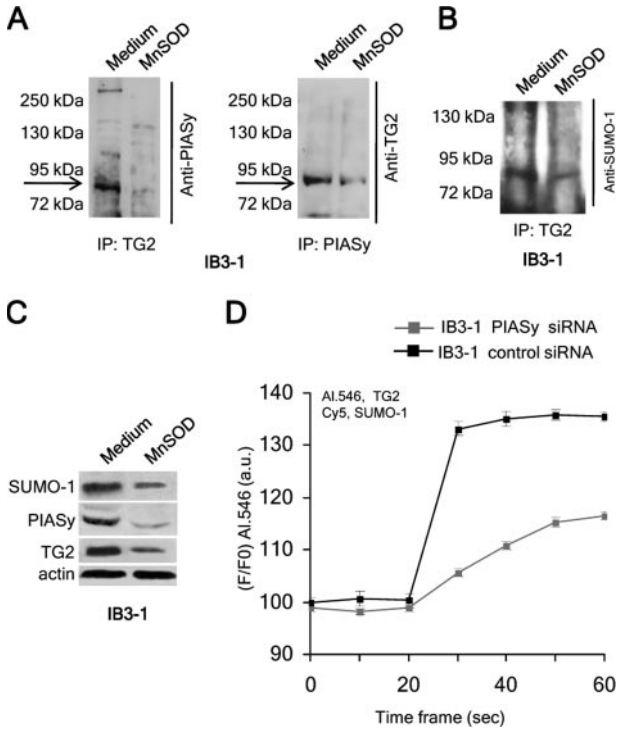

FIGURE 2. PIASy mediates TG2 SUMOylation in CF airway epithelial cells. *A–C*, IB3-1 cells were transduced with either human MnSOD or antisense cDNAs in pAd5CMVK vector. *A*, Immunoblot analysis of TG2 (*left*) or PIASy (*right*) immunoprecipitates (IP) with anti-PIASy (*left*) or anti-TG2 (*right*) Abs, respectively. *B*, Immunoblot analysis with anti-SUMO-1 Ab of TG2 immunoprecipitates. *C*, Immunoblot analysis of SUMO-1, PIASy, and TG2 protein. β-actin levels were used as loading control. *D*, IB3-1 cells were transfected with either 50 nM human PIASy siRNA or control siRNA. FRET analysis of SUMO-1-TG2 interaction.

washing, the immunoprecipitated proteins were electrophoresed through 10% polyacrylamide gels (Bio-Rad), transferred onto blotting membranes (PolyScreen polyvinylidene difluoride; NEN), and analyzed.

Patients and ex vivo cultures of nasal polyp mucosal biopsies

Seven consecutive CF patients carrying the common CFTR mutations (F508del/F508del, F508del/W1282X, F508del/N1303K, or F508del/G542X) (mean age, 19 years; range, 13–29 years) with chronic sinusitis and nasal polyposis and seven consecutive non-CF patients (mean age, 21 years; range, 16–32 years) with idiopathic polyposis underwent surgical treatment. Informed consent was obtained from all subjects and the ethical committee of Regione Campania Health Authority approved the study. CF nasal polyp biopsies were cultured for 4 h, as previously reported (22), with or without ROS scavenger EUK 134 (50 μg/ml). Control nasal polyp biopsies were also cultured for 1 h with H_2O_2 (2 mM; Sigma-Aldrich).

Mice

Young adult female CF mice homozygous for the F508del mutation in the 129/FVB outbred background (36) and their wild-type littermates were housed in static isolator cages at the animal care specific pathogen-free facility of the University of Louvain following recommendations of the Federation of European Laboratory Animal Science Associations (37). To prevent intestinal obstruction CF mice were weaned to a liquid diet (Peptamen; Nestlé Nutrition). Peptamen was replaced daily. The genotype of each animal was checked at 21 days of age, as previously described (36). These studies and procedures were approved by the local Ethics Committee for Animal Welfare and conformed to the European Community regulations for animal use in research (CEE no. 86/609). CF ($n = 7$) and normal homozygous wild-type mice ($n = 7$), 10 to 14 wk of age, were treated i.p. (38) for 7 days with a daily dose of 100 μl of 0.01 M cystamine or PBS solution. Mice were then killed by i.p. injection of 20 mg of sodium pentobarbital (Abbott Laboratories).

ROS detection

Cell lines were pulsed with 10 μM 5-(and-6)-chloromethyl-2′7′-dichlorodihydrofluorescein diacetate acetyl ester (CM-H2DCFDA) (Molecular Probes/Invitrogen) according to the manufacturer's suggestions. The cells were analyzed with a Wallac 1420 multilabel counter (PerkinElmer) or detected by a LSM510 Zeiss confocal laser scanning unit. Seven-micrometer frozen lung tissue sections from each mouse were pulsed with 10 μM CM-H2DCFDA and analyzed by confocal microscopy.

Confocal microscopy

Cell lines. Treated or untreated cells were fixed in methanol, permeabilized with 0.5% Triton X-100, and incubated with Abs against PPARγ (1/100 dilution; Santa Cruz Biotechnology), SUMO-1 (1/100; Santa Cruz Biotechnology), TG2 (1/100; NeoMarkers), PIASy (1/100; Santa Cruz Biotechnology), and nuclear co-repressor (N-CoR, 1/200; Santa Cruz Biotechnology) according to the previously described procedure (22).

Human tissue sections. Five-micrometer frozen human lung tissue sections were fixed in acetone for 10 min. The sections were incubated for 2 h at room temperature with Abs against SUMO-1 (1/100; Santa Cruz Biotechnology), PIASy (1/100; Santa Cruz Biotechnology), and TG2 (1/100; NeoMarkers) as previously described (22).

Mice lung tissue. Seven-micrometer frozen lung tissue sections from each mice were fixed in acetone for 10 min. The sections were incubated for 2 h at room temperature with the following Abs: anti-phospho-p42/p44 MAP kinases (1/200; Cell Signaling Technology), PPARγ (clone H100 sc-7196, rabbit polyclonal IgG, 1/100; Santa Cruz Biotechnology), TG2 (clone H237 sc20261, rabbit polyclonal IgG, 1/100; Santa Cruz Biotechnology), and SUMO-1 (clone S-18 sc31852, goat polyclonal IgG, 1/100). This was followed by incubation with Alexa 488 donkey anti-rabbit (used for detection of phospho-p42–44, PPARγ, and TG2 protein, 1/200; Invitrogen) or 546 donkey anti-goat (used for detection of SUMO-1 protein, 1/200; Invitrogen). Data were analyzed under fluorescence examination by confocal microscopy as previously described (22).

In situ detection of TG2 enzymatic activity

TG2 activity in cell lines was detected by incubating live cells with biotinylated monodansylcadaverine for 1 h at 37°C (16). The incorporation of labeled substrate was visualized by incubation with Alexa 546-conjugated streptavidin (1/100; Molecular Probes/Invitrogen) for 30 min (22). TG2

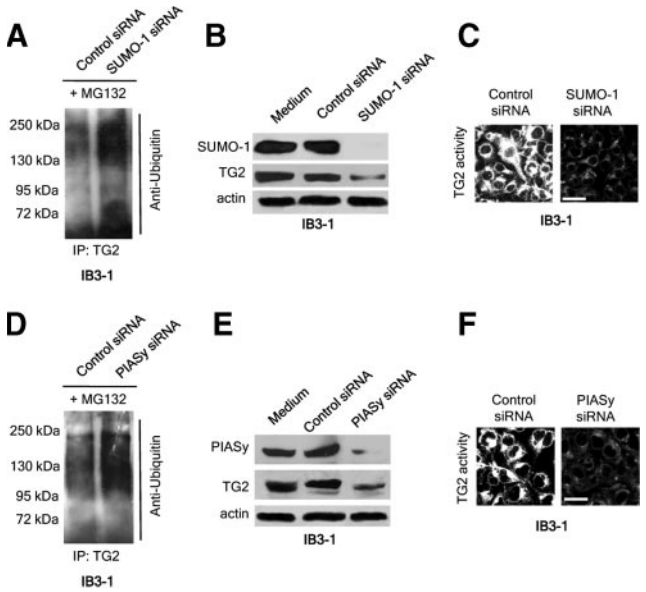

FIGURE 3. Decrease of TG2 protein levels and TG2 activity by either SUMO or PIASy gene silencing. *A–C*, IB3-1 cells were transfected with either 50 nM human SUMO-1 siRNA or control siRNA. *A*, Immunoblot analysis with anti-ubiquitin Ab of TG2 immunoprecipitates upon SUMO-1 gene silencing followed by a 6-h incubation with 50 μM proteasome inhibitor MG132. *B*, Immunoblot analysis of SUMO-1 and TG2 protein in IB3-1 cells upon SUMO-1 gene silencing. β-actin levels were used as loading control. *C*, TG2 activity (white) in IB3-1 cells upon SUMO-1 gene silencing. Confocal microscopy, scale bar, 10 μm. *D–F*, IB3-1 cells were transfected with either 50 nM human PIASy siRNA or control siRNA. *D*, Immunoblot analysis with anti-ubiquitin Ab of TG2 immunoprecipitates upon PIASy gene silencing followed by a 6-h incubation with 50 μM proteasome inhibitor MG132. *E*, Immunoblot analysis of PIASy and TG2 protein upon PIASy gene silencing. β-actin levels were used as loading control. *F*, TG2 activity (white) in IB3-1 cells upon PIASy gene silencing. Confocal microscopy, scale bar, 10 μm.

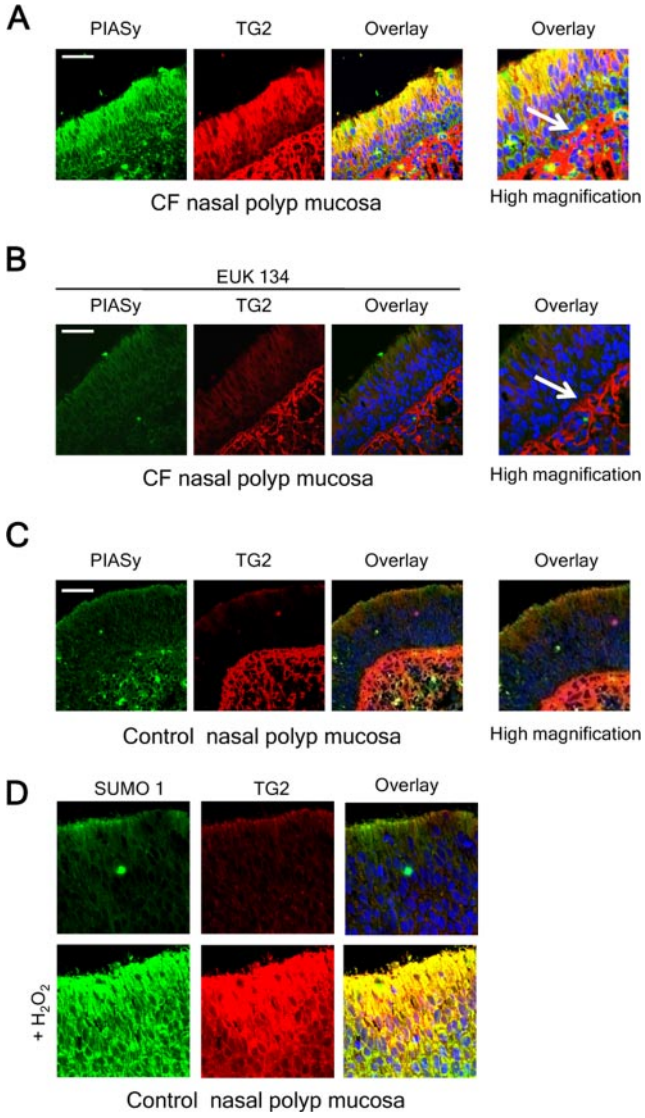

FIGURE 4. ROS-mediated PIASy-TG2 interaction in human nasal polyp mucosa. *A*, Confocal images of PIASγ (green) and TG2 protein (red) in CF nasal polyp mucosa. The same pattern is observed after a 4-h incubation with medium alone. *B*, Confocal images of PIASγ and TG2 in CF nasal polyp mucosa cultured for 4 h with EUK-134. *C*, Confocal images of PIASγ (green) and TG2 protein (red) in control nasal polyp mucosa. *D*, Confocal images of PIASγ and TG2 in control nasal polyp mucosa cultured for 1 h with 2 mM H_2O_2. *A–D*, Overlay shows the merged images. DAPI (4,6-diamidino-2-phenylindole) (blue), nuclear counterstaining. Scale bar, 10 μm.

enzymatic activity on human or mice lung sections was detected by incubating unfixed sections with biotinylated monodansylcadaverine for 1 h at room temperature, as previously described (22).

Fluorescence resonance energy transfer (FRET) microscopy

For acceptor photobleaching, cells were fixed with buffered 2% paraformaldheyde and permeabilized with 0.5% Triton X-100. Upon fixation, cells were immunostained with Alexa 546-anti-TG2 (Molecular Probes/Invitrogen)/Cy5-anti-SUMO-1 (Santa Cruz Biotechnology) or Alexa 546-anti-TG2/Cy5-anti-PIASy (Santa Cruz Biotechnology). Seven-micrometer frozen lung tissue sections from each mouse were fixed with buffered 2% paraformaldheyde. Upon fixation, tissue sections were immunostained with Alexa 546-anti-TG2/Cy5-anti-SUMO-1 (Santa Cruz Biotechnology). Cells or tissue sections were then mounted for performing FRET assay by confocal microscopy. Cy5 was bleached at $\leq$10% of its initial fluorescence, by 200 pulses (2.56 ms) of 5 mW 633 nm laser per pixel, sampling 0.01 mm^2 of the specimen. Alexa 546 fluorescence was detected before and after Cy5 photobleaching (39).

ELISA

Human or murine TNF-α secretion was measured using the BD OptEIA TNF-α ELISA kit II (BD Biosciences). Measurements were performed at least in triplicate. Values were normalized to 10^6 cells; results were expressed as means $\pm$ SEM.

Statistical analysis

All experiments were performed at least in triplicate. Data distribution was analyzed, and statistical differences were evaluated by using ANOVA Tukey-Kramer test by SPSS 12 software. Results of experiments on mice were expressed as means $\pm$ SEM. Between-group comparisons were evaluated by one-way ANOVA, and post hoc comparisons were made using ANOVA Tukey-Kramer test. A p value of <0.05 was considered significant.

Results

PIASy-mediated TG2 SUMOylation increases TG2 protein levels in CF airway epithelial cells

To investigate whether posttranslational modifications could result in the persistence of high levels of TG2 protein, we first analyzed IB3-1 CF epithelial cell lines carrying F508-del/W1282X CFTR mutations and the isogenic stably rescued C38 cells. Western blots revealed that SUMO-1 was increased in IB3-1 cells as compared with C38 cell lines (Fig. 1*A*). Furthermore, acceptor photobleaching FRET revealed that SUMO-1 interacted with TG2 in IB3-1 cells (Fig. 1*B*), and SUMO-1 immunoreactivity was detected on

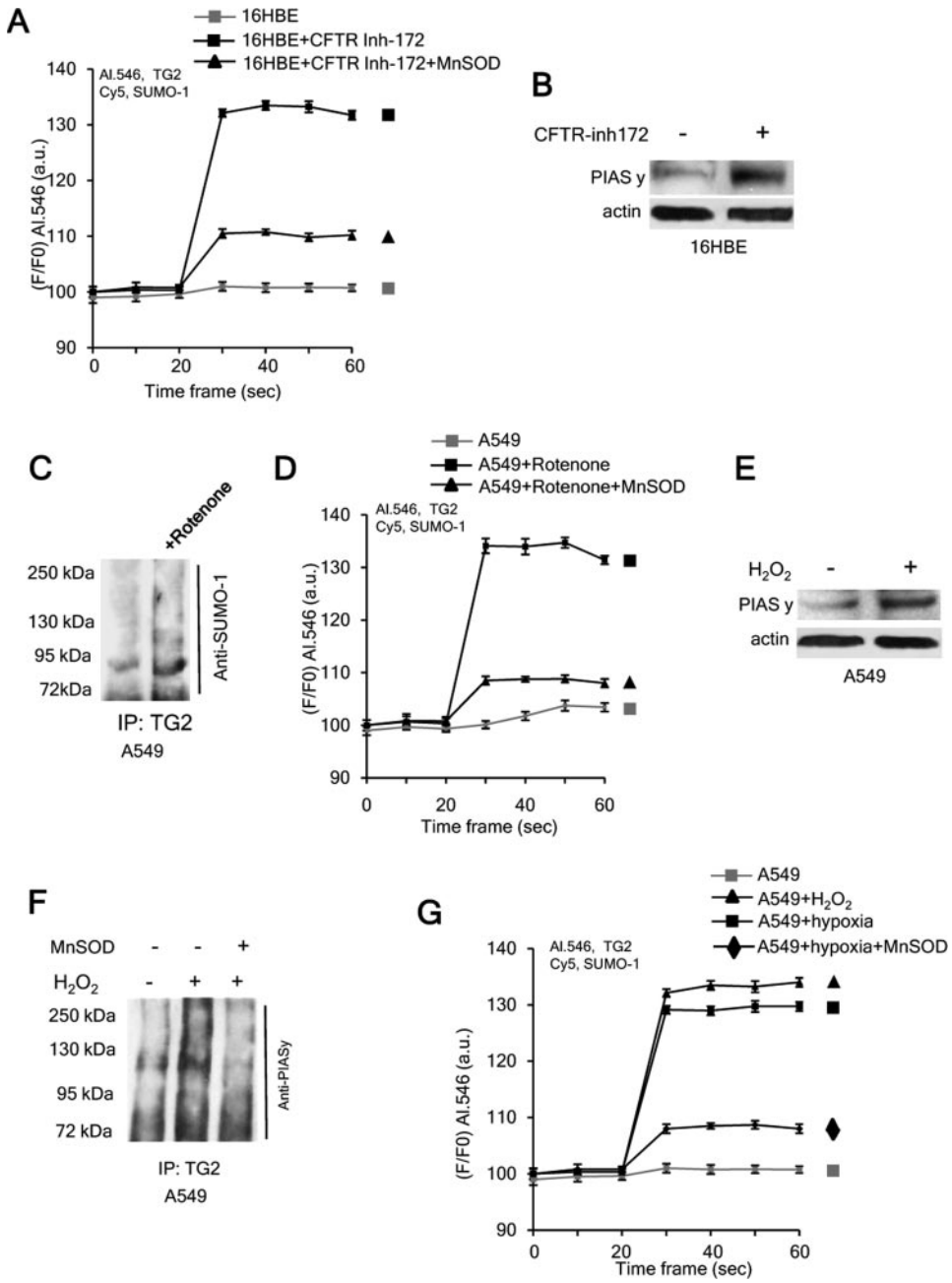

FIGURE 5. Deregulation of ROS machinery mediates TG2 SUMOylation in 16HBE and A549 cells. *A* and *B*, 16HBE cell lines were cultured with or without CFTRinh-172 in the presence or absence of MnSOD overexpression. *A*, FRET analysis reveals SUMO-1-TG2 interaction after CFTR inhibition that was controlled by MnSOD overexpression. *B*, Immunoblot analysis of PIASy protein. β-actin levels were used as loading control. *C* and *D*, A549 cells were cultured with or without rotenone. *C*, Immunoprecipitated (IP) TG2 species from whole-cell extracts are immunoreactive for the anti-SUMO-1 Ab upon rotenone treatment. *D*, FRET analysis reveals SUMO-1-TG2 interaction after incubation with rotenone. MnSOD overexpression controls rotenone-induced TG2 SUMOylation. *E–G*, A549 cells were cultured with H_2O_2 or under hypoxic conditions. *E*, Immunoblot analysis of PIASy protein after H_2O_2 treatment. β-actin levels were used as loading control. *F*, Immunoblot analysis of TG2 immunoprecipitates (IP) with anti-PIASy Ab after H_2O_2 treatment in presence or absence of MnSOD overexpression. *G*, FRET analysis reveals SUMO-1-TG2 interaction after H_2O_2 treatment as well as when A549 cells were cultured upon hypoxic conditions. The effects of hypoxia on TG2 SUMOylation are controlled by MnSOD overexpression.

TG2 immunoprecipitates (Fig. 1*C*). When TG2 immunoprecipitates from IB3-1 cells were probed with the anti-TG2 Ab, two TG2 bands were detected, with the upper band corresponding to the SUMOylated TG2 (Fig. 1*D*). Moreover, TG2 protein levels were higher in IB3-1 than in C38 cell lysates (Fig. 1*E*). Sequence analysis and SUMO motif screening revealed three SUMO acceptor sites (ψ_kxE) (32) in TG2 sequence (supplemental Fig. 1).[4]

We investigated whether PIASy could mediate TG2 SUMOylation. We found that PIASy and TG2 coimmunoprecipitated in IB3-1 cells (Fig. 2*A*). Since PIASy SUMO-1 E3-ligase activity is influenced by ROS (33), we investigated whether the CF intracellular prooxidative environment (22) could mediated TG2-PIASy interaction and TG2 SUMOylation. The overexpression of human MnSOD (35) controlled PIASy-TG2 coimmunoprecipitation (Fig. 2*A*) as well as SUMO-TG2 coimmunoprecipitation (Fig. 2*B*), thus reducing TG2 protein levels (Fig. 2*C*). Furthermore, MnSOD overexpression reduced PIASy protein levels (Fig. 2*C*). The antioxidant synthetic SOD mimetic EUK-134 (22) showed the same effects as MnSOD (supplemental Fig. 2). We confirmed the involvement of PIASy in TG2 SUMOylation by PIASy gene silencing. We reduced PIASy cellular expression by >90%, using PIASy siRNA. Indeed, PIASy siRNA inhibited TG2-SUMO-1 interaction (Fig. 2*D*) and TG2-SUMO-1 coimmunoprecipitation (data not shown). This suggests that the increase of ROS levels induces PIASy-TG2 interaction and TG2 SUMOylation.

SUMOylation may induce protein stabilization by blocking ubiquitination of the same lysine residues (40). We demonstrated that SUMO gene silencing by SUMO-1-specific siRNA increased TG2 ubiquitination upon proteasome inhibition by MG132 (Fig. 3*A*), thus allowing TG2 to be targeted to proteasome for degradation. This induced decreases of TG2 protein (Fig. 3*B*) and TG2 activity (Fig. 3*C*). PIASy siRNA showed the same effects as

[4] The online version of this article contains supplemental material.

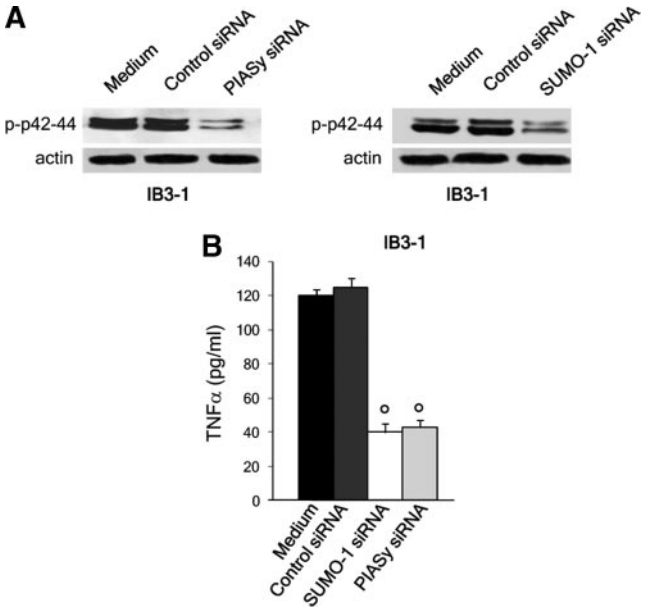

FIGURE 6. SUMO-1 or PIASy gene silencing control inflammation in CF airway epithelial cells. IB3-1 cells were transfected with either 50 nM human SUMO-1 siRNA, PIASy siRNA, or control siRNA. *A*, Immunoblot analysis of p42–44 phosphorylation upon PIASy siRNA (*left*) and SUMO-1 siRNA (*right*). β-actin levels were used as loading control. *B*, TNF-α protein upon SUMO-1 or PIASy gene silencing (each bar represents the mean plus SEM of three separate experiments, each with $n = 3$; ∗, $p < 0.008$ vs control siRNA).

SUMO-1 siRNA on TG2 ubiquitination (Fig. 3*D*) and TG2 protein levels (Fig. 3*E*) and activity (Fig. 3*F*).

To investigate whether TG2-PIASy interaction and TG2 SUMOylation may take place in human airways of CF patients and whether it was induced by the oxidative stress, we used a well-established tissue culture model of biopsies of human CF nasal polyps (22, 41). We have already validated this experimental model (22, 41) and reported that increased TG2 levels are a feature of CF nasal polyp mucosa and that the inhibition of TG2 is effective in controlling mucosal inflammation by restoring normal levels of PPARγ protein (22). We found that TG2-PIASy colocalized in human CF airways (Fig. 4*A*) and that this interaction was inhibited upon treatment with the EUK-134 (Fig. 4*B*). EUK-134 reduced TG2 expression at epithelial but not in the subepithelial compartment (Fig. 4*B*, arrow), where PIASy did not colocalize with TG2 protein (arrow in Fig. 4*A*). After EUK-134 treatment the distribution of TG2 in CF nasal polyp biopsies was similar to that observed in non-CF controls (22). This suggests that the inhibition of TG2-PIASy interaction restores the physiological levels and distribution of TG2 in CF airways (22). Furthermore, in CF nasal polyp mucosa TG2 colocalizes with SUMO-1, and the incubation with EUK-134 inhibited TG2-SUMO-1 colocalization (data not shown). Non-CF control nasal polyp mucosa showed very faint TG2, PIASy, or SUMO-1 expression at the epithelial level (Fig. 4, *C* and *D*). In nasal control biopsies the treatment with H_2O_2 was highly effective in increasing epithelial SUMO-1 and TG2 expression and their colocalization (Fig. 4*D*).

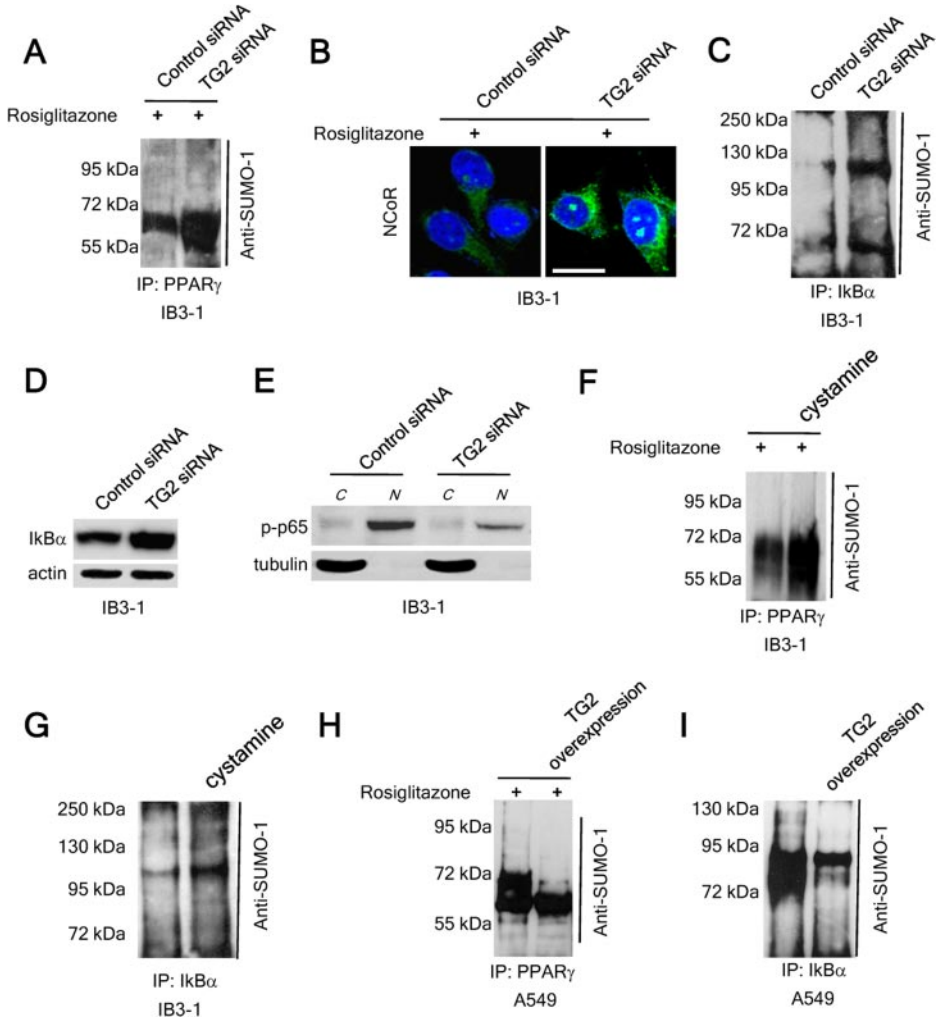

FIGURE 7. TG2 inhibition modulates PPARγ and IkBα pathways in CF airway epithelia. *A* and *B*, IB3-I cells were incubated for 6 h with rosiglitazone in presence or absence of TG2 gene silencing. *A*, Immunoprecipitated (IP) PPARγ from whole-cell extracts are immunoreactive for the anti-SUMO-1 Ab upon TG2 siRNA. *B*, Confocal images of IB3-1 cells immunostained with N-CoR (green). DAPI (4,6-diamidino-2-phenylindole) nuclear counterstaining. Scale bar, 10 μm. *C* and *D*, IB3-1 cells were transfected with either 50 nM human TG2 siRNA or control siRNA. *C*, Immunoprecipitated IkBα species from whole-cell extracts are immunoreactive for the anti-SUMO-1 Ab upon TG2 siRNA. *D*, Immunoblot analysis of IkBα expression upon TG2 gene silencing. *E*, Immunoblot analysis of phospho-p65(Ser^{536}) in cytoplasmic (C) and nuclear (N) cell fractions upon TG2 gene silencing. *F*, IB3-1 cells were incubated with rosiglitazone in the presence or absence of 400 μM cystamine. Increased immunoreactivity of immunoprecipitated PPARγ species from whole-cell extracts for the anti-SUMO-1 Ab after cystamine treatment is shown. *G*, Increased immunoreactivity of immunoprecipitated IkBα species from whole-cell extracts of IB3-1 cells for the anti-SUMO-1 Ab after cystamine treatment. *H* and *I*, IB3-1 cells were transfected with wild-type TG2 cloned into the pLPCX vector (pLPCX-TG2) or empty vector (pLPCX). Decrease of SUMO-1 immunoreactivity of immunoprecipitated PPARγ (*H*) or IkBα (*I*) species from whole-cell extracts after TG2 overexpression.

Deregulation of ROS machinery mediates TG2 SUMOylation in human airway epithelial cell lines

Since we have previously demonstrated that the inhibition of CFTR function by CFTR-172inh leads to increases of ROS levels and TG2 activation (22), we investigated whether a deregulation of ROS machinery could mediate TG2 SUMOylation in airway epithelia. We inhibited CFTR function by CFTR-172inh in 16HBE cell lines and demonstrated that PIASy-TG2 interaction (data not shown) and TG2 SUMOylation (Fig. 5*A*) were induced upon CFTR inhibition, which up-regulates intracellular ROS (22). MnSOD overexpression was highly effective in controlling CFTR-172inh-induced TG2 SUMOylation (Fig. 5*A*). The same effects were observed in A549 epithelial cell lines (data not shown). CFTR-172inh also increased PIASy protein levels (Fig. 5*B*). Moreover, rotenone, the most commonly used complex I inhibitor that increases ROS production in mitochondria (42), induced TG2-SUMO-1 coimmunoprecipitation (Fig. 5*C*) and interaction (Fig. 5*D*) in A549 cells. The effects of rotenone (1 μM) were neutralized by MnSOD overexpression (Fig. 5*D*) as well as by EUK-134 (data not shown). Buthionine sulfoximine, an inhibitor of the glutathione pathway (42), showed the same effects as those observed after treatment with rotenone (supplemental Fig. 2).

The treatment of A549 cells with H_2O_2 induced increased PIASy protein levels (Fig. 5*E*) as well as PIASy-TG2 interaction (Fig. 5*F*) and TG2 SUMOylation (Fig. 5*G*). These effects were controlled by MnSOD overexpression (Fig. 5*F*). Moreover, when A549 cells were cultured under hypoxic conditions (34), increased TG2 SUMOylation was observed (Fig. 5*G*). The effects of hypoxia were likely mediated by ROS (43) since MnSOD overexpression controlled hypoxia-induced TG2 SUMOylation (Fig. 5*G*).

These data suggest that TG2 SUMOylation occurs as a consequence of the deregulation of the oxidative control machinery.

SUMO-1 or PIASy gene silencing controls inflammation in CF airway epithelial cells

TG2 SUMOylation might provide the missing link between cellular stress and inflammation. We tested whether the control of TG2 SUMOylation might modulate TG2-driven inflammation we have described in CF epithelia (22). We demonstrated that gene silencing of either PIASy or SUMO by specific siRNAs induced a significant decrease of p42–44 phosphorylation (Fig. 6*A*) and TNF-α release (Fig. 6*B*) in IB3-1 cells.

TG2 inhibition modulates PPARγ and IkBα SUMOylation in CF airway epithelia

Since PPARγ may undergo SUMOylation in response to a PPARγ agonist (22, 44), thus interacting with N-CoR-histone deacetylase 3 (HDAC3) complex and thereby blocks its ubiquitination (44), we investigated whether increased TG2 protein levels might interfere with PPARγ SUMOylation. We demonstrated that blocking TG2 through specific gene silencing (22) increased SUMO-1 immunoreactivity in PPARγ immunoprecipitates in response to rosiglitazone (Fig. 7*A*), enhanced N-CoR protein and its nuclear localization (Fig. 7*B*), and favored N-CoR-PPARγ interaction (data not shown). TG2 might also mediate NF-κB activation (45) by favoring cross-linking, ubiquitination, and proteasome degradation of IkBα, a key NF-κB modulator (45) and known TG2 substrate (45). Conversely, SUMO enhancers induce SUMOylation and stabilization of IkBα, thus preventing NF-κB activation (34). We demonstrated that in IB3-1 cells the inhibition of TG2 by gene silencing increased SUMO-1 immunoreactivity in IkBα immunoprecipitates (Fig. 7*C*) and increased IkBα protein levels (Fig. 7*D*). Moreover, reduced p-65 NF-κB was detected in nuclear extracts of IB3-1 cells after TG2 inhibition (Fig. 7*E*). TG2 specific inhibitors such as cystamine (38) (Fig. 7, *F* and *G*), R283, or KCC009 (22) (data not shown) showed the same effects as TG2 gene silencing. Furthermore, TG2 overexpression in A549 cells was effective in reducing PPARγ and IkBα SUMOylation (Fig. 7, *H* and *I*). TG2 SUMOylation may therefore switch off the intracellular regulatory machinery, preventing PPARγ SUMOylation, IkBα stabilization, and leading to an uncontrolled inflammatory response.

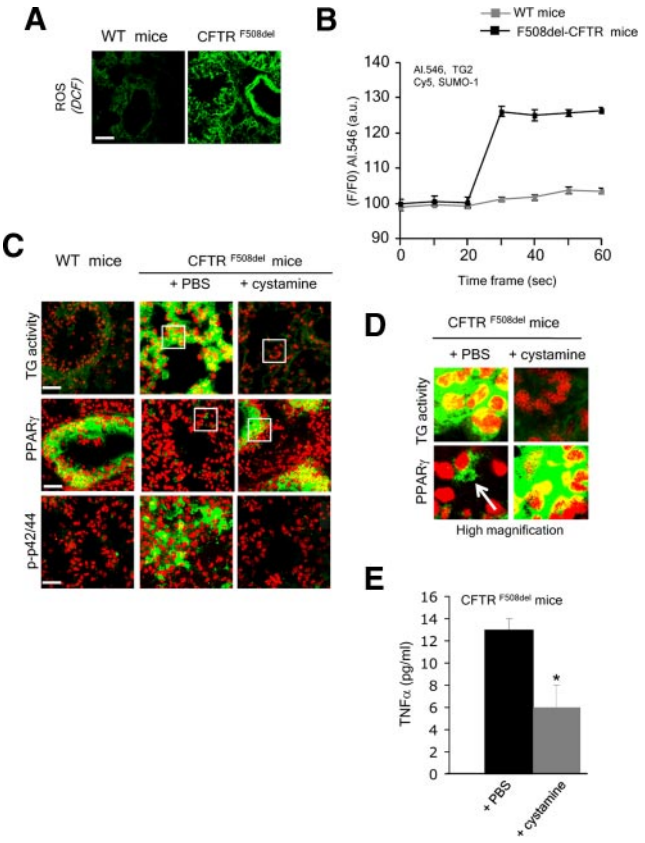

FIGURE 8. TG2 inhibition by cystamine controls airway inflammation in F508del-CFTR homozygous mice. *A*, Increase of intracellular ROS (DCF immunofluorescence) in F508del-CFTR mice as compared with wild-type (WT) littermates. Confocal microscopy. Scale bar, 10 μm. *B*, FRET analysis of TG2-SUMO-1 interaction in homozygous F508del-CFTR mice and WT littermates. *C–E*, Homozygous F508del-CFTR mice treated with cystamine (daily i.p. injection of 100 μl of 0.01 M in PBS/7 days) or PBS. The pattern observed after PBS treatment was similar to that observed in untreated mice. *C*, Confocal images identified increased TG2 activity, low expression of PPARγ protein with localization in perinuclear aggregates, and increased p42–44 phopshorylation in lung tissues of PBS-treated CF mice as compared with control littermates. Cystamine reduces TG2 activity and phospho-p42–44 and restores high epithelial expression and nuclear localization of PPARγ as observed in WT mice. *D*, High magnification of *C*. Confocal microscopy, CyTRAK Orange nuclear counterstaining, yellow indicates nuclear localization. One representative case of seven mice for each group is shown. *E*, TNF-α protein in mouse lung homogenates (mean plus SEM of three separate experiments, each with $n = 7$; $*$, $p < 0.017$ vs PBS-treated mice).

TG2 inhibition controls inflammation in F508del-CFTR homozygous mice

To test the effects of TG2 inhibition in vivo, we treated CF mutant mice homozygous for F508del-CFTR mutation (36) and their control littermates (36) with cystamine, previously reported to inhibit TG2 and ameliorate disease manifestations in a mouse model of

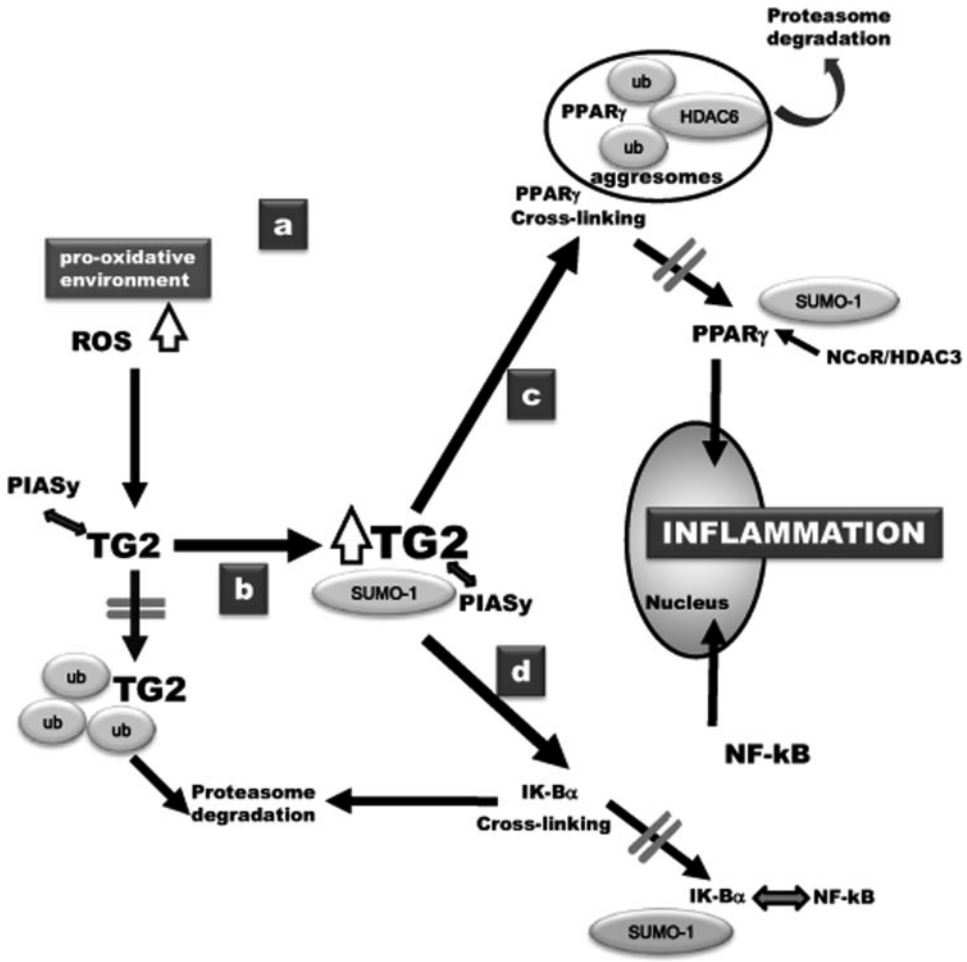

FIGURE 9. Schematic representation of the main finding of the paper. *a*, Increased intracellular levels of ROS favor PIASy-TG2 interaction. *b*, PIASy-TG2 interaction leads to TG2 sumoylation and inhibits TG2 ubiquitination and proteasome degradation, thus leading to uncontrolled TG2 activation. *c*, TG2 favors PPARγ cross-linking and proteasome degradation and inhibits PPARγ SUMOylation and PPARγ-NCoR complex interaction, thus inhibiting transrepressing activity. *d*, TG2 induces IkBα cross-linking and proteasome degradation, favoring NF-κB activation and nuclear translocation.

Huntington's disease (38). We treated CF and wild-type mice with a daily injection of cystamine (i.p. injection of 100 μl of 0.01 M in PBS for 7 days) or PBS (i.p. injection of 100 μl of PBS for 7 days). After treatment with PBS the expression and distribution of the tested markers remained unaltered as compared with the pattern observed in untreated CF mice. Before treatment, as well as after treatment with PBS, all seven tested CF mice showed increase of ROS (Fig. 8*A*) and SUMO-TG2 interaction (Fig. 8*B*), as well as TG2 activity (Fig. 8, *C* and *D*; *D* is a high magnification of *C*), as compared with control littermates. PPARγ was also reduced and sequestered in aggresomes (Fig. 8, *C* and *D*), whereas phosphorylation of p42–44 (Fig. 8*C*) and increase of TNF-α protein were observed (Fig. 8*E*). In all CF mice, the treatment with cystamine controlled TG2 activity (Fig. 8, *C* and *D*), increased PPARγ levels and its nuclear localization (Fig. 8, *C* and *D*), and reduced p42–44 phosphorylation (Fig. 8*C*) and TNF-α protein levels (Fig. 8*E*), thus restoring the pattern observed in their control littermates. Cystamine did not induce any changes in wild-type mice (data not shown).

Discussion

In this report we have underpinned the relationship between CFTR defective function, oxidative stress, and chronic airway inflammation in CF. We have identified TG2 SUMOylation as a pivot in driving the proinflammatory CF phenotype.

The cellular response to stress involves a finely tuned posttranslational network that provides proteins with functional ability at the right time and place, and its perturbations have been shown to contribute to the etiology of various human diseases (46). SUMOylation has been defined as a key player of the posttranslational network to regulate key cellular functions, including transcription, nuclear translocation, stress response, and chromatin structure, as well as of diversifying localization and even stability of the modified proteins (31, 32, 46). SUMOylation is accomplished via an enzymatic cascade involving, among others, E3 ligases, that catalyze the transfer of SUMO from the conjugating enzyme UBC9 to a substrate (31). E3 ligases have gained a central role in the SUMO machinery, since they regulate SUMOylation in response to different stresses (31). Herein we demonstrate that in CF airway epithelia the increased levels of ROS lead to TG2 SUMOylation via interaction of TG2 with PIASy, an E3 ligase already reported to mediate NEMO SUMOylation upon genotoxic stress through ROS generation (33). Oxidative stress increases PIASy protein levels and favors TG2 SUMOylation that leads to the persistence of high TG2 tissue levels by down-regulating TG2 ubiquitination and proteasome degradation.

Our results also indicate that TG2 SUMOylation is a general response to oxidative stress inducers since the impairment of the intracellular ROS balance, either by perturbing mitochondrial oxidative regulation by rotenone or by interfering with gluthatione pathway, is also effective in inducing TG2 SUMOylation and enhancing TG2 activity in airway epithelia. The persistence of high levels of TG2 might in turn increase the intracellular ROS since TG2 may also contribute to the functionality of the mitochondrial respiratory chain (27). Moreover, the PPARγ down-regulation might also interfere with the appropriate control of the redox machinery since it can also modulate oxidative stress (47). Thus, TG2

may sustain a vicious cycle that leads to a progressive and uncontrolled impairment of the cellular homeostasis.

TG2 SUMOylation may therefore switch off the posttranslational regulatory mechanisms in response to the oxidative stress. Most proteins involved in the pathogenesis of chronic human diseases, as huntingtin, ataxin-1, tau, and α-synuclein, were reported to be SUMO (48) as well as TG2 substrates (49). PPARγ, which may be targeted by TG2 to cross-linking and proteasome degradation (22), may also be targeted by SUMO-1 and undergo SUMOylation in response to a PPARγ agonists, such as rosiglitazone (22, 44). SUMOylated PPARγ interacts with the N-CoR-histone deacetylase 3 (HDAC3) complex and thereby blocks its ubiquitination, thus maintaining a repressor condition (44). Herein we demonstrated that sustained TG2 activation inhibits PPARγ SUMOylation and its interaction with the N-CoR (44), thus favoring inflammation. Moreover TG2-mediated cross-linking and degradation of IkBα, a known TG2 substrate (45), inhibits IkBα SUMOylation and favors NF-κB activation. Therefore, TG2 may function as a link between oxidative stress and inflammation by driving the decision as to whether a protein should undergo SUMO-mediated regulation or degradation (Fig. 9).

The rheostat role of TG2 makes this enzyme an attractive target to restore cellular homeostasis and dampen chronic inflammation in CF airways. The regulation of the high levels of TG2 protein or the inhibition of sustained TG2 enzyme activation may represent a new attractive approach to control disease evolution in CF patients.

To provide the rationale and the proof-of-principle for the putative use of TG2 inhibitors in CF patients, we checked whether the mechanisms described in cell lines also take place in human CF airways. The inflammatory response is a complex event involving different cell types interacting within their natural environment. We took advantage of a well-established model of in vitro cultures of explants of CF nasal polyps, which are routinely removed surgically and represent CF chronic airway inflammation (22, 41). We demonstrated that ROS-mediated PIASy-TG2 as well as SUMO-1-TG2 interactions take place in human CF airways.

To evaluate whether we can translate our in vitro findings into an appropriate animal model and confirm their biological relevance in vivo we have studied CF mutant mice homozygous for F508del-CFTR (36). We have demonstrated TG2-SUMO colocalization and increased TG2 activity in lung tissues from F508del-CFTR homozygous mice. In the lungs of these mice, PPARγ is also reduced and sequestered in aggresomes, and inflammation is present. We treated these CF mice with daily i.p. injections of cystamine, already used in a mouse model of Huntington's disease (38). Cystamine is known to inactivate TG2 through a disulfide-exchange reaction and is a substrate for TG2 (38). We have shown that daily injections of cystamine inhibit TG2 activation, increase PPARγ protein expression, and control inflammation.

Our results highlight TG2 as an unforeseen unifying link between genetic defect, deregulation of cellular homeostasis, and inflammation (Fig. 9). They also indicate TG2 as a candidate target for the design of a pathogenic-based therapy in CF and add to the rationale for attempting inhibition of TG2 in CF patients. This study also suggests that targeting TG2 SUMOylation through inhibition of TG2-SUMO interactions might be helpful to control the unwanted persistence of TG2, thus favoring TG2 ubiquitination and proteasome degradation. Therefore, TG2 inhibition might represent a new attractive option to control the evolution of chronic inflammatory diseases, neurodegenerative diseases, and even cancer.

Acknowledgments

We thank Michael Bownlee (Albert Einstein College of Medicine, New York, NY) for the gift of the adenoviral vectors, G. M. Fimia (National Institute for Infectious Diseases, Istituto di Ricovero e Cura a Carattere Scientifico, "L. Spallanzani", Rome, Italy) for the gift of the TG2 plasmid, Fabio Formiggini (Dynamic Imaging Microscopy, Centro di Ingegneria Genetica, Naples, Italy) for the technical support in FRET analysis, and Delphine Labrousse (Cancer Research UK Oncology Unit, University of Southampton, Southampton, U.K.) for the technical support in performing experiments on mice. Cftrtm1EUR (F508del (FVB/129) mice were obtained from Bob Scholte (Erasmus Medical Center Rotterdam, Rotterdam, The Netherlands) (European Economic Community European Coordination Action for Research in Cystic Fibrosis program EU FP6 LSHM-CT-2005-018932).

Disclosures

The authors have no financial conflicts of interest.

References

1. Ratjen, F., and G. Doring. 2003. Cystic fibrosis. *Lancet* 361: 681–689.
2. Thelin, W. R., Y. Chen, M. Gentzsch, S. M. Kreda, J. L. Sallee, C. O. Scarlett, C. H. Borchers, K. Jacobson, M. J. Stutts, and S. L. Milgram. 2007. Direct interaction with filamins modulates the stability and plasma membrane expression of CFTR. *J. Clin. Invest.* 117: 364–374.
3. Gelman, M. S., and R. R. Kopito. 2003. Cystic fibrosis: premature degradation of mutant proteins as a molecular disease mechanism. *Methods Mol. Biol.* 232: 27–37.
4. Kopito, R. R. 1999. Biosynthesis and degradation of CFTR. *Physiol. Rev.* 79: S167–S173.
5. Reddy, M. M., P. M. Quinton, C. Haws, J. J. Wine, R. Grygorczyk, J. A. Tabcharani, J. W. Hanrahan, K. L. Gunderson, and R. R. Kopito. 1996. Failure of the cystic fibrosis transmembrane conductance regulator to conduct ATP. *Science* 271: 1876–1879.
6. Ward, C. L., S. Omura, and R. R. Kopito. 1995. Degradation of CFTR by the ubiquitin-proteasome pathway. *Cell* 83: 121–127.
7. Proesmans, M., F. Vermeulen, and K. De Boeck. 2008. What's new in cystic fibrosis?: from treating symptoms to correction of the basic defect. *Eur. J. Pediatr.* 167: 839–849.
8. Verkman, A. S., and L. J. Galietta. 2009. Chloride channels as drug targets. *Nat. Rev. Drug Discov.* 8: 153–171.
9. Caputo, A., E. Caci, L. Ferrera, N. Pedemonte, C. Barsanti, E. Sondo, U. Pfeffer, R. Ravazzolo, O. Zegarra-Moran, and L. J. Galietta. 2008. TMEM16A, a membrane protein associated with calcium-dependent chloride channel activity. *Science* 322: 590–594.
10. Scheid, P., L. Kempster, U. Griesenbach, J. C. Davies, A. Dewar, P. P. Weber, W. H. Colledge, M. J. Evans, D. M. Geddes, and E. W. Alton. 2001. Inflammation in cystic fibrosis airways: relationship to increased bacterial adherence. *Eur. Respir. J.* 17: 27–35.
11. Smith, J. J., S. M. Travis, E. P. Greenberg, and M. J. Welsh. 1996. Cystic fibrosis airway epithelia fail to kill bacteria because of abnormal airway surface fluid. *Cell* 85: 229–236.
12. Kowalski, M. P., A. Dubouix-Bourandy, M. Bajmoczi, D. E. Golan, T. Zaidi, Y. S. Coutinho-Sledge, M. P. Gygi, S. P. Gygi, E. A. Wiemer, and G. B. Pier. 2007. Host resistance to lung infection mediated by major vault protein in epithelial cells. *Science* 6: 130–132.
13. Thelin, W. R., and R. C. Boucher. 2007. The epithelium as a target for therapy in cystic fibrosis. *Curr. Opin. Pharmacol.* 7: 290–295.
14. Escotte, S., O. Tabary, D. Dusser, C. Majer-Teboul, E. Puchelle, and J. Jacquot. 2003. Fluticasone reduces IL-6 and IL-8 production of cystic fibrosis bronchial epithelial cells via IKK-β kinase pathway. *Eur. Respir. J.* 21: 574–581.
15. Rottner, M., C. Kunzelmann, M. Mergey, J. M. Freyssinet, and M. C. Martinez. 2007. Exaggerated apoptosis and NF-κB activation in pancreatic and tracheal cystic fibrosis cells. *FASEB J.* 21: 2939–2948.
16. Venkatakrishnan, A., A. A. Stecenko, G. King, T. R. Blackwell, K. Brigham, J. W. Christman, and T. S. Blackwell. 2000. Exaggerated activation of nuclear factor-κB and altered IκB-beta processing in cystic fibrosis bronchial epithelial cells. *Am. J. Respir. Cell Mol. Biol.* 23: 396–403.
17. Becker, M. N., M. S. Sauer, M. S. Muhlebach, A. J. Hirsh, Q. Wu, M. W. Verghese, and S. H. Randell. 2004. Cytokine secretion by cystic fibrosis airway epithelial cells. *Am. J. Respir. Crit. Care Med.* 169: 645–653.
18. Hybiske, K., Z. Fu, C. Schwarzer, J. Tseng, J. Do, N. Huang, and T. E. Machen. 2007. Effects of cystic fibrosis transmembrane conductance regulator and ΔF508CFTR on inflammatory response, ER stress, and Ca^{2+} of airway epithelia. *Am. J. Physiol.* 293: L1250–L1260.
19. Teichgräber, V., M. Ulrich, N. Endlich, J. Riethmüller, B. Wilker, C. C. De Oliveira-Munding, A. M. van Heeckeren, M. L. Barr, G. von Kürthy, K. W. Schmid, et al. 2008. Ceramide accumulation mediates inflammation, cell death and infection susceptibility in cystic fibrosis. *Nat. Med.* 14: 382–391.
20. Perez, A., A. C. Issler, C. U. Cotton, T. J. Kelley, A. S. Verkman, and P. B. Davis. 2007. CFTR inhibition mimics the cystic fibrosis inflammatory profile. *Am. J. Physiol.* 292: L383–L395.

21. Verhaeghe, C., C. Remouchamps, B. Hennuy, A. Vanderplasschen, A. Chariot, S. Tabruyn, C. Oury, and V. Bours. 2007. Role of IKK and ERK pathways in intrinsic inflammation of cystic fibrosis airways. *Biochem. Pharmacol.* 73: 1982–1994.
22. Maiuri, L., A. Luciani, I. Giardino, V. Raia, V. R. Villella, M. D'Apolito, M. Pettoello-Mantovani, S. Guido, C. Ciacci, M. Cimmino, et al. 2008. Tissue transglutaminase activation modulates inflammation in cystic fibrosis via PPARγ down-regulation. *J. Immunol.* 180: 7697–7705.
23. Rottner, M., J. M. Freyssinet, and M. C. Martínez. 2009. Mechanisms of the noxious inflammatory cycle in cystic fibrosis. *Respir. Res.* 10: 23.
24. Vij, N., S. Mazur, and P. L. Zeitlin. 2009. CFTR is a negative regulator of NFκB mediated innate immune response. *PLoS ONE* 4: e4664.
25. Lorand, L., and R. M. Graham. 2003. Transglutaminases: crosslinking enzymes with pleiotropic functions. *Nat. Rev. Mol. Cell Biol.* 4: 140–156.
26. Daynes, R. A., and D. C. Jones. 2002. Emerging roles of PPARs in inflammation and immunity. *Nat. Rev. Immunol.* 2: 748–759.
27. Malorni, W., M. G. Farrace, C. Rodolfo, and M. Piacentini. 2008. Type 2 transglutaminase in neurodegenerative diseases: the mitochondrial connection. *Curr. Pharm. Des.* 14: 278–288.
28. Lorand, L. 1996. Neurodegenerative diseases and transglutaminase. *Proc. Natl. Acad. Sci. USA* 93: 14310–14313.
29. Molberg, O., S. N. Mcadam, R. Körner, H. Quarsten, C. Kristiansen, L. Madsen, L. Fugger, H. Scott, O. Norén, P. Roepstorff, et al. 1998. Tissue transglutaminase selectively modifies gliadin peptides that are recognized by gut-derived T cells in celiac disease. *Nat. Med.* 4: 713–717.
30. Verna, A., H. Wang, B. Manavathi, J. Y. Fok, A. P. Mann, R. Kumar, and K. Mehta. 2006. Increased expression of tissue transglutaminase in pancreatic ductal adenocarcinoma and its implications in drug resistance and metastasis. *Cancer Res.* 66: 10525–10533.
31. Meulmeester, E., and F. Melchior. 2008. Cell biology: SUMO. *Nature* 452: 709–711.
32. Geiss-Friedlander, R., and F. Melchior. 2007. Concepts in sumoylation: a decade on. *Nat. Rev. Mol. Cell Biol.* 8: 947–956.
33. Mabb, A. M., and S. M. Wuerzberger-Davis. 2006. PIASy mediates NEMO sumoylation and NF-κB activation in response to genotoxic stress. *Nat. Cell Biol.* 8: 986–993.
34. Carbia-Nagashima, A., J. Gerez, C. Perez-Castro, M. Paez-Pereda, S. Silberstein, G. K. Stalla, F. Holsboer, and E. Arzt. 2007. RSUME, a small RWD-containing protein, enhances SUMO conjugation and stabilizes HIF-1α during hypoxia. *Cell* 131: 309–323.
35. Du, X., D. Edelstein, S. Obici, N. Higham, M. H. Zou, and M. Brownlee. 2006. Insulin resistance reduces arterial prostacyclin synthase and eNOS activities by increasing endothelial fatty acid oxidation. *J. Clin. Invest.* 116: 1071–1079.
36. Legssyer, R., F. Huaux, J. Lebacq, M. Delos, E. Marbaix, P. Lebecque, D. Lison, B. J. Scholte, P. Wallemacq, and T. Leal. 2006. Azithromycin reduces spontaneous and induced inflammation in ΔF508 cystic fibrosis mice. *Respir. Res.* 7: 134.
37. Nicklas, W., P. Baneux, R. Boot, T. Decelle, A. A. Deeny, M. Fumanelli, and B. Illgen-Wilcke; for FELASA (Federation of European Laboratory Animal Science Associations Working Group on Health Monitoring of Rodent and Rabbit Colonies). 2002. Recommendation for the health monitoring of rodent and rabbit colonies in breeding and experimental units. *Lab. Anim.* 36: 20–42.
38. Karpuj, M. V., M. W. Becher, J. E. Springer, D. Chabas, S. Youssef, R. Pedotti, D. Mitchell, and L. Steinman. 2002. Prolonged survival and decreased abnormal movements in transgenic model of Huntington disease, with administration of the transglutaminase inhibitor cystamine. *Nat. Med.* 8: 143–149.
39. Kenworthy, A. K. 2001. Imaging protein-protein interactions using fluorescence resonance energy transfer microscopy. *Methods* 24: 289–296.
40. Müller, S., and C. Hoege. 2001. SUMO-1, ubiquitin's mysterious cousin. *Nat. Rev. Mol. Cell Biol.* 2: 202–210.
41. Raia, V., L. Maiuri, C. Ciacci, I. Ricciardelli, L. Vacca, S. Auricchio, M. Cimmino, M. Cavaliere, M. Nardone, A. Cesaro, et al. 2005. Inhibition of p38 mitogen activated protein kinase controls airway inflammation in cystic fibrosis. *Thorax* 60: 773–780.
42. Martinvalet, D., D. M. Dykxhoorn, R. Ferrini, and J. Lieberman. 2008. Granzyme A cleaves a mitochondrial complex I protein to initiate caspase-independent cell death. *Cell* 133: 681–692.
43. Muniyappa, H. B., S. Song, C. K. Mathews, and K. C. Das. 2009. Reactive oxygen species-independent oxidation of thioredoxin in hypoxia: inactivation of ribonucleotide reductase and redox-mediated checkpoint control. *J. Biol. Chem.* 284: 17069–17081.
44. Pascual, G., A. L. Fong, S. Ogawa, A. Gamliel, A. C. Li, V. Perissi, D. W. Rose, T. M. Willson, M. G. Rosenfeld, and C. K. Glass. 2005. A SUMOylation-dependent pathway mediates transrepression of inflammatory response genes by PPAR-γ. *Nature* 437: 759–763.
45. Kim, D. S., S. S. Park, B. H. Nam, I. H. Kim, and S. Y. Kim. 2006. Reversal of drug resistance in breast cancer cells by transglutaminase 2 inhibition and nuclear factor-κB inactivation. *Cancer Res.* 66: 10936–10943.
46. Tempè, D., M. Piechaczyk, and G. Bossis. 2008. SUMO under stress. *Biochem. Soc. Trans.* 36: 874–878.
47. Quintanilla, R. A., Y. N. Jin, K. Fuenzalida, M. Bronfman, and G. V. Johnson. 2008. Rosiglitazone treatment prevents mitochondrial dysfunction in mutant huntingtin-expressing cells: possible role of peroxisome proliferator-activated receptor-γ (PPARγ) in the pathogenesis of Huntington disease. *J. Biol. Chem.* 283: 25628–25637.
48. Steffan, J. S., N. Agrawal, J. Pallos, E. Rockabrand, L. C. Trotman, N. Slepko, K. Illes, T. Lukacsovich, Y. Z. Zhu, E. Cattaneo, et al. 2004. SUMO modification of huntingtin and Huntington's disease pathology. *Science* 304: 100–104.
49. Juun, E., R. D. Ronchetti, M. M. Quezado, S. Y. Kim, and M. M. Mouradian. 2003. Tissue transglutaminase-induced aggregation of α-synuclein: implication for Lewy body formation in Parkinson's disease and dementia with Lewy bodies. *Proc. Natl. Acad. Sci. USA* 100: 2047–2052.

Tissue Transglutaminase Activation Modulates Inflammation in Cystic Fibrosis via PPARγ Down-Regulation[1]

Luigi Maiuri,[2]*† Alessandro Luciani,†‡ Ida Giardino,§ Valeria Raia,¶ Valeria R. Villella,‖ Maria D'Apolito,† Massimo Pettoello-Mantovani,† Stefano Guido,‖ Carolina Ciacci,‡ Mariano Cimmino,# Olivier N. Cexus, Marco Londei,††‡‡ and Sonia Quaratino[2]**††**

Cystic fibrosis (CF), the most common life-threatening inherited disease in Caucasians, is due to mutations in the CF transmembrane conductance regulator (CFTR) gene and is characterized by airways chronic inflammation and pulmonary infections. The inflammatory response is not secondary to the pulmonary infections. Indeed, several studies have shown an increased proinflammatory activity in the CF tissues, regardless of bacterial infections, because inflammation is similarly observed in CFTR-defective cell lines kept in sterile conditions. Despite recent studies that have indicated that CF airway epithelial cells can spontaneously initiate the inflammatory cascade, we still do not have a clear insight of the molecular mechanisms involved in this increased inflammatory response. In this study, to understand these mechanisms, we investigated ex vivo cultures of nasal polyp mucosal explants of CF patients and controls, CFTR-defective IB3-1 bronchial epithelial cells, C38 isogenic CFTR corrected, and 16HBE normal bronchial epithelial cell lines. We have shown that a defective CFTR induces a remarkable up-regulation of tissue transglutaminase (TG2) in both tissues and cell lines. The increased TG2 activity leads to functional sequestration of the anti-inflammatory peroxisome proliferator-activated receptor γ and increase of the classic parameters of inflammation, such as TNF-α, tyrosine phosphorylation, and MAPKs. Specific inhibition of TG2 was able to reinstate normal levels of peroxisome proliferator-activated receptor-γ and dampen down inflammation both in CF tissues and CFTR-defective cells. Our results highlight an unpredicted central role of TG2 in the mechanistic pathway of CF inflammation, also opening a possible new wave of therapies for sufferers of chronic inflammatory diseases. ***The Journal of Immunology,*** **2008, 180: 7697–7705.**

The breach of the innate immune system and a chronically infected and inflamed lung are the characteristic features of cystic fibrosis (CF)[3] (1). It has been estimated that ~30,000 children and adults in the U.S. (70,000 worldwide) are affected by CF, with a frequency of ~1 in 2,500 livebirths (1).

The direct link between CF transmembrane conductance regulator (CFTR) dysfunction and airway infection has been shown. Defects in the CFTR result in an impaired clearance of lung pathogens, especially *Pseudomonas aeruginosa* (2, 3). Infections are then further exacerbated by the poor mucociliary clearance due to ciliary dysfunction and the hyperabsorption of water by the airways epithelium (4).

The mechanisms by which CFTR mutations might contribute to airways inflammation are, however, still elusive. Defects of the CFTR are also associated with a marked increase of proinflammatory cytokines, such as TNF-α, IL-6, IL-1β, IL-17 (5, 6), and the potent neutrophil chemoattractant and activator IL-8, which recruits large numbers of neutrophils into the airways (1). Chronic inflammation, however, is not merely the consequence of repetitive infections, because CFTR-defective cell lines spontaneously develop similar proinflammatory features when kept in vitro in sterile conditions (7, 8). Indeed, CFTR-defective cells have been reported to have an intrinsically proinflammatory phenotype, and despite different intracellular pathways that have been considered, none to date has been demonstrated to be associated (7, 8).

To underpin the molecular link between a defected CFTR and the excessive inflammatory responses typical of CF airways here we have studied nasal polyp mucosa from CF patients (9) as well as CFTR-defective bronchial epithelial cell lines (2, 10). The rationale to extend the study to the cell lines was to specifically target the role of the defective CFTR on peroxisome proliferator-activated receptor-γ (PPARγ) in sterile conditions, excluding the influence that recurrent infections might have on the epithelium and the generation of inflammation.

We have highlighted how a defected CFTR induces high levels of tissue transglutaminase (TG2) in the airways. TG2 has a pivotal

*European Institute for Cystic Fibrosis Research, San Raffaele Scientific Institute, Milan, Italy; †Institute of Pediatrics, University of Foggia, Foggia, Italy; ‡Department of Experimental Medicine, University Federico II, Naples, Italy; §Department of Laboratory Medicine, University of Foggia, Foggia, Italy; ¶Department of Pediatrics, University Federico II, Naples, Italy; ‖Department of Chemical Engineering, University Federico II, Naples, Italy; #Department of Otolaryngology, University Federico II, Naples, Italy; **Cancer Research UK Oncology Unit, University of Southampton, Southampton, United Kingdom; ††Institute of Child Health, University College, London, United Kingdom; and ‡‡Novartis Pharma AG Translational Medicine, Basel, Switzerland

Received for publication January 8, 2008. Accepted for publication March 28, 2008.

The costs of publication of this article were defrayed in part by the payment of page charges. This article must therefore be hereby marked *advertisement* in accordance with 18 U.S.C. Section 1734 solely to indicate this fact.

[1] This work was supported by the European Institute for Cystic Fibrosis Research, Cancer Research U.K., and Rothschild Trust.

[2] Address correspondence and reprint requests to Dr. Sonia Quaratino, Cancer Research UK Oncology Unit, University of Southampton, SO16 6YD Southampton, UK. E-mail address: sq@soton.ac.uk or Luigi Maiuri, European Institute for Cystic Fibrosis Research, San Raffaele Scientific Institute, via Olgettina 58, 20132, Milan, Italy. E-mail address: maiuri@unina.it

[3] Abbreviations used in this paper: CF, cystic fibrosis; bio-MDC, biotinylated monodansylcadaverine; CFTR, CF transmembrane conductance regulator; CM-H2DCFDA, 5(and 6)-chloromethyl-2′7′-dichlorodihydrofluorescein diacetate acetyl ester; HDAC6, histone deacetylase 6; NAC, *N*-acetyl-cysteine; PPARγ, peroxisome proliferator-activated receptor-γ; ROS, reactive oxygen species; siRNA, small interfering RNA; TG2, tissue transglutaminase.

role in the initiation of inflammation by sequestering PPARγ, a nuclear hormone receptor expressed in monocytes, macrophages, and epithelial cells that negatively regulates inflammatory gene expression by transrepressing inflammatory responses (11). This work also suggests that TG2 inhibition could become a therapeutic target to control inflammation in CF and possibly in other chronic inflammatory diseases.

Materials and Methods

Human airway biopsies and ex vivo cultures

Nasal polyp explants from 10 CF patients carrying the common CFTR mutations (ΔF508/ΔF508, ΔF508/W1282X, ΔF508/N1303K, or ΔF508/G542X) and 10 non-CF patients with nonallergic idiopathic polyposis were cultured, for 4–24 h (9), with or without specific TG2 inhibitors 1,3-dymethyl-2-[(2-oxopropyl) thio] imidazolium (R283) (250 μM) (12) or halo-dihydroisoxazole-derivate transglutaminase inhibitor KCC009 (250 μM), reactive oxygen species (ROS) scavenger EUK 134 (50 μg/ml; Alexis Biochemical), *N*-acetylcysteine (NAC, 10 mM; Alexis Biochemical), PPARγ antagonist GW9662 (1 μM; Alexis Biochemical), or R283 for 24 h, followed by GW9662 (1 μM) for 4 h. Informed consent was obtained from all subjects, and the ethical committee of Regione Campania Health Authority approved the study.

Cell lines and cultures

IB3-1 (human CF bronchial epithelial cell line with the common ΔF508/W1282X CFTR mutation) and C38 (isogenic stably rescued with functional CFTR) cell lines (LGC Promochem) (2, 7, 10) were stimulated for 6 h with R283 (250 μM) or KCC009 (250 μM), ionomycin (1 μM; Calbiochem), BAPTA-AM (5 μM, Calbiochem), EUK 134 (50 μg/ml), rosiglitazone (10 μμ), NAC (10 mM), proteasome inhibitor MG132 (50 μM for 6 h; Calbiochem), or R283 for 24 h, followed by 6-h rosiglitazone. Normal human bronchial epithelial 16HBE cells were cultured, as previously described (8).

Quantitative RT-PCR

Quantitative RT-PCR was performed using iCycler iQ Multicolour Real-Time PCR Detector (Bio-Rad) with iQ TM SYBR Green supermix (Bio-Rad). A relative quantitative method was applied for TG2 mRNA (Qiagen; catalog QT00081277), normalized by the control GAPDH mRNA.

RNA interference

IB3-1 cells were transfected with 50 nM human TG2, human PPARγ, and scramble small interfering RNAs (siRNAs) duplex using Hiperfect Transfection Reagent (Qiagen) at 37°C for 72 h. The target sequence of TG2 siRNA was 5′-CCGCGTCGTGACCAACTACAA-3′, and the whole-cell lysate was then analyzed for Western blot. The PPARγ siRNA is a pool of three sequences, as follows: CCAAGUAACUCUCCUCAAAtt, GAAUG UGAAGCCCAUUGAAtt, and CUACUGCAGGUGAUCAAGAtt. Transfected cells were then analyzed by confocal microscopy for expression using anti-PPARγ mAb clone E8.

Western blot

First Abs anti-phospho-p42/p44 MAPKs (Cell Signaling Technology), PPARγ (clone E8 sc-7273; Santa Cruz Biotechnology), TG2 (clone CUB7402; DakoCytomation), Nε(γ-L-glutamyl)-L-lysine isopeptide (clone 81DIC2; Covalab), and ubiquitin (1:100 clone FL-76, rabbit polyclonal IgG) were counterstained by a HRP-conjugated anti-IgG Ab (Amersham, General Healthcare). The amounts of proteins were determined by a Bio-Rad protein assay to ensure equal protein loading before Western blot analysis. Fifty micrograms of cell lysate were loaded in each lane.

Immunoprecipitation

Following cell lysis, 500 μg of proteins was incubated at 4°C overnight with anti-PPARγ Ab (clone E8) and then mixed with protein G-Sepharose beads for 2 h. The beads were washed three times with lysis buffer, and immunoprecipitates were resuspended in SDS loading buffer. Equal amounts of immunoprecipitate were loaded and analyzed for Western blot.

ROS detection

Cell lines were pulsed with 10 μM 5(and 6)-chloromethyl-2′7′-dichlorodihydrofluorescein diacetate acetyl ester (CM-H2DCFDA; Molecular Probes, Invitrogen), according to manufacturer suggestions, and analyzed with Wallac 1420 multilabel counter (PerkinElmer). Tissue sections (5 μm) of nasal mucosa and cells were incubated with 10 μM CM-H2DCFDA, according to manufacturer suggestions, and an LSM510 Zeiss confocal laser-scanning unit (Carl Zeiss, Germany) was used for detection.

In situ detection of TG2 activity and protein

TG2 protein and enzyme activity were detected and analyzed by confocal microscopy. Briefly, for detection of TG2 enzyme activity, live cells were preincubated with TG2 assay buffer (965 μl of 100 mM Tris/HCl (pH 7.4), 25 μl of 200 mM $CaCl_2$) for 15 min and then with the same TG2 assay buffer added with 10 μl of 10 mM biotinylated monodansylcadaverine (bio-MDC; Molecular Probes) for 1 h at room temperature. The reaction was stopped with 25 mM EDTA for 5 min. The cells were then fixed in 4% paraformaldehyde for 10 min. The incorporation of labeled substrate was visualized by incubation with PE-conjugated streptavidin (DakoCytomation; 1:50) for 30 min. Control experiments included the omission of bio-MDC, as well as replacement of 200 mM $CaCl_2$ with 200 mM EDTA. Blocking experiments were also conducted by incubating cells with the active site inhibitor R283 (250 μM) for 1 h before incubation with the substrates (bio-MDC or biotinylated peptides) and detection of TG2 enzymatic activity. Data were analyzed under fluorescence examination by LSM510 Zeiss confocal laser-scanning unit (Carl Zeiss).

The simultaneous detection of TG2 protein and activity was performed by incubating live cells with bio-MDC for 1 h at room temperature, according to the above described procedure, and then with anti-TG2 CUB 7402 mAb (NeoMarkers; 1:50) for 1 h at room temperature. This was followed by simultaneous incubation with PE-conjugated streptavidin (DakoCytomation; 1:50) and FITC-conjugated rabbit anti-mouse Ig $F(ab')_2$ (DakoCytomation; 1:20) for 1 h.

The detection of TG2 activity and protein on tissue sections was performed, as reported in our previous paper (12).

Confocal microscopy

Cell lines were fixed in methanol and permeabilized with 0.5% Triton X-100 prior incubation with primary Abs. Frozen tissue sections were fixed in acetone for 10 min. Anti-phospho-p42/p44 (1:500; Cell Signaling Technology), anti-phosphotyrosine PY99 mAb (1:80, mouse IgG2b), anti-PPARγ (clone E8, sc-7273, 1:100, mouse IgG1; clone H100, sc-7196, 1:100, rabbit polyclonal IgG; Santa Cruz Biotechnology), anti-ubiquitin (1:100 clone FL-76, rabbit polyclonal IgG), anti-histone deacetylase 6 (HDAC6; 1:100 clone H300, rabbit polyclonal IgG), anti-p65 NF-κB (F-6; 1:100), and anti-ICAM-1 (15.2; 1:200) (Santa Cruz Biotechnology) Abs were used for first Ab. The Ag expression and distribution were visualized by indirect immunofluorescence, as previously described (12).

ELISA

Human TNF-α secretion was measured using the BD OptEIATM TNF-α ELISA kit II (BD Biosciences). Measurements were performed at least in triplicate. Values were normalized to 10^6 cells; results were expressed as mean ± SEMs.

Statistical analysis

All experiments were performed at least in triplicate. Data distribution was analyzed, and statistical differences were evaluated by using ANOVA Tukey-Kramer test by SPSS 12 software. A p value of <0.05 was considered significant.

Results

PPARγ colocalizes in perinuclear aggresomes with ubiquitin and HDAC6 in CF epithelium

We initially determined whether PPARγ, a key inflammation regulator implicated in the prevention of several immunoinflammatory disorders (13), had any role in CF. PPARγ, produced by several cell types, including epithelial cells, regulates inflammation via the specific inhibition of proinflammatory cytokines, such as TNF-α, IL-6, IL-1β, and the NF-κB pathway, and by modulating oxidative stress (13–15).

Nasal polyp mucosal biopsies from CF patients and controls were ex vivo cultured, as previously reported, so that epithelial, myeloid, and lymphoid components can retain all the interactions with neighboring cells within their natural environment (9).

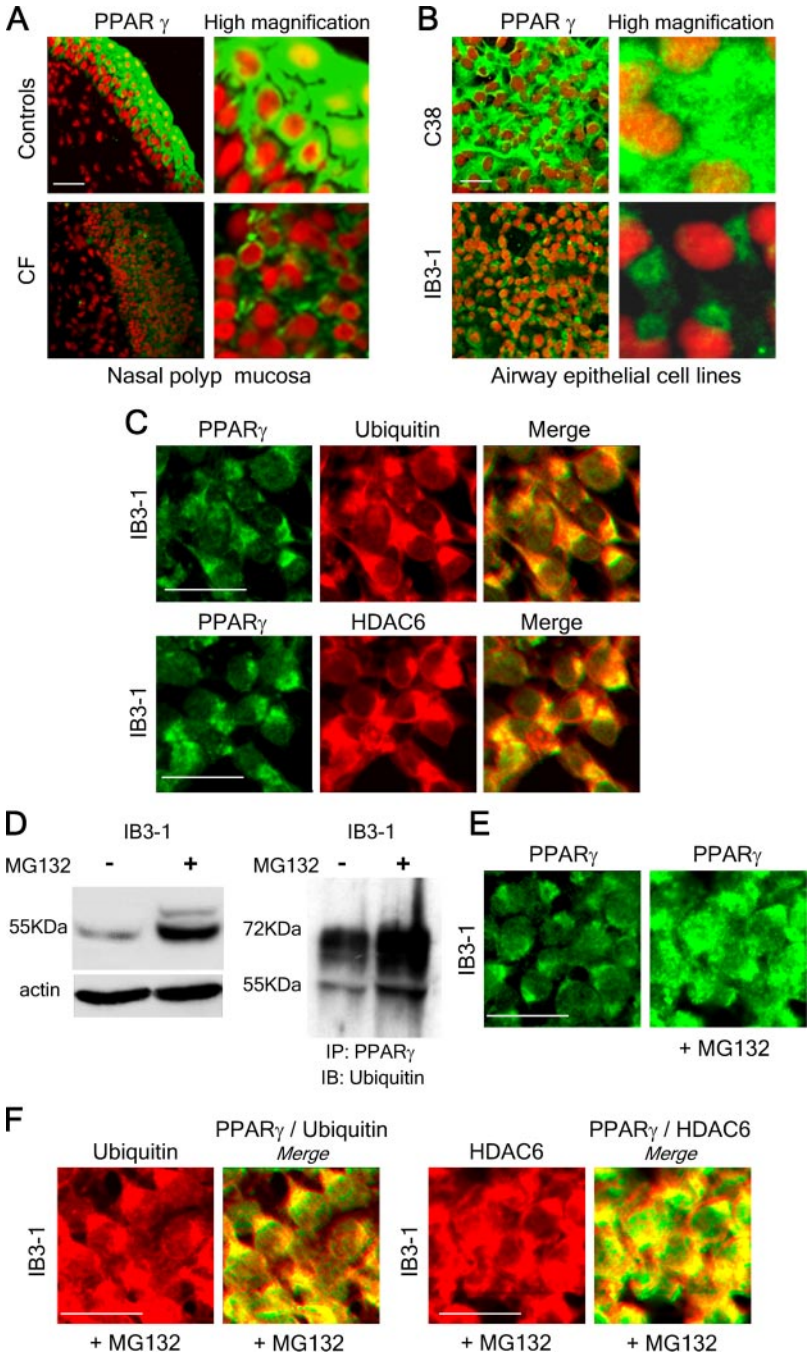

FIGURE 1. PPARγ expression in airway epithelial cells. Confocal images of nasal polyp mucosa from CF patients and controls (*A*) and IB3-1 and C38 cells (*B*): low PPARγ expression (green) (as detected by clone E8 Ab) with perinuclear aggregates in nasal CF epithelia and in IB3-1 cells; CyTRAK Orange (red), nuclear counterstaining. Yellow color indicates nuclear localization of PPARγ. *C*, Confocal images of IB3-1 cells: colocalization (yellow) of ubiquitin (red, *top line*) or HDAC6 (red, *bottom line*) in perinuclear aggregates of PPARγ (green). *D*, *Left panel*, Immunoblot detection of PPARγ in C38 and IB3-1 cells incubated with or without the proteasome inhibitor MG132. *Right panel*, Immunoprecipitated PPARγ species from whole-cell extracts of IB3-1 cells are immunoreactive for the anti-ubiquitin Ab. Immunoprecipitation (IP): anti-PPARγ Ab; immunoblot (IB): anti-ubiquitin Ab. *E*, Confocal images of IB3-1 cells: high PPARγ expression (green) in perinuclear aggregates upon MG132 incubation. *F*, IB3-1 cells after incubation with MG132: expression and colocalization of ubiquitin/PPARγ (yellow, *left panel*) or HDAC6/PPARγ (yellow, *right panel*) in aggresomes. *A–C* and *E* and *F*, Scale bar, 10 μm.

We found that PPARγ expression in nasal biopsies from CF patients and the CFTR-defective IB3-1 cell line was significantly reduced compared with controls and the isogenic C38 cell line with functional CFTR (Fig. 1, *A* and *B*). Remarkably, PPARγ was mainly limited to perinuclear localization in CF tissues and CFTR-defective IB3-1 cell line (Fig. 1, *A* and *B*).

This perinuclear localization was suggestive of aggresomes, a specific cellular response against accumulation of ubiquitinated misfolded and/or aggregated proteins (16), which might also result from impaired proteasome function (16). Although aggresomes containing PPARγ have not been described before, aggresomes containing ubiquitinated misfolded ΔF508 CFTR molecules have been previously observed as result of overexpression of the defective CFTR (16). The aggresomes of CFTR also contain HDAC6, a microtubule-associated deacetylase that interacts with ubiquitin and stabilizes polyubiquitin chains (17). We have shown that in the CFTR-defective IB3-1 cell line, the perinuclear aggregates of PPARγ also colocalize with both HDAC6 and ubiquitin (Fig. 1*C*), thus demonstrating the aggresome nature of these aggregates. Because the presence of aggresomes and HDAC6 is usually the cellular response to eliminate cytoplasmic misfolded proteins (17), we have then investigated whether PPARγ was subjected to proteasome degradation. Treatment with the specific proteasome inhibitor MG132 (18) led to an increase in PPARγ protein levels (Fig. 1, *D* and *E*) and PPARγ ubiquitination (Fig. 1*D*) in CFTR-defective IB3-1 cells. Treatment with MG132 also led to an impressive perinuclear increase of HDAC6- and ubiquitin-PPARγ colocalization (Fig. 1*F*) in IB3-1 cells, suggesting a role for proteasome degradation.

Similar results were obtained using a polyclonal anti-PPARγ Ab with different epitope specificity (data not shown). To confirm the anti-PPARγ Ab specificity, IB3-1 cells were transfected with

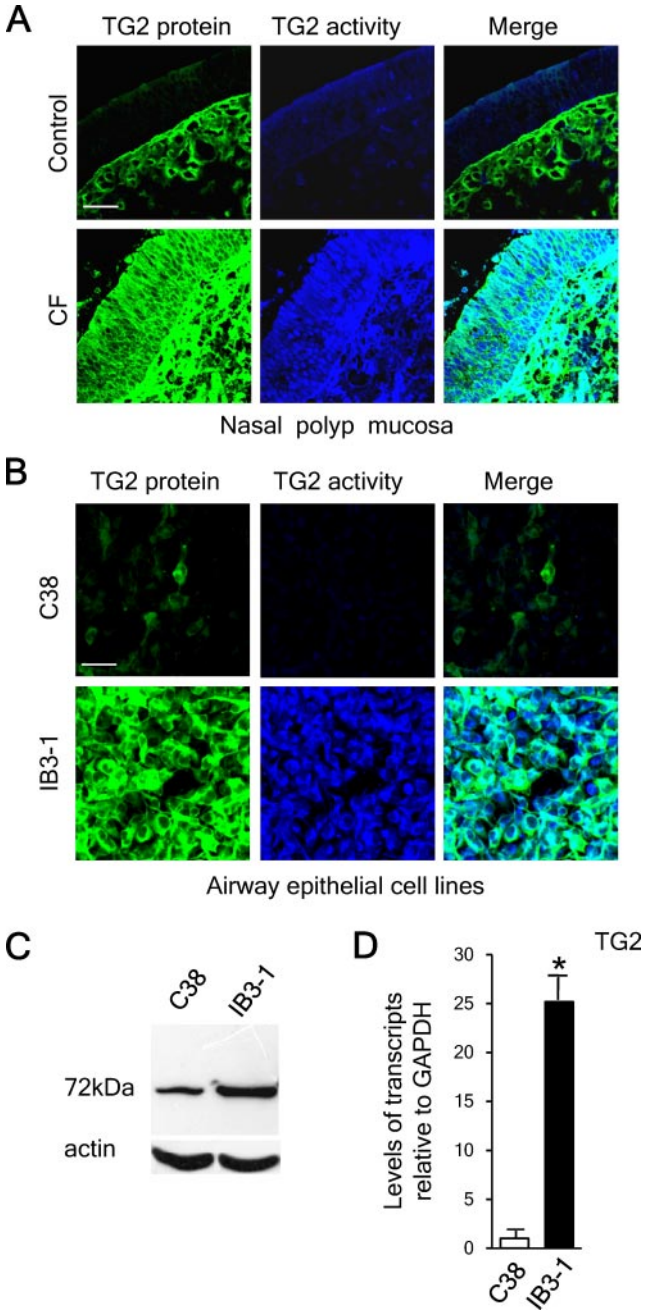

FIGURE 2. TG2 expression in airway epithelial cells. Confocal images identified expression of TG2 (green) and its activity (blue) in epithelial cells of nasal polyp mucosa from CF patients (*A*) and IB3-1 CF cells (*B*) as compared with controls. Merge indicates overlay of individual channels (cyan). Scale bar, 10 μm. *C*, Lysates of C38 and IB3-1 cells were immunoblotted with anti-TG2 Abs. *D*, Real-time PCR of TG2 mRNA in C38 and IB3-1 cells. TG2 transcript was significantly higher in IB3-1 than C38 cells (*, $p < 0.05$ vs C38 cells). Error bars represent SEMs.

human PPARγ siRNA and then immunostained with anti-PPARγ mAb clone E8. We did not detect any PPARγ in the IB3-1 cell transfected with human PPARγ siRNA (data not shown).

TG2 is up-regulated in human CFTR-defective cells

Aggresomes are a prominent cytopathological feature of most neurodegenerative disorders, including Parkinson's and Huntington's diseases (19). In these pathologies, there is also an increase in TG2, responsible for the aggregation of α-synuclein in Parkinson's (20–23). TG2 is a pleiotropic enzyme expressed by many cell types, including epithelial cells, often up-regulated in many chronic inflammatory conditions (22, 23). Therefore, we explored whether TG2 levels or its enzymatic activity were up-regulated in CF tissues and CFTR-defective cell lines.

We observed a significant increase of TG2 protein and enzymatic activity in CF tissues as well as the IB3-1 cell line (Fig. 2, *A–C*). The increase of TG2 was demonstrated by immunoblot and confocal microscopy, whereas real-time PCR showed that TG2 transcript was significantly higher in IB3-1 than C38 cell lines (Fig. 2*D*). These results clearly indicate that CFTR-defective epithelial cells are characterized by an intrinsic TG2 functional increase.

TG2 induces cross-linking of PPARγ and mediates aggresome formation

We then tested the hypothesis that TG2 might induce posttranslational modifications (cross-linking) of PPARγ in CFTR-defective cells, because the QG and QXXP motifs in the PPARγ sequence could be recognized as specific sites for TG2 activity (22).

Double labeling immunofluorescence with anti-PPARγ Ab and an isopeptide cross-link specifically catalyzed by TG2 (22) demonstrated colocalization only in IB3-1 perinuclear aggregates (Fig. 3*A*). Furthermore, using an anti-PPARγ Ab, several high molecular mass bands ranging between 72 and 250 kDa were immunoprecipitated and detected by the anti-isopeptide Ab in the IB3-1 line (Fig. 3*B*). Normal 55-kDa PPARγ in IB3-1 cells was reduced (Fig. 3*C*), whereas C38 cell line presented only faint levels of the high molecular mass and a considerable amount of the normal 55-kDa PPARγ (Fig. 3, *B* and *C*). Exposure of the IB3-1 cells to the irreversible TG2-specific inhibitor R283 (a gift from M. Griffin, Aston University, Birmingham, U.K.) (12, 23, 24) tested at increasing concentrations 50–500 μM with similar results and induced a significant reduction of high molecular mass PPARγ (Fig. 3*D*) and a significant increase of the normal 55-kDa PPARγ in the IB3-1 cells (Fig. 3*E*). This indicated that the cross-linked PPARγ was due to increased TG2 activity. A similar result was achieved through TG2 gene silencing by siRNA (Fig. 3*F*). Exposure of both CF tissues and IB3-1 cells to R283 also resulted in a significant reduction of PPARγ aggregates, restoring a wider intracellular distribution of PPARγ (Fig. 3*G*).

In IB3-1 cells, PPARγ nuclear translocation was promoted only by R283, whereas rosiglitazone, a PPARγ agonist with potent anti-inflammatory activity used in clinic (25), induced only a marginal nuclear PPARγ increase (Fig. 3*H*). In contrast, rosiglitazone alone was able to induce an impressive PPARγ nuclear translocation in C38 cells (Fig. 3*H*).

These results indicate that PPARγ aggregates in CFTR-defective cells are induced by TG2.

TG2 inhibition controls inflammation in CF epithelial cells

TG2 activity does not only control the levels and function of PPARγ, but also influences other markers of inflammation. Inhibition of TG2 with either R283 or KCC009 (another TG2-specific inhibitor, gift from C. Khosla, Stanford University, Palo Alto, CA; data not shown) induced a significant reduction of the phosphorylated p42/p44 MAPKs (Fig. 4*A*), ICAM-1, and NF-κB activation (data not shown) both in CF tissues and IB3-1 cells. Inhibition of TG2 by siRNA also induced a significant decrease of the phosphorylated p42/p44 (Fig. 4*B*) and TNF-α release (Fig. 4*C*) in IB3-1 cells.

The inhibitory activity of R283 on tyrosine phosphorylation, a well-established marker of epithelial inflammation in human CF airway mucosa (9), was abrogated by 4-h incubation with the PPARγ antagonist GW9662 (Fig. 4*D*), further indicating that TG2 controls inflammation through PPARγ.

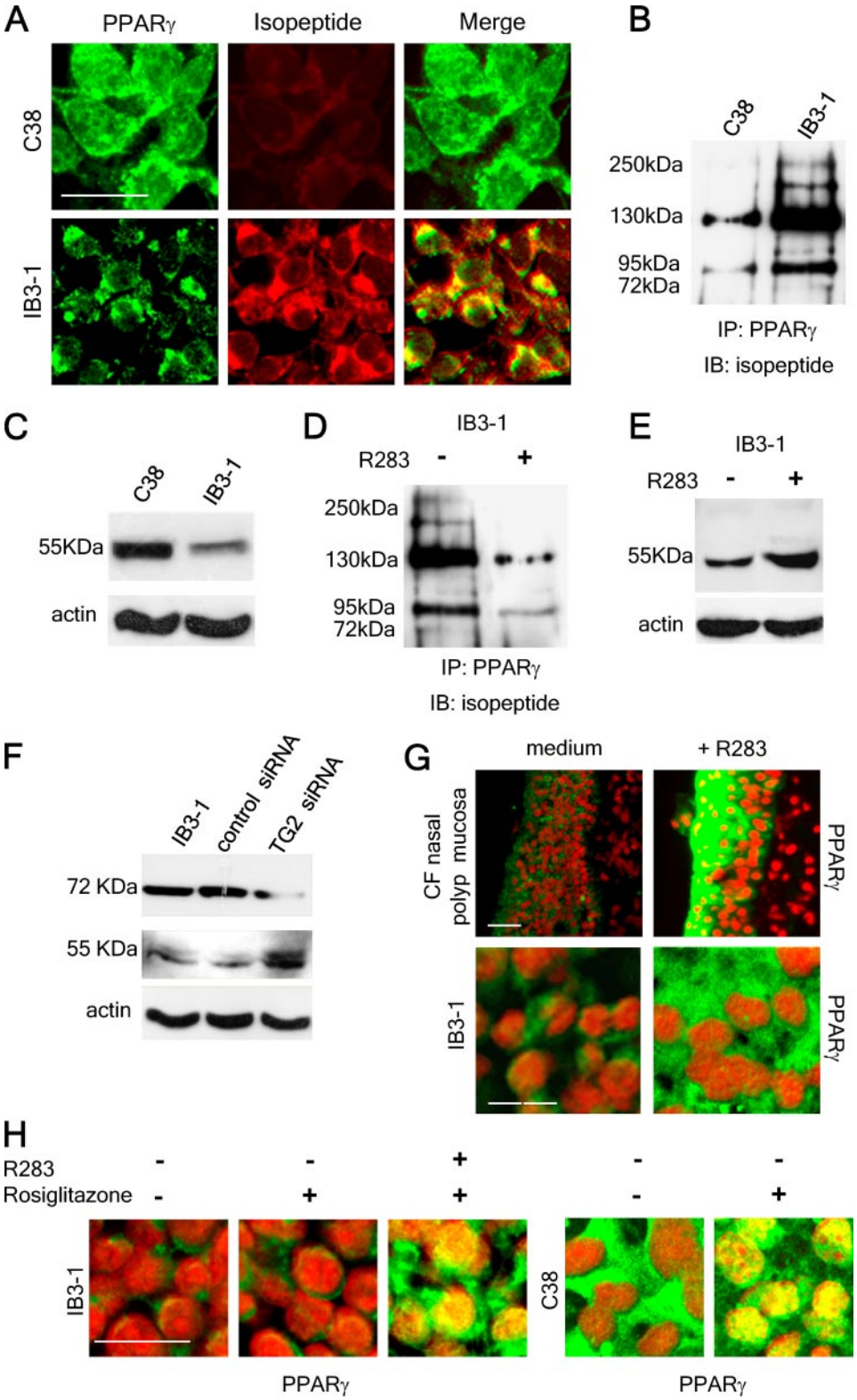

FIGURE 3. Effects of TG2 on PPARγ protein expression and localization. *A*, Confocal images of IB3-1 and C38 cells immunostained with PPARγ (green) and the anti-isopeptide Ab (red). Merge of individual channels shows colocalization (yellow) in perinuclear aggregates. *B*, Immunoprecipitated PPARγ species from whole-cell extracts of C38 and IB3-1 cells are immunoreactive for the anti-isopeptide cross-link Ab. Immunoprecipitation (IP): anti-PPARγ Ab; immunoblot (IB): anti-isopeptide Ab. *C*, Immunoblot of PPARγ in C38 and IB3-1 cells. *D*, Effect of R283 on PPARγ immunoreactivity for the anti-isopeptide Ab in IB3-1 cells. IP: anti-PPARγ Ab; IB: anti-isopeptide Ab. *E*, Immunoblot analysis of PPARγ in IB3-1 cells with or without R283. *F*, Immunoblot of PPARγ in IB3-1 cells: effect of TG2 siRNA. Scramble siRNA was used as a negative control. 72 kDa, TG2; 55 kDa, PPARγ. Confocal images of *G*, PPARγ (green) immunostaining of CF nasal mucosa and IB3-1 cells with or without R283, and *H*, PPARγ (green) in IB3-1 cells (*left panel*) and in C38 cells (*right panel*) after incubation with PPARγ agonist rosiglitazone (10 μM for 6 h) with or without prior incubation with R283. CyTRAK Orange (red) nuclear counterstaining. Yellow color indicates nuclear localization of PPARγ. *A*, *G*, and *H*, Scale bar, 10 μm.

Intracellular Ca^{2+} and ROS levels modulate TG2 activity and inflammation in CFTR-defective cells

We then investigated the mechanisms underlying TG2 up-regulation in CFTR-defective cells. Because TG2 activity is strictly Ca^{2+} dependent (22), and high Ca^{2+} mobilization has been shown in CF nasal or bronchial epithelia (26), we looked at the role of Ca^{2+} in CFTR-defective cells.

Ca^{2+} decrease, induced by the Ca^{2+} chelator BAPTA-AM (27), significantly reduced TG2 activity (Fig. 4*E*) as well as p42/44 phosphorylation (Fig. 4*E*) in IB3-1 cells. The Ca^{2+} ionophore ionomycin (27), on the contrary, increased TG2 activity (Fig. 4*E*) and phospho-p42/p44 (Fig. 4*E*) in C38 cells. These results demonstrated that Ca^{2+} ions drive TG2 activation and thus inflammation in CF epithelium.

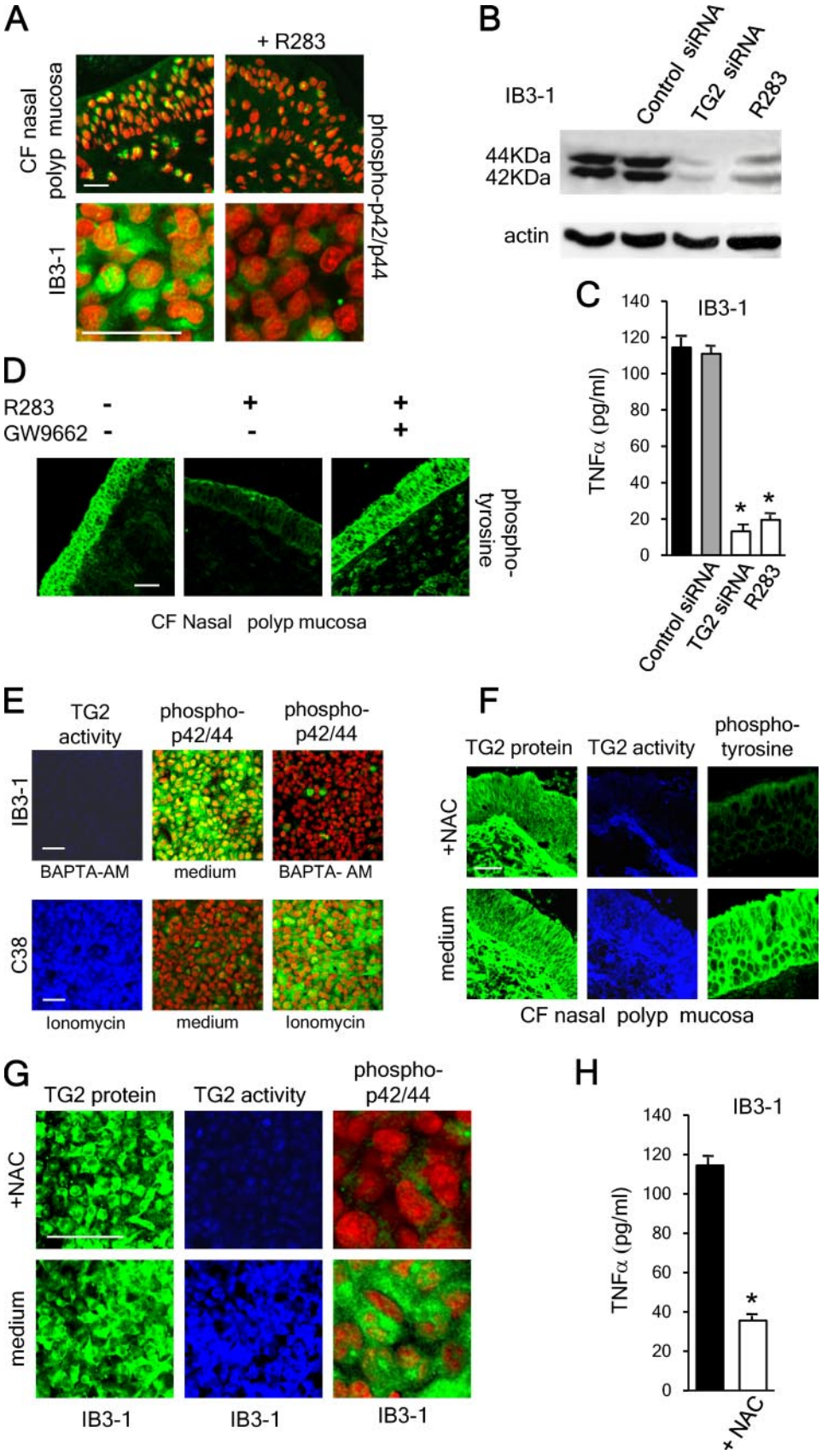

FIGURE 4. Inhibition of TG2 activity controls inflammation in human airway CF epithelia and CFTR-defective cells. *A*, Confocal images of phospho-p42/p44 MAPK expression (green) by CF nasal mucosa and IB3-1 cells cultured with or without R283; CyTRAK Orange (red) nuclear counterstaining. *B*, Immunoblot of phospho-p42/p44 MAPKs in IB3-1 cells after TG2 gene silencing or incubation with R283. Scramble siRNA was used as a negative control. *C*, TNF-α ELISA in IB3-1 cells after TG2 silencing or incubation with R283. The experiment was repeated three times (*, $p < 0.05$ vs IB3-1 cells cultured in medium alone). Error bars represent SEMs. Confocal images of *D*, phospho-*tyr* expression (Py99 Ab) by CF nasal mucosa after incubation with R283 or R283, followed by GW9662, and *E*, TG2 activity (blue) in IB3-1 cells with Ca^{2+}-chelator BAPTA-AM and in C38 cells with Ca^{2+}-ionophore ionomycin. Phospho-p42/p44 MAPK expression (green) by IB3-1 cells cultured with or without BAPTA-AM and by C38 cells cultured with or without ionomycin. CyTRAK Orange (red) nuclear counterstaining. *F* and *G*, NAC decreases expression of TG2 activity (blue), phospho-*tyr*, phospho-p42/p44 (green) in CF nasal polyp mucosa (*F*), and in IB3-1 cells (*G*). Expression of TG2 protein (green) in both CF nasal polyp mucosa and IB3-1 is not affected by NAC treatment (*F* and *G*). *H*, TNF-α secretion in IB3-1 cell line cultured for 48 h with or without NAC. The experiment was repeated three times (*, $p < 0.05$ vs IB3-1 cells cultured in medium alone). Error bars represent SEMs. *A* and *D–G*, Scale bar, 10 μm.

Because TG2 activity is also regulated by ROS (27), we tested whether ROS influenced the TG2-induced inflammation in CF.

In agreement with previous reports, high levels of ROS were only detected in CF tissues and CFTR-defective cells (data not shown) (28). The ROS scavenger NAC significantly reduced TG2

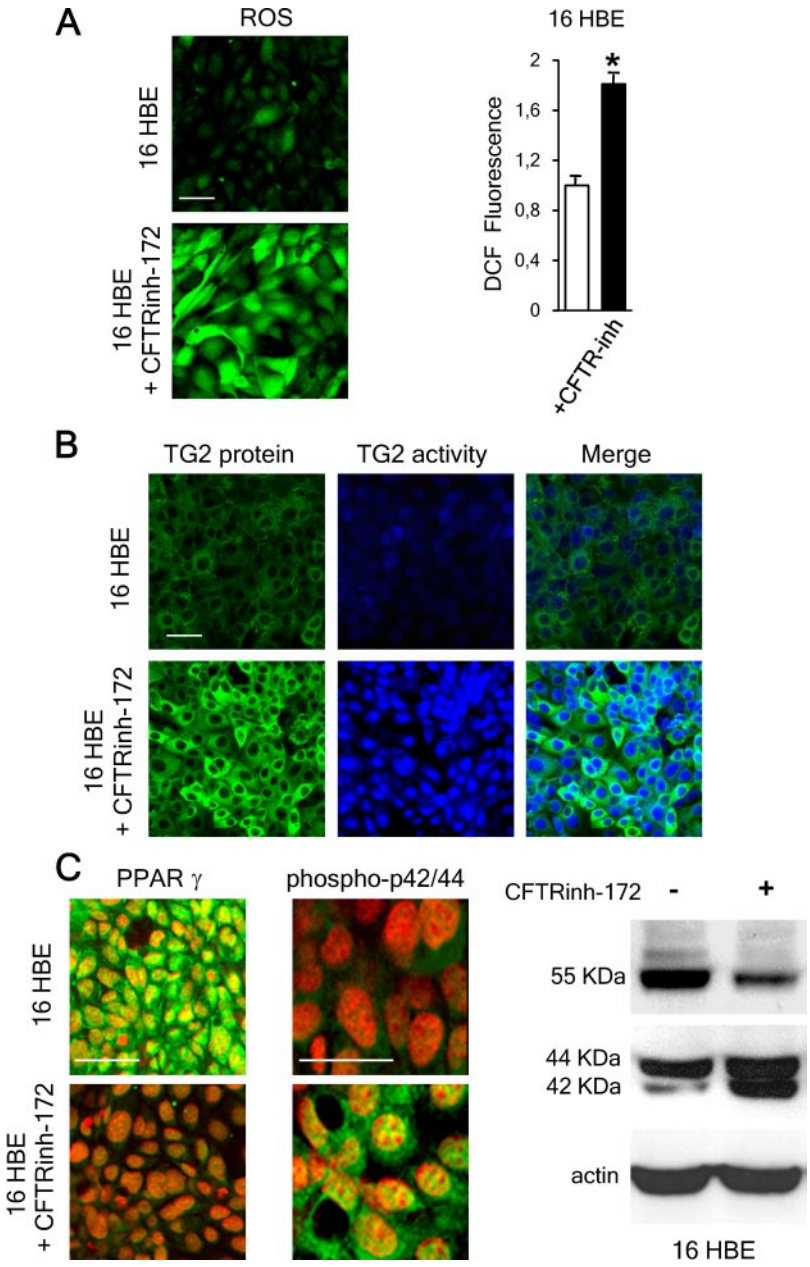

FIGURE 5. CTR inhibition induces airways inflammation. The 16HBE cells were cultured with or without CFTRinh-172 inhibitor. *A*, Confocal microscopy of intracellular ROS (CM-H2DCFDA detection, green) or a Wallac 1420 multilabel counter (each bar represents the mean plus SEMs of three separate experiments, each with $n = 8$; $*$, $p < 0.01$ compared with C38 cells). *B*, Confocal images of TG2 (green) and its activity (blue). Merge indicates overlay of individual channels (cyan). *C*, Confocal images of PPARγ and phospho-p42/44 MAPKs (green); CyTRAK Orange (red) nuclear counterstaining. Immunoblot analysis of PPARγ (55 kDa) and phospho-p42/44 MAPKs (42 and 44 kDa). *A–C*, Scale bar, 10 μm.

activity (Fig. 4, *F* and *G*), phosphotyrosine expression (Fig. 4*F*), p42/44 phosphorylation (Fig. 4*G*), and TNF-α release (Fig. 4*H*) in both CF tissues and IB3-1 cells. Similar results were obtained after inhibition of ROS by another ROS scavenger, EUK 134 (data not shown).

CFTR inhibition induces TG2 up-regulation and inflammation in normal bronchial 16HBE cells

To assess that the pathway described to date was a direct consequence of CFTR dysfunction, we blocked the functional CFTR in the normal bronchial 16HBE cell line with the selective inhibitor CFTRinh-172 (8). We observed all the modifications we have reported above, such as increase of intracellular ROS (Fig. 5*A*), increase of TG2 protein and its activity (Fig. 5*B*), decrease of PPARγ (Fig. 5*C*), and increase of p42/44 phosphorylation (Fig. 5*C*).

Altogether, these results clearly demonstrated how CFTR disruption directly leads to the development of airway inflammation in CF.

Discussion

The novel finding of the present study is the demonstration that CFTR mutations lead to an increase of TG2 levels and activity that, in turn, down-regulate the anti-inflammatory effects of PPARγ. In *cftr*$^{-/-}$ mice, PPARγ expression is down-regulated both at the mRNA and protein levels, and its function is reduced compared with wild-type littermates (29). Therefore, PPARγ agonists have been exploited in therapeutic approaches to control inflammation in airway diseases in animal models (30, 31).

We have shown that PPARγ is not only reduced in CF epithelium and CFTR-defective cell lines, but also confined to perinuclear aggresomes, prominent pathological features common to many neurodegenerative conditions such as Huntington and Parkinson's diseases (32). Aggresomes are generated in response to alterations of the ubiquitin proteasome system, the principal cellular mechanism to eliminate misfolded proteins before they aggregate (33). Aggresomes often develop when a

threshold of misfolded protein is exceeded, and are usually enriched of molecular chaperone, proteasome subunits, ubiquitin conjugates, and the histone deacetylase HDAC6. In CF, the defective CFTR is often not transported beyond the endoplasmic reticulum and accumulates in aggresomes (16, 33). The data shown in Fig. 1*C* clearly indicate that also PPARγ colocalizes in aggresomes with ubiquitin and HDAC6. In CFTR-defective cells, the specific inhibition of the ubiquitin-proteasome system with MG-132 led to a significant increase of PPARγ, HDAC6-, and ubiquitin-PPARγ colocalization in aggresomes (Fig. 1, *D–F*). This suggests that the formation of these aggresomes in CF is caused by the accumulation of misfolded proteins fated to final degradation by the proteasome-ubiquitination system.

The report that in Parkinson's disease TG2 cross-links α-synuclein and induces its aggregation in high molecular mass aggresomes (34) prompted us to investigate whether TG2 also had a role in the aggresome formation in CF. TG2 is a pleiotropic enzyme with a calcium-dependent transamidating activity that results in cross-linking of proteins via ε(γ-glutamyl) lysine bonds (22, 23). Our results clearly demonstrated a significant increase of TG2 protein and enzymatic activity in CF epithelium and CFTR-defective cell lines. TG2 up-regulation was also responsible for the aggresome formation in CF. Importantly, TG2 induced cross-linking of PPARγ and its sequestration into aggresomes (Fig. 3, *A–D*), because the TG2-inhibitor R283 produced a significant reduction of PPARγ protein aggregates and restored a wider intracellular protein distribution (Fig. 3, *E–G*). We have proven the unequivocal role of TG2 in controlling PPARγ and inflammation by blocking TG2 enzymatic activity (R283) as well as its translation (siRNA). Furthermore, the inhibition of the normal CFTR in a normal 16HBE bronchial cell line led to a dramatic up-regulation of TG2 and inflammation, clearly showing the direct link between CFTR defectiveness and TG2 up-regulation and inflammation.

Collectively, our study provides a molecular explanation of the reported association between CFTR malfunction and sterile inflammation. Highlighting the role of TG2 in CF, we have also indicated novel ways to modulate inflammation, a key component in CF pathogenesis.

Furthermore, increased amounts of TG2 have been recently described in other diseases, including cancer, in which up-regulation of TG2 is associated with an increased metastatic activity (35) or drug resistance, as in breast cancer, through the activation of NF-κB (36, 37). Because of its capacity to activate NF-κB, a crucial mediator of inflammation-induced tumor growth and metastatic progression, through depletion of free IκBα (38), TG2 provides a mechanistic link between inflammation and cancer.

In this view, our study may have a wider impact in the whole area of inflammation and cancer.

Acknowledgments

We thank Martin Griffin (Aston University, Birmingham, U.K.) and Chaitan Khosla (Stanford University, Palo Alto, CA) for the gift of the TG2-specific inhibitors R283 and KCC009, respectively.

Disclosures

The authors have no financial conflict of interest.

References

1. Ratjen, F., and G. Doring. 2003. Cystic fibrosis. *Lancet* 361: 681–689.
2. Smith, J. J., S. M. Travis, E. P. Greenberg, and M. J. Welsh. 1996. Cystic fibrosis airway epithelia fail to kill bacteria because of abnormal airway surface fluid. *Cell* 85: 229–236.
3. Kowalski, M. P., A. Dubouix-Bourandy, M. Bajmoczi, D. E. Golan, T. Zaidi, Y. S. Coutinho-Sledge, M. P. Gygi, S. P. Gygi, E. A. Wiemer, and G. B. Pier. 2007. Host resistance to lung infection mediated by major vault protein in epithelial cells. *Science* 6: 130–132.
4. Thelin, W. R., and R. C. Boucher. 2007. The epithelium as a target for therapy in cystic fibrosis. *Curr. Opin. Pharmacol.* 7: 290–295.
5. Osika, E., J. M. Cavaillon, K. Chadelat, M. Boule, C. Fitting, G. Tournier, and A. Clement. 1999. Distinct sputum cytokine profiles in cystic fibrosis and other chronic inflammatory airway disease. *Eur. Respir. J.* 14: 339–346.
6. Dubin, P. J., F. McAllister, and J. K. Kolls. 2007. Is cystic fibrosis a TH17 disease? *Inflamm. Res.* 56: 221–227.
7. Verhaeghe, C., C. Remouchamps, B. Hennuy, A. Vanderplasschen, A. Chariot, S. P. Tabruyn, C. Oury, and V. Bours. 2007. Role of IKK and ERK pathways in intrinsic inflammation of cystic fibrosis airways. *Biochem. Pharmacol.* 73: 1982–1994.
8. Perez, A., A. C. Issler, C. U. Cotton, T. J. Kelley, A. S. Verkman, and P. B. Davis. 2007. CFTR inhibition mimics the cystic fibrosis inflammatory profile. *Am. J. Physiol.* 292: L383–L395.
9. Raia, V., L. Maiuri, C. Ciacci, I. Ricciardelli, L. Vacca, S. Auricchio, M. Cimmino, M. Cavaliere, M. Nardone, A. Cesaro, et al. 2005. Inhibition of p38 mitogen activated protein kinase controls airway inflammation in cystic fibrosis. *Thorax* 60: 773–780.
10. Egan, M. E., J. Glöckner-Pagel, C. Ambrose, P. A. Cahill, L. Pappoe, N. Balamuth, E. Cho, S. Canny, C. A. Wagner, J. Geibel, and M. J. Caplan. 2002. Calcium-pump inhibitors induce functional surface expression of Delta F508-CFTR protein in cystic fibrosis epithelial cells. *Nat. Med.* 8: 485–492.
11. Daynes, R. A., and D. C. Jones. 2002. Emerging roles of PPARs in inflammation and immunity. *Nat. Rev. Immunol.* 2: 748–759.
12. Maiuri, L., C. Ciacci, I. Ricciardelli, L. Vacca, V. Raia, A. Rispo, M. Griffin, T. Issekutz, S. Quaratino, and M. Londei. 2005. Unexpected role of surface transglutaminase type II in celiac disease. *Gastroenterology* 129: 1400–1413.
13. Bailey, S. T., and S. Ghosh. 2005. 'PPAR'ting ways with inflammation. *Nat. Immunol.* 6: 966–967.
14. Kelly, D., J. I. Campbell, T. P. King, G. Grant, E. A. Jansson, A. G. Coutts, S. Pettersson, and S. Conway. 2004. Commensal anaerobic gut bacteria attenuate inflammation by regulating nuclear cytoplasmic shuttling of PPAR-γ and RelA. *Nat. Immunol.* 5: 104–112.
15. Collino, M., M. Aragno, R. Mastrocola, M. Gallicchio, A. C. Rosa, C. Dianzani, O. Danni, C. Thiemermann, and R. Fantozzi. 2006. Modulation of the oxidative stress and inflammatory response by PPAR-γ agonists in the hippocampus of rats exposed to cerebral ischemia/reperfusion. *Eur. J. Pharmacol.* 530: 70–80.
16. Kopito, R. R. 2000. Aggresomes, inclusion bodies and protein aggregation. *Trends Cell Biol.* 10: 524–530.
17. Kawaguchi, Y., J. J. Kovacs, A. McLaurin, J. M. Vance, A. Ito, and T. P. Yao. 2003. The deacetylase HDAC6 regulates aggresome formation and cell viability in response to misfolded protein stress. *Cell* 115: 727–738.
18. Hauser, S., G. Adelmant, P. Sarraf, H. M. Wright, E. Mueller, and B. M. Spiegelman. 2000. Degradation of the peroxisome proliferator-activated receptor γ is linked to ligand dependent activation. *J. Biol. Chem.* 275: 18527–18533.
19. Taylor, J. P., J. Hardy, and K. H. Fischebeck. 2002. Toxic proteins in neurodegenerative disease. *Science* 296: 2354–2360.
20. Zainelli, G. M., C. A. Ross, J. C. Troncoso, and N. A. Muma. 2003. Transglutaminase cross-links in intranuclear inclusions in Huntington disease. *J. Neuropathol. Exp. Neurol.* 62: 14–24.
21. Andringa, G., K. Y. Lam, M. Chegary, X. Wang, T. N. Chase, and M. C. Bennett. 2004. Tissue transglutaminase catalyzes the formation of α-synuclein cross-links in Parkinson's disease. *FASEB J.* 18: 932–934.
22. Lorand, L., and R. M. Graham. 2003. Transglutaminases: cross-linking enzymes with pleiotropic functions. *Nat. Rev. Mol. Cell Biol.* 4: 140–156.
23. Siegel, M., and C. Khosla. 2007. Transglutaminase 2 inhibitors and their therapeutic role in disease states. *Pharmacol. Ther.* 115: 232–245.
24. Skill, N. J., T. S. Johnson, I. G. Coutts, R. E. Saint, M. Fisher, L. Huang, A. M. El Nahas, R. J. Collighan, and M. Griffin. 2004. Inhibition of transglutaminase activity reduces extracellular matrix accumulation induced by high glucose levels in proximal tubular epithelial cells. *J. Biol. Chem.* 279: 47754–47762.
25. Belvisi, M. G., D. J. Hele, and M. A. Berrel. 2006. Peroxisome proliferator-activated receptor γ agonists as therapy for chronic airway inflammation. *Eur. J. Pharmacol.* 533: 101–109.
26. Ribeiro, C. M., A. M. Paradiso, M. A. Carew, S. B. Shears, and R. C. Boucher. 2005. Cystic fibrosis airway epithelial Ca^{2+} i signaling: the mechanism for the larger agonist-mediated Ca^{2+} signals in human cystic fibrosis airway epithelia. *J. Biol. Chem.* 280: 10202–10209.
27. Yi, S. J., K. H. Kim, H. J. Choi, J. O. Yoo, H. I. Jung, J. A. Han, Y. M. Kim, I. B. Suh, and K. S. Ha. 2006. $[Ca^{(2+)}]$-dependent generation of intracellular reactive oxygen species mediates maitotoxin-induced cellular responses in human umbilical vein endothelial cells. *Mol. Cells* 21: 121–128.
28. Starosta, V., E. Rietschel, K. Paul, U. Baumann, and M. Griese. 2006. Oxidative changes of bronchoalveolar proteins in cystic fibrosis. *Chest* 129: 431–437.
29. Ollero, M., O. Junaidi, M. M. Zaman, I. Tzameli, A. A. Ferrando, C. Andersson, P. G. Blanco, E. Bialecki, and S. D. Freedman. 2004. Decreased expression of

peroxisome proliferator activated receptor γ in cftr$^{-/-}$ mice. *J. Cell. Physiol.* 200: 235–244.
30. Rizzo, G., and S. Fiorucci. 2006. PPARs and other nuclear receptors in inflammation. *Curr. Opin. Pharmacol.* 6: 421–427.
31. Lee, K. S., S. J. Park, S. R. Kim, K. H. Min, S. M. Jin, H. K. Lee, and Y. C. Lee. 2006. Modulation of airway remodeling and airway inflammation by peroxisome proliferator-activated receptor γ in a murine model of toluene diisocyanate-induced asthma. *J. Immunol.* 177: 5248–5257.
32. Taylor, J. P., F. Tanaka, J. Robitschek, C. M. Sandoval, A. Taye, S. Markovic-Plese, and K. H. Fischbeck. 2003. Aggresomes protect cells by enhancing the degradation of toxic polyglutamine containing protein. *Hum. Mol. Genet.* 12: 749–757.
33. Johnston, J. A., C. L. Ward, and R. R. Kopito. 1998. Aggresomes: a cellular response to misfolded proteins. *J. Cell Biol.* 143: 1883–1898.
34. Juun, E., R. D. Ronchetti, M. M. Quezado, S. Y. Kim, and M. M. Mouradian. 2003. Tissue transglutaminase induced aggregation of α synuclein: implication for Lewy body formation in Parkinson's disease and dementia with Lewy bodies. *Proc. Natl. Acad. Sci. USA* 100: 2047–2052.
35. Satpathy, M., L. Cao, R. Pincheira, R. Emerson, R. Bigsby, H. Nakshatri, and D. Matei. 2007. Enhanced peritoneal ovarian tumor dissemination by tissue transglutaminase. *Cancer Res.* 67: 7194–7202.
36. Antonyak, M. A., A. M. Miller, J. M. Jansen, J. E. Boehm, C. E. Balkman, J. J. Wakshlag, R. L. Page, and R. A. Cerione. 2004. Augmentation of tissue transglutaminase expression and activation by epidermal growth factor inhibit doxorubicin-induced apoptosis in human breast cancer cells. *J. Biol. Chem.* 279: 41461–41467.
37. Kim, D. S., S. S. Park, B. H. Nam, I. H. Kim, and S. Y. Kim. 2006. Reversal of drug resistance in breast cancer cells by transglutaminase 2 inhibition and nuclear factor-κB inactivation. *Cancer Res.* 66: 10936–10943.
38. Karin, M., and F. R. Greten. 2005. NF-κB: linking inflammation and immunity to cancer development and progression. *Nat. Rev. Immunol.* 5: 749–759.